State Space Models for Epidemiological Surveillance of COVID-19

Stefan Heyder

Computational Methods and Applications to German data

2025-10-05 20:45:33+02:00 – Draft v 0.9

Abstract

A major challenge for scientific inquiry during an ongoing epidemic is the multitude of uncertainties one must consider. In this thesis, we detail the demands that epidemiological data impose and demonstrate that state space models (SSMs) offer a flexible class of statistical models capable of capturing these effects while delivering results that are straightforward to interpret. To facilitate inference and predictions in these models, we use importance sampling techniques, for which two popular choices are the Cross-Entropy method (CE-method) and Efficient Importance Sampling (EIS), which are based on Kullback-Leibler and least-squares loss, respectively. For these two methods we provide central limit theorems that shed light on the empirical observation that EIS provides better importance sampling approximations. Our theoretical results reveal that this is likely due to the lower asymptotic variance of EIS.

To demonstrate the capabilities of such models, we fit models for three real-world applications using Germany's COVID-19 data. The first model illustrates how SSMs can be employed to account for the reporting process in detail, which may be used to handle reporting artifacts caused by factors such as holiday periods. Second, we provide a model that explicitly accounts for the exchange of cases between spatial regions. We use this model to perform one-week-ahead forecasts of reported cases for Germany and validate them against the ECDC's ForecastHub dataset, consisting of such forecasts made in real-time. Finally, we introduce a model for the delayed reporting of hospitalizations in Germany, which we use to nowcast the hospitalization incidence. We also compare the predictive performance of this model to real-time nowcasts provided by the German NowcastHub.

Zusammenfassung

Eine zentrale Herausforderung, der sich die Wissenschaft während einer laufenden Epidemie stellen muss, ist die Mannigfaltigkeit von Unsicherheiten. In dieser Dissertation erläutern wir die Anforderungen, die epidemiologische Daten stellen, und zeigen, dass Zustandsraummodelle (engl. State Space Models, SSMs) eine flexible Klasse statistischer Modelle bieten, die diese Effekte erfassen und gleichzeitig leicht interpretierbare Ergebnisse liefern können. Um Inferenz und Vorhersagen in diesen Modellen zu ermöglichen, verwenden wir Importance-Sampling-Techniken, für die zwei populäre Ansätze existieren: Die Cross-Entropy-Methode (CE-Methode) optimiert die Kullback-Leibler Divergenz zwischen Vorschlags- und Zielverteilung, währen die Efficient Importance Sampling (EIS) Method einen geeignenten Kleinste-Quadrate Abstand minimiert. Für diese beiden Methoden stellen wir neue zentrale Grenzwertsätze vor, die die empirische Beobachtung erklären, dass EIS bessere Importance-Sampling-Approximationen liefert. Unsere theoretischen Ergebnisse zeigen, dass dies wahrscheinlich auf die niedrigere asymptotische Varianz von EIS zurückzuführen ist.

Um die Anwendungsmöglichkeiten dieser Modelle zu demonstrieren, wenden wir diese auf drei reale Anwendungen von COVID-19-Daten aus Deutschland an. Das erste Modell veranschaulicht, wie SSMs eingesetzt werden können, um den Meldeprozess von COVID-19 Infektionen detailliert zu berücksichtigen und damit Meldeanomalien, wie sie beispielsweise durch Ferienzeiten entstehen, zu behandeln. Als Zweites stellen wir ein Modell vor, das explizit den Austausch von Fällen zwischen räumlichen Regionen berücksichtigt. Wir nutzen dieses Modell für Kurzzeitprognosen gemeldeter Fälle für Deutschland und validieren diese anhand des ECDC-ForecastHub-Datensatzes, der aus solchen Echtzeit-Prognosen besteht. Schließlich führen wir ein Modell für die verzögerte Meldung von Hospitalisierungen in Deutschland ein, das wir zur Nowcasting der Hospitalisierungsinzidenz verwenden. Wir vergleichen auch die Vorhersageleistung dieses Modells mit Echtzeit-Nowcasts, die vom deutschen NowcastHub bereitgestellt werden.

Publications and Contributions

This thesis consists mostly of unpublished work. During my time as a PhD student, I have, however, been fortunate to collaborate with many scientists on problems in mathematical epidemiology with a focus on COVID-19, resulting in several preprints and publications. In this section I aim to clarify what my contributions to these works were and distinguish them from the contributions of the present thesis. Peer-reviewed publications are marked with a superscript[¶]. For the original contributions of this thesis, refer to the contribution statements located at the beginning of each chapter.

During my time as a PhD student I was also serving as a statistical consultant at TU Ilmenau. In that role, I was lucky to be co-author of some publications as well. However, as these do not directly relate to the thesis at hand, I chose to omit them here.

The first set of works follows the convention of sorting authors by their last name.

Hotz et al., 2020 Thomas Hotz conceived the initial idea for this paper, derived most of the results, and wrote the initial manuscript. Matthias Glock and I managed the data cleaning, estimation of reproduction numbers and automation of the associated dashboard. Alexander Krämer, Anne Böhle, and Sebastian Semper provided consultation on epidemiological and practical relevance.

Grundel et al., 2022[¶] Sara Grundel and Karl Worthmann developed the idea of using optimal control techniques to balance testing with non-pharmaceutical interventions under societal constraints. Thomas Hotz and I designed the compartmental model, incorporating realistic parameters, and derived the epidemiological implications of the optimal strategies. Tobias Ritschel and Philipp Sauerteig established the mathematical and numerical results related to optimal control theory. The writing for the initial version of the paper was divided among Tobias Ritschel, Philipp Sauerteig and myself.

Grundel et al., 2021[¶] Sara Grundel and Karl Worthmann came up with the idea of applying the optimal control techniques from testing to vaccination strategies. Thomas Hotz and myself consulted on how to adapt the compartmental model to account for vaccination instead of testing and contributed to the epidemiological interpretation of the results. The initial version of the paper was written by Tobias Ritschel and Philipp Sauerteig.

Heyder and Hotz, 2023 Thomas Hotz and I conceived with the idea of comparing different measures of COVID-19 spread with respect to ease of interpretation and communication. I then developed these ideas into an initial manuscript, except for the derivation of the renewal equation, which was contributed by Thomas Hotz.

The second set of works follows the convention of sorting authors by contribution.

Bracher et al., 2021¶ and Bracher et al., 2022¶ These two papers are a result of the joint efforts of the German and Polish ForecastHub[1], organized by the Chair of Econometrics and Statistics at Karlsruhe Institute of Technology and the Computational Statistics Group at Heidelberg Institute for Theoretical Studies. Together with the authors of (Burgard et al., 2021), I contributed the `ITWW_country_repro` model, based on the same reference. This included automating the weekly submission of forecasts and actively participating in the weekly group discussions. Based on a pre-registered study protocol, these discussions, and extensive evaluations, the group from Karlsruhe, led by Johannes Bracher, wrote the initial manuscripts.

Heyder et al., 2022¶ Thomas Hotz initially suggested applying small area estimation techniques to reproduction number estimates. I developed the model, estimator and simulation study, consulting with Thomas Hotz throughout the process. I wrote the first draft of the paper. Jan Pablo Burgard provided consultations on the small-area aspect of the paper, and Tyll Krüger on the epidemiological implications.

Sherratt et al., 2022¶ This paper is based on the results of the European ForecastHub[2], spearheaded by the European Centre for Disease Prevention and Control (ECDC). Again, Thomas Hotz and I contributed the `ITWW` model from the German and Polish ForecastHub, participated in weekly discussions and additionally contributed the `ILM-EKF` model, based on Thomas Hotz's initial idea.

Brockhaus et al., 2023¶ This paper was conceived and written by Elisabeth Brockhaus and Johannes Bracher. My contribution includes the estimates of the Ilmenau model for reproduction numbers over time, I participated in discussion as well as interpretation of results and consulted on the final manuscript.

Wolffram et al., 2023¶ The results of this work are based on the German NowcastHub[3], which Thomas Hotz and I contributed daily nowcasts of the `ILM-prop` to. Again, the results of this paper are based on weekly group discussions, and the initial manuscript was prepared by Daniel Wolffram and Johannes Bracher. I then consulted on the interpretation of the results, in particular the surprisingly good performance of the ILM-prop model.

Own publications

Bracher, J. et al. (Aug. 27, 2021). "A Pre-Registered Short-Term Forecasting Study of COVID-19 in Germany and Poland during the Second Wave." In: *Nat Commun* 12.1 (1), p. 5173. ISSN: 2041-1723. DOI: 10.1038/s41467-021-25207-0.

Bracher, J. et al. (Oct. 31, 2022). "National and Subnational Short-Term Forecasting of COVID-19 in Germany and Poland during Early 2021." In: *Commun Med* 2.1 (1), pp. 1–17. ISSN: 2730-664X. DOI: 10.1038/s43856-022-00191-8.

Brockhaus, E. K. et al. (Nov. 27, 2023). "Why Are Different Estimates of the Effective Reproductive Number so Different? A Case Study on COVID-19 in Germany." In: *PLOS Computational Biology* 19.11, e1011653. ISSN: 1553-7358. DOI: 10.1371/journal.pcbi.1011653.

Burgard, J. P. et al. (Aug. 31, 2021). "Regional Estimates of Reproduction Numbers with Application to COVID-19." arXiv: 2108.13842 [stat]. URL: http://arxiv.org/abs/2108.13842 (visited on 09/30/2021).

Grundel, S. et al. (Jan. 1, 2021). "How to Coordinate Vaccination and Social Distancing to Mitigate SARS-CoV-2 Outbreaks." In: *SIAM J. Appl. Dyn. Syst.* 20.2, pp. 1135–1157. DOI: 10.1137/20M1387687.

[1] https://github.com/KITmetricslab/covid19-forecast-hub-de
[2] https://covid19forecasthub.eu/
[3] https://covid19nowcasthub.de/

– (Apr. 1, 2022). “How Much Testing and Social Distancing Is Required to Control COVID-19? Some Insight Based on an Age-Differentiated Compartmental Model.” In: *SIAM J. Control Optim.* 60.2, S145–S169. ISSN: 0363-0129, 1095-7138. DOI: 10.1137/20M1377783.

Heyder, S. et al. (2022). “Regional Estimates of Reproduction Numbers with Application to COVID-19.” In: *Progress in Industrial Mathematics at ECMI 2021*. Ed. by M. Ehrhardt et al. Mathematics in Industry. Cham: Springer International Publishing, pp. 163–171. ISBN: 978-3-031-11818-0. DOI: 10.1007/978-3-031-11818-0_22.

Heyder, S. et al. (Oct. 4, 2023). “Measures of COVID-19 Spread.” In: *Covid-19 pandisziplinär und international: Gesundheitswissenschaftliche, gesellschaftspolitische und philosophische Hintergründe*. Ed. by A. Kraemer et al. Medizin, Kultur, Gesellschaft. Wiesbaden: Springer Fachmedien, pp. 51–66. ISBN: 978-3-658-40525-0. DOI: 10.1007/978-3-658-40525-0_3.

Hotz, T. et al. (Apr. 18, 2020). “Monitoring the Spread of COVID-19 by Estimating Reproduction Numbers over Time.” arXiv: 2004.08557 [q-bio, stat]. URL: http://arxiv.org/abs/2004.08557 (visited on 07/20/2020).

Sherratt, K. et al. (June 16, 2022). *Predictive Performance of Multi-Model Ensemble Forecasts of COVID-19 across European Nations*. DOI: 10.1101/2022.06.16.22276024. Pre-published.

Wolffram, D. et al. (Aug. 11, 2023). “Collaborative Nowcasting of COVID-19 Hospitalization Incidences in Germany.” In: *PLOS Computational Biology* 19.8, e1011394. ISSN: 1553-7358. DOI: 10.1371/journal.pcbi.1011394.

Du musst bereit sein Dinge zu tun.

— A meme on the internet, 2022.

Acknowledgments

Put your acknowledgments here.

Contents

Chapter 1

Introduction

The Coronavirus disease 2019 (COVID-19) pandemic put the scientific community to the test: How infectious, morbid, and mortal was the disease? When and for how long did infected people become infectious? How effective are the countermeasures taken? How safe and effective are the vaccines that were developed at an unprecedented speed? Some of these questions, such as those about the epidemiology of COVID-19, are confined to well-established areas of research, while others, e.g. those about the efficacy of countermeasures, required collaboration across a wide range of disciplines — from infectious disease epidemiology, mathematical and statistical modeling, social and communication science, to non-scientific actors such as legislators, journalists and politicians.

Although there is still a significant amount of scientific and societal follow-up work to be done, given the magnitude of this challenge, it is astonishing how well the scientific community and society as a whole have dealt with the pandemic. A key factor in this accomplishment is the large-scale availability of data surrounding the pandemic. In many countries, including Germany, data on reported cases, deaths, vaccinations, and deaths were published daily by the respective national health authorities, which for Germany is the Robert Koch-Institut (RKI) (Robert Koch-Institut, 2021, 2022). As the news chronicled daily on the number of reported cases and deaths, numerous dashboards with analyses of COVID-19 data were made available and an abundant number of scientific works were created. Effectively communicating with the public, whose cooperation with countermeasures was critical, became increasingly important. To disseminate insights to the public, we need to understand and communicate the underlying dynamics of an epidemic.

An epidemic outbreak is inherently a random phenomenon (Diekmann, Heesterbeek, and Britton, 2013). Who becomes infected, how long they stay infectious, whom they meet while they are infectious and whom they ultimately infect are all aspects that depend to a certain degree on chance. If one is interested in large-scale phenomena, e.g. effects of immunization in a large population, one relies on a deterministic model (Britton et al., 2019), such as the classical S(E)IR model (Kermack and McKendrick, 1927) or its variants. However, as soon as one is interested in more detailed phenomena, as we are in this thesis, stochastic and statistical modeling becomes essential.

As statisticians, having access to vast amounts of data is both a blessing and a curse. While more, and ideally better, data enables us to formulate and address more relevant questions, the models we create to accommodate these data become increasingly complex. A major complexity of epidemic models are the dependencies across time, requiring the use of methods from time-series analysis. However, such models require more care in modeling, fitting, and interpretation, as there are more opportunities for error along the way. As we incorporate more detailed effects into our models, fitting the models to data becomes difficult to practically impossible using established techniques. While there are some remedies for this curse of dimensionality, e.g. exploiting as much available structure as possible, there is an ongoing need for new procedures enabling inference in these settings. As of the writing of this thesis, there is no comprehensive framework for creating such models that details how to incorporate the various phenomena practitioners are interested in. Additionally, we need both mathematical and practical insight into the performance of these procedures to make

informed decisions in applied settings: which methods should we prefer under which circumstances?

These considerations set the stage for this thesis. Driven by the need for good statistical models that allow us to answer urgent questions in infectious disease epidemiology, with COVID-19 as a prime example, we will start in Chapter 2 with an analysis of what is required of these sought-after models. We will define and discuss the role of several epidemiological indicators, namely quantities that have an interpretation related to the epidemic. It turns out that we will usually be interested in quantifying the speed at which the epidemic proliferates, and we discuss several popular indicators that measure this speed. A useful statistical analysis should provide interpretable insight into the problem at hand, so we focus on how straightforward this interpretation is, offering recommendations on when to use which indicator. To estimate these indicators from data, we must create statistical models that include them. Before we do so, we will compile a list of desiderata from the context of COVID-19 to identify a suitable class of such models.

Many of these desiderata can be modeled by state space models, a flexible framework for modeling non-stationary time series. Unfortunately, we will require that these SSMs include integer-valued, non-Gaussian, observations, which makes fitting the models to data analytically impossible and numerically difficult, as one is faced with an intractable high-dimensional distribution; similar to challenges arising in Bayesian inference. Instead of analytical derivations, inference will have to rely on simulation methods, most notably importance sampling. This is at the heart of Chapter 3. To apply these methods, the practitioner has some flexibility in the so-called proposal distribution, a tractable approximation to the sought-after distribution. Different disciplines have developed simulation-based techniques that allow the user to choose optimal proposals, where optimality is based on different performance criteria for different methods. In this thesis, we focus on two methods: the Cross-Entropy method (CE-method) and Efficient Importance Sampling (EIS), corresponding to Kullback Leibler divergence and least-squares loss respectively. In the literature, a comparison between these two methods is missing: there are neither mathematical nor empirical results comparing the two. We fill this gap by first proving central limit theorems for both methods, allowing for a theoretical comparison. Additionally, we provide extensive simulation studies comparing the methods on instructive univariate and SSMs examples. To this end, we also develop a new algorithm that allows the CE-method to be applied to state space models (SSMs).

Finally, we demonstrate in Chapter 3 how to solve a selection of infectious disease epidemiology problems using the mathematical insights we have gained. These examples focus on the COVID-19 epidemic in Germany and illustrate the modeling, computational, and applied aspects of this thesis. We focus on the following three challenges by providing models and insights for German data: How does one model and account for the complex and artifact-prone reporting process of incident cases? How does one incorporate cross-regional infections into these models? And, finally, how does one account for the long reporting delays present in hospitalizations?

In summary, this thesis contributes to both theoretical and applied problems in the context of statistical modeling of infectious diseases. We hope that its results will enhance our ability to respond to future epidemic outbreaks.

Chapter 2

Epidemiological considerations

Contributions of this chapter

The main contribution of this chapter is the analysis of desiderata for epidemiological models (Section 2.4). Furthermore, Section 2.2.4 is based on the ideas of (Heyder and Hotz, 2023) and has been adapted to this thesis.

The spread of infectious diseases, such as COVID-19, is a complex phenomenon. For COVID-19, this complexity arises from the interplay of many factors. Studying these factors will allow us to define the aims and challenges of epidemiological modeling in the context of this thesis. It will also guide us towards desirable and achievable outcomes of our efforts from an applied perspective.

First of all, there is considerable heterogeneity in the progression of the disease once an individual is infected (Salzberger et al., 2021). Some infectees may show few to no symptoms but are still highly infectious (Byambasuren et al., 2020), and disease progression is closely linked to age and preexisting comorbidities (Biswas et al., 2020). Additionally, different variants of SARS-CoV-2 differ in key epidemiological characteristics such as the reproduction number (Z. Du et al., 2022) and mortality (Hughes et al., 2023).

Second, the spread is highly dependent on the contact behavior within the population, as the infector must be in close physical proximity to the infectee to infect them. These contact patterns are an essential component of any mathematical model for infectious diseases, as they define how the epidemic evolves. Some empirical studies (Mossong et al., 2008; Tomori et al., 2021) capture contact behavior at specific time points. However, during an ongoing epidemic these patterns change both in intensity and shape (Tomori et al., 2021).

Finally, as the disease spreads in the population and vaccinations become available, the population develops partial immunity against the disease, if not against infection (Wu et al., 2023). This immunity affects the spread as well: if an infector has contact with a partially immune individual, the probability of transmission is reduced. Additionally, partial immunity may lead infectors to develop fewer or no symptoms so they may not be aware of being infectious, foregoing quarantine.

As statisticians, we face a challenging problem: Which of these factors should we include in our model and how should we incorporate them? The answer certainly depends on the specific epidemiological question under consideration and the availability and quality of the data.

Parts of this chapter, especially Sections 2.2 to 2.4, consist of the ideas published in (Heyder and Hotz, 2023), but have been rewritten to fit better into this thesis.

2.1 Objectives of epidemiological modelling

Before considering the mathematical modeling of epidemics, it's important to clarify what the goals of our investigation are. In this thesis, we aim at providing models informed by real-world data, that enable other scientists to learn about the past, current or future state of the epidemic and whose results are, ideally, easy to communicate to non-experts, such as political stakeholders. These targets roughly translate to the following three tasks for epidemiological modeling:

Retrospective Analysis Here we are interested in an ex-post analysis of a period of interest in the past. The goal is to infer intrinsic epidemiological quantities, such as the time-varying reproduction number R_t, e.g. as in (Abbott et al., 2020), or to evaluate the performance of non-pharmaceutical interventions (NPIs) taken, see e.g. (Brauner et al., 2021; Flaxman et al., 2020; Khazaei et al., 2023). Such analyses can inform future decisions on which countermeasures to implement, highlighting causal links between NPIs prescribed and reductions in reported cases. This objective is challenging due to the observational nature of the data and data quality issues, see Section 2.3. The interplay between NPIs and voluntary change of behavior of the population adds complexity, as such changes may precede enforced social distancing (Gupta, Simon, and Wing, 2020).

For examples focusing on the efficacy of NPIs, we refer the reader to (Brauner et al., 2021; Flaxman et al., 2020; Khazaei et al., 2023), especially the discussion and limitation sections therein. In such analyses, we can assume that all data related to that period is as complete as possible. Methods range from estimating parameters for each day individually, e.g. using the EpiEstim (Cori, 2021) method (Abbott et al., 2020), to constructing complex Bayesian mechanistic (Flaxman et al., 2020) and hierarchical models (Brauner et al., 2021; Khazaei et al., 2023).

Monitoring For monitoring, we are interested in real-time inference about the current state of the epidemic. This includes the recent past and near future and may include nowcasts and forecasts of cases, hospitalizations or deaths. In this setting, data is not yet final, and inference is complicated by slow reporting and data revisions, see Section 2.3. The results of monitoring can be used to inform current policy, i.e. whether current NPIs should be lifted or new ones enforced. Most online dashboards that emerged at the beginning of the pandemic fall into this category. The result of monitoring may be an estimate of an epidemiological indicator, but may also consist of short-term forecasts. Examples of the former include the daily reproduction number estimates of the RKI (An Der Heiden and Hamouda, 2020), the Helmholtz Centre for Infection Research's dashboard (Khailaie et al., 2021) or the dashboard of the authors team (Hotz et al., 2020).

While some of these dashboards also provide forecasts of cases, a more concerted effort of forecasts is provided by the U.S. ForecastHub (Ray et al., 2020), its German/Polish (Bracher et al., 2021a; Bracher et al., 2022) and EU/EFTA (Sherratt et al., 2022) equivalents. These collaborative platforms gathered real-time forecasts of COVID-19 cases and deaths in the upcoming four weeks, based on an ensemble that aggregates predictions from several models provided by expert modelers. In a real-time setting, these forecasts can be evaluated without hindsight bias, which informs practitioners as to which model to prefer. For forecasting, methods can range from classical time series analysis methods (Arroyo-Marioli et al., 2021) to compartmental models (Khailaie et al., 2021) and computationally intensive agent-based models (Adamik et al., 2020).

Scenario Modeling Scenario modeling concerns itself with the impact that changes of current circumstances, e.g. variants, seasonality, policies, vaccination or NPIs, have on public health outcomes. Unlike monitoring, the goal is to quantify the influence over longer periods with scenarios reaching multiple months into the future. The parameters of scenarios are assumed to be uncertain, making the task at hand challenging. These forecasts are difficult to evaluate, as the scenario specifications rely on assumptions that are hard to verify in practice. Nevertheless, these scenarios help policymakers make informed decisions (Borchering et al., 2023).

In the context of this thesis, we are primarily interested in performing retrospective analyses and providing tools for monitoring as well as short-term forecasting. While scenario modeling has its own merits, evaluating the performance of models is much harder, as there is no ground truth for comparison. Additionally, the methods developed in this thesis rely on having recurring observations on a daily or weekly time scale, usually in the form of reported cases, deaths, or hospitalizations, which for scenario modeling are not available. If such observations are not available, i.e. because we are forecasting months ahead, the uncertainty produced by our models will be much too large to be sensible. To produce short-term forecast, we need to specify how fast the epidemic is spreading.

2.2 Measures of epidemic spread

A key component of any epidemiological model is how the spread of the epidemic is accounted for. As previously argued, an epidemic is a complex process, driven by a multitude of factors. To make this complexity manageable, we will employ simplified models for the spread of cases. We are interested not only in the spread of the epidemic but also in the speed, i.e. the change over time, with which cases proliferate, because it allows us to make predictions about future cases and thus provide recommendations on whether countermeasures should be employed or lifted.

In this thesis, our primary focus lies on the growth factor; however, for the sake of completeness, we also introduce and discuss the reproduction number in this section. As we will argue, these two measures offer simple interpretations and, as such, are valuable in communicating the results of our modeling efforts not only to other researchers but also to non-experts, such as the public and political stakeholders.

Additionally, we will be interested in measures that capture the severity of the epidemic, i.e. the morbidities and mortalities caused by the epidemic. Since these events are consequences of infection that occur after a delay, they can be inferred from incidence data. Thus, modeling the spread of

the epidemic serves two goals: making inferences and predictions about the cases and associated measures, as well as morbidities.

To introduce the different measures in the following, we will initially make some simplifying assumptions about the population in which the epidemic spreads and the time frame considered. Subsequently, we will relax these assumptions to accommodate more realistic populations.

First, we consider a homogenous population with homogeneous mixing. This means that any two individuals in the population are affected by the epidemic in the same way: the probabilities of becoming infected, infectious, hospitalized, or recovering from infection are the same for every individual in the population. Additionally, homogenous mixing indicates that once an individual is infected, they meet and infect every other individual in the population with the same probability.

Furthermore, we assume that the population is large enough that the probability of duplicate infections — i.e. becoming infected twice either from the same or different individuals — is negligibly small, and we assume that infections occur independently from one another. Similarly, we could also assume that the population is infinitely large or that the time frame under consideration is sufficiently short.

Finally, we assume that the behavior of the population is constant over the period modeled, which implies that, except for negligible effects such as the decline of susceptibles in the population, the indicators of interest are constant as well. Without this assumption, estimating the indicators is hopeless. The following subsections are loosely based on (Diekmann, Heesterbeek, and Britton, 2013; Hotz et al., 2020)

2.2.1 Reproduction number

We will model the evolution of the epidemic in discrete time, as this is the time scale on which data are available. Denote by $I_0 \in \mathbf{N}$ the initial number of infected individuals on a reference day 0, and for a day $t \in \mathbf{Z}$ let I_t be the number of newly infected individuals on that day. Note that I_t is random. For $\tau \in \mathbf{Z}$ let β_τ be the expected number of secondary cases a primary case infects τ days after it becomes infectious, and assume that the expected number of secondary cases $R_c = \sum_{\tau \in \mathbf{N}} \beta_\tau$ is non-zero and finite $0 < R_c < \infty$. R_c is called the case reproduction number.

As we have assumed that R_c is finite, we may write $\beta_\tau = R_c w_\tau$ where $w_\tau = \frac{\beta_\tau}{R_c}$. $w = (w_\tau)_{\tau \in \mathbf{N}}$ is called the generation time distribution or the infectivity profile. On day t the conditional expectation of newly infected individuals given all past incidences $\mathbb{E}\left(I_t | I_{t-1}, I_{t-2}, \dots\right)$ can then be written as a convolution of w and the number of past cases

$$\mathbb{E}\left(I_t | I_{t-1}, I_{t-2}, \dots\right) = R_c \sum_{\tau=1}^{\infty} I_{t-\tau} w_\tau, \tag{2.1}$$

the so-called renewal equation. Here we have implicitly assumed that $w_0 = 0$, i.e. infected individuals need at least one day to become infectious themselves. For COVID-19 this is a reasonable assumption (Lauer et al., 2020). If case numbers are small, e.g. if the assumptions we demand hold, the conditional distribution of I_t given past cases is, by the law of small numbers, well approximated by a Poisson distribution and combined with the renewal equation we obtain the renewal equation model (C. Fraser, 2007)

$$I_t | I_{t-1}, I_{t-2}, \cdots \sim \text{Pois}\left(R_t \sum_{\tau=1}^{\infty} I_{t-\tau} w_\tau\right), \tag{2.2}$$

where the time-varying or instantaneous reproduction number R_t can vary over time as well. Working with the time-varying reproduction number R_t instead of the case reproduction number R_c has multiple advantages. First, R_c is a measure of the future behavior of a case, i.e. it does not capture the current state of the epidemic[1]. Second, R_t can be estimated from data until day t alone, while $R_c = \sum_{\tau=1}^{\infty} w_\tau R_{t+\tau}$ depends on future cases (C. Fraser, 2007).

[1] Note that R_c also depends on t here and in the following, which we suppress for ease of notation.

Given incidence data $I_t, I_{t-1}, \dots$ we can perform frequentist inference on R_t in Equation (2.2) by estimating

$$\hat{R}_t = \frac{I_t}{\sum_{\tau=1}^{\infty} I_{t-\tau} w_\tau}, \tag{2.3}$$

which is a moment- and maximum-likelihood estimator (Hotz et al., 2020). Additionally (Cori, 2021) provides a Bayesian framework, using conjugate gamma priors for R_t. If one is interested in the case reproduction number R_c, one can recover it from estimates of R_t as $\hat{R}_c = \sum_{\tau=1}^{\infty} w_\tau \hat{R}_{t+\tau}$ or using the Wallinga-Teunis estimator (Wallinga and Teunis, 2004).

The reproduction numbers R_c and R_t have a mechanistic interpretation: R_c is the number of secondary cases an infectious individual can expect to infect over the time of their disease, and so is R_t with the additional assumption that the behavior of the infection process stays the same for the whole duration of infection. Assuming that contacts lead to infection independently and with the same probability, this means that the reproduction numbers are proportional to the total number of contacts a person has, and as such, they are an excellent measure of the efficacy of NPIs (Brauner et al., 2021; Flaxman et al., 2020; Khazaei et al., 2023). An additional advantage is that the model (2.2) can be interpreted mechanistically, i.e. R_t gives a mechanical model of why the number of cases increases. In contrast, the model of exponential growth that we will address next is more phenomenological in nature, based on the observation that the number of cases tend to increase or decrease exponentially.

2.2.2 Growth Factor

If I_0 is small compared to the total population size, a sensible assumption, one can show that under the above model, the expected number of cases grows approximately exponentially (Diekmann, Heesterbeek, and Britton, 2013, Section 1.2),

$$\mathbb{E}I_t \approx \rho \mathbb{E}I_{t-1} \approx \rho^t \mathbb{E}I_0. \tag{2.4}$$

ρ is called the daily exponential growth factor and can be recovered from Equation (2.1) by an exponential ansatz (Wallinga and Lipsitch, 2007):

$$\rho^t \mathbb{E}I_0 = \mathbb{E}I_t = R_c \sum_{\tau=1}^{\infty} \mathbb{E}I_{t-\tau} w_\tau = R_c \sum_{\tau=1}^{\infty} \mathbb{E}I_0 \rho^{t-\tau} w_\tau = \rho^t \mathbb{E}I_0 \left(R_c \sum_{\tau=1}^{\infty} \rho^{-\tau} w_\tau \right)$$

which shows that unless ρ or $\mathbb{E}I_0$ is zero,

$$\sum_{\tau=1}^{\infty} \rho^{-\tau} w_\tau = \frac{1}{R_c}$$

has to hold. The left-hand side is the probability generating function $\mathbb{E}\rho^{-W}$ for $W \sim \sum_{\tau=1}^{\infty} w_\tau \delta_\tau$. Unless w is degenerate, i.e. there is only a single $\tau \in \mathbf{N}_{\geq 1}$ with $w_\tau \neq 0$, the left-hand side is strictly decreasing in ρ with limits 0 and ∞ as ρ goes to 0 and ∞ respectively. Under these circumstances, there is exactly one solution $\rho \in \mathbf{R}_{>0}$ for any given R_c. Thus, once the infectivity profile w is fixed, there is a one-to one relationship between ρ and R_c. For the remainder of this section, we will use the generation time distribution given by Figure 2.1.

Similarly to the time-varying reproduction number, we may alter Equation (2.4) by introducing for $t \in \mathbf{N}$ a time-varying growth factor $\rho_t \in \mathbf{R}_{>0}$, resulting in

$$\mathbb{E}I_t = \rho_t \mathbb{E}I_{t-1}, \tag{2.5}$$

which can be estimated, e.g. by the moment-estimator $\hat{\rho}_t = \frac{I_t}{I_{t-1}}$.

Focusing on the growth factor over the reproduction number has the advantage that one does not need to specify a generation time distribution w to estimate ρ_t, whereas it is essential for estimating R_t.

2.2.3 Other indicators

Instead of concentrating on the daily evolution of the epidemic, it may be beneficial to consider the weekly behavior. Under the assumption of constant exponential growth, the weekly growth factor is simply ρ^7. However, for the reproduction number a weekly time scale is too coarse to be sensible, at least for COVID-19, with infections occurring on the daily, rather than weekly, scale.

As we will see in Section 2.3, the incidence data available in Germany is strongly affected by weekday effects, with fewer cases reported on weekends and more during the week. To avoid explicitly modeling these effects, we will, in Section 4.2, group the case data by weeks. In this case one could estimate the weekly growth factor ρ^7, e.g., by

$$\widehat{\rho^7} \approx \frac{\mathbb{E}\sum_{s=0}^{6} I_{t-s}}{\mathbb{E}\sum_{s=0}^{6} I_{t-7-s}}. \tag{2.6}$$

Here we assumed, again, that the circumstances of the epidemic do not change over the period considered. By slight abuse of notation, we let ρ_t^7 be this weekly growth factor, where now t is counting weeks instead of days. Notice that when ρ_t is time-varying, it is not necessarily the case that $\rho_t^7 = \prod_{s=0}^{6} \rho_{t-s}$. Notice that if $\mathbb{E}W = 7$, i.e. the average infectious period is one week, linearization yields

$$R_c = \frac{1}{\mathbb{E}\rho^{-W}} \approx \rho^7.$$

Let us hasten to add that there is no reason for the error in this approximation to be small. However, at $R_c = 1$, the threshold for growth or decline, we have $\rho = \rho^7 = 1 = R_c$, which suggests that the error around $R_c = 1$ should be small. Indeed, for the generation time distribution presented in Figure 2.1 (with $\mathbb{E}W = 5.6$), the maximum difference between R_c and $\rho^{\mathbb{E}W}$ is 0.001, while the maximum difference between R_c and ρ^7 is 0.06 for $R_c \in [0.8, 1.2]$, the relevant epidemiological range for reproduction numbers for COVID-19 (see, e.g. Figure 2.6). Thus, if we accept slight numerical errors, for COVID-19 we may think of ρ^7 as, approximately, the case reproduction number.

The exponential growth rate r and doubling time d are closely related to the growth factor, and are given by

$$r = \log \rho \qquad\qquad d = \log_\rho 2 = \frac{\log 2}{\log \rho}.$$

Thus r is the growth rate of the exponentially increasing cases, $\mathbb{E}I_t \approx \exp(rt)\mathbb{E}I_0$ and d is the time it takes for cases to double under this exponential growth, $\mathbb{E}I_{t+d} \approx 2\mathbb{E}I_t$. Notice that the last equation only makes sense if $d \in \mathbf{N}$, or if we model the epidemic to evolve in continuous time instead. These two quantities are not as easy to interpret as, e.g., the weekly growth factor or the reproduction number.

2.2.4 Usefulness of indicators

This subsection briefly summarizes the ideas published in (Heyder and Hotz, 2023).

Given incidence data, which of the above indicators should one estimate and report? The answer depends, of course, on the goals of one's investigations and the data at hand as well as the audience to whom one communicates these estimates.

When the audience is the general public, reproduction numbers and growth factors help convey the exponential growth of the epidemic, either by an argument based on generations (reproduction number) or by exponential growth in time (growth factor).

If data about the infectivity profile w is available, e.g. from contact-tracing studies, reproduction numbers have the advantage of having a concrete, mechanistic interpretation as numbers of infectious contacts. If one is interested in containing the epidemic, i.e., "flattening the curve", reducing contacts uniformly in the population by a factor of $c = 1 - \frac{1}{R}$ works. That is if $R = 1.25$, we have to reduce contacts by 20% to reach $R = 1$. Such information is useful not only for policymakers but also for the general population.

Another concern of monitoring is short-term forecasts of future cases, say, for one to four weeks ahead. Given just the estimated growth factor or reproduction number, this task is more easily achieved by the growth factor: it suffices to multiply current incidences by ρ^7 to get the expected number of cases in the next week. For reproduction numbers, forecasting is more involved, relying on simulation to repeatedly sample from Equation (2.2).

We recommend avoiding the communication of exponential growth rates and doubling times if at all possible. Exponential growth rates come with the disadvantages of the growth factor without the upside of having easily accessible forecasts. While doubling times allow for forecasts in terms of when the number of cases will double, such forecasts are usually not of primary interest.

How well we can estimate these indicators depends on the available data and, in particular, its quality.

2.3 Available data and its quality

Early during the COVID-19 epidemic, a surprising amount of publicly accessible data on the severity became available quickly. This data was provided by national health authorities such as the Robert Koch-Institut (RKI) in Germany, and was also made available through aggregate data repositories, e.g. by the Johns Hopkins University Center for Systems Science and Engineering (JHU CSSE) (Dong, H. Du, and Gardner, 2020b). These data contain information about the number of cases and deaths reported each day and, depending on the data source, further information, e.g., the age, sex, or location of the case may be included.

The main type of data we use for the models in Chapter 4 consists of case and hospitalization data. In the following, we will present some peculiarities of these data, through descriptive statistics and explorative data analyses. Based on the findings in this section, the next section, Section 2.4 will derive desiderata for estimating the indicators introduced in Section 2.2.

Let us note that several other data could be of interest as well, depending on the epidemiological question at hand. Useful data include the DIVI-Intensivregister data monitoring the intensive care unit (ICU) occupancy and capacity in Germany as well as data on the number of tests and vaccines administered. In our later analyses, we will also make use of other, non-epidemiological, data, e.g. commuting data. As these are not directly related to the epidemic data, we present them separately in the respective sections.

To estimate reproduction numbers by Equation (2.3) we need to assume a generation time distribution. Here we use a trapezoidal shape with mean generation time $\bar{w} = 5.6$ days, used also in (Burgard et al., 2021). Its shape is motivated by the fact that primary cases take some days to become infectious themselves, i.e. the incubation period is several days. Additionally, we deem infection after 11 days unlikely, as symptomatic individuals are most likely quarantined or hospitalized after this time. We display this generation time distribution in Figure 2.1. Note that the generation time distribution varies across variants (Hart et al., 2022), and should thus be adapted in periods when newer variants become dominant. However, the main focus of this thesis lies in the estimation of growth factors, which are not affected by this, and so we stick to the generation time distribution given in Figure 2.1.

2.3.1 Incidence and death data

In this thesis, we focus on the data available for Germany, provided by the RKI available on Zenodo (Robert Koch-Institut, 2024c) or GitHub (Robert Koch-Institut, 2024d). In these repositories, the RKI publishes daily data on the number of cases in the aforementioned strata. On some days, data has not been published to Zenodo or GitHub, e.g. for May 31st, 2020. In this case, we use the data provided by the ard-data RKI-archive on GitHub (MichaelKreil and fossdd, 2022).

This data contains the following information for each case and death:

- the county (Landkreis) where the infectee is registered,

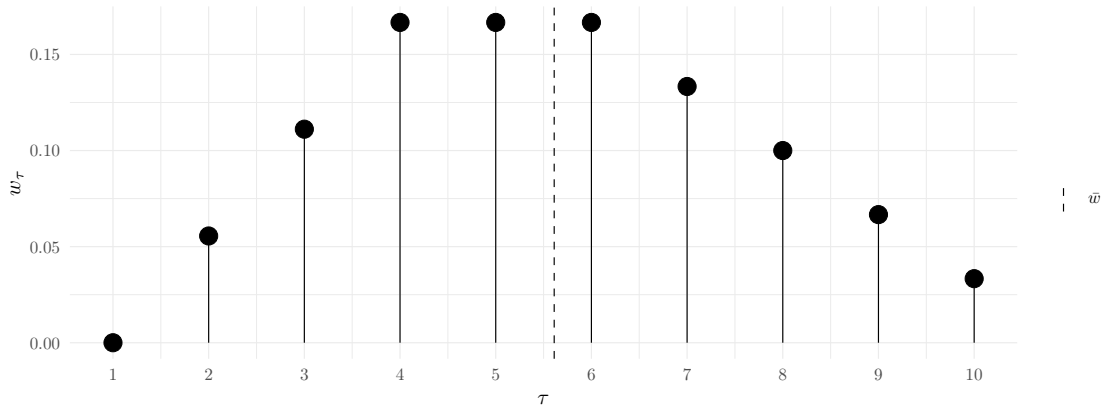

Figure 2.1: Generation time distribution used to estimate reproduction numbers throughout this thesis.

- sex (male, female or unknown), and age group (00-04, 05-14, 15-34, 35-59, 60-79, 80+, unknown),
- the dates of reporting (Meldedatum) and symptom onset (Refdatum), as well as
- meta-information on whether the case was already present in the past dataset.

The dates of reporting and symptom onset are of particular importance: the date of reporting is the date that the local health authorities became aware of the case, which may be several days after the symptom onset or infection date, but also several days before the RKI is aware of the case. Thus, there are several dates of interest, ordered roughly by occurrence:

- the date of infection,
- the date of symptom onset (if the case is symptomatic),
- the date of reporting to the local health authorities,
- the date of publication by the RKI and potentially,
- the date of death.

Exceptions to this order include the possibility that the date of death could occur before any, of the two reporting dates and symptom onset could begin after the first date of reporting, i.e. because testing is due to contact tracing.

The date of infection is generally unknown. While the date of symptom onset is close to the date of infection, unfortunately, it is only known for roughly 25% of the reported cases. Therefore, we restrict our analyses to the date of reporting. An Der Heiden and Hamouda (2020) use multiple imputation to address this problem; however, this method assumes that the symptom onset dates are missing completely at random, which is questionable as asymptomatic infections will produce no date of symptom onset. There can be considerable delay between the two reporting dates, as we will explore later, see, e.g., Figures 2.3 and 2.4.

We restrict ourselves to data available from April 1st, 2020. This dataset already includes cases with earlier reporting date. Additionally, we consider only data reported up to and including May 5th 2023, the date when the WHO declared COVID-19 no longer a global health emergency. Figure 2.2 shows the number of daily reported cases (**A**) and deaths (**B**) with a centered weekly running mean. Apparent from this figure is the considerable day-to-day variation, the so-called weekday effect. As the reporting date is tied to the working hours of the local health authorities, fewer cases are processed, and thus reported, on weekends and more during the week. The weekday effect is less pronounced for the symptom onset date, if it is known (figure not shown).

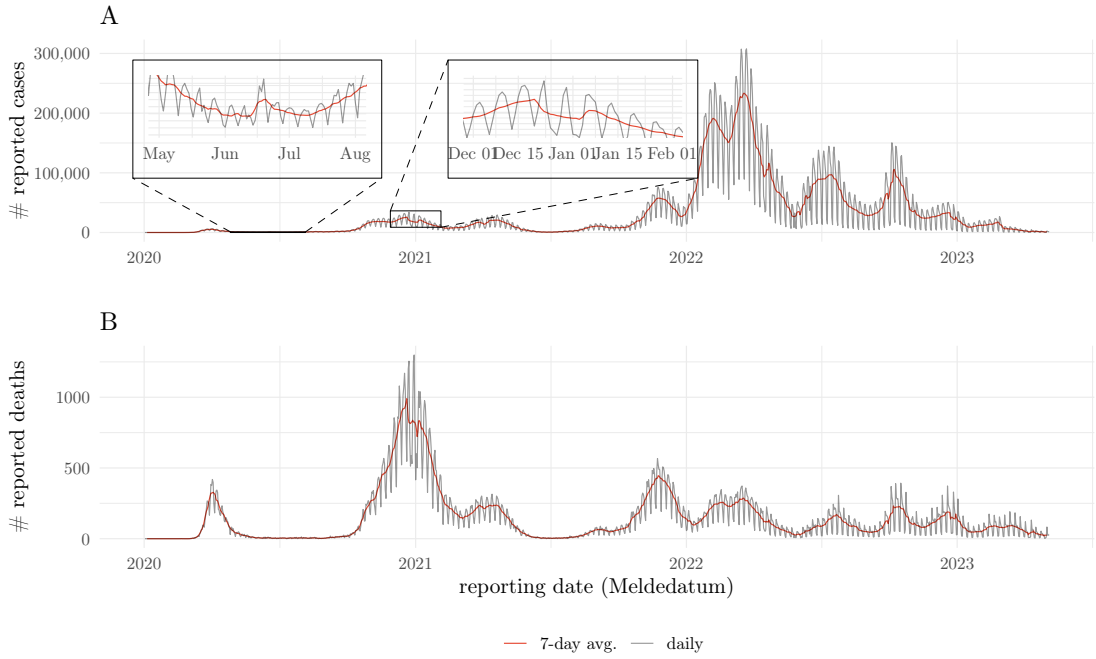

Figure 2.2: **A**: daily reported cases in Germany by reporting date, as well as a 7-day running average, to smoothen out the weekday effect. The first inset shows the impact that a local outbreak (T. Günther et al., 2020) has on country-wide case numbers, while the second inset shows under-reporting during the holiday season. **B**: the number of reported deaths in Germany for each reporting date, together with a 7-day running average.

We want to highlight two periods of irregularities during the early stage of the epidemic, magnified in Figure 2.2 **A**. The first concerns a local outbreak in a German meat processing plant (T. Günther et al., 2020). Over two weeks in early June 2020, 1 413 positive cases were reported for Gütersloh county. Due to the low number of reported cases everywhere else, this locally confined outbreak is visible even when aggregating over all counties in Germany. The second period concerns the Christmas holiday break, where we observe a sudden decline in reported cases, compensated by a large increase in cases in the second week of January. Due to the holiday leave, we'd expect this drop in cases to be related to fewer staff working at the local health authorities, rather than a true decrease in cases. Similar patterns are visible for Easter 2021 and Christmas 2021.

Due to late reporting and other reporting artifacts, the number of reported cases for any day s will, usually, increase over time. The RKI does not report incidences on the same day and so on any day $t > s$ we obtain incidences $I_{s,t}$ for day s. We say these cases are reported with delay $\tau = t - s > 0$. This results in the so-called reporting triangle, depicted for April 2020 in Figure 2.3 **A**.

To quantify the amount of reporting delay, we will focus on the number of newly reported cases on each day, i.e. we want to determine

$$I_{s,t} = \sum_{\tau=1}^{t-s} i_{s,\tau},$$

where $i_{s,\tau} \in \mathbf{N}_0$ is the number of newly reported cases for day s with delay τ, i.e. on day $t = s + \tau$. However, due to reporting artifacts, it may occur that $i_{s,\tau}$ is negative in some instances, e.g. because the reporting dates of cases have been misattributed. To deal with this issue, we set

$$\tilde{I}_{s,t} = \min\{\max\{I_{s,s+1}, \ldots, I_{s,t}\}, I_{s,T}\},$$

where T is the last date in our dataset, i.e. 13th October 2023. This running maximum, cut-off at

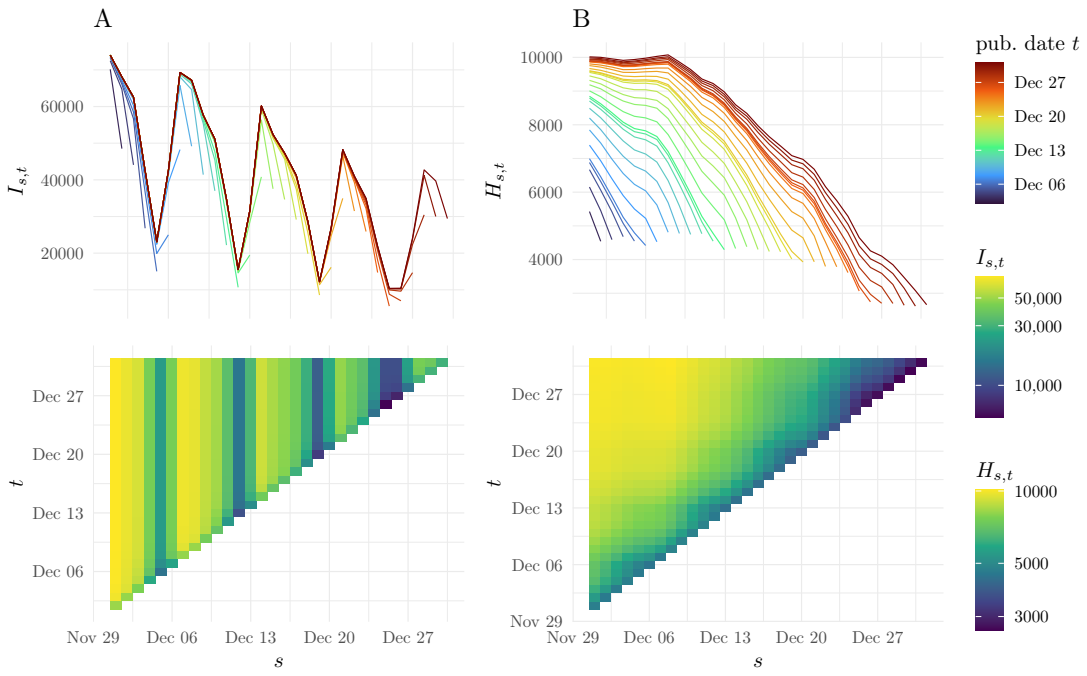

Figure 2.3: Cases (**A**) and hospitalizations (**B**) by publication date and time. The top figures show the number of reported cases $I_{s,t}$ / hospitalizations $H_{s,t}$ over time. Each line corresponds to a different publication date t, as indicated by color, while the x-axis denotes time s. The bottom figure shows the associated reporting triangles, i.e. $I_{s,t}$ for date s and publication date t, $t \geq s$. For **A**, notice that due to late reporting the number of reported cases stabilizes only after roughly 4 days. For **B**, hospitalizations are reported on a weekly basis. Notice that delays are much longer than those of cases, as it takes weeks to become hospitalized after infection.

the final value, ensures that we can write

$$\tilde{I}_{s,t} = \sum_{\tau=1}^{t-s} i_{s,\tau},$$

where $i_{s,\tau} \in \mathbf{N}_0$. Cutting off at $I_{s,T}$ ensures that if a large amount of cases is misattributed, we still treat the last reported value as the truth. Large positive relative differences $\frac{I_{s,t}-I_{s,T}}{I_{s,T}} > 0$, possibly due to such misattributions, are quite rare, with the 99.9% quantile of these positive relative differences still being only 16%.

From Figure 2.3 we get the impression that most reporting delays of cases are on the order of days rather than weeks, and indeed this is the case. For day s, let

$$p_{s,\tau} = \frac{i_{s,\tau}}{\sum_{\tau'=1}^{\infty} i_{s,s+\tau'}}$$

be the proportion of cases that are reported with delay $\tau \in \mathbf{N}$. The corresponding empirical survival function

$$\hat{S}_s(\tau) = 1 - \sum_{\tau' \leq \tau} p_{s,\tau'}$$

is the share of cases reported with at most τ days of delay. We compute $\hat{S}_s(\tau)$ for each day present in the dataset. Figure 2.4 **A** shows box plots of $\hat{S}_s(\tau)$ for each delay. We observe that the upper quartile of $\hat{S}_s(4)$ is already below 5%, while the upper quartile of $\hat{S}_s(10)$ is close to 1%.

Additionally, we estimate

$$\hat{S}_q(\tau) = \frac{\sum_{s \in q} i_{s,s+\tau}}{\sum_{s \in q, \tau' \geq 1} i_{s,s+\tau'}}$$

for each q of the 15 quarters present in our dataset separately, as the reporting behavior may have changed over time. Here $s \in q$ means that the day s lies in the quarter q. The results are shown in Figure 2.4 **B**, where we observe that for most quarters, 95% of the cases have been reported after 4 days delay and 99% of the cases have been reported after 8 days delay. Furthermore, we see that the amount of next-day ($\tau = 1$) reporting slightly increased in 2021 and 2022, compared to the beginning of the pandemic.

Reporting delays and artifacts are not the only obstacles we have to overcome when analyzing these data. By definition, the number of reported cases consists of cases with a positive PCR test. To compare reported incidences between two points in time, one has to assume that the so-called dark figure, i.e. the ratio of undetected to detected cases, is the same. However, there is are some objections to this assumption: the capacity and total number of PCR tests per week, as well as the ratio of positive tests, has been changing throughout the whole epidemic, see e.g. (Willrich et al., 2021). Additionally, the wide-spread availability of rapidtests, and the 2G (access to workplace and social gatherings only for vaccinated and recovered individuals) and 3G (like 2G, but also access with a negative test) NPIs introduced in fall 2021 likely changed the characteristics of those still getting PCR tests. Nevertheless, for short durations without such events we may still assume a

In summary, we see that handling case data turns out to be quite involved: we have to account for reporting artifacts, delays and keep in mind that the reported number of cases is not the same as the actual number of cases.

2.3.2 Hospitalization data

In addition to reported cases and deaths, starting April 2021 the RKI published the number of hospitalizations of reported COVID-19 cases each day on Zenodo (Robert Koch-Institut, 2024a) and GitHub (Robert Koch-Institut, 2024b). Similar to incident cases, weekly hospitalizations are reported by federal state and age group (00-04, 05-14, 15-34, 35-59, 60-79, 80+, and unknown; same as for cases). However, hospitalizations are not reported on the county level, and are only available as weekly rolling sums.

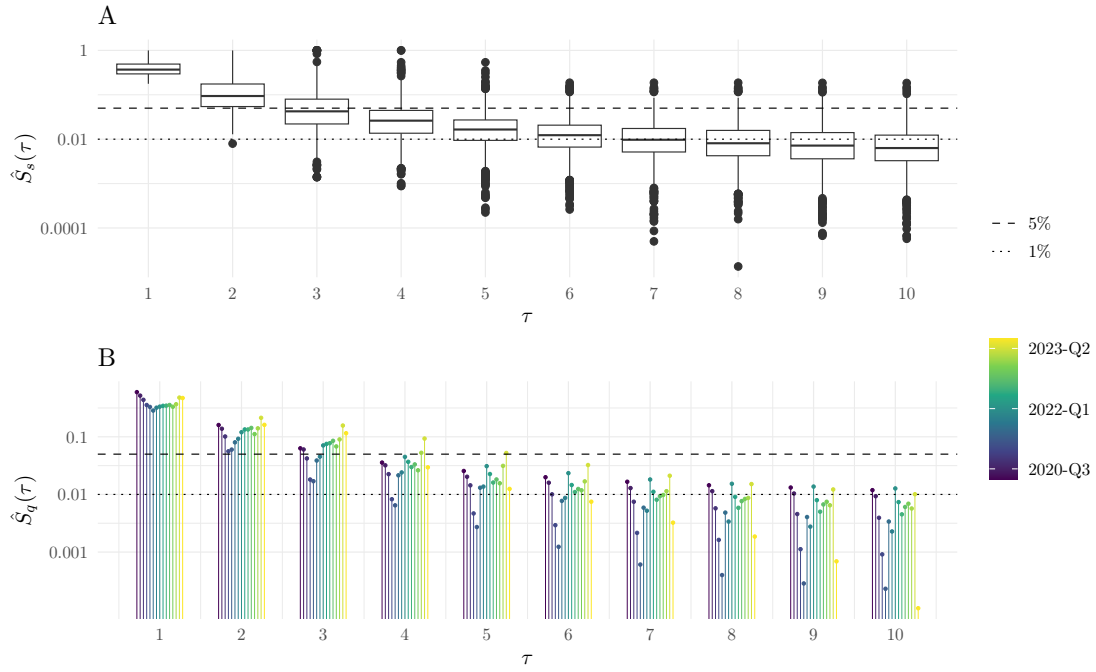

Figure 2.4: **A**: Box plots for the empirical survival function $\hat{S}_s(\tau)$ for all days s in the dataset, after 4 (10) days, the upper quartile of $\hat{S}_s$ is close to 5% (1%).**B**: Empirical survival function $\hat{S}(\tau)$ for every quarter present in the COVID-19 dataset. In most quarters 95% (99%) of the cases have been reported after 4 (8) days of delay.

In these data, the number of hospitalizations is linked to the date of reporting of the associated case, so the "true" value of the indicator for today, which will only be observed after a long delay, i.e. after the last hospitalization associated with today is reported. While this association requires a careful interpretation of the indicator (see Section 4.3) it was, besides case incidences and ICU occupancy, one of the main official indicators in Germany informing countermeasures in 2021.

The extent of delays is visible in the reporting triangle Figure 2.3 **B**: the reported number of hospitalizations on December 1st 2021 roughly doubled over the course of one month. By the aforementioned reporting scheme of hospitalizations, there are two reporting dates for a single hospitalized case: the reporting date of the case — the date when local health authorities were made aware of the positive test — and the reporting date of the hospitalization — the date when the hospitalization was reported to the RKI. This induces a double weekday effect in the reporting delays which we make visible in Figure 2.5. In this figure, we can observe that the increment $h_{s,\tau}$ — defined similarly to $i_{s,\tau}$ — exhibits a weekday effect for both fixed delay τ and fixed date of hospitalization $s + \tau$.

Hospitalizations are associated with the *reporting date of the corresponding case* and no information is available on the actual date of hospitalization. In addition, hospitalizations are published only as weekly sums over the past seven days. This means that the number of hospitalizations reported for today consists of all hospitalizations that correspond to cases with a *case reporting date* in the past seven days. In particular, if the case reporting date of a hospitalized case is today, the case will *not* count towards today's hospitalization count. The reporting date of hospitalization is not available in the dataset but can be inferred by comparing datasets from consecutive days.

We show the empirical survival function of hospitalizations for a fixed date in Figure 2.5 **C**, split by age groups. We observe that delays have long tails, with most cases reported after 12 weeks (84 days). After such a long delay between infection and hospitalization, it is unlikely that hospitalization is due to the original infection with COVID-19, and will disregard all longer delays in our analyses accordingly.

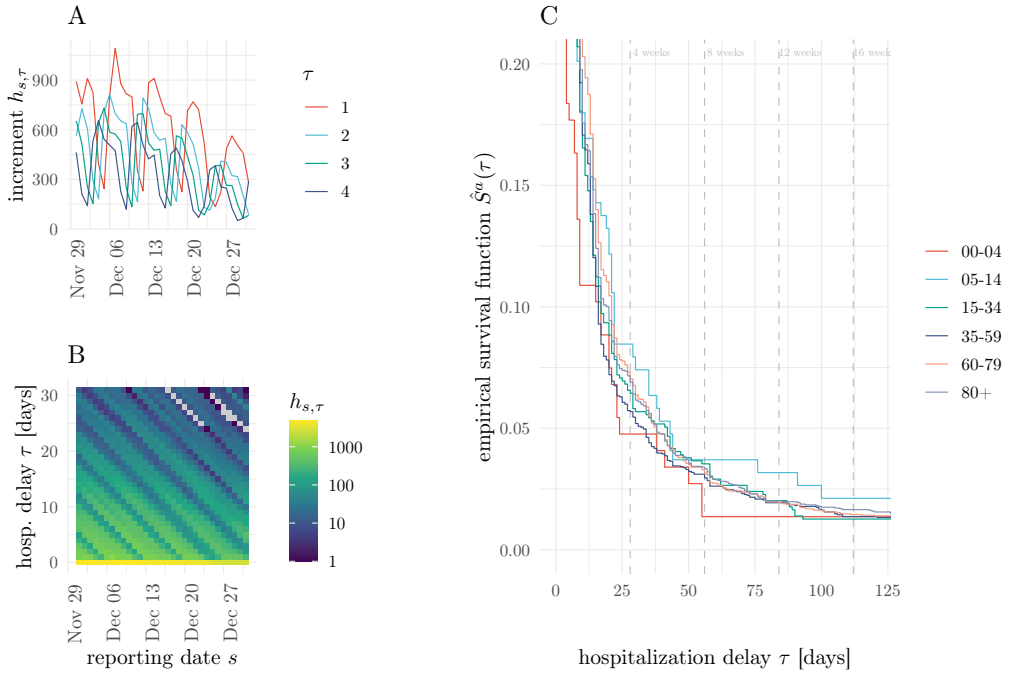

Figure 2.5: **A**: the newly reported hospitalizations on days s in December 2021, by delay τ. Notice the double weekday effect in both s and $s + \tau$.**B**: newly reported hospitalizations during December 2021. The double weekday effect is visible in the striped pattern. **C**: empirical survival function of hospitalization delays for cases with case reporting date December 1st 2021 with vertical dashed lines indicating four-week increments.

As is apparent from these data quality issues, the models we construct will have to account for, e.g. the weekday effect and reporting delays, to make sensible inferences about the true state of the epidemic.

2.4 Desiderata for epidemiological models

In what follows, we provide give a non-exhaustive list of requirements we have identified as important when modeling the COVID-19 epidemic. To begin, we present a naïve analysis of reproduction numbers and weekly growth factors for the German data to illustrate where this simple approach breaks down. This will be our starting point to motivate which effects to include in our modeling considerations.

For the reproduction number, we first estimate $\hat{R}$ by the moment estimator (2.3) using the raw incidences I_t for the whole of Germany and the generation time distribution from Figure 2.1. As these estimates are affected by the weekday effect present in the raw incidences, we repeat the estimation, now based on the seven-day averages $\frac{1}{7}\sum_{\tau=-3}^{3} I_{t-\tau}$, producing smoother estimates. Similarly, we estimate the weekly growth factor once by the raw incidences, $\hat{\rho}^7 = \frac{I_t}{I_{t-7}}$ and the smoothed estimate Equation (2.6).

The results of these procedures are displayed in Figure 2.6, and from this figure, we can deduce the shortcomings of this naïve analysis. When considering the estimates based on daily incidences, the weekday effect is very noticeable in the reproduction number estimates, which makes interpretation of these estimates on any given day difficult. The growth factor estimates are affected less, because the seven-day period coincides with that of the weekday effect. However, the growth factor estimates are prone to large variances in periods of few incidences, e.g. in the summer of 2020. All estimators are, naturally, susceptible to reporting artifacts, e.g. in the Christmas period already highlighted in

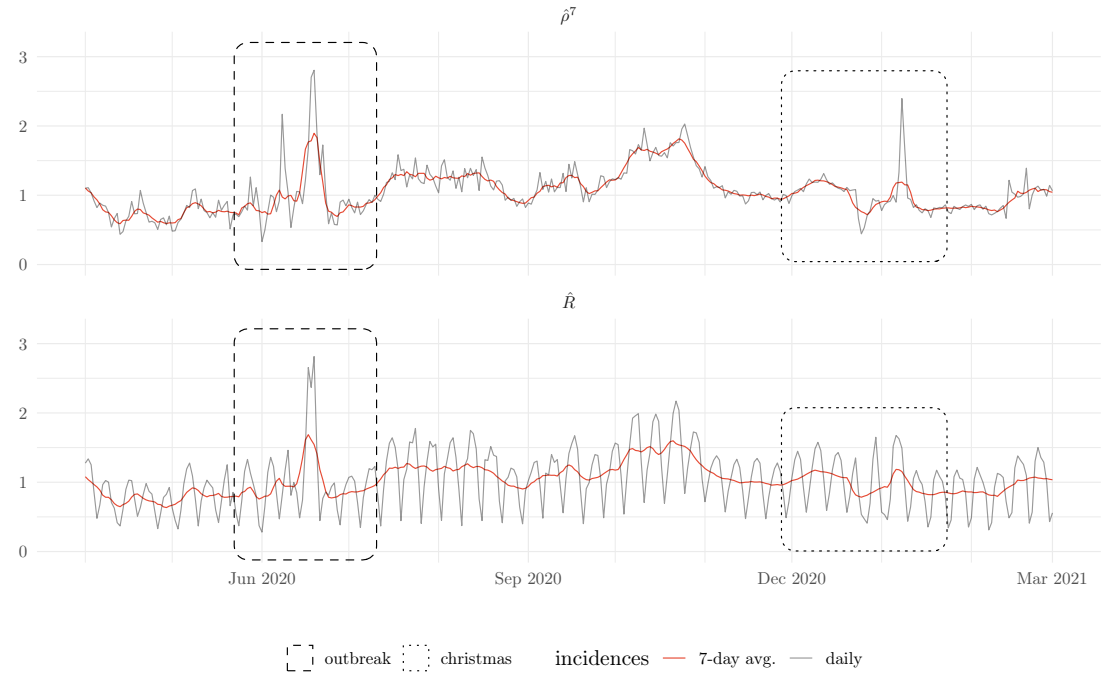

Figure 2.6: Naïve estimates of weekly growth factors $\hat{\rho}^7$ and reproduction numbers $\hat{R}$ from April 2020 to the end of March 2021. The estimates are based on daily (gray lines) and seven-day average (red line) cases.

Figure 2.2.

In addition, we want to draw the reader's attention to the local outbreak highlighted already in Figure 2.2. In this period, a large share of the country-wide cases were reported in a single, small, region, Gütersloh county. If we want to interpret the reproduction number and growth factor estimates as representing the speed of the epidemic at the country level, the estimates corresponding to these dates are exaggerated: we would not expect the number of cases, on the country level, to grow at the same speed as in this single county. Furthermore, the estimates in the weeks following the outbreak are unrealistically low, because the outbreak now contributes towards the denominator in the estimates of R and ρ.

More problems arise when we consider inferences based on these estimators. While confidence intervals for the reproduction numbers can be obtained by assuming a Poisson distribution, Equation (2.2), these confidence intervals apply only to the marginal distribution of a single estimate. Constructing joint confidence intervals for, e.g., the difference in reproduction numbers is not feasible, as the dependencies given by the renewal equation model, (2.2), are non-linear and non-Gaussian. While applying the estimators to the weekly average of cases does produce smoother estimates, it also introduces bias. Indeed, the renewal equation model is no longer valid for these incidences, as $\frac{1}{7}\sum_{\tau=-3}^{3} I_{t+\tau}$ is not independent of the past incidences $\frac{1}{7}\sum_{\tau=-3}^{3} I_{t-s+\tau}$ if $t - s < 7$.

Given these difficulties, we cannot expect precise inferences using such simple models. Instead, we will need to extend these models to account for some of the following phenomena, depending on the problem considered. For each of the phenomena we will provide a brief rationale on its importance and offer some ideas on how we could include them in our models.

regularization in time We would generally expect the day-to-day variation in contact, and thus infection, behavior to be small. Even if new NPIs are introduced, a mix of early and late adoption in different regions should lead to only small changes in R and ρ each day on the country level.

To achieve this smoothing, we may model the absolute or relative change in the indicators to be

locally linear or constant.

weekday effects Related to the previous point, weekday effects are a major obstacle in our way to obtain smooth estimates of R and ρ over time. These effects are due to the reporting process, where infections are more likely to be reported during the week than on the weekend.

While smoothing seems to remove weekday effects visually, the above analysis shows that for reproduction number estimation, smoothing is not suited to properly account for weekday variation in reporting. The reason for this is that the weekday effect can be thought of as the result of a discrete-time convolution of reported infections and a delay distribution that is different for each day of the week. Instead of smoothing, one should solve the inverse problem related to this convolution instead, i.e. perform a deconvolution.

reporting delays When data are subject to reporting delays, estimates of indicators will differ between data availability dates. Thus, the most recent estimates are biased downwards, i.e. for both the reproduction number and growth factor estimates the numerator is subject to more delay than the denominator, as the numerator relies on more recent data. Failing to account for reporting delays will thus give a false sense of security. Additionally, if one is interested in forecasts of future cases, these forecasts will in turn underpredict.

Assuming that reporting behavior is locally constant, we can deal with reporting delays, by estimating their distribution and using this estimate to correct the most recent reported cases, making sure to account for any uncertainties introduced.

reporting artifacts During periods of low attendance at the local health authorities, e.g. due to holiday breaks, fewer cases are reported. This is visible, e.g., during the Christmas break in 2020, see Figure 2.2. However, people are still infected and as such a backlog of unreported cases accumulates. Once the break is over, case numbers suddenly start to increase. As a result, the indicators we study first point towards declining, then increasing cases, stabilizing again after the backlog of late reported cases disappears from the denominators of $\hat{R}$ and $\hat{\rho}$.

To deal with this unsatisfactory behavior, we can mark the number of cases in the offending period as missing. This will allow the fitting procedure to rearrange cases in this period so as to best fit the data. If necessary, the total number of missing cases can be fixed at the true number of cases in that period, a linear constraint that is easily enforced.

regional variation The outbreak in Gütersloh county, June 2020, shows what can go wrong if we neglect regional variation of the spread of COVID-19. Similar to the effect of reporting artifacts, reproduction number and growth factor estimates are not representative during and shortly after the outbreak. Additionally, we would expect the spread of COVID-19 to be heterogeneous due to other factors as well: different regions possess different levels of immunity, be it by infection or vaccination, implement different NPIs and, arguably, exhibit different contact behavior: inhabitants of rural counties will probably commute to work by car, while inhabitants of larger cities use public transportation, exposing them to many more infectors. Furthermore, inhabitants can travel between different regions, so our models should include an exchange of infections as well.

Deterministically modeling different reproduction numbers / growth factors for each of the 400 counties in Germany will be a difficult task, as the number of cases within each region can be quite low, especially between waves, so uncertainty in estimates will be high. Instead, we will implement an idea from small-area estimation, modeling for each day the indicator in a region as random with common marginals. Similar to mixed effects models, this allows regions with few incidences to "borrow statistical strength" from regions with large incidences. For fixed time-points, we have already implemented such a model in (Burgard et al., 2021). Actually, restricting ourselves to the same marginals is not necessary, as we will see in Section 4.2.

exchange of cases between regions As infected individuals travel from their home region to another region — e.g. commuting to work or for leisure — cross-regional infections can occur, that is a transmission where the primary case is attributed to a region which is not the same as the region to which the secondary case is attributed to. Ignoring this exchange can lead to several problems:

- Epidemic indicators in the region of the primary case are underestimated, while they are overestimated in the region of the secondary case. While this is not a problem when the total number of exchanged cases is roughly equal between the two regions, there is no reason to assume that this is usually the case. The main reason for this is that the total number of currently infectious individuals varies from region to region. Additionally, regions vary in population size, and commuting between regions is not symmetric (see Section 4.2).
- When case numbers are low, there may be prolonged periods of time when there are no reported infections in a region, e.g. between the first and second wave in 2020. Solely modeling the epidemic in this region would imply an infinite rate of change, i.e. both the renewal equation Equation (2.1) and Equation (2.4) break down.

count data By definition, the number of infected or reported cases are count data. When case numbers are high, an appropriate central limit theorem suggests modeling these discrete data with a Gaussian distribution. However, when case numbers are low, no such central limit theorem is applicable, and we have to resort to discrete distributions, such as the Poisson distribution (motivated by the law of small numbers) or the Negative Binomial distribution (a Poisson-Gamma mixture). This is the case whenever we are interested in time periods with overall low incidence, or data on the regional level. In such models, analytical solutions are usually not available, and we have to resort to numerical methods, e.g. MC-integration, to derive quantities of interest.

In this chapter, we have set the stage for the remainder of this thesis: now that we have defined precisely what data we have at our hands and what epidemiological application requires, we turn our attention to the models that will allow us to meet many of the requirements.

Chapter 3

Importance Sampling in State Space Models

Contributions

The main contribution of this chapter consists of a rigorous comparison of two importance sampling frameworks: the Cross-Entropy method (CE-method) and Efficient Importance Sampling (EIS). Both methods determine optimal importance sampling proposals, but have, until now, been studied in separate communities: the CE-method is popular in rare-event estimation and engineering disciplines, while EIS is popular in the financial time series community.
The contributions of the individual sections are as follows:

Gaussian Linear State Space Models This section is loosely based on (Durbin and Koopman, 2012).

Partially Gaussian state space models This section is loosely based on (Brown, 1986; Durbin and Koopman, 2012).

Importance Sampling While the general treatment of importance sampling is based on (Chopin and Papaspiliopoulos, 2020; Durbin and Koopman, 2012), we contribute the following:

- We prove Lemma 3.5 and Corollary 3.1.
- Discussion surrounding Theorem 3.2, especially Example 3.2.
- The analysis of asymptotics of importance sampling methods, i.e. Propositions 3.3 and 3.4.
- The consistency and CLT results for the CE-method (Theorems 3.4 and 3.6) and EIS (Theorems 3.8 and 3.9).
- The discussion of assumptions required in the CLTs for practical applications.

Interim discussion The whole section is newly contributed.

Gaussian importance sampling for state space models

- The discussion surrounding the difficulties the CE-method faces when applied to the GLSSM proposal.
- The derivation of the CE-method for Markov-proposals (Theorem 3.12), resulting in Algorithm 7 and the optimized Algorithm 8.

Inference in PGSSMs This section is for the largest part based on literature, however the following points are new:

- The discussion of calculating the gradient, Equation (3.44), for the LA / EIS.
- We make the antithetic variable construction of (Durbin and Koopman, 1997) rigorous.
- Section 3.6.2 is a rigorous reformulation of (Durbin and Koopman, 2012, Section 11.5).

Comparison of the CE-method and EIS This whole section is a new contribution, extensively comparing the CE-method with EIS.

In the last chapter, we have detailed the need for models capable of modeling complex epidemiological phenomena. Crucially, we must account for the time-series and discrete nature of the data at hand. State space models (SSMs) form a versatile class of statistical models that allow modeling of non-stationary time series data while providing a straightforward, mechanistic interpretation of the time series' dynamics. The main idea of these models is to introduce unobserved **latent states** whose joint distribution is governed by a Markov process, and to model the observed time series conditional on these states. By exploiting this structure, inference in SSMs becomes computationally efficient, as the complexity of algorithms is linear in the number n of time points considered. In this chapter, we provide a mathematical introduction to the theory of SSMs and the main tool we will use for inference: importance sampling. The foundations of SSMs presented in this chapter are, if not mentioned otherwise, based on (Chopin and Papaspiliopoulos, 2020; Durbin and Koopman, 2012).

Let us start from a very general definition of a SSM.

Definition 3.1 (State Space Model)**.** A **state space model** is a discrete time stochastic process $(X_t, Y_t)_{t=0,\dots,n}$ taking values in the measurable space $(\mathcal{X} \times \mathcal{Y}, \mathcal{B}_\mathcal{X} \otimes \mathcal{B}_\mathcal{Y})$ such that

(i) The marginal distribution of the **states** $(X_0, \dots, X_n)$ is a discrete time Markov process, i.e. for $t = 1, \dots, n$

$$\mathbf{P}\left(X_t \in B | X_0, \dots, X_{t-1}\right) = \mathbf{P}\left(X_t \in B | X_{t-1}\right) \text{ a.s.} \tag{3.1}$$

for all measurable $B \in \mathcal{B}_\mathcal{X}$.

(ii) Conditional on the state X_t and observation Y_{t-1}, Y_t is independent of X_s and Y_{s-1}, $s < t$, i.e.

$$\mathbf{P}\left(Y_t \in B | X_0, \dots, X_t, Y_0, \dots, Y_{t-1}\right) = \mathbf{P}\left(Y_t \in B | X_t, Y_{t-1}\right)$$

for all measurable $B \in \mathcal{B}_\mathcal{Y}$.

For notational convenience, we will write $X_{s:t} = (X_s, \dots, X_t)$ for the vector that contains all states from s to t, $s \leq t$, dropping the first index if we consider the whole set of observations up to time t, so $X_{:t} = X_{0:t}$, and dropping the subscript if we consider all states at once, $X = X_{:n}$. Similarly we set $Y_{s:t} = (Y_s, \dots, Y_t)$, $Y_{:t} = Y_{0:t}$ and $Y = Y_{:n}$.

The models that we consider in this thesis will usually assume that densities for the state transitions with respect to a common dominating measure $\mu_\mathcal{X}$ and similar for the observations with respect to some dominating measure $\mu_\mathcal{Y}$.

Notation 3.1 (Densities, conditional densities)**.** We will use the standard abuse of notation for densities that makes the type of density "obvious" from the arguments used. This means that $p(x)$ is the density for all states X, evaluated at x, $p(x_t|x_{t-1})$ the conditional density of $X_t|X_{t-1}$, evaluated at x_t and x_{t-1} and similarly for observations: $p(y|x)$ is the density of the conditional distribution of all observations Y conditioned on all states X, evaluated at y and x.

Note that this notation also implicitly includes the time t and allows for changes in, e.g., the state transition over time.

When densities come from a parametric model parametrized by $\theta \in \Theta \subseteq \mathbf{R}^l$ and the dependence of the model on θ is of interest, i.e. because we try to estimate θ, we indicate this by adding a subscript to the densities. If this dependence is not of interest, e.g. because θ is fixed, we omit θ for better readability.

In this notation, the joint density of a parametric SSM factorizes as

$$\begin{aligned} p_\theta(x, y) &= p_\theta(x_0, \dots, x_n, y_0, \dots, y_n) \\ &= p_\theta(x_0) \prod_{t=1}^{n} p_\theta(x_t|x_{t-1}) \prod_{t=0}^{n} p_\theta(y_t|x_t, y_{t-1}), \end{aligned} \tag{3.2}$$

where $p_\theta(y_0|x_0, y_{-1}) = p_\theta(y_0|x_0)$.

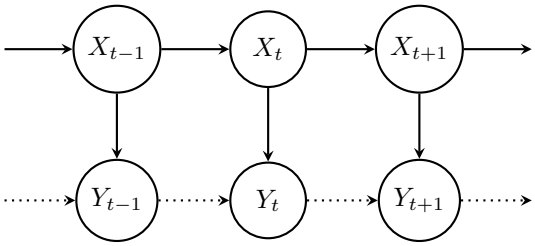

Figure 3.1: Dependency structure in a SSM as given by Definition 3.1. The dependencies between observations Y_{t-1} (indicated by dotted arrows) are usually not part of the standard definition of a SSM, but can be incorporated in a straightforward manner.

As inferences made in this thesis depend on the SSM only through the likelihood we identify almost sure versions of (X, Y) with themselves, i.e. all equations involving X or Y are understood almost surely.

Remark 3.1 (dependence on Y_{t-1}, dimensions)**.** Contrary to the standard definition of a SSM, as found in, e.g., (Chopin and Papaspiliopoulos, 2020, Chapter 2) or (Durbin and Koopman, 2012, Chapter 9), our Definition 3.1 allows Y_t to depend on Y_{t-1}. As the models considered in Chapter 4 will make extensive use of SSMs with this dependency structure we opt to use this non-standard definition here. This is of course not a limitation of the standard definition: given a SSM of the form described in Definition 3.1, we can transform it to the standard form by choosing states $(X_t, Y_t) \in \mathcal{X} \times \mathcal{Y}$ and observations $Y_t \in \mathcal{Y}$ such that the SSM becomes a stochastic process on $(\mathcal{X} \times \mathcal{Y}) \times \mathcal{Y}$.

Additionally, the goal of our inferences will always be functionals of the conditional distribution $X|Y$ for a single, fixed, set of observations y. Assuming all densities exist, the conditional density $p(x|y)$ is given, up to a constant not depending on x, by Equation (3.2):

$$p(x|y) \propto p(x, y) = p(x_0) \prod_{t=1}^{n} p(x_t|x_{t-1}) \prod_{t=0}^{n} p(y_t|x_t, y_{t-1}).$$

Thus, the dependence of Y_t on Y_{t-1} only affects our inferences through $p(y_t|x_t, y_{t-1})$, where, as Y_{t-1} is observed, the argument y_{t-1} is fixed. Consequently, all results we present in this chapter for SSMs where Y_t depends only on X_t that concern only the conditional distribution $X|Y = y$ carry over to those given by Definition 3.1. We will reiterate this argument at appropriate points in this thesis.

In most SSMs we consider in this thesis we use $\mathcal{X} = \mathbf{R}^m$ and $\mathcal{Y} = \mathbf{R}^p$ or $\mathcal{Y} = \mathbf{Z}^p$ so that $\mathcal{X}$ is m dimensional and $\mathcal{Y}$ is p dimensional and equip these spaces with the usual σ-Algebras. Unless noted otherwise, we use for $\mu_{\mathcal{X}}$ the m-dimensional Lebesgue measure and for $\mu_{\mathcal{Y}}$ either the p-dimensional Lebesgue measure ($\mathcal{Y} = \mathbf{R}^p$) or the p-dimensional counting measure ($\mathcal{Y} = \mathbf{Z}^p$).

Given data $y = (y_t)_{t=0,\dots,n}$ that may be modeled with a SSM the practitioner is confronted with several tasks, which provide the structure of this chapter:

(i) Choosing a suitable, usually parametric, class of SSMs that include the effects of interest.

(ii) Fitting such a parametric model to the data at hand by either frequentist or Bayesian techniques.

(iii) Infer the latent states X from the observations by determining, either analytically or through simulation, the smoothing distribution $X|Y$.

The first step, Item (i), requires that the practitioner specifies a joint probability distribution for the states and observations (see Chapter 4 for examples of this). Due to the assumed dependency structure, this boils down to specifying transition kernels for the states and observations. The setting given in Definition 3.1 is too abstract to perform inference in, so further assumptions on the types of distributions for the latent states and observations are needed. In this chapter, we

will discuss Gaussian linear state space model (GLSSM) (Section 3.1), where both the posterior distribution and the likelihood can be derived analytically. For the epidemiological application we have in mind, these are, however, insufficient due to the non-linear behavior of incidences and the low count per region (Section 2.4). Such observations are better modeled with distributions on the natural numbers, i.e. with a Poisson or negative binomial distribution, both of which are exponential families of distributions. This will lead to the class of Partially Gaussian state space models (PGSSMs) (Section 3.2) which will become the main focus of our study.

Regarding the second step, Item (ii), a frequentist practitioner will want to perform maximum likelihood inference on θ. While asymptotic confidence intervals for the maximum likelihood estimator (MLE) $\hat{\theta}$ can be derived both theoretically and practically (Durbin and Koopman, 2012, Chapter 7), they are, in the context of this thesis, usually of little interest. For these asymptotic frequentist procedures to be meaningful, an appropriate central limit theorem must hold. However, as the time series we study are non-stationary and the dependence on parameters θ is allowed to be arbitrary, it is in general not obvious that such a theorem holds for the model under consideration. Instead, we approach this fitting as an Empirical Bayes procedure and our main practical interest lies in analyzing the posterior distribution $X|Y$ where we set θ equal to $\hat{\theta}$.

To obtain the maximum likelihood estimates $\hat{\theta}$ one needs access to the likelihood

$$p_\theta(y) = \int_{\mathcal{X}^n} p_\theta(x, y)\,\mathrm{d}x = \int_{\mathcal{X}^n} p_\theta(y|x)p_\theta(x)\,\mathrm{d}x \tag{3.3}$$

which is usually not analytically available. Direct numerical evaluation of Equation (3.3) is hopeless due to the high dimensionality of the state space $\mathcal{X}^n$. Instead, we will resort to simulation-based inference by importance sampling (see Section 3.3), a Monte-Carlo method that approximates $p(y)$ by constructing a global tractable approximation to the integrand in Equation (3.3). Alternatively, sequential Monte Carlo (SMC) methods, i.e. particle filters, that perform importance sampling sequentially across the $n+1$ time steps can be used. We will not follow this approach for reasons described later, but refer the reader to the excellent reference (Chopin and Papaspiliopoulos, 2020) for an introduction to these methods.

The performance of these simulations depends crucially on our ability to construct distributions that are close to the posterior $p(x|y)$ but are easy to sample from. To this end, we construct either Gaussian linear state space models (GLSSMs) (Section 3.5.1) in which sampling from the posterior is analytically possible, or Gaussian Markov processes (Section 3.5.2) which are directly amenable to simulation. These two approaches are motivated by what we term "optimal importance sampling", where we use a proposal distribution that solves an optimization problem. Two popular approaches for choosing such a proposal are Efficient Importance Sampling and the Cross-Entropy method, which minimize an L^2 or KL-divergence loss, respectively. Empirically, it has been shown that EIS outperforms the CE-method, to which we add theoretical insight in the form of two central limit theorems (Section 3.3): As both methods rely on importance sampling to determine an optimal proposal, the asymptotic variance of this procedure is of practical relevance, and we argue that this asymptotic variance is likely smaller for EIS. To this end, we provide extensive simulation studies investigating the asymptotic variance of the two methods in Section 3.7. To the best of the authors' knowledge, this is the first rigorous investigation comparing these two methods.

As an alternative to the MLE approach, a fully Bayesian approach would regard θ as random and administer a prior distribution, say with density $p(\theta)$. In this setting, the main interest still lies in determining the posterior distribution of $X|Y = y$, but due to the prior put on θ, its density, should it exist, is now given by

$$p(x|y) = \int p(x, \theta|y)\,\mathrm{d}\theta,$$

where $p(x, \theta|y)$ is the joint posterior of states and hyperparameters, conditional on observations y. To tackle this problem, one may again use importance sampling methods, see e.g. (Durbin and Koopman, 2012, Chapter 13.1), or use MCMC-methods tailored to SSMs, e.g. Particle-MCMC (Chopin and Papaspiliopoulos, 2020, Chapter 16) — however this approach is outside the scope of this thesis.

To perform the above tasks, the setting defined in Definition 3.1 is too general to have numerically tractable solutions, as such we restrict our studies to more structured SSMs. We begin with assuming a joint Gaussian distribution for states and observations. Subsequently, we will relax this assumption to allow the observations Y to have more general distributions.

3.1 Gaussian Linear State Space Models

Gaussian linear state space models (GLSSMs) are the working horses of most methods used in this thesis because many of the interesting quantities, e.g. the smoothing distribution, are analytically tractable and can be obtained computationally efficient. Indeed, for fixed dimension of states m and observations p the runtime of algorithms that we consider in this thesis is $\mathcal{O}(n)$, i.e. linear in the number of time points observed.

Definition 3.2 (GLSSM)**.** A Gaussian linear state space model (GLSSM) is a joint distribution over states and observations (X, Y) where states a.s. obey the transition equation

$$X_{t+1} = A_t X_t + u_t + \varepsilon_{t+1} \qquad t = 0, \dots, n-1, \tag{3.4}$$

and observations a.s. obey the observation equation

$$Y_t = B_t X_t + v_t + \eta_t \qquad t = 0, \dots, n. \tag{3.5}$$

Here $A_t \in \mathbf{R}^{m \times m}$ and $B_t \in \mathbf{R}^{p \times m}$ are matrices that specify the systems dynamics. The **innovations** $(\varepsilon_{t+1})_{t=0,\dots,n-1}$ and **measurement noise** $(\eta_t)_{t=0,\dots,n}$ and the starting value $X_0 \sim \mathcal{N}(\mathbb{E}X_0, \Sigma_0)$ are jointly independent. Furthermore, $\varepsilon_{t+1} \sim \mathcal{N}(0, \Sigma_t)$ and $\eta_t \sim \mathcal{N}(0, \Omega_t)$ are centered Gaussian random variables and $u_t \in \mathbf{R}^m, t = 0, \dots, n-1$, $v_t \in \mathbf{R}^p, t = 0, \dots, n$ are deterministic biases.

Remark 3.2. From Equation (3.4) it is easy to see that the states $X = (X_0, \dots, X_n)$ form a Gaussian Markov process and that conditional on X_t, $t \in \{0, \dots, n\}$, Y_t is independent of X_s and Y_s, $s < t$. Thus a GLSSM is indeed a SSM.

The defining feature of a GLSSM is that the joint distribution of (X, Y) is Gaussian, as (X, Y) may be written as an affine combination of the jointly Gaussian $(X_0, \varepsilon_1, \dots, \varepsilon_n, \eta_0, \dots, \eta_n)$ and it is often useful to perform inferences in terms of innovations and measurement noise instead of states, see e.g. (Durbin and Koopman, 2012, Section 4.5).

As the joint distribution of (X, Y) is Gaussian, so are conditional distributions of states given any set of observations.

Lemma 3.1 (Gaussian conditional distributions)**.** *Let (X, Y) be jointly Gaussian with distribution $\mathcal{N}(\mu, \Sigma)$ where*

$$\mu = (\mu_X, \mu_Y)$$

and

$$\Sigma = \begin{pmatrix} \Sigma_{XX} & \Sigma_{XY} \\ \Sigma_{YX} & \Sigma_{YY} \end{pmatrix},$$

where μ and Σ are partitioned according to the dimensions of X and Y.

Then the following holds:

(i) If Σ_{YY} is non-singular, $X|Y = y$ follows a Gaussian distribution with conditional expectation

$$\mu_{X|Y=y} = \mathbb{E}(X|Y = y) = \mu_X + \Sigma_{XY}\Sigma_{YY}^{-1}(y - \mu_Y)$$

and conditional covariance matrix

$$\Sigma_{X|Y=y} = \mathrm{Cov}(X|Y = y) = \Sigma_{XX} - \Sigma_{XY}\Sigma_{YY}^{-1}\Sigma_{YX}.$$

(ii) In particular, let $X \sim \mathcal{N}(\mu, \Sigma)$ and $Y = BX + \varepsilon$ for a matrix $B \in \mathbf{R}^{p \times m}$ and $\mathbf{R}^p \ni \varepsilon \sim \mathcal{N}(0, \Omega)$ independent of X where $\Omega \in \mathbf{R}^{p \times p}$. Then, as $\mathbb{E}Y = B\mu$, $\mathrm{Cov}(X, Y) = \mathrm{Cov}(Y, X)^T = \Sigma B^T$ and $\mathrm{Cov}(Y) = B\Sigma B^T + \Omega$, we have

$$\mathbb{E}(X|Y = y) = \mu + K(y - B\mu)$$

and

$$\operatorname{Cov}(X|Y=y) = \Sigma - K\Sigma K^T = (I - KB)\,\Sigma,$$

as long as $B\Sigma B^T + \Omega$ *is non-singular. Here* $K = \Sigma B^T \left(B\Sigma B^T + \Omega\right)^{-1}$.

(iii) If Σ_{XX} *is non-singular, then* $Y - BX$ *is independent of* X *for* $B = \Sigma_{YX}\Sigma_{XX}^{-1}$ *and we may write*

$$Y = BX + v + \eta$$

for an $\eta \sim \mathcal{N}(0, \Omega)$ *with covariance matrix* $\Omega = \Sigma_{YY} - \Sigma_{YX}\Sigma_{XX}^{-1}\Sigma_{XY}$ *independent of* X*, and deterministic* $v = \mu_Y - B\mu_X$.

(iv) Suppose that (X, Y, Z) *is jointly Gaussian with mean* μ *and covariance matrix* Σ*, partitioned similarly as before. If the conditional distribution of* X *given* $Y = y$ *and* $Z = z$ *is given by*

$$X|Y = y, Z = z \sim \mathcal{N}(Ky + Gz + v, \Xi),$$

then the conditional distribution of X *given only* $Y = y$ *is*

$$X|Y = y \sim \mathcal{N}\left(Ky + G\mu_{Z|Y=y} + v, \Xi + G\operatorname{Cov}(Z|Y)G^T\right).$$

Remark 3.3 (generalized inverse)**.** If Σ_{YY} in Lemma 3.1 (i) is singular, the statement remains true if we choose as Σ_{YY}^{-1} a generalized inverse of Σ_{YY}, see (Rao, 2002, 8.a Note 3). A generalized inverse for a matrix $A \in \mathbf{R}^{m\times p}$ is any matrix $A^- \in \mathbf{R}^{m\times p}$ such that $AA^-A = A$. Given a singular value decomposition $A = UDV^T$, we may obtain the Moore-Penrose inverse $A^\dagger = VD^-U^T$ of A, which is a generalized inverse of A, by inverting the non-zero diagonal elements of D, i.e.

$$D^-_{i,i} = \begin{cases} \frac{1}{D_{i,i}} & \text{if } D_{i,i} \neq 0 \\ 0 & \text{else} \end{cases}$$

for all $i = 1, \ldots, \min(m, p)$.

Proof. For the first statement, we refer the reader to (Durbin and Koopman, 2012, Chapter 4, Lemma 1).

The second statement follows from substituting the value of K.

The third statement follows from noting that $Y - BX = \begin{pmatrix} -B & I \end{pmatrix}\begin{pmatrix} X \\ Y \end{pmatrix}$ follows a Gaussian distribution. A quick calculation reveals that

$$\operatorname{Cov}(Y - BX, X) = \Sigma_{YX} - B\Sigma_{XX} = \Sigma_{YX} - \Sigma_{YX} = 0,$$

showing the independence. Thus $\eta = Y - BX - v$ follows a centered Gaussian distribution and equating covariance matrices, we see that Ω has the desired form.

For the final statement, notice that $\xi = X - KY - GZ - v$ fulfills

$$\xi|Y = y, Z = z \sim \mathcal{N}(0, \Xi)$$

which does not depend on y or z. Thus the unconditional distribution of ξ is $\mathcal{N}(0, \Xi)$ as well, and ξ is independent of (Y, Z). Rewriting X in terms of Y, Z and ξ, we obtain

$$X = KY + GZ + v + \xi,$$

and so

$$\mathbb{E}(X|Y = y) = Ky + G\mathbb{E}(Z|Y = y) + v,$$

as well as

$$\begin{aligned}\operatorname{Cov}(X|Y=y) &= \operatorname{Cov}(KY+GZ+v+\xi|Y=y)\\ &= \operatorname{Cov}(GZ+\xi|Y=y)\\ &= \operatorname{Cov}(GZ+\xi) - \operatorname{Cov}(GZ+\xi,Y)\Sigma_{YY}^{-1}\operatorname{Cov}(Y,GZ+\varepsilon)\\ &= G\Sigma_{ZZ}G^T + \Xi - G\Sigma_{ZY}\Sigma_{YY}^{-1}\Sigma_{YZ}G^T\\ &= \Xi + G\operatorname{Cov}(Z|Y)G^T.\end{aligned}$$

□

After having observed $Y=y$, our main interest lies in the conditional distribution of states X given $Y=y$, which we could obtain by applying Lemma 3.1, i.e. where $B=\text{block-diag}(B_0,\dots,B_n)$ and $\Omega=\text{block-diag}(\Omega_0,\dots,\Omega_n)$ are block-diagonal matrices. However, this would require inversion of the $(n+1)p\times(n+1)p$ matrix $(B\Sigma B+\Omega)$ which becomes numerical infeasible quickly. Instead, we can exploit the sequential structure of the GLSSM, which will allow us to perform conditioning on only a single observation at a time.

To this end, let us denote by $\hat{X}_{t|s}=\mathbb{E}(X_t|Y_{:s}=y_{:s})$ the conditional expectation of X_t given a set of observations $y_{:s}$ and by $\Xi_{t|s}=\operatorname{Cov}(X_t|Y_{:s}=y_{:s})$ the conditional covariance matrix of X_t given $Y_{:s}=y_{:s}$. Then

$$X_t|Y_{:s}=y_{:s}\sim\mathcal{N}\left(\hat{X}_{t|s},\Xi_{t|s}\right).$$

For a given t, three values of s are of particular interest: If $s=t-1$ determining this conditional distribution is called a **prediction problem**, if $s=t$ this is a **filtering problem** and if $s=n$ a **smoothing problem**, and we call the distributions we seek the **predictive, filtering** or **smoothing distribution** respectively. Similarly we define $\hat{Y}_{t|s}=\mathbb{E}(Y_t|Y_{:s}=y_{:s})$ to be the conditional expectation of Y_t given $Y_{:s}=y_{:s}$, note that $\hat{Y}_{t|s}=Y_t$ if $s\geq t$. Finally, let $\Psi_{t|s}=\operatorname{Cov}(Y_t|Y_{:s}=y_{:s})$ be the conditional covariance matrix of Y_t given $Y_{:s}=y_{:s}$. Again $\Psi_{t|s}=0$ if $s\geq t$.

These distributions may be obtained efficiently using the celebrated Kalman filter (Algorithm 1) and smoother (Algorithm 2) algorithms, which we state here for completeness.

Algorithm 1 Kalman filter, with runtime $\mathcal{O}(n(m^2+p^3))$

Require: GLSSM (Definition 3.2), observations $y_0,\dots,y_n$.

$A_{-1}\leftarrow I\in\mathbf{R}^{m\times m}$ ▷ Identity Matrix
$u_{-1}\leftarrow\mathbf{0}\in\mathbf{R}^m$
$\hat{X}_{-1|-1}\leftarrow\mathbb{E}X_0$
$\Xi_{0|-1}\leftarrow\mathbf{0}_{m\times m}$
$\ell_{-1}\leftarrow 0$
for $t\leftarrow 0,\dots,n$ **do**
  $\hat{X}_{t|t-1}\leftarrow A_{t-1}\hat{X}_{t-1|t-1}+u_{t-1}$ ▷ prediction
  $\Xi_{t|t-1}\leftarrow A_{t-1}\Xi_{t-1|t-1}A_{t-1}^T+\Sigma_t$
  $\hat{Y}_{t|t-1}\leftarrow B_t\hat{X}_{t|t-1}+v_t$
  $\Psi_{t|t-1}\leftarrow B_t\Xi_{t|t-1}B_t^T+\Omega_t$
  $K_t\leftarrow\Xi_{t|t-1}B_t^T\Psi_{t|t-1}^{-1}$ ▷ filtering
  $\hat{X}_{t|t}\leftarrow\hat{X}_{t|t-1}+K_t(y_t-\hat{Y}_{t|t-1})$
  $\Xi_{t|t}\leftarrow\Xi_{t|t-1}-K_t\Psi_{t|t-1}K_t^T$
  $\ell_t\leftarrow\ell_{t-1}+\frac{p}{2}\log(2\pi)+\frac{1}{2}\log\det\Psi_{t|t-1}+\frac{1}{2}\left(y_t-\hat{Y}_{t|t-1}\right)^T\Psi_{t|t-1}^{-1}\left(y_t-\hat{Y}_{t|t-1}\right)$ ▷ NLL
end for

In Algorithm 1 every time point $t=0,\dots,n$ is processed in the same way, with a two-step procedure: first we predict the new observation Y_t based on $Y_{:t-1}$. Using the linearity of the system as well as the assumed conditional independence, this is achieved by applying the system dynamics to the current conditional expectation and covariance matrices. After Y_t has been observed, we can update

the conditional distribution of the states by appealing to Lemma 3.1. For a rigorous derivation of the Kalman filter, we refer the reader to (Durbin and Koopman, 2012, Chapter 4) or the excellent monograph of (Schneider, 1986).

The Kalman filter is very efficient: each loop iteration requires inversion of the $p \times p$ matrix $\Psi_{t|t-1}$. Assuming this operation dominates the time complexity, e.g. because $m \approx p$, the time complexity of the Kalman filter is $\mathcal{O}(n\, p^3)$, a drastic improvement over the naïve $\mathcal{O}(n^3\, m^3)$, obtained by applying Lemma 3.1 to the joint distribution of (X, Y). Similarly, the space complexity of Algorithm 1 is $\mathcal{O}\left(n\left(m^2 + p^2\right)\right)$, and grows only linearly in n.

Notice that the Kalman filter iteratively calculates the negative log-likelihood ℓ_t

$$\ell_t = -\log p(y_{:t}) = -\log \sum_{s=0}^{t} \log p(y_s | y_{:(s-1)})$$

while filtering. This is possible because of the dependency structure of the GLSSM, which makes the increments in ℓ_t tractable, as

$$Y_s | Y_{:(s-1)} \sim \mathcal{N}\left(\hat{Y}_{s|s-1}, \Psi_{s|s-1}\right),$$

for $s = 0, \ldots, n$, which is shown in the derivation of the Kalman filter. Thus, the Kalman filter enables us to perform MLE by giving us access to ℓ_n.

From this discussion we can see how we may alter the Kalman filter to accommodate a similar dependency structure as proposed in Definition 3.1 (depicted in Figure 3.1): If we allow to have

$$Y_t = B_t X_t + C_{t-1} Y_{t-1} + \eta_t \qquad\qquad t = 0, \ldots, n$$

we would still be able to perform the filtering step of Algorithm 1 by determining the conditional distribution of Y_t given $Y_{:(t-1)}$ using Lemma 3.1 — .

Depending on the situation at hand, one of the many variants of the basic algorithm presented in Algorithm 1 may be used. If the inversion of $\Psi_{t|t-1}$ is numerically unstable, the filtered covariance matrices $\Xi_{t|t}$ may become numerically non-positive definite. In this case, the square root filter and smoother (Morf and Kailath, 1975) may be used. It is based on Cholesky roots of the involved covariance matrices, ensuring them to be PSD.

When the dimension of observations is much larger than that of the states, $p \gg m$, the information filter (D. Fraser and Potter, 1969) can be used. Instead of performing operations on the covariance matrices, i.e. $\Xi_{t|t-1}$ and $\Psi_{t|t-1}$, the information filter operates on their inverses, the precision matrices $\Xi^{-1}_{t|t-1}$ and $\Psi^{-1}_{t|t-1}$ as well as rescaled states $\Xi^{-1}_{t|t-1}\hat{X}_{t|t-1}$ and observation $\Psi^{-1}_{t|t-1}\hat{Y}_{t|t-1}$ estimates. This makes the filtering step more efficient, as the most intensive step is the calculation of $\Psi^{-1}_{t|t-1}$. However, the price one pays is that the prediction step now requires inversion of a $m \times m$ matrix, and as such the computational gains only manifest when p is sufficiently large compared to m (Assimakis, Adam, and Douladiris, 2012).

If the dimensions of the model are so large that calculating the $m \times m$ and $p \times p$ covariance matrices becomes an issue, the simulation based Ensemble Kalman filter (EnKF) (Evensen, 1994) can be used. Instead of calculating the covariance matrices analytically, the EnKF stores a particle approximation to the Gaussian filtering distribution and iteratively performs a prediction and update step with a particle approximation, similar to the analytical update the Kalman filter performs. Despite being based on linear Gaussian dynamics, the EnKF is successfully employed in many high-dimensional non-linear non Gaussian problems (Katzfuss, Stroud, and Wikle, 2016).

For non-linear problems of moderate dimension, i.e. those where we replace the right-hand side of both state (Equation (3.4)) and observation (Equation (3.5)) equations by non-linear functions, other variants such as the Extended Kalman filter (EKF) (Jazwinski, 1970) and the unscented Kalman filter (UKF) (Julier and Uhlmann, 1997) may be used. The EKF applies the Kalman filter to a linearization of the non-linear system around the current conditional means $\hat{X}_{t|t-1}$ and $\hat{X}_{t|t}$. If the systems dynamics are highly non-linear, this approximation can fail. Alternatively, the

UKF, which is based on the unscented transform, directly approximates the predicted means and covariance matrix, by constructing a set of deterministic points that are propagated through the systems dynamics.

The Kalman smoother (Algorithm 2) computes the marginal distributions $X_t|Y$ for $t = 0, \dots, n$. Upon closer inspection, the mean and covariance updates resemble that of the Kalman filter (Algorithm 1). This is no coincidence: By the assumed dependence structure (Figure 3.1, except for the dashed arrows), we obtain the following lemma, which will allow us to prove the recursions.

Lemma 3.2 (conditional independence from future observations)**.** *Let $t \in \{0, \dots, n-1\}$ and $s > t$. In a GLSSM, conditional on X_{t+1}, X_t is independent of Y_s, $s > t$.*

Proof. As $s > t$, we have

$$p(x_t, y_s|x_{t+1}) = p(y_s|x_{t+1}, x_t)p(x_t|x_{t+1}) = p(y_s|x_{t+1})p(x_t|x_{t+1})$$

where the second equality follows from the dependency structure of the model. □

Algorithm 2 Kalman smoother. Note that the Kalman filter already outputs the smoothed last state $\hat{X}_{n|n}$ and covariance $\Xi_{n|n}$.

Require: GLSSM (Definition 3.2), outputs from Kalman filter (Algorithm 1)

1: **for** $t \leftarrow n-1, \dots, 0$ **do**
2: $\quad G_t = \Xi_{t|t} A_t \Xi_{t+1|t}^{-1}$
3: $\quad \hat{X}_{t|n} = \hat{X}_{t|t} + G_t \left(\hat{X}_{t+1|n} - \hat{X}_{t+1|t} \right)$
4: $\quad \Xi_{t|n} = \Xi_{t|t} - G_t \left(\Xi_{t+1|t} - \Xi_{t+1|n} \right) G_t^T$
5: **end for**

We can now sketch the proof for the Kalman smoother recursions, based on the arguments in (Chopin and Papaspiliopoulos, 2020, Chapter 7.3). By the preceding lemma, the conditional distribution of X_t given $Y_{:n}$ and X_{t+1} is the same as that given $Y_{:t}$ and X_{t+1}. We may now regard $X_{t+1} = A_t X_t + u_t + \varepsilon_{t+1}$ as an additional observation at time t, and use the Kalman filter update to determine this conditional distribution:

$$X_t|Y_{:n} = y_{:n}, X_{t+1} = x_{t+1} \sim \mathcal{N}\left(\hat{X}_{t|t} + G_t(x_{t+1} - \hat{X}_{t+1|t}), \Xi_{t|t} - G_t \Xi_{t+1|t} G_t^T \right).$$

As $\hat{X}_{t|t}$ and $\hat{X}_{t+1|t}$ are linear functions of $Y_{:n}$ (actually $Y_{:t}$), we may apply the last statement of Lemma 3.1, to see that, conditional on $Y_{:n} = y_{:n}$, the distribution of X_t is Gaussian with mean

$$\hat{X}_{t|t} + G_t \left(\hat{X}_{t+1|n} - \hat{X}_{t+1|t} \right)$$

and covariance matrix

$$\Xi_{t|t} - G_t \Xi_{t+1|t} G_t^T + G_t \Xi_{t+1|n} G_t^T = \Xi_{t|t} - G_t \left(\Xi_{t+1|t} - \Xi_{t+1|n} \right) G_t^T.$$

These quantities are calculated by the Kalman smoother (Algorithm 2).

Going back to the proof of the last statement in Lemma 3.1, we see that we can represent X_t as

$$X_t = \hat{X}_{t|t} + G_t(X_{t+1} - \hat{X}_{t+1|t}) + \xi_t, \tag{3.6}$$

for a $\xi_t \sim \mathcal{N}\left(0, \Xi_{t|t} - G_t \Xi_{t+1|t} G_t\right)$ which is independent of $Y_{:n}$ and X_{t+1}. This recurrence may be used to generate samples from the joint smoothing distribution, which is useful if one is interested in non-linear functionals of the smoothing distribution that involve multiple states at once, such as a moving median or maximum. It is based on the following decomposition of the smoothing density

$$p(x|y) = p(x_n|y) \prod_{t=n-1}^{0} p(x_t|x_{t+1}, y_{:t}).$$

Algorithm 3 Forwards filter, backwards smoother (Frühwirth-Schnatter, 1994, Proposition 1)

Require: GLSSM (Definition 3.2), outputs from Kalman filter (Algorithm 1)

1: Simulate $\check{X}_{n|n} \sim \mathcal{N}(\hat{X}_{n|n}, \Xi_{n|n})$
2: **for** $t \leftarrow n-1, \ldots, 0$ **do**
3: $\quad G_t = \Xi_{t|t} A_t \Xi_{t+1|t}^{-1}$
4: $\quad$ Simulate $\xi_t \sim \mathcal{N}(0, \Xi_{t|t} - G_t \Xi_{t+1|t} G_t^T)$
5: $\quad$ Set $\check{X}_{t|n} = \hat{X}_{t|t} + G_t \left(\check{X}_{t+1} - \hat{X}_{t+1|t} \right) + \xi_t$
6: **end for**

The resulting algorithm is called the Forwards Filter, Backwards Sampling (FFBS) (Algorithm 3) and was first described in (Frühwirth-Schnatter, 1994) in the context of a data augmentation algorithm for Bayesian analysis of GLSSM.

Remark 3.4 (regularity of Σ_t and Ω_t)**.** Throughout this section, we have assumed, either explicitly or implicitly, that the innovation and observation covariance matrices Σ_t and Ω_t are non-singular, i.e. SPD.

For the Kalman filter we require that for every t, $\Psi_{t|t-1}$ is non-singular, i.e. that we can apply Lemma 3.1 (i). This is fulfilled as soon as Ω_t is non-singular, which is a reasonable assumption in most models. Following the remark after Lemma 3.1, we could also replace $\Psi_{t|t-1}^{-1}$ in Algorithm 1 by its Moore-Penrose inverse.

A similar argument can be made for singular $\Xi_{t+1|t}$, where we replace $\Xi_{t+1|t}^{-1}$ by its Moore-Penrose inverse in the Kalman smoother (Algorithm 2) and the FFBS (Algorithm 3).

In the context of COVID-19, variants of the Kalman filter have been employed to analyse the time-varying behavior of epidemiological parameters. Usually the models start from some theoretical, e.g. compartmental, model of how the epidemic spreads. After time-discretization and possibly linearization, one ends up with a GLSSM, to which the Kalman filter or one of its variants may be applied. In (Arroyo-Marioli et al., 2021) the authors construct a simple GLSSM to reconstruct the time-varying reproduction number from observed growth factors, exploiting the linear relationship between the two quantities in the SIR compartmental model and using the Kalman filter and smoother to perform inference. (Song et al., 2021; Zhu et al., 2021) directly apply the EKF to time-discretized compartmental models, fitting them either to simulated (Zhu et al., 2021) or real (Song et al., 2021) data. Similarly, (Engbert et al., 2020) use the EnKF to fit a stochastic compartmental model to German regional data, where the EnKF allows to deal with the non-linear and non-Gaussian properties on these small spatial scales.

The attractive feature of GLSSMs is that a large part of inference is analytically feasible: we can calculate the likelihood, smoothing distribution and sample from it. However, the modeling capacity of GLSSMs is limited: most interesting phenomena in the context of this thesis follow neither linear dynamics nor are well modeled by a Gaussian distribution.

Nevertheless, linearization of non-linear dynamics suggests that GLSSMs can have some use as approximations to these more complicated phenomena, provided they are sufficiently close to Gaussian models, e.g. unimodal and without heavy tails. We start to move away from linear Gaussian models by allowing observations that are non-Gaussian.

3.2 Partially Gaussian state space models

For the applications considered in this thesis the distribution of observations is never Gaussian — see Section 2.4 — and all we can hope for is that the data-generating mechanism is close enough to a Gaussian distribution that inferences made in a GLSSM may carry over. For epidemiological models, Gaussian distributions may be appropriate if incidences are high, e.g. during large outbreaks in a whole country. When case numbers are small, the discrete nature of incidences is better captured by a distribution on $\mathbf{N}_0$, and standard distributions used are the Poisson and negative binomial

distributions, see e.g. (Lloyd-Smith et al., 2005). We thus want SSMs where observations are allowed to follow these non-Gaussian distributions.

Concerning the distribution of states, we keep the linear Gaussian assumption, i.e. Equation (3.4). As demonstrated in Chapter 4, using Gaussian states and transitions allows for flexible modeling of many epidemiological desiderata. Furthermore, keeping the states Gaussian will enable us to use Efficient Importance Sampling (EIS) effectively, by constructing approximations via GLSSM which possess the same state dynamics. Alternatively, t-distributed innovations or more general transition kernels could be employed and we refer the interested reader to (Durbin and Koopman, 2012, Part II) for a selection of these models. The following definition is that of (Koopman, Lit, and Nguyen, 2019), which itself is an extension of earlier work of (Shephard, 1994). (Shephard, 1994) considered only SSMs where, conditional on another Markov process $Z = (Z_t)_{t=0,\dots,n}$, model is a full GLSSM, which allows for efficient inference if the conditional distribution $Z|(X,Y)$ is tractable. As their definition involves a conditional GLSSM, the observations still take values in $\mathbf{R}^p$, not $\mathbf{N}^p$ as is necessary for our endeavors. Thus we opt for the definition presented in (Koopman, Lit, and Nguyen, 2019), where we replace the Gaussian observations (Equation (3.5)) with arbitrary distributions.

Definition 3.3 (Partially Gaussian state space model (PGSSM))**.** A Partially Gaussian state space model (PGSSM) is a joint distribution for (X,Y) where states X follow Equation (3.4), i.e.

$$X_{t+1} = A_t X_t + u_t + \varepsilon_{t+1} \qquad\qquad t = 0,\dots,n-1,$$

with $X_0 \sim \mathcal{N}(0,\Sigma_0)$, $\varepsilon_t \sim \mathcal{N}(0,\Sigma_t), u_t \in \mathbf{R}^m$ for $t = 1,\dots,n$ and X_0, $(\varepsilon_t)_{t=1,\dots,n}$ jointly independent.

Furthermore, the observations Y form a conditional Markov process, conditional on states X, where the conditional densities of observations, given states admit the following form

$$p(y|x) = \prod_{t=0}^{n} p(y_t|x_t, y_{t-1}),$$

with respect to the dominating measure $\bigotimes_{t=0}^{n} \mu_{\mathcal{Y}}$. Here $p(y_t|x_t,y_{t-1})$ are allowed to take any arbitrary density[1].

It is straightforward to check that a PGSSM is indeed a SSM.

Remark 3.5. Recalling Remark 3.1, if our main interest lies in the conditional distribution $X|Y=y$ for a fixed set of observations y, it will suffice to consider models where

$$p(y|x) = \prod_{t=0}^{n} p(y_t|x_t)$$

holds, and we will do so in the following to enhance readability.

Both the Poisson and negative binomial distribution belong to the class of exponential family distributions. As such, their densities have a convenient structure, allowing only for a linear interaction between the natural parameter and the densities' argument. We refer to (Brown, 1986) for a comprehensive treatment of exponential families and use their definitions throughout this section.

Definition 3.4 (exponential family)**.** Let μ be a σ-finite measure on $\mathbf{R}^p$ and denote by

$$\Psi = \left\{ \psi \in \mathbf{R}^p : \int \exp\left(\psi^T y\right)\, \mathrm{d}\mu(y) < \infty \right\}$$

the set of parameters ψ such that the moment-generating function of μ is finite. For every $\psi \in \Psi$

$$p_\psi(y) = Z(\psi)^{-1} \exp(\psi^T y)$$

[1] Recall that we have not specified $\mu_{\mathcal{Y}}$, so it is always possible to use $p = \mathbf{1}_{\mathcal{Y}}$, the constant function.

defines a probability density with respect to the measure μ, where

$$Z(\psi) = \int \exp\left(\psi^T x\right) \, \mathrm{d}\mu(y)$$

is the normalizing constant. We call both the densities p_ψ and induced probability measures

$$\mathbf{P}_\psi(A) = \int_A p_\psi(y) \, \mathrm{d}\mu(y),$$

for measurable $A \subset \mathbf{R}^p$, a **standard exponential family**.

Conversely, let $\mathbf{P}_\psi, \psi \in \Psi$ be a given parametric family of probability measures on some space $\mathcal{Y}$ that is absolutely continuous with respect to a common dominating measure μ. Suppose there exist a reparametrization $\eta : \Psi \to \mathbf{R}^p$, a statistic $T : \mathcal{Y} \to \mathbf{R}^p$ and functions $Z : \Psi \to \mathbf{R}$, $h : \mathcal{Y} \to \mathbf{R}$, such that

$$p_\psi(y) = \frac{\mathrm{d}\mathbf{P}_\psi}{\mathrm{d}\mu} = \frac{h(y)}{Z(\psi)} \exp\left(\eta(\psi)^T T(y)\right),$$

then we call $(\mathbf{P}_\psi)_{\psi\in\Psi}$ and $(p_\psi)_{\psi\in\Psi}$ a **p-dimensional exponential family**. If $\eta(\psi) = \psi$ is the identity, we call ψ the natural parameter. If $T(y) = y$, we call y the natural observation. If ψ is the natural parameter, we call $(\mathbf{P}_\psi)_{\psi\in\Psi}$ a **natural exponential family**. By reparametrization (in ψ) and sufficiency (in y) every p-dimensional exponential family can be written as an equivalent standard exponential family, see the elaborations in (Brown, 1986, Chapter 1).

Exponential families have the attractive property that they are log-concave in their parameters. As such the Fisher-information is always positive semidefinite, which will be crucial in defining surrogate Gaussian models in Section 3.5.

Lemma 3.3 (log-concavity of exponential family distributions)**.** *Let $(p_\psi)_{\psi\in\Psi}$ be a natural p-dimensional exponential family and Ψ convex and open in $\mathbf{R}^p$. In this case $\psi \mapsto \log p_\psi(y)$ is concave for every $y \in \mathbf{R}^p$.*

Proof. As $\log p_\psi(y) = -\log Z(\psi) + \psi^T y$ it suffices to show that $\psi \mapsto \log Z(\psi)$ is convex. However,

$$\psi \mapsto \log Z(\psi) = \log \int \exp\left(\psi^T y\right) \mathrm{d}\mu(y)$$

is the cumulant generating function of the base measure μ, which is convex (Billingsley, 1995, p. 144f). □

Additionally, the moment generating function $\psi \mapsto Z(\psi)$ is smooth on the interior of Ψ and allows to switch the order of integration and differentiation.

Theorem 3.1 ((Brown, 1986, Theorem 2.2, Corollary 2.3))**.** *Let $\psi \in \operatorname{int}\Psi$ be an interior point. Then the moment generating function $Z : \Psi \to \mathbf{R}$ is infinitely often differentiable with derivatives*

$$\frac{\partial^{|\alpha|}}{\partial^\alpha \psi} Z(\psi) = \int y^\alpha \exp\left(\psi^T y\right) \, \mathrm{d}\mu(y)$$

for any multi-index $\alpha \in \mathbf{N}^k$.

Additionally, the gradient of $\log Z$, $\nabla_\psi \log Z(\psi)$ is given by

$$\nabla_\psi \log Z(\psi) = \mathbb{E}T(X),$$

and the Hessian of $\log Z$, $H_\psi \log Z(\psi)$ by

$$H_\psi \log Z(\psi) = \operatorname{Cov}(T(X)),$$

where $X \sim \mathbf{P}_\psi$.

Example 3.1 (Poisson & negative binomial distribution)**.** Both the family of Poisson distributions, parameterized by rate λ and the negative binomial distribution, parameterized by success probability q with fixed overdispersion r form an exponential family.

The log-density of the Poisson distribution with rate λ, Pois(λ) w.r.t. the counting measure on $\mathbf{N}_0$ is

$$\log p_\lambda(x) = -\lambda + x \log \lambda - \log x!.$$

Thus the Poisson distribution forms an exponential family with natural parameter $\log \lambda$, natural statistic id (the identity), base measure $h(x) = \frac{1}{x!}$ and moment-generating function function $Z(\lambda) = \exp(-\lambda)$.

The log-density of the negative binomial distribution with overdispersion parameter r and success probability p NegBinom (q, r) is

$$\log p_{q,r}(x) = \log \binom{x+r-1}{x} + x \log(1-q) + r \log q.$$

For fixed r these distributions form an exponential family with natural parameter $\log(1-q)$, natural statistic $T = \mathrm{id}$, base measure $h(x) = \binom{x+r-1}{x}$ and moment-generating function $Z(q) = r \log q$.

In this parametrization the mean of the NegBinom(q, r) distribution is $\mu = r\frac{1-q}{q}$ and its variance is $r\frac{1-q}{q^2}$. An alternative parametrization that will become useful Chapter 4 is that by the log mean $\xi = \log \mu$ and overdisperision r, with variance $\mu + \frac{\mu^2}{r}$. Thus, the NegBinom distribution has $1 + \frac{\mu}{r}$ times the variance of a Poisson distribution with the same mean. As $q = \frac{r}{r+\mu}$, this parametrization has log-density

$$\log p_{r,\xi}(x) = \log \binom{x+r-1}{x} + x\xi - (r+x)\log(\exp \xi + r) - r \log r,$$

which does not form a natural exponential family. However, it retains the log-concavity of Lemma 3.3, as a quick calculation reveals that

$$\partial^2_{\xi^2} \log p_{r,\xi}(x) = -(r+x)\frac{r\exp(-\xi)}{(r\exp(-\xi)+1)^2} < 0$$

for all $x \in \mathbf{N}_0$.

The models we study in Chapter 4 belong, for the most part, to the following subclass of PGSSM models.

Definition 3.5 (Exponential Family Partially Gaussian state space model (EGSSM))**.** An Exponential Family Partially Gaussian state space model (EGSSM) is a PGSSM where the conditional distribution of Y_t given X_t comes from an exponential family with respect to a base measure μ_t, i.e.

$$p(y_t|x_t) = h_t(y_t) Z_t(x_t) \exp\left(\eta_t(x_t)^T T_t(y_t)\right)$$

for suitable functions h_t, Z_t, η_t, T_t. If Y_t in the PGSSM is allowed to depend on the previous Y_{t-1}, the functions h_t, Z_t, η_t and T_t may depend on y_{t-1}.

If, additionally, matrices $B_t \in \mathbf{R}^{p\times m}$ exist, such that for the signal $S_t = B_t X_t \in \mathbf{R}^p$, Y_t only depends on X_t through S_t, i.e. it holds

$$p(y_t|x_t) = \prod_{i=1}^{p} h_t^i(y_t^i)\, Z_t^i(s_t)\, \exp\left(\eta_t^i(s_t^i)\, T(y_t^i)\right),$$

for functions $h_t^i : \mathbf{R} \to \mathbf{R}, Z_t^i : \mathbf{R} \to \mathbf{R}, \eta_t^i : \mathbf{R} \to \mathbf{R}, T : \mathbf{R} \to \mathbf{R}$, $i = 1, \ldots p$, we say the EGSSM has a **linear signal**, similar to the treatment in (Durbin and Koopman, 2012, Part II).

Remark 3.6. To simplify notation we will usually assume that the functions h, Z and T are the same for all t (and i, if the EGSSM has a linear signal) and drop in our notation the dependence of h, Z, and T on t (and i). Similarly, we assume that the base measure μ_t is the same for all t.

From Lemma 3.3, we immediately obtain the following results (Durbin and Koopman, 2012, Section 10.6.4)

Lemma 3.4 (log-concavity of the smoothing distribution)**.** *Consider an EGSSM, where* $\eta_t = \mathrm{id}$ *for all* t*. Then* $x \mapsto \log p(x|y)$ *is concave for* $\mu_{\mathcal{Y}}$*-a.e.* y*.*

Proof. We may write

$$\log p(x|y) = \log p(y|x) + \log p(x) - \log p(y),$$

where the last term does not depend on x. $\log p(x)$ is concave in x, as $p(x)$ is the joint density of a multivariate Gaussian distribution. Furthermore

$$\log p(y|x) = \sum_{t=0}^{n} \log p(y_t|x_t, y_{t-1}),$$

which, by Lemma 3.3 is concave in x. □

Notice that the dependence of Y_t on Y_{t-1} does not influence the statement of this lemma, as we are interested in properties of $x \mapsto p(x|y)$.

As in the previous chapter, after having observed Y, one is interested in the conditional distribution of states X, given Y. If the observations are not Gaussian, this is a difficult task as the distribution is not analytically tractable. Instead, approximations, e.g. the Laplace approximation (LA), which will exploit the log-concavity developed here or simulation-based inference, e.g. importance sampling (Sections 3.3 and 3.5), sequential Monte Carlo (Chopin and Papaspiliopoulos, 2020) or MCMC-methods (Brooks et al., 2011) are used. Similarly, fitting hyperparameters ψ by maximum likelihood inference becomes more difficult as evaluating $\ell(\psi) = p(y) = \int p(x, y)\,\mathrm{d}x$ is not analytically available, thus requiring numerical or simulation methods for evaluation and gradient descent or EM-techniques for optimization, see Section 3.6.

In this thesis, we will focus on importance sampling methods, which are the focus of the next section.

3.3 Importance Sampling

Importance sampling is a simulation technique that allows us to approximate integrals w.r.t a measure of interest, the target, by sampling from a tractable approximation, the proposal, instead, thus performing Monte-Carlo integration. To account for the fact that we did not sample from the correct probability measure, we weight samples according to their importance. As the user has freedom in the choice of approximation (except for some technical conditions), importance sampling also acts as a variance reduction technique with better approximations resulting in smaller Monte-Carlo variance. Thus the role that importance sampling plays is twofold: first, it enables Monte-Carlo integration even if sampling from the target is not possible, and second it allows us to do so in an efficient way by choosing, to be defined precisely below, the approximation in an optimal way.

Alternative approaches to importance sampling for performing inference in SSMs include Markov chain Monte Carlo (MCMC) and SMC. Recall from the introduction to this chapter that this inference concerns three objectives: maximum likelihood estimation, i.e. evaluation and optimization of the likelihood, access to the posterior distribution $X_{:n}|Y_{:n}$ and prediction of future states and observations. Let us give a concise comparison of these alternative approaches, weighing their advantages and disadvantages over importance sampling, in particular for the SSMs that this thesis deals with.

MCMC (Brooks et al., 2011) is a simulation technique that allows to simulation of correlated samples from a target distribution by constructing an ergodic Markov chain that has as its invariant distribution the desired distribution. If one is able to simulate from such a Markov chain, one can generate samples whose marginal distributions are close to the target distribution. Thus, these samples can be used in MC-integration to estimate expectations of interest, though one

has to be mindful of autocorrelation of these samples. For standard variants of MCMC, such as Metropolis-Hastings MCMC or Hamiltonian Monte Carlo, one needs access to the density of the sought after distribution up to a constant to simulate a step in the Markov chain. While these methods are very general, in high dimensions, these are affected by the curse of dimensionality.

Let us argue for our choice of using IS over MCMC for estimating conditional expectations of the form $\mathbb{E}(f(X)|Y)$ for PGSSMs. For the models we consider in this thesis, the dimension of X ($(n+1)m$) can become quite large, so MCMC suffers from the aforementioned curse of dimensionality. IS can also suffer from this curse, especially if the proposal is far from the target. If, however, the proposal is close to the target, IS can perform surprisingly well, see e.g. (Chopin and Ridgway, 2017) where it is used as the gold standard method against which other methods are benchmarked.

As IS is based on independent samples, it can be parallelized easily, whereas parallelizing MCMC is more involved, using e.g. (Neiswanger, Wang, and Xing, 2014). Additionally, analysis of convergence is much simpler than that of MCMC, which requires consideration of burn-in samples, autocorrelation of samples and investigating trace plots for the chain getting stuck.

SMC (Chopin and Papaspiliopoulos, 2020) or particle filters, use sequential importance sampling to provide a particle approximation to the filtering distributions $X_t|Y_{:t}$, essentially decomposing the problem into a n importance sampling steps. To avoid particle collapse, SMC is usually equipped with a resampling step once the effective sample size of the current set of particles drops below a specified level. Once the final filtering distribution $X_n|Y_{:n}$ is approximated, the smoothing distribution may be obtained in several ways, e.g., backwards sampling or a two-filter approach, see (Chopin and Papaspiliopoulos, 2020, Chapter 12).

Conveniently, SMC allows us to approximate the likelihood $\ell(\theta)$ for a single parameter by a single pass of the particle filter. However, the discrete nature of resampling makes the approximated likelihood non-continuous, complicating maximum likelihood inference. (Chopin and Papaspiliopoulos, 2020, Chapter 14) discusses several strategies: the first amounts to importance sampling of the order as discussed in this thesis, where one fixes a reference parameter θ_0 to perform importance sampling with $p_{\theta_0}(x|y)$ against $p_\theta(x|y)$. The second strategy only works in the univariate case and consists of approximating the non-continuous inverse CDFs appearing in the resampling step by continuous ones. Finally, if the dependence on the hyperparameters θ allows for application of the EM-algorithm, it may be used to perform the optimization. Contrary to SMC, the global importance sampling approach we discuss in Sections 3.5 and 3.6 allows us to perform importance sampling in an optimal way, and allows for use of numerical differentiation as the dependence of $\log p_y(\theta)$ on θ is smooth, as there is no resampling involved.

This chapter proceeds with a general treatment of importance sampling, loosely based on (Chopin and Papaspiliopoulos, 2020, Chapter 8) and (Durbin and Koopman, 2012, Chapter 11). Subsequently, we will focus our attention on methods to obtain good importance sampling proposals.

Suppose we have a function $h : \mathcal{X} \to \mathbf{R}$ whose integral w.r.t. to some measure μ,

$$\zeta = \int_{\mathcal{X}} h(x)\,\mathrm{d}\mu(x),$$

exists and whose value we want to compute. Furthermore, suppose that we can write

$$\int_{\mathcal{X}} h(x)\,\mathrm{d}\mu(x) = \int_{\mathcal{X}} f(x)\,\mathrm{d}\mathbf{P}(x) = \mathbf{P}[f],$$

for a probability measure $\mathbf{P}$ and function $f : \mathcal{X} \to \mathbf{R}$, e.g. because $\mathbf{P} = p\mu$ and $h(x) = f(x)p(x)$ μ-a.s.. Here, and in the remainder of this chapter, we use the operator shorthand notation $\mathbf{P}[f] = \int f\,\mathrm{d}\mathbf{P}$ for a measure $\mathbf{P}$ and a $\mathbf{P}$-integrable function f. Let $\mathbf{G}$ be a another probability measure on $\mathcal{X}$ such that $f\mathbf{P}$ is absolutely continuous with respect to $\mathbf{G}$, $f\mathbf{P} \ll \mathbf{G}$, and let $v = \frac{\mathrm{d}f\mathbf{P}}{\mathrm{d}\mathbf{G}}$ be the corresponding Radon-Nikodym derivative. Then

$$\zeta = \mathbf{P}[f] = \int_{\mathcal{X}} f(x)\,\mathrm{d}\mathbf{P}(x) = \int_{\mathcal{X}} \left(\frac{\mathrm{d}f\mathbf{P}}{\mathrm{d}\mathbf{G}}\right)(x)\,\mathrm{d}\mathbf{G}(x) = \mathbf{G}[v]$$

which suggests estimating ζ by Monte-Carlo integration:

$$\hat{\zeta} = \frac{1}{N}\sum_{i=1}^{N} v(X^i),$$

the importance sampling estimate of ζ. The importance samples $X^i, i = 1, \dots, N$ have distribution $\mathbf{G}$, and will usually be i.i.d. For this procedure to work, we want $\hat{\zeta}$ to fulfill a law of large numbers and a central limit theorem, so we will want $v \in L^2(\mathbf{G})$, where $L^p(\nu)$ is the space of p-times ν-integrable functions for a measure ν. We call such a proposal admissible, and inadmissible otherwise. The i.i.d. assumption could also be dropped, e.g. when we employ antithetic variables, see (Ripley, 2009, Section 5.3) and Section 3.6. Here we call $\hat{\zeta}$ the importance sampling estimate of ζ.

If $v \in L^2(\mathbf{G})$ and under i.i.d. sampling the Monte-Carlo variance of $\hat{\zeta}$ is $\frac{\mathrm{Var}\left(v(X^i)\right)}{N}$, and so naturally we want $\mathrm{Var}\left(v(X^i)\right)$ to be small to ensure fast convergence of $\hat{\zeta}$. As v depends on the proposal $\mathbf{G}$, and we have flexibility in choosing $\mathbf{G}$, importance sampling acts as a variance reduction technique: the better $\mathbf{G}$ approximates $f\mathbf{P}$, in the sense that the variance of v w.r.t. $\mathbf{G}$ is small, the faster importance sampling will converge.

A classical result is that the minimum MSE proposal $\mathbf{G}^*$ has a closed form. Indeed it is given by the total variation measure of $f\mathbf{P}$, renormalized to be a probability measure, which can be shown by a simple application of Jensen's inequality.

Proposition 3.1 (Chopin and Papaspiliopoulos, 2020, Proposition 8.2)**.** *[minimum MSE proposal] The proposal $\mathbf{G}^*$ that minimizes the MSE of importance sampling is given by*

$$\mathbf{G}^* = \frac{|f|}{\mathbf{P}\left[|f|\right]}\mathbf{P}.$$

Unfortunately, this optimality result has no practical use, indeed if f is positive we would need to obtain $\mathbf{P}[f]$ first, the overall target of our endeavor. Additionally, sampling from $\mathbf{G}^*$ is not guaranteed to be practically feasible.

If the Radon-Nikodym derivative $w = \frac{\mathrm{d}\mathbf{P}}{\mathrm{d}\mathbf{G}}$ exists, then $v = fw$, which, for the problems we will study, is the case. Then

$$\hat{\zeta} = \frac{1}{N}\sum_{i=1}^{N} f(X^i)w(X^i),$$

where $w(X^i)$ is called the importance weight, or just weight, of the i-th sample. If the samples are clear from the context we sometimes write $w^i = w(X^i)$. This motivates us to regard

$$\hat{\mathbf{P}}_N = \frac{1}{N}\sum_{i=1}^{N} w(X_i)\delta_{X_i}, \tag{3.7}$$

as a particle approximation of $\mathbf{P}$, in the sense that for sufficiently well behaved test functions f, as $N \to \infty$

$$\hat{\mathbf{P}}_N[f] = \frac{1}{N}\sum_{i=1}^{N} f(X^i)w(X^i) \to \mathbf{P}[f].$$

We will return to the question of which functions f to consider further below and assume in the following discussion $fw \in L^2(\mathbf{G})$.

To perform importance sampling one must be able to evaluate w. In the context of PGSSMs this is usually not possible: if $\mathbf{P}$ is the intractable conditional distribution of $X|Y$, then the integration constant of its density $p(y)$ is not analytically available. Still, we can usually evaluate the weights up to a constant, i.e.

$$\tilde{w}(x) \propto \frac{\mathrm{d}\mathbf{P}}{\mathrm{d}\mathbf{G}}(x)$$

is available. The missing constant is then $\mathbf{G}\tilde{w}$, which is itself amenable to importance sampling: we may estimate it by $\frac{1}{N}\sum_{i=1}^{N}\tilde{w}(X^i)$. This leads to the so-called self-normalized importance sampling weights

$$W_i = \frac{w(X^i)}{\sum_{i=1}^{N} w(X^i)},$$

Monte Carlo estimates

$$\hat{\zeta} = \sum_{i=1}^{N} W_i f(X^i),$$

and particle approximation

$$\hat{\mathbf{P}}_N = \sum_{i=1}^{N} W_i \delta_{X^i}.$$

Unless $\tilde{w}$ is degenerate, i.e. constant,

$$\hat{\zeta} = \frac{\sum_{i=1}^{N}\tilde{w}(X^i f(X^i))}{\sum_{i=1}^{N}\tilde{w}(X^i)}$$

is a ratio of two non-constant, unbiased estimators and so is itself biased. Nevertheless, noticing that the rescaled denominator $\frac{1}{N}\sum_{i=1}^{N}\tilde{w}(X^i)$ consistently estimates the integration constant $\mathbf{G}\tilde{w}$, allows us to apply Slutsky's lemma and obtain a central limit theorem for $\hat{\zeta}$ (recall that we assumed $fw \in L^2(\mathbf{G})$).

The class for test functions f for which this holds depends on $\mathbf{P}$ and $\mathbf{G}$. (Agapiou et al., 2017) study the behavior of uniformly bounded test functions $\|f\| \leq 1$. For these functions it suffices that $w \in L^2(\mathbf{G})$ to ensure asymptotic normality of ζ. Thus an important quantity is

$$\rho = \frac{1}{(\mathbf{G}\tilde{w})^2}\mathbf{G}[\tilde{w}^2] = \mathbf{G}[w^2] = \mathbf{P}[w],$$

the second moment of the importance sampling weights. (Agapiou et al., 2017) show that the bias

$$\left|\mathbb{E}(\hat{\mathbf{P}}_N - \mathbf{P})[f]\right|$$

and mean-squared error (MSE)

$$\mathbb{E}\left((\hat{\mathbf{P}}_N - \mathbf{P})[f]\right)^2$$

of importance sampling are both, for bounded f, of order $\mathcal{O}\left(\frac{\rho}{N}\right)$. Here the expectation $\mathbb{E}$ is with respect to the random particles $X^1, \ldots, X^N$. Consequently, for bounded functions, keeping $\frac{\rho}{N}$ small produces importance sampling estimates with small bias and MSE. This can be achieved in two ways: either we choose $\mathbf{G}$ „close enough“ to $\mathbf{P}$ to ensure small ρ, or we choose N large enough to compensate for a large ρ.

Applying Jensen's inequality, we see that

$$\mathcal{D}_{\mathrm{KL}}(\mathbf{P}||\mathbf{G}) = \mathbf{P}[\log w] \leq \log \mathbf{P}[w] = \log \rho,$$

so small ρ implies a small KL-divergence between $\mathbf{P}$ and $\mathbf{G}$ as well. Conversely, the following theorem of Chatterjee and Diaconis implies that a small KL-divergence is both sufficient and necessary for importance sampling to perform well.

Theorem 3.2 (Chatterjee and Diaconis, 2018, Theorem 1.1)**.** *Let $\mathbf{P}$ and $\mathbf{G}$ be probability measures on a measurable space $(\mathcal{X}, \mathcal{B})$ such that $\mathbf{P} \ll \mathbf{G}$ and let $f \in \mathbf{L}^2(\mathbf{P})$ be a function with $\|f\|_{L^2(\mathbf{P})} = \left(\mathbf{P}f^2\right)^{1/2} < \infty$. Let Y be an $\mathcal{X}$ valued random variable with law $\mathbf{P}$.*

Let $L = \mathcal{D}_{KL}(\mathbf{P}||\mathbf{G}) = \mathbb{E}\log w(Y)$ be the KL-divergence between $\mathbf{P}$ and $\mathbf{G}$, and let

$$\hat{\mathbf{P}}_N = \sum_{i=1}^{N} w(X^i)\delta_{X^i}$$

be the particle approximations of $\mathbf{P}$ *based on samples* $X^1, \ldots, X^N \overset{i.i.d}{\sim} \mathbf{G}$, $N \in \mathbf{N}$.

If the sample size N *is given by* $N = \exp(L + t)$ *for a* $t \geq 0$,

$$\mathbb{E}\left|\hat{\mathbf{P}}_N[f] - \mathbf{P}[f]\right| \leq \|f\|_{L^2(\mathbf{P})}\left(\exp(-t/4) + 2\sqrt{\mathbb{P}\left(\log w(Z) > L + t/2\right)}\right). \tag{3.8}$$

Conversely, if $N = \exp(L - s)$ *for* $s \geq 0$, *then for any* $\delta \in (0, 1)$

$$\mathbb{P}(\hat{\mathbf{P}}_N[\mathbf{1}] \geq 1 - \delta) \leq \exp\left(-\frac{s}{2}\right) + \frac{\mathbb{P}\left(\log w(Z) \leq L - \frac{s}{2}\right)}{1 - \delta}, \tag{3.9}$$

where $\mathbf{1}$ *is the constant function* $x \mapsto 1$.

Notice the boldface $\mathbb{P}$ *and* $\mathbb{E}$ *to differentiate the measures* $\mathbf{P}$ *and* $\mathbf{G}$ *from expectations and probabilities with respect to the abstract probability space* $(\Omega, \mathcal{A}, \mathbb{P})$ *where the random variables* $X_1, \ldots, X_N$ *and* Y *live.*

The proof of this theorem is based on splitting $\mathcal{X}$ into $\{\log w \leq L + \frac{t}{2}\}$ and its complement and straightforward, it may be found in the Appendix of (Chatterjee and Diaconis, 2018). Theorem 1.2 in the same paper provides a qualitatively similar result for autonormalised importance sampling.

Let us consider the implications of Theorem 3.2, starting with Equation (3.8), by devising heuristics to decide when $\mathbf{G}$ is a good proposal for fixed sample size N, and assume for simplicity that $\|f\|_{L^2(\mathbf{P})} = 1$. First of all, as $t = \log N - L$, we have $\exp(-t/4) = \exp(L/4)N^{-\frac{1}{4}}$, so for large N this term becomes negligible, and the interesting term in inequality (3.8) is the second one. As $\mathbb{E}\log w(Z) = L$, this term is a tail probability and we can use standard mass-concentration inequalities to analyze its behavior as t (and so N) grows. Markov's inequality tells us that

$$\mathbb{P}\left(\log w(Z) > L + \frac{t}{2}\right) \leq \frac{L}{L + t/2} = \frac{2}{1 + \frac{\log N}{L}}.$$

Second, if, additionally, $\log w(Z)$ has finite variance, Chebyshev's inequality yields

$$\mathbb{P}\left(\log w(Z) > L + \frac{t}{2}\right) \leq \frac{4\operatorname{Var}(\log w(Z))}{t^2} = \frac{4\operatorname{Var}(\log w(Z))}{(\log N - L)^2}.$$

In both upper bounds provided by the concentration inequalities, all else being equal, a smaller KL-divergence will yield a tighter bound. However, in Chebyshev's inequality, the variance of log weights also plays a role, and will surely be different for different proposals. Assuming $\mathbf{G} \ll \mathbf{P}$, we have $\frac{\mathrm{d}\mathbf{G}}{\mathrm{d}\mathbf{P}} = \frac{1}{w}$ and so

$$\mathbb{E}\exp(-\log w(Z)) = \mathbb{E}\frac{1}{w(Z)} = \mathbf{P}\left[\frac{\mathrm{d}\mathbf{G}}{\mathrm{d}\mathbf{P}}\right] = 1,$$

If the log-weights are bounded from above and below, the following lemma shows that as the variance of $U = -\log w(Z)$ goes to 0, their mean,

$$\mathbb{E}U = \mathbb{E} - \log w(Z) = -\mathcal{D}_{\mathrm{KL}}(\mathbf{P}||\mathbf{G})$$

goes to 0 as well.

Lemma 3.5. *For* $a, b \in \mathbf{R}$, *let* $U \in [a, b]$ *be a bounded random variable with variance* σ^2 *and* $\mathbb{E}\exp U = 1$. *Let* $\mu = \mathbb{E}U$ *be the mean of* U. *Then there exists a* $\delta \in [\exp(a), \exp(b)]$, *such that*

$$0 \geq \mu = \log\left(1 - \delta\frac{\sigma^2}{2}\right).$$

If, additionally, $\sigma^2 < \frac{2}{\exp(b)}$ *then*

$$\mu \geq \log\left(1 - \exp(b)\frac{\sigma^2}{2}\right).$$

Proof. As U is bounded, all involved expectations exist and are finite. That $\mu \leq 0$ follows from Jensen's inequality. We perform a first-order Taylor expansion of $\exp(U-\mu)$, where the random variable ξ is between $U-\mu$ and 0:

$$1 = \exp(\mu)\mathbb{E}\exp(U-\mu) = \exp(\mu)\left(1 + \mathbb{E}(U-\mu) + \mathbb{E}\left(\frac{(U-\mu)^2}{2}\exp(\xi)\right)\right).$$

Then $\xi' = \xi + \mu$ is in $[a,b]$, and note that, unless $U = 1$ a.s., $\mathbb{E}\exp U = 1$ forces $a < 0 < b$. Thus

$$1 = \exp(\mu) + \mathbb{E}\left(\frac{(U-\mu)^2}{2}\exp(\xi')\right),$$

and as $\xi' \in [a,b]$, the expectation is in $\left[\exp(a)\frac{\sigma^2}{2}, \exp(b)\frac{\sigma^2}{2}\right]$, i.e. $\mathbb{E}\left(\frac{(U-\mu)^2}{2}\exp(\xi')\right) = \delta\frac{\sigma^2}{2}$ for some $\delta \in [\exp(a), \exp(b)]$. Solving for μ, we get

$$\mu = \log\left(1 - \delta\frac{\sigma^2}{2}\right),$$

as promised.

The second statement follows from $\delta \leq \exp(b)$ and the monotonicity of log, where the condition ensures that the argument is positive. □

Corollary 3.1. *Let* $\mathbf{P}$ *and* $\mathbf{G}$ *be equivalent probability measures with bounded Radon-Nikodym derivative* $w = \frac{\mathrm{d}\mathbf{P}}{\mathrm{d}\mathbf{G}} \in [a,b]$, $a, b \in \mathbf{R}$ *and KL-divergence* $\mathcal{D}_{KL}(\mathbf{P}||\mathbf{G}) = \mathbf{P}[\log w]$.
If $\log w \in L^2(\mathbf{P})$ *with variance* $\sigma^2 = \mathbf{P}[(\log w - L)^2]$, *and* $\sigma^2 < \frac{2}{\exp(b)}$, *then*

$$\mathcal{D}_{KL}(\mathbf{P}||\mathbf{G}) \leq -\log\left(1 - \exp(b)\frac{\sigma^2}{2}\right).$$

Under the assumptions of this corollary, we see that a small variance of the log-weights implies a small KL-divergence, which in turn implies good importance sampling performance.

Let us now discuss the implications of Equation (3.9). We see that for large s, i.e. $N \ll \exp(L)$, the right-hand side is small, and so the probability that importance sampling fails for the constant function is practically relevant. Observe that here

$$\hat{\mathbf{P}}_N[\mathbf{1}] = \frac{1}{N}\sum_{i=1}^{N} w_i$$

is the mean of weights, which does not have to sum to 1. As a result, Chatterjee and Diaconis recommend to choose $N = \mathcal{O}(\exp(\mathcal{D}_{\mathrm{KL}}(\mathbf{P}||\mathbf{G})))$.

Based on this discussion, we see that choosing $\mathbf{G}$ such that either the KL-divergence or the variance of the log-weights is small is sensible. Making the variance small has the additional advantage that it, at least for bounded log-weights, also implies an upper bound for the KL-divergence. We will return to this train of thought when we discuss optimal ways of performing importance sampling, such as the CE-method (minimizing the KL-divergence) and EIS (minimizing the variance of log-weights) in the following sub-chapters.

In practice, we will want to judge whether for an actual sample $X^1, \ldots, X^N \overset{\text{i.i.d}}{\sim} \mathbf{G}$ importance sampling has converged, and there are several criteria available in the literature. The classic effective sample size (ESS)(Kong, Liu, and Wong, 1994)

$$\mathrm{ESS} = \frac{1}{\sum_{i=1}^{N} W_i^2} \in [1, N]$$

arises from an analysis of the asymptotic efficiency of importance sampling estimates: Consider additional $Y^1, \dots, Y^N \overset{\text{i.i.d}}{\sim} \mathbf{P}$, a test function $f \in L^2(\mathbf{P})$ and assume that $\rho < \infty$. We may then estimate $\zeta = \mathbf{P}f$ in two ways: either by using the importance sampling estimate

$$\hat{\zeta}_{\text{IS}} = \hat{\mathbf{P}}_N(f) = \sum_{i=1}^N W_i f(X^i) = \frac{1}{N}\sum_{i=1}^N (NW_i) f(X^i),$$

or by standard Monte-Carlo integration

$$\hat{\zeta}_{\text{MC}} = \frac{1}{N}\sum_{i=1}^N f(Y^i).$$

(Kong, 1992) applies the delta method to $\text{Var}\left(\hat{\zeta}_{\text{IS}}\right)$, obtaining

$$\text{Var}\left(\hat{\zeta}_{\text{IS}}\right) \approx \text{Var}\left(\hat{\zeta}_{\text{MC}}\right)\left(1 + \text{Var}\left(NW_1\right)\right).$$

Note that this approximation does not depend on the specific f considered, and it is not guaranteed that for large N the remainder goes to 0, as (Kong, 1992) mentions. In particular, the approximation has to fail whenever $\text{Var}\left(\hat{\zeta}_{\text{IS}}\right) < \text{Var}\left(\hat{\zeta}_{\text{MC}}\right)$, i.e. when importance sampling actually performs variance reduction. Nevertheless, whenever the approximation is valid, we may interpret

$$\frac{N}{1 + \text{Var}\left(NW_1\right)}$$

as an effective sample size, in the sense that N times the relative efficiency of $\hat{\zeta}_{\text{MC}}$ relative to $\hat{\zeta}_{\text{IS}}$ is approximately given by this expression. As the self-normalized weights $W_1, \dots, W_N$ are exchangeable and sum to 1, their expected value is $\mathbb{E}W_1 = \frac{1}{N}$. Estimating $\text{Var}\left(W_1\right)$ by the unadjusted sample covariance $\frac{1}{N}\sum_{i=1}^N W_i^2 - \frac{1}{N^2}$ then results in the promised

$$\text{ESS} = \frac{N}{1 + N^2\left(\frac{1}{N}\sum_{i=1}^N W_i^2 - \frac{1}{N^2}\right)} = \frac{1}{\sum_{i=1}^N W_i^2}.$$

Notice that as the self-normalized weights sum to 1, the ESS is at least 1, as $0 \leq W_i \leq 1$ and at most N by the Cauchy-Schwarz inequality.

If we write the ESS in terms of the unnormalized weights $\tilde{w}$ we see that the efficiency factor (EF) $\text{EF} = \frac{\text{ESS}}{N}$ fulfills, as $N \to \infty$,

$$\text{EF} = \frac{\text{ESS}}{N} = \frac{\left(\frac{1}{N}\sum_{i=1}^N \tilde{w}_i\right)^2}{\frac{1}{N}\sum_{i=1}\tilde{w}_i^2} \overset{a.s}{\to} \frac{(\mathbf{G}[\tilde{w}])^2}{\mathbf{G}[\tilde{w}^2]} = \rho^{-1}, \tag{3.10}$$

if $\tilde{w} \in L^2(\mathbf{G})$ (Agapiou et al., 2017, Section 2.3.2). Thus, asymptotically, a large ESS leads to small bias and MSE for bounded functions f. Additionally, the above derivations allow us to interpret the second moment

$$\rho = \mathbf{G}[(NW_1)^2] = \left(\mathbf{G}[NW_1]\right)^2 + \text{Var}\left(NW_1\right) = 1 + \text{Var}\left(NW_1\right) \approx \frac{\text{Var}\left(\hat{\zeta}_{\text{IS}}\right)}{\text{Var}\left(\hat{\zeta}_{\text{MC}}\right)}$$

as the asymptotic relative efficiency of the two estimators, as long as this approximation is valid. In practice, a small ESS can be an indicator that importance sampling with $\mathbf{G}$ may be inadequate. Note that relying solely on the empirical ESS may lead to problems, see the following example. To prepare, we prove a lemma regarding ρ for Gaussian targets and proposals.

Lemma 3.6. *Let $\mathbf{P} = \mathcal{N}(\mu, \Sigma)$ and $\mathbf{G} = \mathcal{N}(\nu, \Omega)$ be two p-dimensional Gaussian distributions with means $\mu, \nu \in \mathbf{R}^p$ and SPD covariance matrices $\Sigma, \Omega \in \mathbf{R}^{p\times p}$. Then ρ is finite if, and only if, $\Omega \succ \frac{1}{2}\Sigma$.*

Proof. For the weights $w = \frac{p}{g}$ we have

$$\begin{aligned}\rho = \mathbf{G}[w^2] &= \int \frac{p^2(x)}{g^2(x)} g(x)\mathrm{d}x = \int \frac{p^2(x)}{g(x)}\mathrm{d}x \\ &= \int \frac{\sqrt{\det \Omega}}{\sqrt{(2\pi)^p}\det \Sigma} \exp\left(-(x-\mu)^T\Sigma^{-1}(x-\mu) + \frac{1}{2}(x-\nu)^T\Omega^{-1}(x-\nu)\right)\mathrm{d}x.\end{aligned}$$

The exponent is a quadratic form in x, and so the integral is finite if, and only if, the matrix of coefficients, $-\Sigma^{-1} + \frac{1}{2}\Omega^{-1}$ is negative definite. Rearranging terms, we see that this is equivalent to $\Omega \succ \frac{1}{2}\Sigma$. □

Example 3.2 (failure of the ESS)**.** Consider the Gaussian scale mixture

$$\mathbf{P} = \frac{1}{2}\left(\mathcal{N}(0,1) + \mathcal{N}(0,\varepsilon^{-2})\right)$$

and proposal $\mathbf{G} = \mathcal{N}(0,1)$. The weights are then given by

$$w(x) = \frac{1}{2}\left(1 + \frac{\varepsilon}{\sqrt{2\pi}}\exp\left(-\frac{x^2}{2}\left(\varepsilon^2 - 1\right)\right)\right)$$

and their second moment w.r.t. $\mathbf{G}$

$$\rho = \int w^2(x)\frac{1}{\sqrt{2\pi}}\exp\left(-\frac{x^2}{2}\right)\mathrm{d}x$$

is finite if, and only if, $\varepsilon^2 > \frac{1}{2}$, by the preceding lemma. Thus, for $\varepsilon^2 \leq \frac{1}{2}$ interpreting the ESS or EF is not sensible. Nevertheless, given samples $X^1, \ldots, X^N \overset{\text{i.i.d}}{\sim} \mathbf{G}$, we may calculate the ESS in the usual way. If N is only moderately large, there is a high probability that most samples do not lie in a region where weights are small, i.e. in the tails of the second component. Thus, unless N is large, the empirical ESS will be large, deceiving us to think that importance sampling with $\mathbf{G}$ is feasible.

We illustrate this by a simulation study, where we calculate the EF $M = 100$ times for different values of N and ε. We used $N = 100, 1\,000, 10\,000$ and $\varepsilon^2 = 0.01, 0.1, 0.5$; the results may be found in Figure 3.2. Notice that for all values of ε considered, we have $\rho = \infty$. We see that even for $N = 1\,000$ and $\varepsilon = \frac{1}{2}$ the upper quartile of EFs is 71%, which seems reasonable to declare importance sampling to perform well.

Let us note that having access to the normalized weights w here allows us to spot this deficiency of the ESS by recognizing that while ESS is high, the weights w are not close to 1, but rather $\frac{1}{2}$.

As an alternative, we may want to assess whether importance sampling has converged through the empirical variance of $\hat{\zeta}_N$,[2] i.e.,

$$\widehat{\mathrm{Var}}\left(\hat{\zeta}_N\right) = \frac{1}{N}\left(\frac{1}{N}\sum_{i=1}^{N} w_i^2 f(X^i)^2 - \hat{\zeta}_N^2\right)$$

is, while seemingly natural, flawed (Chatterjee and Diaconis, 2018). Indeed, the authors show that for any given threshold ϵ we may find an N which only depends on ϵ, such that the probability that the empirical variance exceeds ϵ for this N is small. This is summarized in the following theorem.

Theorem 3.3 (Chatterjee and Diaconis, 2018, Theorem 2.1)**.** *Given any $\epsilon > 0$, there exists $N \leq \epsilon^{-2}2^{1+\epsilon^{-3}}$ such that the following is true. Take any $\mathbf{G}$ and $\mathbf{P}$ as in Theorem 3.2, and any $f : \mathcal{X} \to \mathbf{R}$ such that $\|f\|_{L^2(\mathbf{P})} \leq 1$. Then*

$$\mathbb{P}\left(\widehat{\mathrm{Var}}\left(\hat{\zeta}_N\right) < \epsilon\right) \geq 1 - 4\epsilon.$$

[2] As the following arguments depend on the sample size N, we mark this dependency by adding N to the subscript of the estimator.

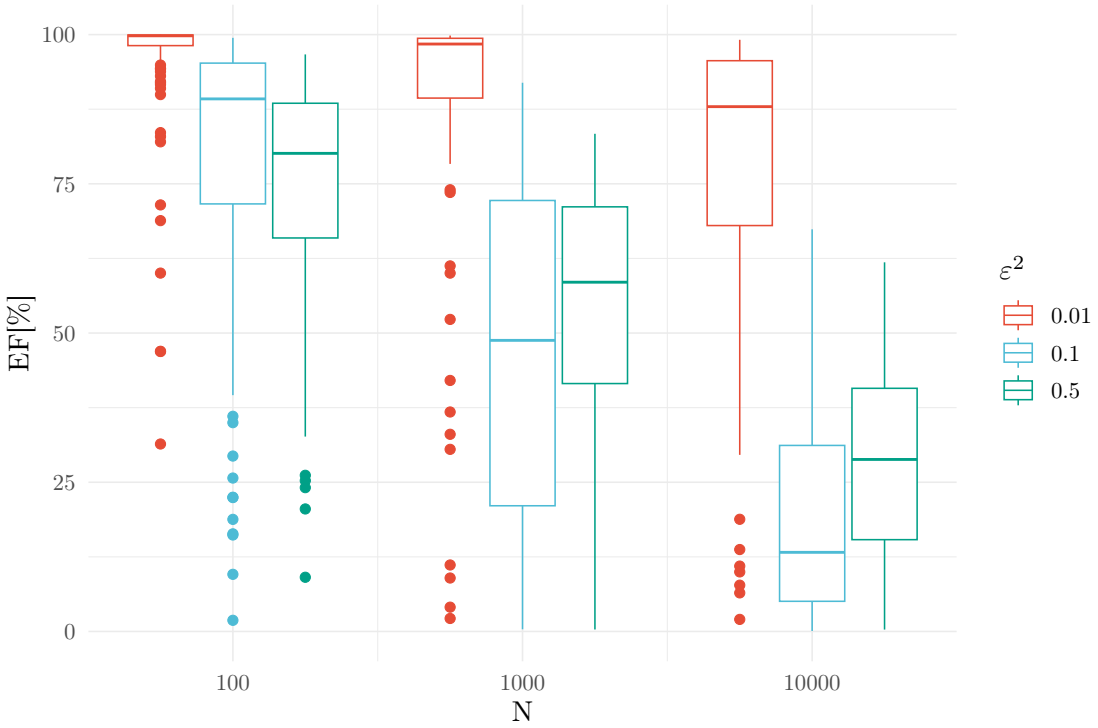

Figure 3.2: Empirical EF for the setup of Example 3.2 for varying sample sizes N and ε^2 and $M = 100$ replications. Here $\mathbf{G} = \mathcal{N}(0,1)$ and $\mathbf{P} = \frac{1}{2}\left(\mathcal{N}(0,1) + \mathcal{N}(0,\varepsilon^{-2})\right)$. In all scenarios the second moment ρ is infinite, thus high EFs are misleading us to believe that importance sampling performs well when it does not.

The problem here is that N does not depend on $\mathbf{G}$ and $\mathbf{P}$, so we may choose $\mathbf{G}$ almost singular to $\mathbf{P}$. As an example, take $\mathbf{P} = \mathcal{N}(0,1)$ and $\mathbf{G} = \mathcal{N}(0,\sigma^2)$ for $\sigma^2 > \frac{1}{2}$. The weights are then given by

$$w(x) = \sigma \exp\left(-\frac{x^2}{2}\left(1 - \frac{1}{\sigma^2}\right)\right),$$

and for $X \sim \mathbf{G}$ the variance of $w(X)X$ is

$$\tau^2 = \operatorname{Var}\left(w(X)X\right) = \frac{\sigma^4}{(2\sigma^2 - 1)^{\frac{3}{2}}} \tag{3.11}$$

which goes to ∞ as σ^2 does. To show Equation (3.11) we calculate the second moment of $w(X)X$,

$$\begin{aligned}
\mathbb{E}(w(X)X)^2 &= \int w(x)^2 x^2 g(x)\,\mathrm{d}x \\
&= \int \sigma^2 \exp\left(-x^2\left(1 - \frac{1}{\sigma^2}\right)\right) x^2 \frac{1}{\sqrt{2\pi\sigma^2}} \exp\left(-\frac{x^2}{2\sigma^2}\right) \mathrm{d}x \\
&= \int \sigma x^2 \frac{1}{\sqrt{2\pi}} \exp\left(-\frac{x^2}{2}\left(2 - \frac{2}{\sigma^2} + \frac{1}{\sigma^2}\right)\right) \mathrm{d}x \\
&= \int \sigma x^2 \frac{1}{\sqrt{2\pi}} \exp\left(-\frac{x^2}{2}\frac{2\sigma^2 - 1}{\sigma^2}\right) \mathrm{d}x \\
&= \nu\sigma \int x^2 \frac{1}{\sqrt{2\pi\nu^2}} \exp\left(-\frac{x^2}{2\nu^2}\right) \mathrm{d}x \\
&= \nu^3\sigma = \frac{\sigma^4}{(2\sigma^2 - 1)^{\frac{3}{2}}}
\end{aligned}$$

where $\nu^2 = \frac{\sigma^2}{2\sigma^2 - 1}$.

Thus, for a pre-specified $\epsilon > 0$, let N be as in Theorem 3.3 and choose σ^2 such that $\operatorname{Var}\left(\hat{\zeta}_N\right) = \frac{\tau^2}{N}$ is larger than, say, 10ϵ. By the preceding theorem, we would, with large probability, observe a small empirical variance and thus declare $\hat{\zeta}_N$ to have converged, whereas, in reality, we would need a sample size that is 100 times as large.

Thus using the empirical variance as a threshold for convergence should be avoided, at least for importance sampling where the weights can be evaluated exactly. For self-normalized importance sampling, the authors do not provide such a theorem. As a remedy (Chatterjee and Diaconis, 2018) suggest the heuristic $q_N = \mathbb{E}Q_N$ where

$$Q_N = \max_{1 \le i \le N} W_i \in [0,1].$$

This judges whether importance sampling has collapsed to just a few particles and is itself amenable to Monte-Carlo integration, by repeatedly sampling N samples from $\mathbf{G}$ and calculating the weights. As this requires multiple runs of importance sampling, it may, however, be prohibitively expensive in practice.

In the following sections, we will predominantly take the position that we are interested in finding a good particle approximation $\hat{\mathbf{P}}_N$ of the form Equation (3.7) over finding the optimal proposal $\mathbf{G}^*$ from Proposition 3.1 and assume that the importance sampling weights can only be evaluated up to a constant. This has several reasons: First of all, for most problems considered in this thesis $\mathbf{P}$ is usually a conditional distribution, e.g. $\mathbf{P} = \mathbb{P}^{X|Y=y}$ for states X and observations Y in the SSM context. Should the appropriate densities exist, evaluating the weights amounts to calculating

$$\frac{\mathrm{d}\mathbb{P}^{X|Y=y}}{\mathrm{d}\mathbf{G}}(x) = \frac{p(x|y)}{g(x)} = \frac{p(y|x)p(x)}{g(x)p(y)} \propto \frac{p(y|x)p(x)}{g(x)}.$$

In these situations $p(y) = \int p(x,y)\,\mathrm{d}x$ is usually intractable. For $\mathbf{G}^*$ we are in the same situation, where the evaluation of the integration constant $\mathbf{P}|f|$ is infeasible, but the density $|f(x)|p(x)$

is available. Second, focusing on the particle approximation allows us to consider multiple test functions f, e.g. focus on different marginals of $\mathbf{P}$, which is usually what practitioners are interested in. Finally, this allows us to simplify the notation used in this thesis. $\mathbf{P}$ will always be the probability measure of interest and $\mathbf{G}$ the proposal. In later parts of this thesis, we will predominantly perform Gaussian importance sampling, i.e. $\mathbf{G} = \mathcal{N}(\mu, \Sigma)$, hence a handy mnemonic is to think of $\mathbf{G}$ as a **G**aussian proposal.

Let us now turn towards the problem of finding a good proposal $\mathbf{G}$ for a given $\mathbf{P}$.

3.3.1 Laplace approximation (LA)

The Laplace approximation (LA) goes back to Laplace (Laplace, 1986) who invented the technique to approximate moments of otherwise intractable distributions. Since (Tierney and Kadane, 1986; Tierney, Kass, and Kadane, 1989) rediscovered its use to approximate posterior means and variances, it has been a staple method for approximate inference. The method is based on a second-order Taylor series expansion of the log target density $\log p(x)$ around its mode $\hat{x}$, i.e. matching mode and curvature. Assuming the density is sufficiently smooth, we have

$$\log p(x) \approx \log p(\hat{x}) + \underbrace{\nabla_x \log p(\hat{x})}_{=0} (x - \hat{x}) + \frac{1}{2}(x - \hat{x})^T H (x - \hat{x}) \tag{3.12}$$

where H is the Hessian of $\log p$ evaluated at $\hat{x}$. As $\log p(\hat{x})$ does not depend on x, the right-hand side can be seen (up to additive constants) as the density of a Gaussian distribution with mean $\hat{x}$ and covariance matrix $\Sigma = -H^{-1}$. Thus using $\mathbf{G} = \mathcal{N}(\hat{x}, -H^{-1})$ as a proposal in importance sampling seems promising. If $\hat{x}$ is the unique global mode of p and H is negative definite, the LA yields an actual Gaussian distribution. To obtain the LA in practice, a Newton-Raphson scheme may be used, which conveniently tracks H as well. Furthermore, if $\mathbf{P}$ includes more structure, e.g. it is the smoothing density in the SSM context, we may be able to exploit this structure to design efficient Newton-Raphson schemes, see Section 3.5.1.

The main advantage of the LA is that it is usually fast to obtain and, for sufficiently well-behaved distributions on a moderate dimensional space, provides reasonably high ESS. Additionally, the Newton-Raphson iterations to find the mode and Hessian are robust and require no simulation, unlike the other methods discussed further below. For the SSMs we consider in this thesis, the numerical methods can be implemented using the Kalman filter and smoother (Durbin and Koopman, 1997; Shephard and Pitt, 1997), even in the degenerate case where H is indefinite (Jungbacker and Koopman, 2007), see also Section 3.5.1.

However, as the LA is a local approximation, it may be an inappropriate description of the global behavior of the target, see Example 3.3 for a breakdown of LA, and the simulation studies presented in Section 3.7. Additionally, even if the LA works in principle, its ESS will usually degenerate quickly once the dimension increases whereas the Cross-Entropy method (CE-method) and Efficient Importance Sampling (EIS) do so at a slower pace.

3.3.2 The Cross-Entropy method (CE-method)

Recall from our discussion surrounding Theorem 3.2 that a small KL-divergence between the target $\mathbf{P}$ and the proposal $\mathbf{G}$ implies good performance for importance sampling. As the KL-divergence depends on global properties of $\mathbf{P}$, i.e. the Radon-Nikodym derivative $\frac{\mathrm{d}\mathbf{P}}{\mathrm{d}\mathbf{G}}$, minimizing it leads to a global approximation of $\mathbf{P}$, improving on the local-approximation provided by the LA.

The Cross-Entropy method (CE-method) (Rubinstein, 1999; Rubinstein and Kroese, 2004) implements this idea and selects from a parametric family $(\mathbf{G}_\psi)_{\psi \in \Psi}$ of proposals the one that minimizes the Kullback Leibler divergence (KL-divergence) to the target. Here Ψ is usually a subset of $\mathbf{R}^k$, which may be open, closed or neither. Thus, the CE-method aims at solving the following optimization problem

$$\min_{\psi \in \Psi} \mathcal{D}_{\mathrm{KL}} \left(\mathbf{P} || \mathbf{G}_\psi \right),$$

for the optimal ψ_{CE}, should the minimum exist. The existence and uniqueness of ψ_{CE} will depend heavily on the choice of parametric family $(\mathbf{G}_\psi)_{\psi\in\Psi}$ and $\mathbf{P}$.

We will assume the existence of a common dominating measure μ for both $\mathbf{P}$ and all $\mathbf{G}_\psi$, $\psi \in \Psi$ with corresponding densities p and g_ψ, $\psi \in \Psi$. The importance sampling weights are then given by

$$w_\psi(x) = \frac{p(x)}{g_\psi(x)},$$

$x \in \mathcal{X}$, or, if at least one of p and g_ψ is only available up to a constant, by

$$\tilde{w}_\psi(x) \propto \frac{p(x)}{g_\psi(x)}.$$

If the dependence on ψ is not of interest or the particular ψ is obvious from the context, we may drop the subscript.

The KL-divergence is given by

$$\mathcal{D}_{\text{KL}}\left(\mathbf{P}||\mathbf{G}_\psi\right) = \mathbf{P}\left[\log w_\psi\right],$$

and can be infinite, e.g. if $\mathbf{P}$ does not possess second moments and $\mathbf{G}_\psi$ are Gaussian distributions. If the KL-divergence is infinite for all $\psi \in \Psi$, the CE-method becomes uninteresting. As such we will require that the KL-divergence is finite for at least one $\psi \in \Psi$, and restrict Ψ, without loss of generality, to those ψ where the KL-divergence is finite.

As the densities w.r.t. a common dominating measure exist, we may reformulate the optimization problem to maximize the cross-entropy between p and g_ψ instead:

$$\begin{aligned}\operatorname{argmin}_{\psi\in\Psi} \mathcal{D}_{\text{KL}}\left(\mathbf{P}||\mathbf{G}_\psi\right) &= \operatorname{argmin}_{\psi\in\Psi} \mathbf{P}\left[\log p\right] - \mathbf{P}\left[\log g_\psi\right] \\ &= \operatorname{argmax}_{\psi\in\Psi} \mathbf{P}\left[\log g_\psi\right].\end{aligned} \tag{3.13}$$

As the KL-divergence is non-negative by the information inequality, the cross-entropy $\mathbf{P}\left[\log g_\psi\right]$ is bounded from above by the differential entropy of $\mathbf{P}$, $\mathbf{P}[\log p]$. For centered distributions with covariance matrix Σ the differential entropy is bounded above by the maximum entropy distribution in this setting, the Gaussian $\mathcal{N}(0,\Sigma)$ (Cover and Thomas, 2006, Example 12.2.8). Thus, if second moments of $\mathbf{P}$ exist, the cross-entropy is bounded from above, and so a maximizer exists if the supremum over Ψ is attained. This would be the case if Ψ is compact and $\psi \mapsto \mathbf{P}[\log g_\psi]$ is continuous, however compact Ψ is too restrictive for our purposes. Instead, we are going to focus on more realistic assumptions.

Suppose now that $\psi \mapsto \log g_\psi(x)$ is (strictly) concave for $\mathbf{P}$-almost every $x \in \mathcal{X}$ and Ψ is a convex subset of $\mathbf{R}^k$. Then $\psi \mapsto \mathbf{P}\left[\log g_\psi\right]$ is (strictly) concave as well. As a consequence, we may apply the usual results from convex optimization, i.e. every local maximum is a global one and if $\psi \mapsto \log g_\psi(x)$ is strictly convex for $\mathbf{P}$-almost every x, there is at most one maximizer (Bazaraa, Sherali, and Shetty, 2006, Theorem 3.4.2).

As we have seen in Lemma 3.3, the densities of exponential families are log-concave in the natural parameter, and as such they will be the primary candidates for our investigations of the CE-method. If we use proposals from an exponential family, we may get rid of the base measure term $h(x)$ in the densities, as the following lemma shows.

Lemma 3.7. *Let $\mathbf{P}$ be a probability measure on $\mathcal{X} = \mathbf{R}^p$ and let $(\mathbf{G}_\psi)_{\psi\in\Psi}$ be a natural exponential family on $\mathcal{X}$ such that $\mathbf{P} \ll \mathbf{G}_\psi$ for all $\psi \in \Psi$. Let μ be the dominating measure of the exponential family, such that*

$$\frac{\mathrm{d}\mathbf{G}_\psi}{\mathrm{d}\mu}(x) = \frac{h(x)}{Z(\psi)} \exp\left(\psi^T T(x)\right),$$

with $h \geq 0$ μ-a.s.

Then $h\mu$ is a dominating measure for both $\mathbf{P}$ and $\mathbf{G}_\psi$ for every ψ in Ψ.

Proof. Let $A \subseteq \mathbf{R}^p$ be measurable. As h is a.s. non-negative, $(h\mu)(A) = 0$ implies that $h\mathbf{1}_A = 0$ μ-a.s. Thus $\mathbf{G}_\psi(A) = \int \mathbf{1}_A(x) \frac{h(x)}{Z(\psi)} \exp(\psi^T T(x)) \, \mathrm{d}\mu = 0$ for all ψ as well. As $\mathbf{G}_\psi \gg \mathbf{P}$ and $\gg$ is transitive, $h\mu$ dominates $\mathbf{P}$ as well. □

As a consequence, when performing importance sampling with target $\mathbf{P}$ and proposal $\mathbf{G}_\psi$ from an exponential family, we will assume in the following that $h \equiv 1$, achieved by taking $h\mu$ as the joint dominating measure.

An additional attractive property of the CE-method for exponential families with natural parameter $\psi \in \mathbf{R}^k$ is that the optimal ψ_{CE} only depends on the expected value $\mathbf{P}[T]$. We first show, that if the covariance of the sufficient statistic is positive definite, the expected value of T under $\mathbf{G}_\psi$ uniquely determines $\psi \in \Psi$, see also (Brown, 1986, Corollary 2.5) for a similar result in minimal exponential families.

Lemma 3.8. *Let $(\mathbf{G}_\psi)_{\psi \in \Psi}$ form a k-dimensional natural exponential family with log-densities*

$$\log g_\psi(x) = \psi^T T(x) - \log Z(\psi),$$

and convex parameter space $\Psi \subseteq \mathbf{R}^k$. Let $\psi, \psi' \in \operatorname{int} \Psi$ with $\mathbf{G}_\psi[T] = \mathbf{G}_{\psi'}[T]$. If $\operatorname{Cov}_{\mathbf{G}_\psi} T$ is positive definite, then ψ and ψ' coincide.

Proof. Consider the function $b : \Psi \to [-\infty, \infty)$

$$\xi \mapsto b(\xi) = \mathbf{G}_{\psi'}[\log g_\xi] = \xi^T \mathbf{G}_{\psi'}[T] - \log Z(\xi).$$

By Theorem 3.1, $\mathbf{G}_{\psi'}[T]$ is finite and b possesses derivatives of every order. Then ψ is a critical point of this map, as the gradient at ψ is

$$\mathbf{G}_{\psi'}[T] - \nabla_\psi \log Z(\psi) = \mathbf{G}_{\psi'}[T] - \mathbf{G}_\psi[T] = 0.$$

The Hessian of this function at ξ is, see Theorem 3.1,

$$-H_\xi \log Z(\xi) = -\operatorname{Cov}_{\mathbf{G}_\xi}[T],$$

which is negative semi-definite, so b is concave. At $\xi = \psi$ it is negative definite, so the critical point ψ is a strict local maximum. By concavity, it is the unique global maximum, and thus the unique critical point, so $\psi = \psi'$. □

Proposition 3.2 (The CE-method for exponential families)**.** *Let $(\mathbf{G}_\psi)_{\psi \in \Psi}$ form a k-dimensional natural exponential family with log-densities*

$$\log g_\psi(x) = \psi^T T(x) - \log Z(\psi),$$

and convex parameter space $\Psi \subseteq \mathbf{R}^k$. Suppose $T \in L^1(\mathbf{P})$.

If there is a $\psi_{CE} \in \Psi$ such that

$$\mathbf{P}[T] = \mathbf{G}_{\psi_{CE}}[T],$$

then ψ_{CE} is a maximizer of Equation (3.13). Furthermore, if $\operatorname{Cov}_{\mathbf{G}_{\psi_{CE}}} T$ is positive definite the maximizer is unique.

Proof. The target may be rewritten as

$$\psi \mapsto f(\psi) = \mathbf{P}\left[\log g_\psi(x)\right] = -\log Z(\psi) + \psi^T \mathbf{P}[T].$$

As $\log Z(\psi)$ is the cumulant-generating function of $\mathbf{G}_\psi$ it is twice differentiable, and so is f. The gradient of $\log Z(\psi)$ is

$$\nabla_\psi \log Z(\psi) = \mathbf{G}_\psi[T]$$

and its Hessian is

$$H_\psi \log Z(\psi) = \operatorname{Cov}_{\mathbf{G}_\psi}(T)$$

the covariance of T under $\mathbf{G}_\psi$. Thus the Hessian of f is

$$H_\psi f = -\operatorname{Cov}_{\mathbf{G}_\psi}(T),$$

which is negative-semi-definite. Therefore f is concave, and any local maximizer ψ is a global maximizer. The gradient of f is

$$\nabla_\psi f(\psi) = \mathbf{P}[T] - \mathbf{G}_\psi[T],$$

which is equal to 0 if, and only if, ψ solves

$$\mathbf{P}[T] = \mathbf{G}_\psi[T].$$

Uniqueness follows from the preceding Lemma 3.8. □

As a consequence, the CE-method for natural exponential families reduces to matching the moments of the sufficient statistic of the target and proposal. In many cases, this system of equations can be solved analytically or by gradient descent algorithms. Let us discuss the assumptions and applicability of this proposition. Assuming that $T \in L^1(\mathbf{P})$ is necessary for the target to be finite, it cannot be dropped. As T typically consists of polynomial, rational or exponential functions, this is not too restrictive, provided the target does not exhibit heavy tails. The proof of uniqueness relies on $\operatorname{Cov}_{\mathbf{G}_\psi} T$ being positive definite, to ensure that $\psi \mapsto \log Z(\psi)$ is strictly convex. This could also be achieved by requiring the exponential family to be minimal, see (Brown, 1986, Theorem 1.13 (iv)). The existence of a ψ such that $\mathbf{P}[T] = \mathbf{G}_\psi[T]$ is not restrictive for most commonly used distributions: for the (multivariate) normal, Poisson, negative binomial and binomial distribution there is always a unique solution, as the sufficient statistics consist of means and covariances.

While $\mathbf{P}[T]$ is usually not available, it is itself amenable to importance sampling. Given a proposal $\mathbf{G}$ we may estimate $\mathbf{P}[T]$ by $\hat{\mathbf{P}}_N T = \sum_{i=1}^N W^i T(X^i)$ for $X^1, \dots, X^N \overset{\text{i.i.d}}{\sim} \mathbf{G}$ and auto-normalized importance sampling weights W^i and in turn, applying Proposition 3.2, estimate ψ_{CE} by $\hat{\psi}_{\text{CE}}$ solving

$$\hat{\mathbf{P}}_N[T] = \mathbf{G}_{\hat{\psi}_{\text{CE}}}[T]. \tag{3.14}$$

As $T \in L^1(\hat{\mathbf{P}}_N)$, the only conditions we have to check to apply the above proposition are that this equation has a unique solution $\mathbf{G}$-almost surely in the interior of Ψ and that Ψ is convex.

To apply the CE-method in practice, one usually iterates the sampling and estimation steps, using the previously found $\hat{\psi}_{\text{CE}}$ to sample in the current iteration and starting the iteration with a proposal from the same exponential family $\mathbf{G} = \mathbf{G}_{\psi^0}$. To ensure numerical convergence, a popular device is that of common random numbers (CRNs), i.e. using the same random number seed in all iterations. A basic version of the CE-method is presented in Algorithm 4.

Algorithm 4 The basic CE-method algorithm for exponential families

Require: exponential family $(\mathbf{G}_\psi)_{\psi\in\Psi}$, initial ψ^0, sample size N, unnormalized weights $\tilde{w}$
1: set $l = 0$
2: store random number seed
3: **repeat**
4: restore random number seed
5: sample $X^1, \dots, X^N \sim \mathbf{G}_{\psi^l}$
6: calculate self-normalized weights W^i for $i = 1, \dots, N$
7: estimate $\hat{\psi}_{\text{CE}}$ ▷ Equation (3.14)
8: set $\psi^{l+1} = \hat{\psi}_{\text{CE}}$
9: set $l = l + 1$
10: **until** $\hat{\psi}^l$ converged
11: **return** $\hat{\psi}_{\text{CE}} = \hat{\psi}^l$

The CE-method is routinely used for estimating failure probabilities for rare events (Homem-de-Mello, 2007) and has been applied to Bayesian posterior inference (Ehre et al., 2023; Engel et al.,

2023), Bayesian marginal likelihood estimation (Chan and Eisenstat, 2012) and optimal control problems (Kappen and Ruiz, 2016; Zhang et al., 2014). Importance sampling is well known to exhibit the curse of dimensionality (COD) (Bengtsson, Bickel, and B. Li, 2008), i.e. the phenomenon that in many problems, unless N grows exponentially with the dimension of $\mathcal{X}$, the weights collapse to a single particle, i.e. $W^{(N)} \to 1$ as the dimension of $\mathcal{X}$ goes to ∞. As the CE-method employs importance sampling to obtain $\hat{\psi}_{\text{CE}}$, it too is affected by this phenomenon, see also Section 3.7. The screening method (Rubinstein and Glynn, 2009) deals with the COD by keeping components of ψ^l that vary too much from iteration to iteration fixed, in essence reducing the dimension of Ψ. Alternatively, the improved cross-entropy method (Chan and Kroese, 2012) suggests generating approximately independent samples from $\mathbf{P}$ by, e.g., MCMC-methods, and replacing the importance sampling version of $\hat{\mathbf{P}}_N$ in Equation (3.14) by the actual empirical distribution. Still, in high dimensions both of these approaches may be difficult to implement: the screening method may not move far from the initial proposal and MCMC-methods are expensive in high dimensions.

As stated in (Chan and Kroese, 2012) there may be two reasons as to why the CE-method fails: either the parametric family is not rich enough to give a good approximation to $\mathbf{P}$, i.e. $\mathcal{D}_{\text{KL}}(\mathbf{P}||\mathbf{G}_{\psi_{\text{CE}}})$ is still large, or the estimate $\hat{\psi}_{\text{CE}}$ fails to be close to ψ_{CE}. As our simulation studies Section 3.7 suggest, the reason for the degeneracy seems to be the latter. It will thus be beneficial to investigate the asymptotic behavior of $\hat{\psi}_{\text{CE}}$.

In the remainder of this section, we will derive novel results on the performance of the estimator $\hat{\psi}_{\text{CE}}$ of ψ_{CE}. In particular, we will investigate under which conditions $\hat{\psi}_{\text{CE}}$ is consistent and asymptotically normal. To focus on the asymptotic behavior, we will only perform a single iteration of the basic CE-method algorithm (Algorithm 4). While we restrict ourselves here to the setting of k-dimensional natural exponential families, these results should generalize to other classes of distributions as well. The advantage that this class of families has is that due to the structure of the densities, they provide straightforward (regularity) conditions for the asymptotic results to hold. As the target functions are concave, these conditions are rather liberal. We start with proving the consistency of $\hat{\psi}_{\text{CE}}$.

Theorem 3.4 (consistency of $\hat{\psi}_{\text{CE}}$)**.** *Adopt the same assumptions as in Proposition 3.2. Furthermore, let $\mathbf{G} \gg \mathbf{P}$ be a proposal distribution and assume that*

(i) ψ_{CE} is the unique maximizer of Equation (3.13),

(ii) ψ_{CE} is in the interior of the convex parameter space Ψ.

Then $\hat{\psi}_{CE}$ is a strongly consistent estimator of ψ_{CE}.

The proof is based on the following theorem of Haberman.

Theorem 3.5 ((Haberman, 1989, Theorem 5.1)[3])**.** *Let $\Psi \subseteq \mathbf{R}^k$, $\mathcal{X}$ a separable, complete metric space and $b_{\mathcal{X}} : \mathcal{X} \times \mathbf{R}^k \to [-\infty, \infty)$ such that for every $x \in \mathcal{X}$ the function*

$$b(x, \cdot) : \mathbf{R}^k \to [-\infty, \infty), \psi \mapsto b(x, \psi)$$

is concave. Let $\mathbf{P}$ be a probability measure on $\mathcal{X}$ such that $\mathbf{P}[b(\cdot, \psi)] < \infty$ for all $\psi \in \mathbf{R}^k$. Assume that $\psi^* \in \Psi$ is the unique maximizer of

$$b_{\Psi} : \Psi \to [-\infty, \infty), \psi \mapsto \mathbf{P}[b(\cdot, \psi)].$$

Let $(X^i)_{i \in \mathbf{N}} \overset{i.i.d}{\sim} \mathbf{P}$ be a sequence of i.i.d. random variables with distribution $\mathbf{P}$ and let for $N \in \mathbf{N}$ let

$$\hat{\mathbf{P}}_N = \frac{1}{N} \sum_{i=1}^{N} \delta_{X^i}$$

be their empirical distribution. Let $\left(\hat{\psi}_N\right)_{N \in \mathbf{N}}$ be a sequence of M-estimators, i.e. a sequence of maximizers of

$$\hat{b}_{\Psi} : \Psi \to [-\infty, \infty), \psi \mapsto \hat{\mathbf{P}}_N[b(\cdot, \psi)].$$

[3]Note that while the actual theorem assumes conditions 1,2,5 and 6 in the paper, C3 as stated here implies conditions 5 and 6, see also the discussion in Sections 2.3 and 2.4 in (Haberman, 1989).

Assume that the following conditions hold:

(C1) For some closed set V, ψ^* is in the interior of V and $\Psi \cap V$ is closed.

(C2) ψ^* is the unique maximizer of

$$b_{\mathrm{cl}(\Psi)} : \mathrm{cl}(\Psi) \to [-\infty, \infty), \psi \mapsto \mathbf{P}[b(\cdot, \psi)],$$

where cl *denotes the closure of Ψ in $\mathbf{R}^k$.*

(C3) Ψ is convex and b_Ψ is finite on a nonempty open set.

Then

$$\hat{\psi}_N \overset{N\to\infty}{\longrightarrow} \psi^*$$

$\mathbf{P}$-almost surely, so $\hat{\psi}_N$ is strongly consistent.

The assumptions of this theorem ensure that the unique optimum is in the interior of Ψ and "well-separated" from its boundary, so there are no additional maximizers on the boundary. In this case, concavity of $b(x, \psi)$ together with the law of large numbers yield uniform convergence of $\hat{\mathbf{P}}_N[b(\cdot, \psi)] \to \mathbf{P}[b(\cdot, \psi)]$ on compacta and thus also for $\hat{\psi}_N$, see (Haberman, 1989, pp. 1652).

To apply this theorem to our setting, let us begin by extending it to incorporate importance sampling.

Proposition 3.3. *Assume that the conditions of Theorem 3.5 are fulfilled and let $\mathbf{G} \gg \mathbf{P}$ be another probability measure with Radon-Nikdoym derivative $w(x) = \frac{\mathrm{d}\mathbf{P}}{\mathrm{d}\mathbf{G}}(x)$. Let $(X^i)_{i\in\mathbf{N}} \overset{i.i.d}{\sim} \mathbf{G}$ and consider the particle approximations*

$$\tilde{\mathbf{P}}_N = \frac{1}{N}\sum_{i=1}^{N} w(X^i)\delta_{X^i},$$
$$\hat{\mathbf{P}}_N = \sum_{i=1}^{N} W^i \delta_{X^i},$$

and suppose for every $N \in \mathbf{N}$ there exist M-estimators

$$\tilde{\psi}_N \in \mathrm{argmax}_{\psi\in\Psi}\, \tilde{\mathbf{P}}_N\left[b(\cdot, \psi)\right],$$
$$\hat{\psi}_N \in \mathrm{argmax}_{\psi\in\Psi}\, \hat{\mathbf{P}}_N\left[b(\cdot, \psi)\right].$$

Then both $\tilde{\psi}_N$ and $\hat{\psi}_N$ are strongly consistent estimators of ψ^*.

Proof. Define a new objective function $\tilde{b} : \mathcal{X} \times \mathbf{R}^k \to [-\infty, \infty)$ by

$$\tilde{b}(x, \psi) = w(x)b(x, \psi).$$

Then $\mathbf{G}\left[\tilde{b}(\cdot, \psi)\right] = \mathbf{P}\left[b(\cdot, \psi)\right]$ for all $\psi \in \Psi$, and so ψ^* is the unique global maximum of

$$\psi \mapsto \mathbf{G}\left[\tilde{b}(\cdot, \psi)\right].$$

As $\mathbf{G}[\tilde{b}(\cdot, \psi)] = \mathbf{P}[b(\cdot, \psi)] < \infty$ and for fixed $x \in \mathcal{X}$ $\tilde{b}(x, \cdot) = w(x)b(x, \cdot)$ is concave, we may directly apply Theorem 3.5 to $\tilde{\psi}_N$, showing its strong consistency.

For $\hat{\psi}_N$, notice that for a fixed sample $X^1, \ldots, X^N \overset{\text{i.i.d}}{\sim} \mathbf{G}$ and any function $f : \mathcal{X} \to [-\infty, \infty)$ we have, a.s.,

$$\hat{\mathbf{P}}_N[f] = \sum_{i=1}^{N} W^i f(X^i) = \frac{\mathbf{G}[\tilde{w}]}{\sum_{i=1}^{N}\tilde{w}(X^i)} \sum_{i=1}^{N} \frac{\tilde{w}(X^i)}{\mathbf{G}[\tilde{w}]} f(X^i) = \frac{\mathbf{G}[\tilde{w}]}{\sum_{i=1}^{N}\tilde{w}(X^i)} \tilde{\mathbf{P}}_N[f] \propto \tilde{\mathbf{P}}_N[f],$$

where $\tilde{w}$ are the unnormalized weights, i.e. $\frac{\tilde{w}(x)}{\mathbf{G}[\tilde{w}]} = w(x), x \in \mathcal{X}$. Thus $\hat{\psi}_N$ maximizes $\tilde{\mathbf{P}}_N[b(\cdot, \psi)]$ as well, and the result follows from the consistency of $\tilde{\psi}_N$. □

Let us now prove the promised consistency of the CE-method.

Proof (Theorem 3.4). We show that the assumptions of Theorem 3.5 are fulfilled. Let

$$b : \mathbf{R}^p \times \mathbf{R}^k \to [-\infty, \infty) \qquad b(x, \psi) = \begin{cases} \log g_\psi(x) & \psi \in \Psi, \\ -\infty & \text{else.} \end{cases}$$

As Ψ is convex and $g_\psi(x)$ is log-concave (see Lemma 3.3), $b(x, \cdot)$ is concave. Let $X^1, \dots, X^N \overset{\text{i.i.d}}{\sim} \mathbf{P}$ and let $\tilde{\mathbf{P}}_N = \frac{1}{N} \sum_{i=1}^N \delta_{X^i}$. For $\psi \in \Psi$ we have

$$\mathbf{P}[b(\cdot, \psi)] = \psi^T \mathbf{P}[T] - \log Z(\psi) < \infty,$$

as $T \in L^1(\mathbf{P})$, while for $\psi \notin \Psi$ this integral is $-\infty$. Thus we only have to check that (C1)-(C3) are fulfilled.

For condition (C1) note that, as ψ_{CE} is in the interior of Ψ, we may choose $\varepsilon > 0$ such that the closed ε ball around ψ_{CE}, $\bar{B}_\varepsilon(\psi_{\text{CE}})$ is completely contained in Ψ, so letting $V = \bar{B}_\varepsilon(\psi_{\text{CE}})$ implies the condition. Condition (C2) is fulfilled by the definition of b and condition (C3) is fulfilled by considering the neighborhood of ψ_{CE} that is assumed to be contained in Ψ. Finally, by Proposition 3.3, $\hat{\psi}_{\text{CE}}$ is strongly consistent. □

The assumptions on ψ_{CE} and Ψ in Theorem 3.4 could be somewhat looser, as the concavity of the target function is a rather strong property. In natural exponential families,

$$\Psi = \left\{ \psi \in \mathbf{R}^k \,:\, Z(\psi) < \infty \right\}$$

is always convex so this is not a strong restriction. In regular exponential families, Ψ is open and so only the existence and uniqueness of ψ_{CE} are required. Uniqueness may be attained, e.g., by Lemma 3.8. It will also hold if the exponential family considered is minimal (Brown, 1986, Corollary 2.5). Existence is a matter of correctly specifying the exponential family. For example, in Section 3.5.2 we will exploit the Markov structure of targets to restrict ourselves to Gaussian Markov processes for $(\mathbf{G}_\psi)_{\psi \in \Psi}$.

Not only is $\log g_\psi$ concave, but it also possesses derivatives of any order, at least on the interior of Ψ. Indeed, its Hessian is given by the inverse of the Fisher-information matrix $I(\psi)^{-1}$:

$$H_\psi \log g_\psi = -H_\psi \log Z(\psi) = -\operatorname{Cov}_{\mathbf{G}_\psi}(T) = -I(\psi)^{-1}.$$

These rather strong properties enable us to derive a central limit theorem for the CE-method with natural exponential family proposals under quite liberal conditions.

Theorem 3.6 (CLT for $\hat{\psi}_{\text{CE}}$)**.** *Adopt the same assumptions as in Proposition 3.2. Furthermore, let $\mathbf{G} \gg \mathbf{P}$ be a proposal distribution with weights $w = \frac{\mathrm{d}\mathbf{P}}{\mathrm{d}\mathbf{G}}$ and assume that*

(i) $\psi_{CE} \in \Psi$ is the unique maximizer of Equation (3.13) which lies in the interior of the convex parameter space Ψ,

(ii) the Fisher information matrix $I(\psi_{CE})$ exists and is positive definite,

(iii) $w, wT \in L^2(\mathbf{G})$, and

(iv) $T \in L^2(\mathbf{P})$.

Then

$$\sqrt{N}(\hat{\psi}_{CE} - \psi_{CE}) \xrightarrow{\mathcal{D}} \mathcal{N}(0, BMB)$$

where $B = I(\psi_{CE}) = \operatorname{Cov}_{\mathbf{G}_{\psi_{CE}}}(T)^{-1}$ and

$$M = \operatorname{Cov}_{\mathbf{G}}(wT) = \mathbf{G}\left[w^2 (T - \mathbf{P}[T])(T - \mathbf{P}[T])^T\right] = \mathbf{P}\left[w (T - \mathbf{P}[T])(T - \mathbf{P}[T])^T\right].$$

To prove Theorem 3.6, let us start again with a general version of a central limit theorem for M-estimators based on concave objective functions.

Theorem 3.7 ((Haberman, 1989, Theorem 6.1)[4]). *Consider the same setting as in Theorem 3.5. Assume further that ψ^* lies in the interior of Ψ and that the following conditions hold:*

(C7) The Hessian $H_\psi \mathbf{P}\left[b(\cdot, \psi^*)\right]$ exists and is non-singular.

(C10) For $X \sim \mathbf{P}$ and some neighborhood V of ψ^*

$$\sigma^2(\psi, \xi) = \mathbb{E}\left(b'(X, \psi, \xi)\right)^2 < \infty \qquad \psi \in V, \xi \in \mathbf{R}^k,$$

where $b'(x, \psi, \xi) = \lim_{a \downarrow} a^{-1}\left(b(x, \psi + a\xi) - b(x, \psi)\right)$ is the directional derivative. Note that if b is differentiable for all $\psi \in V$, $b'(x, \psi, \xi) = \xi^T \nabla_\psi b(x, \psi)$ and it suffices to assume $(\nabla_\psi b(x, \psi))_i (\nabla_\psi b(x, \psi))_j \in L^1(\mathbf{P})$ for all $\psi \in N$ and $i, j = 1, \ldots, k$.

Let $M = \mathrm{Cov}\left(\nabla_\psi b(X, \psi)\right)$ and let $B = -\left(H_\psi \mathbf{P}\left[b(\cdot, \psi)\right]\right)^{-1}$. Then

$$\sqrt{N}\left(\hat{\psi}_N - \psi\right) \xrightarrow{\mathcal{D}} \mathcal{N}(0, BMB). \tag{3.15}$$

Similar to the consistency result above (Proposition 3.3), we need to extend this CLT to account for importance sampling.

Proposition 3.4. *Assume that the conditions of Theorem 3.7 are fulfilled and use the same notation as in Proposition 3.3. Furthermore, assume that*

(i) $w(\cdot) b'(\cdot, \psi, \xi) \in L^2(\mathbf{G})$ in a neighborhood N of ψ^* for all $\xi \in \mathbf{R}^k$.

Then

$$\sqrt{N}\left(\tilde{\psi}_N - \psi^*\right) \xrightarrow{\mathcal{D}} \mathcal{N}(0, BMB), \tag{3.16}$$

where $M = \mathrm{Cov}\left(w(X) \nabla_\psi b(X, \psi^*)\right)$ for $X \sim \mathbf{G}$ and $B = -\left(H_\psi \mathbf{P}\left[b(\cdot, \psi^*)\right]\right)^{-1}$ is as in Theorem 3.7. Additionally

$$\sqrt{N}\left(\hat{\psi}_N - \psi^*\right) \xrightarrow{\mathcal{D}} \mathcal{N}(0, BMB). \tag{3.17}$$

Proof. Similar to the proof of Proposition 3.3, define the new objective function $\tilde{b} : \mathcal{X} \times \mathbf{R}^k \to [-\infty, \infty)$ by

$$\tilde{b}(x, \psi) = w(x) b(x, \psi),$$

and notice that $\mathbf{G}\left[\tilde{b}(\cdot, \psi)\right] = \mathbf{P}\left[b(\cdot, \psi)\right]$. Let us verify the conditions of Theorem 3.7 for $\tilde{b}$ and the probability measure $\mathbf{G}$.

For condition (C7), as $H_\psi \mathbf{P}[b(\cdot, \psi)]$ exists and is non-singular, so does

$$H_\psi \mathbf{G}[\tilde{b}(\cdot, \psi)] = H_\psi \mathbf{P}[b(\cdot, \psi)]$$

exist and is non-singular. Similarly, it is easy to see that $\tilde{b}'(x, \psi, \xi) = w(x) b'(x, \psi, \xi)$ and so for $X \sim \mathbf{G}$

$$\sigma^2_{\tilde{b}}(\psi, \xi) = \mathbb{E}\left(\tilde{b}'(X, \psi, \xi)\right)^2 = \mathbb{E} w^2(X) b'(X, \psi, \xi)^2 < \infty$$

by assumption (i), showing condition (C10). Thus we may apply Theorem 3.7 to $\tilde{b}$ and $\mathbf{G}$, finishing the proof. □

Interestingly, importance sampling only affects the M component of the asymptotic variance. The reason for this is that M is a quadratic function of the weights w, while B only depends linearly on w, allowing to switch integrators from $\mathbf{G}$ to $\mathbf{P}$. We now have all the tools at our disposal to proof Theorem 3.6.

[4] Note, again, that the original theorem is based on conditions 7,8,9 in the paper. However, under (C7), condition (C10) implies conditions 8 and 9 in the paper. See the discussion in Section 3.1 in (Haberman, 1989).

Proof of Theorem 3.6. We show that the assumptions and conditions of Theorem 3.7 for the objective function $b : \mathcal{X} \times \mathbf{R}^k \to [-\infty, \infty)$

$$b(x, \psi) = \begin{cases} \log g_\psi(x) & x \in \Psi \\ -\infty & \text{else,} \end{cases}$$

are fulfilled, which, together with Proposition 3.4 will show the claim.

The Hessian of the objective function is, for $\psi \in \operatorname{int} \Psi$

$$H_\psi \mathbf{P}\left[b(\cdot, \psi)\right] = H_\psi \mathbf{P}\left[\psi^T T - \log Z(\psi)\right] = -H_\psi \log Z(\psi) = -I(\psi),$$

as the cumulant generating function is smooth on $\operatorname{int} \Psi$ (Theorem 3.1). Thus the Hessian is non-singular by assumption (ii), showing that condition (C7) is fulfilled.

For condition (C10), note that for $\psi \in \operatorname{int} \Psi$, b is differentiable with gradient

$$\nabla_\psi b(x, \psi) = T(x) - \nabla_\psi \log Z(\psi) = T(x) - \mathbf{G}_\psi[T].$$

By assumption (iv), $\nabla_\psi b(x, \psi) \in L^2(\mathbf{P})$, showing that condition (C10) is fulfilled.

To show that the central limit theorem applies to $\hat{\psi}_{\mathrm{CE}}$, we additionally show that assumption (i) in Proposition 3.4 is fulfilled, which will finish the proof. To this end, note that

$$w(x) b'(x, \psi, \xi) = w(x) \xi^T \nabla_\psi b(x, \psi) = \xi^T \left(w(x)(T(x) - \mathbf{G}_\psi[T])\right) \in L^2(\mathbf{G})$$

by assumption (iii).

Finally, to show the representation of M, note that by Proposition 3.4 we have for $X \sim \mathbf{G}$

$$M = \operatorname{Cov}\left(w(X)\left(T(X) - G_{\psi_{\mathrm{CE}}}[T]\right)\right),$$

and $\mathbb{E} w(X)\left(T(X) - \mathbf{G}_{\psi_{\mathrm{CE}}}[T]\right) = 0$ as $\mathbf{G}_{\psi_{\mathrm{CE}}}[T] = \mathbf{P}[T]$. □

The form of the asymptotic covariance matrix is that of the sandwich estimator (White, 1982), corrected for the importance sampling with $\mathbf{G}$. This is not surprising: the CE-method essentially performs maximum likelihood estimation of ψ where the data comes from the misspecified $\mathbf{P}$. Additionally, we have to correct the variance for performing importance sampling with $\mathbf{G}$, instead of sampling directly from $\mathbf{P}$.

The assumptions of Theorem 3.6 are minimal to facilitate the proof. The existence and positive definiteness of the Fisher information matrix are easily checked for the exponential family proposal and hold for minimal regular exponential families. Additionally, we have two moment constraints that involve the weights w and the sufficient statistic T. That $wT \in L^2(\mathbf{G})$ may be seen as a generalization of the existence of the second moment $\rho = \mathbf{G}[w^2]$, adapted to the exponential family setting. As such it is a natural requirement. That $T \in L^2(\mathbf{P})$ is required for the application of Theorem 3.7, and, as mentioned before, should not be problematic in practice, except for heavy-tailed distributions.

For our application, we will choose $(\mathbf{G}_\psi)_{\psi \in \Psi}$ to consist of Gaussian distributions with natural parameter $\psi = \left(\Sigma^{-1}\mu, -\frac{1}{2}\Sigma^{-1}\right)$ and sufficient statistic $T(x) = \left(x, xx^T\right)$. Thus $T \in L^2(\mathbf{P})$ is equivalent to $\mathbf{P}$ having fourth order moments, which is reasonable if the target is not heavy-tailed.

If $(\mathbf{G}_\psi)_{\psi \in \Psi}$ do not form an exponential family, $\hat{\psi}_{\mathrm{CE}}$ will still be consistent and asymptotically normal, provided the usual regularity conditions for M-estimators apply. These usually include conditions to ensure the maximum is well-separated and the target is sufficiently smooth such that a Taylor expansion around the maximum is feasible. To extend our results to more involved settings, we refer the reader to (Van der Vaart, 2000) for an empirical process treatment of M- and related Z-estimators, (Haberman, 1989) for asymptotics when the objective function is concave, but the maximum may lie on the border of the parameter space and (Liang and Zeger, 1995) for a review of estimators based on estimating equations.

However, these conditions will become more intricate than the ones we have provided here, as the concavity of the log densities is a rather strong property. As a result, we expect that assessing whether these conditions are satisfied in practice be more difficult.

3.3.3 Efficient Importance Sampling (EIS)

Efficient Importance Sampling (EIS) (Richard and Zhang, 2007) provides an alternative to the CE-method. Instead of minimizing the KL-divergence between the target $\mathbf{P}$ and proposal $\mathbf{G}_\psi, \psi \in \Psi$, EIS aims at minimizing the variance of the logarithm of importance sampling weights. Our discussion of (Chatterjee and Diaconis, 2018), Theorem 3.2, especially Lemma 3.5, suggests that this is worthwhile. Thus, EIS finds ψ_{EIS} which is a feasible solution to the following optimization problem

$$\min_{\psi \in \Psi} \text{Var}_{\mathbf{P}} \left[\log w_\psi\right] = \min_{\psi \in \Psi} \mathbf{P} \left[\log w_\psi - \mathbf{P} \log w_\psi\right]^2, \tag{3.18}$$

where, as in the last section, $\log w_\psi = \log p - \log g_\psi$.

Two problems arise: $\mathbf{P}[\log w_\psi] = \mathcal{D}_{\text{KL}}\left(\mathbf{P} || \mathbf{G}_\psi\right)$ is usually intractable and we usually only have access to the unnormalized weights $\frac{\tilde{w}_\psi}{\mathbf{G}_\psi[w_\psi]} = w_\psi$, with unknown integration constant $\mathbf{G}_\psi\left[w_\psi\right]$. Both can be dealt with by introducing the nuisance parameter $\lambda = \mathbf{P}\left[\log \tilde{w}_\psi\right]$, utilizing the fact that the mean is the minimizer of the squared distance functional with the minimum value equal to the variance, should it exist. Indeed

$$\log w_\psi - \mathbf{P}[\log w_\psi] = \log \tilde{w}_\psi - \log \mathbf{G}_\psi[\tilde{w}_\psi] - \mathbf{P}\left[\log \tilde{w}_\psi\right] + \log \mathbf{G}_\psi[\tilde{w}_\psi] = \log \tilde{w}_\psi - \mathbf{P}\left[\log \tilde{w}_\psi\right],$$

so

$$\min_{\psi \in \Psi} \mathbf{P}\left[\log w_\psi - \mathbf{P}\left[\log w_\psi\right]\right]^2 = \min_{\psi \in \Psi, \lambda \in \mathbf{R}} \mathbf{P}\left[\log \tilde{w}_\psi - \lambda\right]^2,$$

where $\psi \in \Psi$ is a minimizer of the left-hand side if, and only if, $(\psi, \lambda) \in \Psi \times \mathbf{R}$ with $\lambda = \mathbf{P}\left[\log \tilde{w}_\psi\right]$ is a minimizer of the right-hand side.

Similar to the CE-method we restrict our in-depth analysis to natural exponential family proposals where

$$\log g_\psi(x) = \psi^T T(x) - \log Z(\psi).$$

In this case the optimization problem is reduced to

$$\min_{\psi \in \Psi, \lambda \in \mathbf{R}} \mathbf{P}\left[\log p - \psi^T T - \lambda\right]^2, \tag{3.19}$$

a weighted linear least squares problem. As we consider unnormalized weights $\tilde{w}$, we are additionally able to get rid of the potentially non-linear term $\log Z(\psi)$. Noticing that this is a convex objective function in ψ which, similar to the CE-method, will be very useful to derive asymptotics later on. For now, we begin with studying the existence and uniqueness of ψ_{EIS} similar to Proposition 3.2.

Lemma 3.9 (EIS for exponential families)**.** *Let $(\mathbf{G}_\psi)_{\psi \in \Psi}$ form a k-dimensional natural exponential family with log-densities*

$$\log g_\psi(x) = \psi^T T(x) - \log Z(\psi)$$

for $\Psi \subseteq \mathbf{R}^k$. Suppose that $\log p, T \in L^2(\mathbf{P})$.

If there is a $\psi_{EIS} \in \Psi$ with

$$\text{Cov}_{\mathbf{P}}\left(T\right) \psi_{EIS} = \text{Cov}_{\mathbf{P}}\left(T, \log p\right) \tag{3.20}$$

it is a global minimizer of Equation (3.18). If $\text{Cov}_{\mathbf{P}}\left(T\right)$ is non-singular,

$$\psi_{EIS} = \text{Cov}_{\mathbf{P}}(T)^{-1} \text{Cov}_{\mathbf{P}}(T, \log p)$$

is the unique global minimizer.

Proof. Under the proposed conditions, we may consider Equation (3.19) instead, where the moment conditions on $\log p$ and T ensure that the problem is well-posed, i.e. the target is finite for all $\psi \in \Psi$. Thus the optimal $(\psi_{\text{EIS}}, \lambda_{\text{EIS}})$ are given by the best linear unbiased predictor (BLUP) of $\log p$ by the sufficient statistic T under $\mathbf{P}$ for ψ_{EIS} and $\mathbf{P}\left[\log \tilde{w}_{\psi_{\text{EIS}}}\right]$ for λ_{EIS}. Standard results from multivariate regression theory imply that the BLUP is given by any solution of

$$\text{Cov}_{\mathbf{P}}(T)\psi_{\text{EIS}} = \text{Cov}_{\mathbf{P}}(T, \log p),$$

i.e. ψ_{EIS} as stated in the lemma. Furthermore, if $\text{Cov}_{\mathbf{P}}(T)$ is non-singular, the solution to this equation is unique.

□

As the optimal ψ_{EIS} depends on several unknown quantities, EIS proceeds like the CE-method and employs importance sampling with a proposal $\mathbf{G}$, estimating ψ_{EIS} by

$$\left(\hat{\lambda}, \hat{\psi}_{\text{EIS}}\right) = \text{argmin}_{\lambda,\psi} \hat{\mathbf{P}}_N \left[\log \tilde{w}_\psi - \lambda\right]$$

where $X^1, \ldots, X^N \overset{\text{i.i.d}}{\sim} \mathbf{G}$. Again, if $\mathbf{G}_\psi, \psi \in \Psi$ form an exponential family with natural parameter ψ, this optimization problem turns into a weighted least squares problem, so we can estimate ψ_{EIS} with the standard weighted least squares estimator

$$\left(\hat{\lambda}', \hat{\psi}_{\text{EIS}}\right) = \left(\mathbf{X}^T \mathbf{W} \mathbf{X}\right)^{-1} \mathbf{X}^T \mathbf{W} y$$

where the random design matrix $\mathbf{X}$[5] and diagonal weights matrix $\mathbf{W}$ are given by

$$\mathbf{X} = \begin{pmatrix} 1 & T(X^1)^T \\ \ldots & \ldots \\ 1 & T(X^N)^T \end{pmatrix}$$

and

$$\mathbf{W} = \text{diag}\left(W^1, \ldots, W^N\right),$$

and the observations are

$$y = \left(\log p(X^1), \ldots, \log p(X^N)\right)^T \in \mathbf{R}^N.$$

Alternatively, replacing $\mathbf{P}$ by $\hat{\mathbf{P}}_N$ in Equation (3.20), we obtain the equivalent formulation

$$\hat{\psi}_{\text{EIS}} = \text{Cov}_{\hat{\mathbf{P}}_N}(T)^{-1} \text{Cov}_{\hat{\mathbf{P}}_N}(T, \log p), \tag{3.21}$$

as long as $\text{Cov}_{\hat{\mathbf{P}}_N} T$ is non-singular.

An attractive feature of EIS is that if the target $\mathbf{P}$ is a member of the exponential family of proposals, i.e. there is a $\psi_{\mathbf{P}} \in \Psi$ such that $\mathbf{P} = \mathbf{G}_{\psi_{\mathbf{P}}}$, then EIS finds the optimal $\psi_{\text{EIS}} = \psi_{\mathbf{P}}$ a.s. for a finite number of samples.

Proposition 3.5 (Finite sample convergence of EIS)**.** *Suppose $\mathbf{G}_\psi, \psi \in \Psi \subseteq \mathbf{R}^k$ for a natural exponential family w.r.t. Lebesgue measure, where the support of the sufficient statistic $\text{supp}\, T$ is open in $\mathbf{R}^k$. Furthermore let $\mathbf{G}$ be a probability measure on $\mathbf{R}^m$ that is equivalent to $\mathbf{P}$, i.e. $\mathbf{G} \ll \mathbf{P}$ and $\mathbf{P} \ll \mathbf{G}$.*

If there is a $\psi_{\mathbf{P}} \in \Psi$ such that $\mathbf{P} = \mathbf{G}_{\psi_{\mathbf{P}}}$, then $\hat{\psi}_{EIS} = \psi_{\mathbf{P}}$ a.s. for $N \geq k$.

Proof. As $\mathbf{P}$ stems from the same exponential family as $\mathbf{G}_\psi$, the pseudo-observations are

$$\log p = \psi_{\mathbf{P}}^T T - \log Z(\psi_{\mathbf{P}}).$$

Thus $\text{Cov}_{\hat{\mathbf{P}}_N}(T, \log p) = \text{Cov}_{\hat{\mathbf{P}}_N}(T)\, \psi_{\mathbf{P}}$. If we can show that $\text{Cov}_{\hat{\mathbf{P}}_N} T$ is non-singular, Equation (3.21) implies that $\hat{\psi}_{\text{EIS}} = \psi_{\mathbf{P}}$ a.s..

If $\text{Cov}_{\hat{\mathbf{P}}_N} T$ were singular, there would exist a $\psi \in \mathbf{R}^k$ such that

$$\psi^T \text{Cov}_{\hat{\mathbf{P}}_N}(T) \psi = \text{Cov}_{\hat{\mathbf{P}}_N}\left(\psi^T T\right) = 0.$$

In this case the a.s. non-zero $W^i(X^i)T(X^i)$ would lie in the orthogonal complement $\psi^\perp$ for all $i = 1, \ldots, N$. As the weights are a.s. positive by the assumed equivalence of $\mathbf{G}$ and $\mathbf{P}$, the same holds true for $T(X^i), i = 1, \ldots, N$. If N is bigger than k, the probability that this happens is 0, as $\text{supp}\, T$ is open. Thus $\text{Cov}_{\hat{\mathbf{P}}_N} T$ is non-singular almost surely and the result is shown. □

[5] if $\mathbf{XWX}$ is not invertible, replace the inverse by the Moore-Penrose pseudoinverse

Note that if in the above proposition only $\mathbf{G}_\psi \gg \mathbf{P}$ holds, we obtain, by a similar argument, that

$$\mathbb{P}\left(\hat{\psi}_{\text{EIS}} = \psi_{\mathbf{P}}\right) \overset{N\to\infty}{\longrightarrow} 1.$$

Additionally, we then have to take care of the event $\{w(X) = 0\}$, whose probability is now potentially positive.

We now turn to deriving asymptotics for $\hat{\psi}_{\text{EIS}}$. As for the CE-method, we start with proving that $\hat{\psi}_{\text{EIS}}$ consistently estimates ψ_{EIS}. For this we need to ensure that ψ_{EIS} is the unique solution to Equation (3.18), as otherwise, consistent estimators of ψ_{EIS} cannot exist. As Equation (3.19) is a linear least squares problem, the objective function is convex, and so we can apply Theorem 3.5 and Proposition 3.3.

Theorem 3.8 (consistency of $\hat{\psi}_{\text{EIS}}$)**.** *Let $(\mathbf{G}_\psi)_{\psi\in\Psi}$ form a k-dimensional natural exponential family with log-densities*

$$\log g_\psi(x) = \psi^T T(x) - \log Z(\psi)$$

for convex $\Psi \subseteq \mathbf{R}^k$. Let $\mathbf{G} \gg \mathbf{P}$ be a proposal and suppose that

(i) $\log p, T \in L^2(\mathbf{P})$ *and*

(ii) $\text{Cov}_{\mathbf{P}}(T)$ *is non-singular,*

(iii) $\psi_{EIS} \in \operatorname{int}\Psi$.

Then

$$\hat{\psi}_{EIS} \overset{N\to\infty}{\longrightarrow} \psi_{EIS}$$

almost surely.

Proof. We follow the same strategy as in the proof of Theorem 3.4. Let

$$b : \mathbf{R}^p \times \mathbf{R}^{k+1} \to [-\infty, \infty) \qquad b(x, \psi') = \begin{cases} -\frac{1}{2}\left(\log p(x) - \psi^T T(x) - \lambda\right)^2 & \psi \in \Psi \\ -\infty & \text{else,} \end{cases}$$

where $\psi' = (\psi, \lambda) \in \mathbf{R}^{k+1}$. For fixed x this function is concave, as its Hessian is negative semi-definite:

$$H_{\psi'} b(x, \psi') = -\begin{pmatrix} 1 & T(x)^T \\ T(x) & T(x)T(x)^T \end{pmatrix} = -\begin{pmatrix} 1 & T(x)^T \end{pmatrix}\begin{pmatrix} 1 & T(x)^T \end{pmatrix}^T,$$

if $\psi \in \Psi$. Let $X^1, \ldots, X^N \overset{\text{i.i.d}}{\sim} \mathbf{P}$ and let $\tilde{\mathbf{P}}_N$ be their empirical distribution. For $\psi \in \Psi, \lambda \in \mathbf{R}$ we have

$$\mathbf{P}\left[b(\cdot, \psi')\right] = -\frac{1}{2}\mathbf{P}\left[\left(\log p - \psi^T T - \lambda\right)^2\right] < \infty,$$

as $\log p, T \in L^2(\mathbf{P})$. Let us now check that conditions (C1) - (C3) are fulfilled.

(C1) is fulfilled, as we assumed $\psi_{\text{EIS}} \in \operatorname{int}\Psi$. (C2) holds, as ψ_{EIS} is the unique global maximizer by Lemma 3.9, as $\text{Cov}(T)$ is non-singular. (C3) obviously holds.

Thus $\hat{\psi}_{\text{EIS}}$ is strongly consistent if $\mathbf{G} = \mathbf{P}$. If $\mathbf{G}$ is different from $\mathbf{P}$, we can apply Proposition 3.3, where the existence of M-estimators is ensured by Equation (3.21), using the Moore-Penrose inverse if $\text{Cov}_{\tilde{\mathbf{P}}_N}(T)$ is singular. □

As Equation (3.21) expresses $\hat{\psi}_{\text{EIS}}$ in terms of empirical covariances, we could alternatively prove consistency by ensuring that the empirical covariances are consistent as well, for which we would need to ensure that fourth-order moments of $\log p$ and T w.r.t. $\mathbf{P}$ exist. This strategy may be fruitful if ψ_{EIS} does not lie in the interior of Ψ, although the more sophisticated treatment of (Haberman, 1989) may also be applicable under these circumstances.

Additionally, if fourth-order moments exist, we can derive a central limit theorem, similar to Theorem 3.6, for EIS.

Theorem 3.9 (CLT for $\hat{\psi}_{\text{EIS}}$)**.** *Let $(\mathbf{G}_\psi)_{\psi\in\Psi}$ form a k-dimensional natural exponential family with log-densities*

$$\log g_\psi(x) = \psi^T T(x) - \log Z(\psi),$$

and convex parameter space $\Psi \subseteq \mathbf{R}^k$. Let $\mathbf{G} \gg \mathbf{P}$ be a proposal with weights $w = \frac{\mathrm{d}\mathbf{P}}{\mathrm{d}\mathbf{G}}$.

Assume that

(i) $wT_iT_j, w(\log p)^2 \in L^2(\mathbf{G})$ *for* $i,j = 1,\dots,k$,

(ii) $\log p, T_i \in L^4(\mathbf{P})$ *for all* $i = 1,\dots,k$

(iii) $\mathrm{Cov}_{\mathbf{P}}(T)$ *is non-singular and* $\psi_{EIS} \in \operatorname{int}\Psi$.

Then

$$\sqrt{N}(\hat{\psi}_{EIS} - \psi_{EIS}) \xrightarrow{\mathcal{D}} \mathcal{N}(0, BMB)$$

where $B = \mathrm{Cov}_{\mathbf{P}}(T)^{-1}$ *and*

$$M = \mathrm{Cov}_{\mathbf{G}}\left(w\left(\log p - {\psi_{EIS}}^T T - \lambda_{EIS} - \mathbf{P}[T]\right)T\right).$$

Proof. Similar to the proof of Theorem 3.6, we combine Theorem 3.7 and Proposition 3.4. Let

$$b : \mathcal{X}\times\mathbf{R}^{k+1} \to [-\infty,\infty) \qquad b(x,\psi') = \begin{cases} -\frac{1}{2}\left(\log p(x) - \psi'^T T'(x)\right) & x\in\Psi \\ -\infty & \text{else,}\end{cases}$$

where $\psi' = (\psi,\lambda) \in \Psi\times\mathbf{R}$ and $T'(x) = \begin{pmatrix} T(x) & 1\end{pmatrix}$. For $\psi\in\Psi$ the map $(\psi,\lambda)\to\mathbf{P}[b(\cdot,(\psi,\lambda))]$ is differentiable with gradient

$$\nabla_{\psi'}\mathbf{P}[b(\cdot,\psi')] = -\mathbf{P}\left[\left(\log p - \psi'^T T'\right)T'\right] = \begin{pmatrix} -\mathbf{P}\left[T'\log p - T'T'^T\psi'\right] \\ -\mathbf{P}\left[\log p - \psi'^T T'\right]\end{pmatrix}$$

and Hessian

$$H_{\psi'}\mathbf{P}[b(\cdot,\psi')] = -\mathbf{P}\left[T'T'^T\right] = -\begin{pmatrix}\mathbf{P}\left[TT^T\right] & \mathbf{P}[T^T] \\ \mathbf{P}[T] & 1\end{pmatrix}.$$

The Hessian is negative definite, as for all $\psi\in\mathbf{R}^k, \lambda\in\mathbf{R}$ we have

$$\begin{aligned}\begin{pmatrix}\psi^T & \lambda\end{pmatrix} H_{\psi'}\mathbf{P}\left[b(\cdot,\psi')\right]\begin{pmatrix}\psi^T & \lambda\end{pmatrix}^T &= -\left(\psi^T\,\mathrm{Cov}_{\mathbf{P}}(T)\psi + \psi^T\mathbf{P}[T]\mathbf{P}[T]^T\psi + 2\psi^T\mathbf{P}[T]\lambda + \lambda^2\right) \\ &= -\left(\psi^T\,\mathrm{Cov}_{\mathbf{P}}(T)\psi + (\lambda + \psi^T\mathbf{P}[T])^2\right) \le 0,\end{aligned}$$

with equality if, and only if, both λ and ψ are 0, as $\mathrm{Cov}_{\mathbf{P}}(T)$ is assumed to be positive definite. Thus condition (C7) is fulfilled.

For condition (C10), we can verify that for all $i,j = 1,\dots,k+1$

$$(\nabla_{\psi'}b(\cdot,\psi'))_i(\nabla_{\psi'}b(\cdot,\psi'))_j = \left(\log p - \psi'^T T'\right)^2 T'_iT'_j$$

is in $L^1(\mathbf{P})$ by assumption (ii) and the Hölder inequality.

To apply Proposition 3.4 we need to show that $w(\cdot)b'(\cdot,\psi',\xi') \in L^2(\mathbf{G})$ for all $\xi'\in\mathbf{R}^{k+1}$ and all ψ' in a neighborhood of ψ_{EIS}, for this it suffices that we show

$$w^2(\nabla_{\psi'}b(\cdot,\psi'))_i(\nabla_{\psi'}b(\cdot,\psi'))_j = w^2\left(\log p - \psi'^T T'\right)^2 T'_iT'_j$$

is in $L^1(\mathbf{G})$, which holds, again, by assumption Item (i) and the Hölder inequality.

We have thus shown a central limit theorem for $\hat{\psi}'_{\text{EIS}} = \left(\hat{\psi}_{\text{EIS}}, \hat{\lambda}_{\text{EIS}}\right)$, i.e.

$$\sqrt{N}\left(\hat{\psi}'_{\text{EIS}} - \psi_{\text{EIS}}\right) \to \mathcal{N}(0, M'B'M')$$

with $B' = -\left(H_{\psi'_{\text{EIS}}} \mathbf{P}\left[b(\cdot, \psi'_{\text{EIS}})\right]\right)^{-1}$ and $M' = \text{Cov}\left(w(X)\nabla_{\psi'_{\text{EIS}}} b(X, \psi'_{\text{EIS}})\right)$ for $X \sim \mathbf{G}$. By using the inversion formula for block matrices, we obtain

$$\begin{aligned} B' &= \begin{pmatrix} \mathbf{P}\left[TT^T\right] & \mathbf{P}[T^T] \\ \mathbf{P}[T] & 1 \end{pmatrix}^{-1} = \begin{pmatrix} \Sigma + \mu\mu^T & \mu^T \\ \mu & 1 \end{pmatrix}^{-1} \\ &= \begin{pmatrix} (\Sigma + \mu\mu^T - \mu\mu^T)^{-1} & 0 \\ 0 & 1 - \mu^T(\Sigma + \mu\mu^T)^{-1}\mu \end{pmatrix} \begin{pmatrix} I_k & -\mu^T \\ -\mu(\Sigma + \mu\mu^T)^{-1} & 1 \end{pmatrix} \\ &= \begin{pmatrix} \Sigma^{-1} & -\mu^T\Sigma^{-1} \\ -\Sigma^{-1}\mu & 1 - \mu^T\left(\Sigma + \mu\mu^T\right)^{-1}\mu \end{pmatrix} \end{aligned}$$

where $\Sigma = \text{Cov}_{\mathbf{P}}(T)$ and $\mu = \mathbf{P}[T]$. Similarly,

$$M' = \begin{pmatrix} \text{Cov}_{\mathbf{G}}\left(wW_{\psi_{\text{EIS}}} T\right) & \text{Cov}_{\mathbf{G}}\left(wW_{\psi_{\text{EIS}}} T, wW_{\psi_{\text{EIS}}}\right) \\ \text{Cov}_{\mathbf{G}}\left(wW_{\psi_{\text{EIS}}}, wW_{\psi_{\text{EIS}}} T\right) & \text{Cov}_{\mathbf{G}}\left(wW_{\psi_{\text{EIS}}}\right) \end{pmatrix},$$

where $W_{\psi_{\text{EIS}}} = \log p - \psi_{\text{EIS}}^{tT} T'$.

If $\mu \neq 0$, we may change the sufficient statistic of the exponential family such that this holds, i.e. let $\tilde{T} = T - \mathbf{P}[T]$, then

$$\log g_\psi(x) = \psi^T T(x) - \log Z(\psi) = \psi^T \tilde{T}(x) - \log \tilde{Z}(\psi)$$

where $\tilde{Z}(\psi) = \log Z(\psi) + \mathbf{P}[T]$. As ψ_{EIS}, Equation (3.20), only depends on $T - \mathbf{P}[T]$ under $\mathbf{P}$, this does not change ψ_{EIS}. Similarly, $\hat{\psi}_{\text{EIS}}$, Equation (3.21), is unaffected by subtracting a constant from T. Only

$$\tilde{\lambda}_{\text{EIS}} = \lambda_{\text{EIS}} + \mathbf{P}[T]$$

and similarly $\hat{\lambda}_{\text{EIS}}$ are changed.

Thus, without loss of generality, we may assume that $\mathbf{P}[T] = 0$. Then

$$B' = \begin{pmatrix} \Sigma^{-1} & 0 \\ 0 & 1 \end{pmatrix}$$

is a diagonal matrix. Taking the ψ_{EIS} marginal of the asymptotic normal distribution, we arrive at

$$\sqrt{N}\left(\hat{\psi}_{\text{EIS}} - \psi_{\text{EIS}}\right) \to \mathcal{N}(0, BMB)$$

with $B = \text{Cov}_{\mathbf{P}}(T)$ and $M = \text{Cov}_G\left(w\left(\log p - {\psi_{\text{EIS}}}^T T - \lambda_{\text{EIS}} - \mathbf{P}[T]\right) T\right)$, as promised.

□

A discussion of the assumptions of Theorems 3.8 and 3.9 is in order. We start with the consistency result Theorem 3.8. The integrability condition, i.e that $\log p, T \in L^2(\mathbf{P})$ is necessary to ensure existence of ψ_{EIS} and the existence of $\text{Cov}_{\mathbf{P}}(T)$ as well as $\psi_{\text{EIS}} \in \text{int}\,\Psi$ ensure uniqueness, see also Lemma 3.9.

Regarding the central limit theorem Theorem 3.9, requiring the existence of higher order moments is natural. Unfortunately, there is no direct interpretation of these requirements as generalizations of the existence of ρ, as was the case for the CE-method.

The only integrability conditions related to the proposal $\mathbf{G}$ are those for wT_iT_j and $w\log(p)^2$. Choosing $(\mathbf{G}_\psi)_{\psi\in\Psi}$ to consist of Gaussian distributions, the conditions on T translate to the existence of certain polynomial moments of w^2 w.r.t. the proposal $\mathbf{G}$ (or w w.r.t. $\mathbf{P}$). This technical condition, is not easily interpreted, as assuming existence of moments of the target distribution seem more natural than those involving the extra weighting term $w = \frac{p}{g}$, which depends on the proposal $\mathbf{G}$ as well.

3.4 Interim discussion

Before we apply EIS and the CE-method in the SSM context, let us consolidate what we have achieved by the asymptotic analysis in the preceding two subsections and reason which of the two methods should be used in which circumstances.

We start with a discussion of the optimal values ψ_{CE} and ψ_{EIS}. Notice that ψ_{EIS} depends on second-order moments of the sufficient statistic T, as well as the shape of $\log p$, whereas the optimal parameter for the CE-method ψ_{CE} depends only on the first-order moments of T. This dependence on higher-order moments may be beneficial for the EIS method, for example, if the covariance of T under $\mathbf{P}$ is very different from that under $\mathbf{G}_\psi$.

The two methods differ concerning the assumptions that are required for uniqueness, consistency and the central limit theorem to hold if the proposals come from an exponential family. For uniqueness, Proposition 3.2 and lemma 3.9, both methods require that the covariance of T is non-singular, however, the measures under which the covariance are considered differ: for the CE-method we need $\text{Cov}_{\mathbf{G}_{\psi_{\text{CE}}}}(T)$ to be non-singular, while for EIS the same has to hold for $\text{Cov}_{\mathbf{P}}(T)$. While the former is easy to ensure, the latter depends on the intractable target $\mathbf{P}$ and may be more difficult to verify in practice, depending on T.

Regarding the consistency results, Theorems 3.4 and 3.8 as well as the central limit theorems, Theorems 3.6 and 3.9, EIS requires that the sufficient statistic be twice as often $\mathbf{P}$-integrable as the CE-method. Additionally, the EIS results assume that $\log p$ is sufficiently often $\mathbf{P}$-integrable. Therefore, EIS is, at first glance, more restrictive than the CE-method. However, our application will perform importance sampling with Gaussian proposals where $T(x) = \begin{pmatrix} x \\ xx^T \end{pmatrix}$. For importance sampling to be consistent in this setting, we have to assume that the target has thinner tails than the Gaussian proposal, which implies that all polynomial moments of the target, and thus of T exist. A similar argument can be made for $\log p$, and so the assumptions are likely to be fulfilled when Gaussian importance sampling is consistent.

To compare the asymptotic covariance matrices of both methods, note that both covariance matrices have the same "bread-meat-bread" factorization, as they are asymptotic covariance matrices of M-estimators[6]. We see that both $B_{\text{CE}} = I(\psi) = \text{Cov}_{G_{\psi_{\text{CE}}}}(T)^{-1}$ and $B_{\text{EIS}} = \text{Cov}_{\mathbf{P}}(T)^{-1}$ are precision matrices of the sufficient statistic T, one with respect to the optimal CE-method proposal and one with respect to the target. Thus, if $\mathbf{P}$ is well approximated by $\mathbf{G}_{\psi_{\text{CE}}}$, we would expect these two components to be close to one another. For $M_{\text{CE}} = \text{Cov}_{\mathbf{G}}(wT)$ and $M_{\text{EIS}} = \text{Cov}_{\mathbf{G}}\left(w(\log p - \psi_{\text{EIS}}^T T - \lambda_{\text{EIS}} - \mathbf{P}[T])T\right)$, there is a more notable difference, i.e. the presence of the $\log p - \psi_{\text{EIS}}^T T - \lambda_{\text{EIS}}$ term. If the EIS approximation performs well, we can expect this term to be small, as it is the prediction error of the least squares approximation of $\log g_\psi$ to $\log p$. Therefore, we expect that EIS outperforms the CE-method in terms of asymptotic variance in these settings. In agreement with Proposition 3.5, $M_{\text{EIS}} = 0$ if $\log p = \log g_{\psi_{\mathbf{P}}}$ so that $\psi_{\text{EIS}} = \psi_{\mathbf{P}}$.

Additionally, both M_{CE} and M_{EIS} depend on the proposal $\mathbf{G}$, and indicate how one might tailor the initial proposal $\mathbf{G}$ to produce low-variance estimates. For the CE-method we might choose $\mathbf{G}$ such that the trace determinant of $\mathbf{G}[w^2 TT^T]$ becomes small. This is not necessarily achieved by the CE-method proposal $\mathbf{G}_{\hat{\psi}_{\text{CE}}}$, and so it may be worthwhile to investigate using two types of proposals in the CE-method, one that makes M_{CE} small and $\mathbf{G}_{\psi_{\text{CE}}}$. This is especially relevant as our simulation studies, Section 3.7, suggest that the asymptotic covariance of the CE-method is usually larger than that of EIS. For EIS, a similar approach might be fruitful, but is not as urgent as that for the CE-method, as the asymptotic covariance of EIS is usually small enough to be feasible in practice.

Finally, let us stress that these asymptotic considerations are, to the author's knowledge, novel results and should be straightforward to extend if the proposals $(\mathbf{G}_\psi)_{\psi \in \Psi}$ do not form a natural exponential family. As any minimal exponential family may be reduced to a natural exponential family by reparametrization, see (Brown, 1986, Theorem 1.9), the delta method can be used to derive CLTs in this case as well, as Proposition 3.2 and Lemma 3.9 still apply. If the family is not

[6] These are sometimes called sandwich estimators.

minimal the optimal values ψ_{EIS} and ψ_{CE} may be non-unique, so we cannot hope to estimate them consistently. In this case the user should choose a minimal parametrization, see again (Brown, 1986, Theorem 1.9). For non-exponential family proposals our results should also carry over, provided the usual regularity conditions ensuring uniqueness, consistency and asymptotic normality for M-estimators hold. If the objective functions are not concave as they are in our setting one usually requires uniformly bounded third-order derivatives of the objective function to exist.

Furthermore, our results can also be extended to the so-called Variance-Minimization method (VM-method) which determines an optimal proposal by solving the following optimization problem:

$$\min_{\psi\in\Psi} \text{Var}_{\mathbf{G}_\psi}(w_\psi) = \min_{\psi\in\Psi} \mathbf{G}_\psi\left[w_\psi^2\right] = \min_{\psi\in\Psi} \mathbf{P}\left[w_\psi\right],$$

where the first equality holds as $\mathbf{G}_\psi[w_\psi] = 1$ for all ψ. Thus the VM-method chooses ψ such that the second moment of importance sampling weights, ρ, becomes small. Again, this is sensible by the discussion surrounding ρ and the ESS. Similar to the CE-method and EIS, one uses importance sampling with a proposal $\mathbf{G}$ to approximate $\mathbf{P}[w_\psi]$ by $\hat{\mathbf{P}}_N[w_\psi]$, and solves this noisy version of the problem. Unfortunately, there is no closed form for the optimal ψ_{VM} or $\hat{\psi}_{\text{VM}}$, even if the proposals form a natural exponential family. Still, as $x \mapsto w_\psi(x)$ is convex, so is $\psi \mapsto \mathbf{P}[w_\psi]$, and we can apply Theorems 3.5 and 3.7 in combination with Propositions 3.3 and 3.4 to show, under suitable regularity conditions, the consistency and asymptotic normality of the method.

Now that we have gained theoretical insight into optimal importance sampling, let us apply these insights to the SSMs that we are interested in.

3.5 Gaussian importance sampling for state space models

For the types of models considered in this thesis, importance sampling is used to infer the posterior distribution. Given a state space model of the form (3.1) and observations $Y = Y_{:n}$, let $\mathbf{P}$ be the distribution of the states $X = X_{:n}$, conditional on Y and f be a function of interest. The task at hand is now to find a suitable proposal $\mathbf{G}$, using the methods presented in the last section. If n is large, the posterior distribution lives in a high dimensional state of dimension $m \cdot n$, so to obtain $\mathbf{G}$ efficiently, we should exploit the available structure. Additionally, we want $\mathbf{G}$ to be tractable, so simulating from it is possible and evaluating the weights w up to a constant is possible.

The multivariate Gaussian distribution is a good candidate in this setting, as simulating from it is straightforward and its density can be evaluated analytically. However, naively performing the optimal importance sampling methods from the previous section for all multivariate Gaussians is computationally inefficient as the family of distributions has $\mathcal{O}((n \cdot m)^2)$ many parameters. We can, however, exploit the available structure of the SSM to find parameterizations with fewer parameters by either using smoothing distributions of GLSSMs (Section 3.5.1) or approximating with a Gaussian discrete-time Markov process (Section 3.5.2).

Using Gaussian proposals, while computationally efficient, also comes with some drawbacks. The whole procedure hinges on the assumption that there is a Gaussian that is close to the target distribution. In the setting of SSMs this is not guaranteed, as the targets may contain multiple modes or heavy tails, features that may, in the worst case, lead to inconsistent importance sampling estimates. Additionally, even if there is a Gaussian distribution that facilitates consistent importance sampling, finding it in practice may be complicated, as the proposals generated by the LA, CE-method and EIS have deteriorating performance for fixed sample size N (in terms of ESS and convergence) with increasing dimension, see Section 3.7.4.

Using a GLSSM as an importance sampling proposal for non-Gaussian state space models was introduced by (Durbin and Koopman, 1997) to facilitate maximum likelihood estimation using the LA as a proposal. Concurrently, (Shephard and Pitt, 1997) established a similar result in the context of MCMC analysis of SSMs.

3.5.1 The GLSSM-approach

The first approach is motivated by the fact that the target posterior is again a Markov process, as are posteriors in GLSSMs. Additionally, the posterior distribution in GLSSMs is again Gaussian, and straightforward to simulate from by, e.g., the FFBS algorithm (Algorithm 3) or the simulation smoother (Durbin and Koopman, 2002). Thus parameterizing the proposals $\mathbf{G}$ by the posterior of a suitably chosen GLSSM may be a fruitful approach. For the models we consider in this thesis, the distribution of states is already Gaussian and the observations are conditionally independent given the states. Thus a natural GLSSM to use as a proposal consists of keeping the prior distribution of states and replacing the distribution of observations with conditionally independent Gaussian distributions and the actual observations by synthetic ones. By the assumed conditional independence, this model only needs $2p \cdot (n+1)$ many parameters, $p \cdot (n+1)$ for the synthetic observations and $p \cdot (n+1)$ for their variances. We term this approach the **GLSSM-approach** to importance sampling.

In total, the GLSSM-approach considers parametric proposals $\mathbf{G}_\psi$ of the form

$$\begin{aligned} \mathbf{G}_\psi &= \mathcal{L}(X|Z=z), \\ Z_t &= B_t X_t + \eta_t, \\ \eta_t &\sim \mathcal{N}(0, \Omega_t), \\ \Omega_t &= \operatorname{diag}\left(\omega_t^2\right) = \operatorname{diag}\left(\omega_{t,1}^2, \ldots, \omega_{1,p}^2\right). \end{aligned} \tag{3.22}$$

where the distribution of X is given by (3.4), $\psi = \left(z, \omega^2\right)$ for $z = (z_0, \ldots, z_n) \in \mathbf{R}^{(n+1)\times m}$ and $\omega^2 = \left(\omega_0^2, \ldots, \omega_n^2\right) \in \mathbf{R}^{(n+1)\times m}$. Alternatively the natural parametrization

$$\psi = \left(z \oslash \omega^2, -1 \oslash \left(2\omega^2\right)\right) \tag{3.23}$$

may also be used, where $\oslash$ is the Hadamard, i.e. entry-wise, division. Simulation from $\mathbf{G}_\psi$ may be efficiently implemented by the FFBS algorithm, as $\mathbf{G}_\psi$ is the smoothing distribution of a GLSSM.

In this setting, the importance sampling weights are given by

$$w(x) = \frac{p(x|y)}{g(x|z)} = \frac{p(y|x)p(x)}{g(z|x)p(x)} \frac{g(z)}{p(y)} \propto \prod_{t=0}^{n} \frac{p(y_t|x_t)}{g(z_t|x_t)},$$

so they can be computed efficiently. Additionally, for a EGSSM with linear signals, $p(y_t|x_t)$ and $g(z_t|x_t)$ depend on x_t only through the signal $s_t = B_t x_t$, and we have

$$w(x) \propto \prod_{t=0}^{n} \frac{p(y_t|s_t)}{g(z_t|s_t)}, \tag{3.24}$$

which implies that auto-normalized weights may be calculated by using the signal smoother (Jungbacker and Koopman, 2007, Theorem 2). As (Durbin and Koopman, 2012) (Durbin and Koopman, 2012, Section 4.5.3) argue, it is often computationally more efficient to treat only on the signals $S_{:n}$ instead of the states $X_{:n}$, the idea being that the dimension of S_t, p, is usually much smaller than that of X_t, m.

As the joint distribution of (X, S) is a Gaussian distribution, by Lemma 3.1 $X|S = s$ is again Gaussian, with known conditional mean and covariance matrix and density $p(x|s) = g(x|s)$. If $(\tilde{X}_t)_{t=0,\ldots,n}$ is a draw from this conditional distribution a quick calculation reveals that a.s. $B_t\tilde{X}_t = S_t$, and so, as expected, the weights $w(\tilde{X}_t)$ are a.s. constant and given by (up to the integration constant) Equation (3.24). Producing a draw from this conditional distribution can be achieved by the FFBS algorithm (Algorithm 3), as (X, S) form a GLSSM with degenerate observation covariance matrices $\Omega_t = 0$.

By the assumed conditional independence of observations given signals, we have

$$p(x, s|y) \propto p(x|s)p(s|y), \tag{3.25}$$

and so if one is interested in the states, rather than the signals, importance sampling with the proposal Equation (3.22) can be achieved in a two-step procedure: first sample from $g(s|z)$, then run the FFBS algorithm to sample from $g(x|s) = p(x|s)$ using the same weights for MC-integration.

The GLSSM-approach is the standard approach for finding the LA in EGSSM (Durbin and Koopman, 2012; Durbin and Koopman, 1997) and may even be applied when the observation densities are not log-concave as (Jungbacker and Koopman, 2007) show. The approach also leads to efficient implementation for EIS (Koopman, Lit, and Nguyen, 2019). However, as will become apparent in the later part of this section, it is infeasible for the CE-method if n is large.

We now give a concise overview over how to perform the LA and EIS for EGSSM, but refer the reader for more details to the respective literature. (Danielsson and Richard, 1993) were the first to propose minimizing the variance of log-weights, which developed into the EIS method (Liesenfeld and Richard, 2003; Richard and Zhang, 2007). However, as formulated in these earlier works, EIS requires careful tracking of integration constants. For PGSSMs, the modified EIS of (Koopman, Lit, and Nguyen, 2019) provides a more straightforward approach to determine the proposal distribution, by noticing that it may be written as the posterior of an appropriately chosen GLSSM, whose distribtion of states coincides with that of the original PGSSM. Instead of approximating the integrals in EIS using MC-integration, (Koopman, Lucas, and Scharth, 2015) suggest to do so using numerical integration, to reduce sampling error.

The LA for PGSSM can be obtained efficiently, by noticing that the Newton-Raphson scheme to obtain the posterior mode (Equation (3.12)) can be implemented using the Kalman smoother, see (Durbin and Koopman, 2012, Chapter 10). For EGSSM with a linear signal, the LA is particularly easy to implement, as the conditional independence of individual observations translates to an approximating GLSSM with independent observations as well — the resulting algorithm is presented in Algorithm 5.

Algorithm 5 The LA for EGSSM

Require: EGSSM (Definition 3.5) with linear signal and natural parameters s_t, $t = 0, \dots, n$, observations $y_0, \dots, y_n$, initial values $\psi^0 = \left(z^0, (\omega^2)^0\right)$

Set $l = 0$.
repeat
  Run the Kalman smoother Algorithm 2 for the model (3.22) to obtain $\hat{s} = \mathbb{E}_{\mathbf{G}_{\psi^l}}\left(S|Z = z^l\right)$.
  for $t = 0, \dots, n$ **do**
    Set $(\omega^{l+1})^2_{t,i} = H_{s_t^i} Z_t(s_t^i)$ ▷ Hessian evaluated at $\hat{s}_t$
    Set $\Omega_t^{l+1} = \operatorname{diag}\left((\omega^2)^{l+1}_{t,1}, \dots, (\omega^2)^{l+1}_{t,p}\right)$.
    Set $z_t^{l+1} = z_t^l - (\Omega_t^{l+1})^{-1}\left(\nabla \log Z_t(s_t^1), \dots, \nabla \log Z_t(s_t^p)\right))$. ▷ Gradient evaluated at $\hat{s}_t$
  end for
  Set $\psi^{l+1} = \left(z^{l+1} \oslash (\omega^2)^{l+1}, -1 \oslash (\omega^2)^{l+1}\right)$.
  Set $l = l + 1$.
until ψ^l has converged.

As we will show in Section 3.7, the LA may provide poor performance as a proposal, when the dimension of the PGSSM grows. In this case, the EIS proposal may perform better. Recall from Section 3.3.3, that EIS aims at minimizing the mean squared error between $s \mapsto \log p(s|y)$, the target log-density and $s \mapsto \log g_\psi(s|z)$, the proposals log-density with respect to the target. Thus in the context of PGSSMs, EIS aims to minimize

$$(z, \omega^2) \mapsto \mathbb{P}^{S|Y=y}\left[\left(\log p(\cdot|y) - \log g(\cdot|z)\right)^2\right].$$

By reformulating the integrand to $\left(\log p(y|s) - \log g(z|s) - \log p(y) + \log g(z)\right)^2$ and following the discussion surrounding Equation (3.19), we may instead minimize

$$\mathbb{P}^{S|Y=y}\left[\left(\log p(y|\cdot) - \log g(z|\cdot) - \lambda\right)^2\right] = \mathbb{P}^{S|Y=y}\left[\left(\sum_{t=0}^{n} \log p(y_t|\cdot_t) - \log g(z_t|\cdot_t) - \lambda\right)^2\right].$$

over the parameters of interest, (z, ω^2), and the nuisance parameter λ.

However, the dimension of ψ is quite high $(2p(n+1))$, so one resorts to solving the lower dimensional problems

$$\mathbb{P}^{S|Y=y}\left[\left(\log p(y_t|\cdot_t) - \log g(z_t|\cdot_t) - \lambda_t\right)^2\right] = \mathbb{P}^{X_t|Y=y}\left[\left(\log p(y_t|\cdot_t) - \log g(z_t|\cdot_t) - \lambda_t\right)^2\right], \quad (3.26)$$

which only depends on the marginal of X_t. While this only yields approximate solutions to the problem at hand, it turns out that the proposals produced by this procedure perform well (see Section 3.7).

EIS for PGSSM then proceeds as in Section 3.3.3, using importance sampling to obtain a particle approximation $\hat{\mathbf{P}}_N$ to $\mathbb{P}^{S|Y=y}$ and solving the resulting approximate problem. As

$$\log g(z_t|s_t) = -\frac{1}{2}(z_t - s_t)^T \Omega_t^{-1}(z_t - s_t) - \frac{p}{2}\log(2\pi) - \frac{1}{2}\log\det\Omega_t,$$

affine in the natural parameters $\left(z \oslash \omega^2, -1 \oslash (2\omega^2)\right)$, the problem reduces to weighted linear least squares problem, which can be solved analytically. If the model at hand is an EGSSM with linear signal[7], we can further exploit the independence of marginals, to solve only for the univariate marginals, i.e. minimize

$$(z_{t,i}, \omega^2_{t,i}, \lambda_{t,i}) \mapsto \mathbb{P}^{S|Y=y}\left[\left(\log p(y_{t,i}|s_{t,i}) - \log g(z_{t,i}|s_{t,i}) - \lambda_{t,i}\right)^2\right], \quad (3.27)$$

or an importance sampling version of it.

We present the resulting algorithm in Algorithm 6, restricted to the case where the model is an EGSSM with linear signal. As starting values ψ we may take those obtained by the LA.

Algorithm 6 EIS for EGSSMs with linear signal

Require: EGSSM (Definition 3.5) with linear signal and natural parameters s_t, $t = 0, \dots, n$, observations $y_0, \dots, y_n$, initial values $\psi^0 = \left(z^0, (\omega^2)^0\right)$, number of samples N.

1: Set $l = 0$.
2: **repeat**
3: Run the FFBS (Algorithm 3) to obtain samples of the signals $(S^i)_{i=1,\dots,N}$.
4: **for** $t = 0, \dots, n$ **do**
5: **for** $i = 1, \dots, p$ **do**
6: Solve Equation (3.27) for $z_{t,i}^{l+1}$ and $(\omega^2)_{t,i}^{l+1}$ ▷ Using $\hat{P}_N$
7: **end for**
8: **end for**
9: Set $\psi^{l+1} = \left(z^{l+1} \oslash (\omega^2)^{l+1}, -1 \oslash (\omega^2)^{l+1}\right)$.
10: Set $l = l + 1$.
11: **until** ψ^l has converged.

For the CE-method, using the GLSSM-approach turns out to be difficult numerically. For a high-level argument of why this is true, let us ignore the Markov structure of the model for the moment. As the CE-method matches moments of the target and proposal, applying it to fit model (3.22) amounts to matching the moments of $\mathbf{G}_\psi$ to those of the target posterior $\mathcal{L}(X|Y = y)$ in the SSM. Unfortunately, the covariance of $\mathbf{G}_\psi$ is given by $\left(\Sigma^{-1} + B^T\Omega^{-1}B\right)^{-1}$, where Σ is the covariance of all states, $B = \text{block-diag}(B_0, \dots, B_n)$ and $\Omega = \text{block-diag}\,(\Omega_0, \dots, \Omega_n)$. Choosing the diagonal matrix Ω such that the covariance of $\mathbf{G}_\psi$ matches this expression is numerically expensive: we either need to invert the large (dimension $(n+1)m \times (n+1)m$) covariance matrix, or solve numerically for the $(n+1)p$ parameters. The problem at hand is that we cannot decouple this into $(n+1)$

[7] Actually, we do not require the model to be an EGSSM, but only that the univariate marginals are conditionally independent.

equations of dimension p (or even $(n+1)p$ equations) as we did for EIS, because all entries of $(\Sigma^{-1} + B^T\Omega^{-1}B)^{-1}$ depend on all entries of Ω.

To make matters more concrete, the CE-method finds $\psi = (z, \omega^2)$ such that model (3.22) maximizes the cross entropy with the target $\mathbf{P}^{X|Y=y}$. For simplicity, let us assume that $m = p$, B is the identity and we only observe a single y. Using Lemma 3.1, we see that when $X \sim \mathcal{N}(\mu, \Sigma)$, the conditional distribution of X given $Z = z$, $\mathbf{G}_\psi$, is a Gaussian distribution with mean $\tilde{\mu} = \mu + \Sigma\left(\Sigma + \Omega\right)^{-1}(z - \mu)$ and covariance matrix $\tilde{\Sigma} = \left(\Sigma^{-1} + \Omega^{-1}\right)^{-1}$ for $\Omega = \operatorname{diag}\left(\omega^2\right)$, where $\omega^2 > 0$. Assuming that Σ is non-singular, we can reparameterize the objective function of the CE-method by $\tilde{\mu}$,

$$\begin{aligned}\max_{z,\omega^2} \int p(s|y) \log g_\psi(s|z) \mathrm{d}x &= \max_{\tilde{\mu},\omega^2} \int p(s|y) \left(-\frac{1}{2}(s-\tilde{\mu})^T \tilde{\Sigma}^{-1}(s-\tilde{\mu}) - \frac{1}{2}\log\det\tilde{\Sigma}\right) \mathrm{d}x \\ &= \max_{\tilde{\mu},\omega^2} -\frac{1}{2}(\gamma-\tilde{\mu})^T\tilde{\Sigma}^{-1}(\gamma-\tilde{\mu}) - \frac{1}{2}\operatorname{trace}\left(\tilde{\Sigma}^{-1}\Gamma\right) - \frac{1}{2}\log\det\tilde{\Sigma},\end{aligned} \tag{3.28}$$

where $\gamma = \mathbb{E}\left(X|Y=y\right)$ and $\Gamma = \operatorname{Cov}\left(X|Y=y\right)$. Thus the optimal $\tilde{\mu}$ is γ and to find the optimal ω^2 we have to minimize

$$\operatorname{trace}\left(\left(\Sigma^{-1} + \Omega^{-1}\right)\Gamma\right) - \log\det\left(\Sigma^{-1} + \Omega^{-1}\right).$$

Taking the derivative w.r.t. $\frac{1}{\omega^2}$, we see that

$$\Gamma_{i,i} = \left(\left(\Sigma^{-1} + \operatorname{diag}\left(\frac{1}{\omega_1}, \ldots, \frac{1}{\omega_p}\right)\right)^{-1}\right)_{i,i} = \left(\Sigma - \Sigma\left(\Sigma + \Omega\right)^{-1}\Sigma\right)_{i,i} \tag{3.29}$$

has to hold for all $i = 1, \ldots, (p \times (n+1))$, i.e. we have to choose ω^2 such that the posterior marginal variances $\Gamma_{i,i}$ coincide with the marginal variances of $\mathbf{G}_\psi$.

Several problems arise: First of all, Equation (3.29) is not guaranteed to have a solution. For the i-th unit-vector $e_i \in \mathbf{R}^p$ we can reformulate Equation (3.29) to

$$\Sigma_{i,i} - \Gamma_{i,i} = e_i^T\Sigma^T\left(\Sigma + \Omega\right)^{-1}\Sigma e_i > 0$$

and so we require $\Gamma_{i,i} < \Sigma_{i,i}$. While the law of total covariance asserts that

$$\Sigma = \mathbb{E}\operatorname{Cov}\left(X|Y\right) + \operatorname{Cov}\left(\mathbb{E}\left(X|Y\right)\right),$$

it does not guarantee $\Gamma \prec \Sigma$ (which would imply $\Gamma_{i,i} < \Sigma_{i,i}$), as $\operatorname{Cov}(X|Y) = \Gamma$ may not hold in the non-Gaussian case.

Second, even if there is an analytical solution Ω to Equation (3.29), in the CE-method we replace $\Gamma_{i,i}$ by the observed marginal variances $\hat{\Gamma}_{i,i}$ obtained by importance sampling. The variation introduced by simulation can then lead to situations where $\hat{\Gamma}_{i,i} > \Sigma_{i,i}$. As an example take $X \sim \mathcal{N}(0,1)$, and $Y = X + \eta$ for $\eta \sim \mathcal{N}(0, \omega^2)$. Then the conditional variance of X given $Y = y$ is $\Gamma = 1 - \frac{1}{1+\omega^2} < 1$. Given N i.i.d. samples $X^1, \ldots X^N \sim \mathcal{N}(0,1)$, their empirical variance $\hat{\Gamma} = \frac{1}{N}\sum_{i=1}^N (X^i - \bar{X})^2$ follows a scaled χ^2_{N-1} distribution, i.e. $\frac{N\hat{\Gamma}}{\Gamma} \sim \chi^2_{N-1}$. Notice that we use the non-Bessel corrected version of the empirical variance here, as it is the maximum-likelihood estimate.

Then

$$\mathbf{P}\left(\hat{\Gamma} > 1\right) = \mathbf{P}\left(\frac{N\hat{\Gamma}}{\Gamma} > \frac{N}{\Gamma}\right) = 1 - F_{\chi^2_{N-1}}\left(N\left(1 + \frac{1}{\omega^2}\right)\right)$$

is the probability that Equation (3.29) has no solution $\omega^2 \in \mathbf{R}_{\geq 0}$. Here $F_{\chi^2_{N-1}}$ is the cumulative distribution function of the χ^2_{N-1} distribution. As ω^2 goes to ∞, this probability approaches $1 - F_{\chi^2_{N-1}}(N)$ which, for large N, is approximately $1 - F_{\chi^2_{N-1}}(N-1) \approx \frac{1}{2}$, as $\chi^2_{N-1} \approx \mathcal{N}\left(N-1, 2(N-1)\right)$ (Johnson, Kotz, and Balakrishnan, 1994, Section 18.5). Thus, even in the basic univariate Gaussian

setting, for every N there is an ω^2 such that the CE-method fails for Equation (3.22) with practically relevant probability.

In higher-dimensional settings, e.g. when applying the CE-method to SSMs, we can expect this phenomenon to occur even more often. In the extreme case of independent marginals, i.e. when Σ is a diagonal matrix, Equation (3.29) reduces to $(n+1)p$ many decoupled equations, where $\hat{\Gamma}_{i,i}, i = 1, \ldots, (n+1)p$ are independent. If all $q_i = \mathbf{P}(\Gamma_{i,i} > \Sigma_{i,i})$ are identical to $q \in (0,1)$, e.g. because Σ and Ω are multiples of the identity, the number of failures follows a Binom$((n+1)p, q)$ distribution, so that even small q may lead to a non-negligible number of failures if the number of observations is high.

Finally, in the multivariate setting, the system (3.29) has no analytical solution. Instead, we have to resort to numerical methods to find a solution Ω. Unfortunately, even evaluating the right-hand side of (3.29) requires $\mathcal{O}(m^3)$ operations, as we have to invert $\Sigma + \Omega$. Additionally, we cannot hope to reuse a singular-value, LR, or eigenvalue-decomposition for further evaluations, as Σ and Ω are not guaranteed to be jointly diagonalizable. In the SSM context we may use the Kalman-smoother to compute the marginal variances, but have to re-run the smoother for every evaluation, which is expensive.

If we admit noise variance ∞ in the univariate setting, then $\Gamma > 1$ implies that the CE-method chooses this as the estimate, i.e. $\mathbf{G}_{\hat{\psi}_{\text{CE}}}$ is $\mathcal{N}(0,1)$, which is equal to the prior. We can interpret this as having a missing observation, which, going back to the SSM context, the Kalman-filter (Algorithm 1) can handle with only simple modifications, see e.g. (Durbin and Koopman, 2012, Section 4.10). However, if there are a lot of failures, the optimally chosen $\mathbf{G}_{\hat{\psi}_{\text{CE}}}$ will be close to the prior distribution of states X, and importance sampling is unlikely to be effective. Hence, we turn to another approach that allows us to apply the CE-method to SSMs.

3.5.2 The Markov-approach

An alternative family of Gaussian proposals is given by directly modeling a Gaussian Markov process on the states $X_{:n}$. Again, this is sensible given the Markov structure of the target. This parametrization is more flexible than using the posterior of a GLSSM with fixed prior as the proposal. This flexibility, however, comes at the cost of requiring a larger number of parameters. Here we propose with $\mathbf{G}_\psi$ where

$$\begin{aligned}
\mathbf{G}_\psi &= \mathcal{L}(U + v), \\
v &\in \mathbf{R}^{(n+1)m}, \\
U_0 &\sim \mathcal{N}(0, R_0 R_0^T), \\
U_t &= C_t U_{t-1} + R_t \nu_t, \\
C_t &\in \mathbf{R}^{m \times m}, \\
\nu_t &\sim \mathcal{N}(0, I_m), \\
R_t &\in \mathbf{R}^{m \times m} \text{ lower triangular with positive diagonal}
\end{aligned} \tag{3.30}$$

for $t = 1, \ldots, n$, with U_0 and $\nu_1, \ldots, \nu_n$ independent. The number of parameters in

$$\psi = (v, C_1, \ldots, C_n, R_0, \ldots, R_n)$$

is $(n+1) \cdot m$ for the mean v, $n \cdot m^2$ for the transition matrices C_t and $(n+1)\frac{m(m-1)}{2}$ for the Cholesky roots of innovation covariances, totaling $\mathcal{O}(n \cdot m^2)$ many parameters. While these are considerably more parameters than for the GLSSM-approach for large state dimension m, we will see in the later part of this section that finding the optimal parameters for the CE-method can be done analytically, depending only on the posterior first and second moments.

This approach, which we term the **Markov-approach**, was originally proposed by (Richard and Zhang, 2007) for general unnormalized transition kernels as EIS proposals. However, because of its lower number of parameters, one should favor the GLSSM-approach for EIS that operates on the signals, see (Koopman, Lit, and Nguyen, 2019).

To perform importance sampling with $\mathbf{G}_\psi$ in model (3.30) we not only need to simulate from $\mathbf{G}_\psi$ but also evaluate the unnormalized importance sampling weights $w(x) = \frac{p(x|y)}{g_\psi(x)}$. Simulation from $\mathbf{G}_\psi$ is achieved by a simple recursion. For the weights note that

$$w(x) \propto \frac{p(y|x)p(x)}{g_\psi(x)} = \prod_{t=0}^{n} \frac{p(y_t|x_t)p(x_t|x_{t-1})}{g_\psi(x_t|x_{t-1})}, \tag{3.31}$$

where $p(x_0|x_{-1}) = p(x_0)$ and $g_\psi(x_0|x_{-1}) = g_\psi(x_0)$.

The Markov structure of model (3.30) implies that the precision matrix of $\mathbf{G}_\psi$ is sparse, i.e. it has a block-tridiagonal form. This is a well-known property of the precision matrix of Gaussian random vectors, as the following two classical lemmas show. We show their proofs here for completeness. For a general treatment, we refer the reader to (Lauritzen, 1996, Chapters 3 and 5).

Lemma 3.10. *Let (X, Y) be jointly Gaussian with distribution $\mathcal{N}(\mu, \Sigma)$ where*

$$\mu = (\mu_X, \mu_Y)$$

and

$$\Sigma = \begin{pmatrix} \Sigma_{XX} & \Sigma_{XY} \\ \Sigma_{YX} & \Sigma_{YY} \end{pmatrix},$$

are partitioned according to the dimensions of X and Y and Σ is non-singular. If

$$P = \Sigma^{-1} = \begin{pmatrix} \Sigma_{XX} & \Sigma_{XY} \\ \Sigma_{XY} & \Sigma_{YY} \end{pmatrix}^{-1} = \begin{pmatrix} P_{XX} & P_{XY} \\ P_{YX} & P_{YY} \end{pmatrix}$$

is the precision matrix of (X, Y), partitioned as is Σ, then $\mathrm{Cov}(X|Y) = P_{XX}^{-1}$.

Proof. Without loss of generality, assume that both X and Y are centered. The conditional density $p(x|y)$ is proportional (in x) to the joint density $p(x, y)$ with

$$\log p(x, y) = -\frac{1}{2} \begin{pmatrix} x & y \end{pmatrix} P \begin{pmatrix} x \\ y \end{pmatrix} + C = -\frac{1}{2} \left(x^T P_{XX} x + 2x^T P_{XY} y \right) + C',$$

for constants C, C' that do not depend on x. As the conditional distribution of X given $Y = y$ is Gaussian (by Lemma 3.1), its covariance matrix is P_{XX}^{-1}. □

Lemma 3.11. *Let $(X, Y, Z) \sim \mathcal{N}(\mu, \Sigma)$ be jointly Gaussian with non-singular Σ. Then $X \perp Y|Z$ if, and only if, the sub-matrix of the precision matrix $P = \Sigma^{-1}$ whose rows correspond to the entries of X and columns correspond to the entries of Y is the 0 matrix.*

Proof. Partition the conditional covariance matrix into

$$\mathrm{Cov}\left((X, Y)|Z\right) = \begin{pmatrix} \Sigma_{XX|Z} & \Sigma_{XY|Z} \\ \Sigma_{YX|Z} & \Sigma_{YY|Z} \end{pmatrix}.$$

As all distributions involved are Gaussian, $X \perp Y|Z$ is equivalent to $\mathrm{Cov}\left((X, Y)|Z\right)$ being a block-diagonal matrix with blocks $\Sigma_{XX|Z}$ and $\Sigma_{YY|Z}$, which is equivalent to its inverse being a block-diagonal matrix with blocks $\Sigma_{XX|Z}^{-1}$ and $\Sigma_{YY|Z}^{-1}$. Its inverse is, by Lemma 3.10, the sub-matrix of P whose rows and columns correspond to X and Y. □

Applying Lemma 3.11 to model (3.30), we see that its precision matrix P is sparse, i.e. it is a block-tri-diagonal matrix, as $U_t \perp U_s|U_{-t,-s}$ for $|t - s| > 1$ and $U_{-t,-s}$ being the vector of all $U_0, \ldots, U_n$ except for U_t, U_s. Thus, the only entries of P that are potentially non-zero are those whose row and

column correspond to (U_t, U_t) for $t = 0, \dots, n$, (U_t, U_{t-1}) and (U_{t-1}, U_t) for $t = 1, \dots, n$. Therefore, P has the following block-tridiagonal structure:

$$P = \begin{pmatrix} P_{0,0} & P_{0,1} & 0 & \cdots & \cdots & 0 & 0 \\ P_{1,0} & P_{1,1} & P_{1,2} & 0 & \cdots & 0 & 0 \\ 0 & P_{2,1} & P_{2,2} & P_{2,3} & \cdots & 0 & 0 \\ \vdots & \ddots & \ddots & \ddots & \ddots & 0 & 0 \\ 0 & 0 & 0 & \cdots & P_{n-1,n-2} & P_{n-1,n-1} & P_{n-1,n} \\ 0 & 0 & 0 & \cdots & 0 & P_{n,n-1} & P_{n,n} \end{pmatrix}. \tag{3.32}$$

The sparsity of P implies that $P = LL^T$ has a sparse Cholesky root L, which will make computations efficient. To see that L is sparse, we apply the following Theorem, slightly adapted to our notation, from the theory of Gaussian-Markov-Random-fields (GMRF), i.e. Gaussian models whose dependency structure is given by a graph, with edges between nodes indicating non-zero entries in the precision matrix.

Theorem 3.10 ((Gelfand et al., 2010, Theorem 12.14)). *Let $X = (X_0, \dots, X_n) \in \mathbf{R}^{(n+1)m}$ be a GMRF wrt to the labeled graph G, with mean μ and symmetric positive-definite precision matrix P. Let L be the Cholesky factor of P and define for $0 \le t < s \le n$ the future of t except s as*

$$F(t, s) = \{t + 1, \dots, s - 1, s + 1, n\}.$$

Then

$$X_t \perp X_s | X_{F(t,s)} \Leftrightarrow L_{t,s} = 0.$$

In the preceding theorem $X_{F(t,s)}$ is the vector of all X_u for $u \in F(t, s)$ and $L_{t,s} \in \mathbf{R}^{m \times m}$ is the sub-matrix of L whose rows correspond to X_t and columns to X_s. From Theorem 3.10 we immediately obtain the following:

Corollary 3.2 (sparsity of L in model (3.30)). *Let $U \sim \mathbf{G}_\psi$ as in Equation (3.30), $P \succ 0$ be the precision matrix of $\overleftarrow{U} = (U_n, \dots, U_0)$ and L be the Cholesky root of P. Then L is a lower-block-diagonal matrix, with at most $nm^2 + (n + 1)m\frac{m-1}{2}$ non-zero entries:*

$$L = \begin{pmatrix} L_{n,n} & 0 & \cdots & \cdots & \cdots & 0 & 0 \\ L_{n-1,n} & L_{n-1,n-1} & 0 & \cdots & \cdots & 0 & 0 \\ 0 & L_{n-2,n-1} & L_{n-2,n-2} & 0 & \cdots & 0 & 0 \\ \vdots & \ddots & \ddots & \ddots & \ddots & 0 & 0 \\ 0 & 0 & 0 & \cdots & L_{1,2} & L_{1,1} & 0 \\ 0 & 0 & 0 & \cdots & 0 & L_{0,1} & L_{0,0} \end{pmatrix}, \tag{3.33}$$

where $L_{t,t} \in \mathbf{R}^{m \times m}, t = 0, \dots, n$ are lower triangular matrices with positive diagonal entries and $L_{t-1,t} \in \mathbf{R}^{m \times m}, t = 1, \dots, n$ are square matrices.

From L in Corollary 3.2 we obtain an iterative method of sampling from $\mathbf{G}_\psi$: If $v + U \sim \mathbf{G}_\psi$, then, as $\operatorname{Cov} U = \left(LL^T\right)^{-1} = L^{-T}L^{-1}$, it holds that $L^T U \sim \mathcal{N}(0, I)$ follows a standard normal distribution. Thus to simulate from $\mathbf{G}_\psi$ we may solve

$$L^T U = \overleftarrow{Z}$$

where $\overleftarrow{Z} = (Z_n, \dots, Z_0) \sim \mathcal{N}(0, I)$. Using the structure available in L, we see that this is equivalent to first solving

$$L_{0,0}^T U_0 = Z_0$$

and then recursively solving for $t = 1, \dots, n$

$$L_{t,t}^T U_t + L_{t-1,}^T U_{t-1} = Z_{t-1}.$$

Rearranging terms, provided $L_{t,t}$ is non-singular, we end up with the Markov-process

$$U_t = L_{t,t}^{-T} L_{t-1,t}^T U_{t-1} + L_{t,t}^{-T} Z_t, \tag{3.34}$$

where Z_t is, by construction, independent of U_{t-1}. Thus for model (3.30), we obtain

$$\begin{aligned} R_t &= L_{t,t}^{-T} \text{ for } t = 0, \dots, n, \\ C_t &= L_{t,t}^{-T} L_{t-1,t}^T \text{ for } t = 1, \dots, n. \end{aligned} \tag{3.35}$$

Here we see why we chose to use $\overleftarrow{U}$ in Corollary 3.2: had we applied Theorem 3.10 to U directly we would have ended up with a Markov process in reverse time.

We now turn our attention to applying the CE-method to model (3.30). Following a similar argument as in the discussion surrounding Equation (3.28), we see that we may match the mean v to that of $\mathbf{P}$ and it suffices to choose P, the precision matrix of U, such that it minimizes

$$\frac{1}{2} \operatorname{trace}\left(P\hat{\Gamma}\right) - \frac{1}{2} \log\det P \tag{3.36}$$

where $\hat{\Gamma}$ is the importance sampling estimate of the joint covariance matrix of all states X. This is equivalent to minimizing

$$\mathcal{D}_{\mathrm{KL}}\left(\mathcal{N}(0, \hat{\Gamma}) \middle|\middle| \mathcal{N}(0, P^{-1})\right).$$

Here P is restricted to precision matrices that may arise in model (3.30), i.e., by Corollary 3.2, $P = LL^T$ where L possess structure as in (3.33). At first glance, this problem seems more involved than solving Equation (3.29): after all, the optimal P depends on the whole covariance matrix $\hat{\Gamma}$. However, it turns out that the sparsity we enforce in L allows us to compute analytically the optimal $\hat{L}$ that minimizes Equation (3.36). Additionally, due to the Markov-structure of our proposal, $\hat{L}$ depends only on the block-tri-diagonal component of $\hat{\Gamma}$, i.e. only the covariances $\operatorname{Cov}(X_t, X_{t-1})$ and $\operatorname{Cov}(X_0)$ are required. This is sensible - all information about the Markov transitions is encoded in these covariances if we assume that X is a Gaussian Markov process.

To make this argument rigorous, let us apply the following result (stated in our notation).

Theorem 3.11 ((Schäfer, Katzfuss, and Owhadi, 2021, Theorem 2.1))**.** *Let Γ be a positive-definite matrix of size $n \times n$. Given a lower-triangular sparsity set $S \subset \{1, \dots, n\}^2$, i.e. $i \geq j$ for all $(i, j) \in S$, let*

$$\hat{L} = \operatorname{argmin}_{L \in \mathcal{S}} \mathcal{D}_{KL}\left(\mathcal{N}(0, \Gamma) \middle|\middle| \mathcal{N}\left(0, (LL^T)^{-1}\right)\right)$$

be the Cholesky root of the closest Gaussian (wrt. the KL-divergence) with sparsity $\mathcal{S} = \{A \in \mathbf{R}^{n \times n} : A_{i,j} \neq 0 \Rightarrow (i, j) \in S\}$.

Then the following holds: The nonzero entries of the i-th column of $\hat{L}$ are given by

$$L_{s_i, i} = \frac{\Gamma_{s_i, s_i}^{-1} e_1}{\sqrt{e_1^T \Gamma_{s_i, s_i}^{-1} e_1}}, \tag{3.37}$$

where $s_i = \{j : (i, j) \in \mathcal{S}\}$, Γ_{s_i, s_i} is the restriction of Γ to the set of indices s_i and $e_1 \in \mathbf{R}^{|s_i|}$ is the first unit vector.

Exploiting the Markov structure of our proposals, we immediately obtain the following:

Corollary 3.3. *Let $\mathcal{S}$ be the sparsity set of a Gaussian Markov process of the form Equation (3.30), i.e.*

$$\mathcal{S} = \left\{((t, i), (s, j)) \in (\{0, \dots, n\} \times \{1, \dots, m\})^2 \mid (t = s \text{ and } i \geq j) \text{ or } t = s + 1\right\},$$

see also Equation (3.33), and let Γ be a positive definite matrix of size $((n+1)m) \times (n+1)m$ with blocks

$$\Gamma_{s,t} = (\Gamma_{(s,i),(t,j)})_{i,j=1,\dots,m}.$$

Then $\hat{L}$ in Theorem 3.11 depends only on the block-diagonal entries $\Gamma_{t,t}$, $t = 0, \dots, n$ and block off-diagonal entries $\Gamma_{t,t+1}$, $t = 0, \dots, n$.

If, in particular, Γ is the covariance matrix of Gaussian Markov process, $\hat{L} = \mathrm{chol}(\Gamma^{-1})$.

We have thus shown the following: The covariance matrix of the KL-optimal Gaussian Markov process for the positive definite covariance matrix Γ with $\mathcal{O}(n^2m^2)$ entries only depends on $\mathcal{O}(nm^2)$ many entries, the marginal covariances. In particular, if we can find a centered Gaussian Markov process $(X_t)_{t=0,\dots,n}$ whose marginal covariances fulfill

$$\begin{aligned} \mathrm{Cov}(X_t) &= \Gamma_t & t &= 0, \dots, n \\ \mathrm{Cov}(X_t, X_{t+1}) &= \Gamma_{t,t+1} & t &= 0, \dots, n, \end{aligned}$$

then its law $\mathcal{L}(X)$ is the one we seek. The following proposition puts all the pieces together.

Theorem 3.12 (the CE-method for the Markov proposal)**.** *Let $\mathbf{P}$ be a probability measure on $\mathbf{R}^{(n+1)\times m}$ with mean μ and positive definite covariance matrix Γ, partitioned into blocks*

$$\Gamma_{s,t} = (\Gamma_{(s,i),(t,j)})_{i,j=1,\dots,m}.$$

Let

$$\begin{pmatrix} J_{t,t} & 0 \\ J_{t+1,t} & Z_{t+1,t+1} \end{pmatrix} = \mathrm{chol} \begin{pmatrix} \Gamma_{t,t} & \Gamma_{t,t+1} \\ \Gamma_{t+1,t} & \Gamma_{t+1,t+1} \end{pmatrix}.$$

Then the optimal cross-entropy parameter

$$\psi_{CE} = \mathrm{argmin}_{\psi=(v,C_1,\dots,C_n,R_0,\dots,R_n)} \mathcal{D}_{KL}\left(\mathbf{P} || \mathbf{G}_\psi\right)$$

for the Markov proposal $\mathbf{G}_\psi$ from model (3.30) exists and is unique. The components of ψ_{CE} are given by

$$\begin{aligned} v &= \mu \\ R_0 &= \mathrm{chol}(\Gamma_{0,0}) \end{aligned}$$

and for $t = 1, \dots, n$

$$\begin{aligned} C_t &= J_{t+1,t} J_{t,t}^{-1} \\ R_t &= Z_{t+1,t+1} \end{aligned}$$

Thus, given ν and Γ, ψ_{CE} can be obtained in $\mathcal{O}(nm^3)$ many operations.

Proof. It only remains to show the uniqueness and existence of ψ_{CE}, as well as its representation. The discussion surrounding Equation (3.36) shows that $v = \mu$ has to hold, so we may assume that $\mathbf{P}$ and the proposal are both centered. As Γ is positive definite, so are all of its sub-matrices, and we may apply Corollary 3.3. Therefore, if we can show that there is a unique Gaussian Markovian probability measure whose covariance matrix matches Γ as in that corollary we are done.

Let $(U_t)_{t=0,\dots,n} \sim \mathbf{G}_{\psi_{\mathrm{CE}}}$. Then

$$\mathrm{Cov}(U_0) = R_0 R_0^T = \Gamma_{0,0},$$

and from the Cholesky decomposition we obtain for $t = 0, \dots, n-1$

$$\begin{pmatrix} J_{t,t}J_{t,t}^T & J_{t,t}J_{t+1,t}^T \\ J_{t+1,t}J_{t,t}^T & J_{t+1,t}J_{t+1,t}^T + Z_{t+1,t+1}Z_{t+1,t+1}^T. \end{pmatrix} = \begin{pmatrix} \Gamma_{t,t} & \Gamma_{t,t+1} \\ \Gamma_{t+1,t} & \Gamma_{t+1,t+1} \end{pmatrix}.$$

As $Z_{t+1,t+1}$ is a lower triangular matrix with positive diagonal and

$$\Gamma_{t+1,t+1} - \Gamma_{t+1,t}\Gamma_t^{-1}\Gamma_{t,t+1} = Z_{t+1,t+1}Z_{t+1,t+1}^T,$$

it is the Cholesky root of the Schur complement $\Gamma_{t+1,t+1} - \Gamma_{t+1,t}\Gamma_t^{-1}\Gamma_{t,t+1}$, which, recalling Lemma 3.1, we can think of as a conditional covariance matrix. Therefore, using induction over $t = 0, \dots, n-1$, we obtain

$$\begin{aligned}\operatorname{Cov}(U_{t+1}) &= C_{t+1} \operatorname{Cov}(U_t) C_{t+1}^T + R_{t+1} R_{t+1}^T \\ &= J_{t+1,t} J_{t,t}^{-1} \Gamma_{t,t} J_{t,t}^{-T} J_{t+1,t}^T + \Gamma_{t+1,t+1} - \Gamma_{t+1,t}\Gamma_t^{-1}\Gamma_{t,t+1} \\ &= \Gamma_{t+1,t+1}\end{aligned}$$

and

$$\operatorname{Cov}(U_{t+1}, U_t) = C_t \operatorname{Cov}(U_t) = J_{t+1,t} J_{t,t}^{-1} J_{t,t} J_{t,t}^T = \Gamma_{t+1,t}.$$

This shows the existence. For uniqueness, note that model (3.30) enforces that R_t is a lower triangular matrix with positive diagonals. As $R_{t+1}R_{t+1}^T$ is the conditional covariance of U_{t+1} given U_t which is, by Lemma 3.1 given by $\Gamma_{t+1,t+1} - \Gamma_{t+1,t}\Gamma_{t,t}^{-1}\Gamma_{t+1,t}$. Thus the R matrices are unique as well. As $\operatorname{Cov}(U_{t+1}, U_t) = C_t \operatorname{Cov}(U_t)$, we can show that, additionally, also C_t is unique. □

When using the CE-method, we do not have access to the mean and covariances necessary to apply this proposition. Instead, we may apply the CE-method to estimate ψ in model (3.30) by replacing these unknown moments with their importance sampling estimates. Given importance samples $U^1, \dots, U^N$ for $\mathcal{L}(X|Y=y)$ and associated auto-normalized weights $W^1, \dots, W^N$, we estimate v by

$$\hat{v} = \sum_{i=1}^N W^i X^i \tag{3.38}$$

and the empirical covariance matrices

$$\begin{aligned}\widehat{\operatorname{Cov}}(X_t, X_{t-1}) &= \sum_{i=1}^N W^i (X_{t:t-1}^i - \hat{v}_{t-1:t})(X_{t:t-1}^i - \hat{v}_{t-1:t})^T \\ \widehat{\operatorname{Cov}}(X_0) &= \sum_{i=1}^N W^i (X_0^i - \hat{v}_0)(X_0^i - \hat{v}_0)^T\end{aligned} \tag{3.39}$$

These steps are summarized in Algorithm 7.

Algorithm 7 The CE-method for the Markov proposal (3.30)

Require: EGSSM (Definition 3.5), observations Y, initial estimate $\hat{\psi}^0 = (v^0, C^0, R^0)$, sample size N

1: set $l = 0$
2: **repeat**
3: sample $U^1 + v^l, \dots, U^N + v^l \overset{\text{i.i.d}}{\sim} \mathbf{G}_{\hat{\psi}^l}$ with fixed seed ▷ Equation (3.30)
4: determine auto-normalized weights $W^1, \dots, W^N$ ▷ Equation (3.31)
5: estimate $\hat{v}^{l+1}$ ▷ Equation (3.38)
6: estimate $\widehat{\operatorname{Cov}}(U_t, U_{t-1}), t = 1, \dots, n$, and $\widehat{\operatorname{Cov}}(U_0)$ ▷ Equation (3.39)
7: determine C^{l+1} and R^{l+1} ▷ Theorem 3.12
8: set $\hat{\psi}^{l+1} = (\hat{v}^{l+1}, C^{l+1}, R^{l+1})$
9: set $l = l + 1$
10: **until** $\hat{\psi}^l$ converged
11: **return** $\hat{\psi}_{\text{CE}} = \hat{\psi}^l$

To run Algorithm 7 we require an initial value for $\hat{\psi}^0$. If a suitable $\hat{\psi}^0$ is not available, we can obtain one from the LA by sampling $X^1, \dots, X^N$ from the LA and performing steps 5 to 8 from the loop. Alternatively, we could also directly base our initial value on the smoothing distribution of the GLSSM that the LA is based on. The Kalman smoother (Algorithm 2) provides us with the

step	time complexity	space complexity
simulation (Step 3)	$\mathcal{O}\left(Nnm^2\right)$	$\mathcal{O}\left(Nnm\right)$
weights (Step 4)	$\mathcal{O}(Nnm^2)$	$\mathcal{O}\left(N\right)$
estimating v (Step 5)	$\mathcal{O}(Nnm)$	$\mathcal{O}\left(nm\right)$
estimating covariances (Step 6)	$\mathcal{O}(Nnm^2)$	$\mathcal{O}\left(nm\right)$
determining C and R (Step 7)	$\mathcal{O}(nm^3)$	$\mathcal{O}(nm^2)$

Table 3.1: Time and space complexities of individual steps in Algorithm 7.

analytically available covariances $\mathrm{Cov}\left(X_t, X_{t-1}|Z=z\right)$ and the marginal covariance $\mathrm{Cov}\left(X_0|Z=z\right)$ can be computed as well.

The convergence criteria in Algorithm 7 is similar to that used for EIS: we stop until the absolute or entry-wise relative difference of $\hat{\psi}^l$ and $\hat{\psi}^{l+1}$ is smaller than a predetermined threshold, or a fixed number of iterations has passed. For the matrices involved, we use the Frobenius norm and the Euclidean distance for the mean v.

In Algorithm 7 we use the standard praxis of CRNs to ensure numerical convergence. This is similar to EIS and the maximum likelihood estimates from Section 3.6.

We give an overview of the time and space complexities of each line in Algorithm 7 in Table 3.1 The total time complexity of a single iteration of Algorithm 7 is $\mathcal{O}\left(Nnm^2 + nm^3\right)$ and its space complexity is $\mathcal{O}\left(Nnm + nm^2\right)$. Let us elaborate on the complexities of each step:

Step 3 Generate N i.i.d. samples from model (3.30), where each simulation requires $\mathcal{O}(n)$ matrix-vector multiplications of dimension m.

Step 4 To evaluate the weights, Equation (3.31), we have to evaluate for every sample $\mathcal{O}(n)$-times the density of a m-variate Gaussian distribution, while this usually has time-complexity $\mathcal{O}(m^3)$, we have access to the Cholesky root R_t, so this step has only time-complexity $\mathcal{O}(m^2)$. In Equation (3.31) we also need to compute $p(y_t|x_t)$ and $p(x_t|x_{t-1})$. Assuming conditional independence of observations, $p(y_t|x_t) = \prod_{i=1}^m p(y_t^i|(B_t x_t)^i)$, evaluating the first term requires only $\mathcal{O}(m^2)$ operations. For the second term, if we allow pre-computation of the Cholesky roots of innovations off-line (in $\mathcal{O}(m^3)$ time), this step reduces to $\mathcal{O}(m^2)$ as well.

Step 5 Calculating the weighted mean $\hat{v} \in \mathbf{R}^{(n+1)m}$, Equation (3.38), requires $\mathcal{O}(Nnm)$ operations.

Step 6 Calculating the weighted covariance matrices, Equation (3.39), requires $(n+1)$ times multiplying N many $m \times 1$ with $1 \times m$ vectors.

Step 7 For each of the $\mathcal{O}(n)$ many C_t and R_t we have to calculate Cholesky decompositions and invert triangular matrices of dimension m.

An efficient implementation of Algorithm 7 can improve on the practically relevant computational time. There is no need to calculate the C_t matrices explicitly, instead we can calculate $C_t U_{t-1} = J_{t+1,t} J_{t,t}^{-1} U_{t-1}$ efficiently by back-substitution, as $J_{t,t}$ is a lower triangular matrix.

The main bottleneck for space lies in the $\mathcal{O}(Nnm)$ simulation part, and we may reduce this by simulating twice from model (3.30) using CRNs, and only storing the samples for a single time step (dimension $\mathcal{O}(Nm)$) in each simulation. In the first pass, we only calculate the weights, and in the second pass, we calculate $\hat{v}$ and the required covariance matrices. For this, we only need the $2N$ samples of dimension m from time t and $t+1$, i.e. $\mathcal{O}(Nm)$ space. This reduces the total space complexity to $\mathcal{O}(Nm + nm^2)$.

We demonstrate these improvements in Algorithm 8. Additionally, we calculate the weights on the log scale for numerical stability.

The advantage of Algorithms 7 and 8 over applying the CE-method to the GLSSM model (3.22) are multiple: First of all, as long as the involved covariance matrices are positive definite, the two algorithms produce valid proposals, i.e. they do not have the degeneracy problem we observed in

Algorithm 8 Time and space improved version of Algorithm 7. Instructions involving the free index i are to be performed for all $i = 1, \dots, N$ samples. For simplicity of notation we let $R^l = (R_0^l, \dots, R_n^l)$ and $J^l = (J_{0,0}^l, J_{1,0}^l, \dots, J_{n-1,n-1}^l, J_{n,n-1}^l)$ for $l \in \mathbf{N}_0$.

Require: EGSSM (Definition 3.5), observations Y, initial estimate $\hat{\psi}^0 = \left(v^0, R^0, J^0\right)$, sample size N

set $l = 0$
repeat
  simulate $\nu_0^1, \dots, \nu_0^N \overset{\text{i.i.d}}{\sim} \mathcal{N}(0, I)$
  set $U_0^i = R_0^l \nu_0^i$
  set $X_0^i = v_0^l + U_0^i$
  set $\log w^i = \log p(y_0 | X_0^i) + \log p(X_0^i) + \frac{1}{2}\|\nu_0^i\|^2$ ▷ $\log g(X_0^i) = -\frac{1}{2}\|\nu_0^i\|_2^2 + C$
  store current RNG state
  for $t \leftarrow 1, \dots, n$ **do**
    simulate $\nu_t^1, \dots, \nu_t^N \overset{\text{i.i.d}}{\sim} \mathcal{N}(0, I)$
    set $U_t^i = (J_{t+1,t})^T (J_{t,t})^{-1} U_{t-1}^i + R_t^l \nu_t^i$ ▷ backsubstitution
    set $X_t^i = v_t^l + U_t^i$
    set $\log w^i = \log w^i + \log p(y_t | X_t^i) + \log p(X_t^i | X_{t-1}^i) + \frac{1}{2}\|\nu_t^i\|^2$
  end for
  set $\log w^i = \log w^i - \max_{i=1,\dots,N} \log w^i$ ▷ ensure $\log w^i \leq 0$
  set $w^i = \exp(\log w^i)$
  set $W^i = \frac{w^i}{\sum_{i=1}^N w^i}$ ▷ auto-normalized weights
  set $v_0^{l+1} = \sum_{i=1}^N W^i X_0^i$
  restore RNG state
  for $t \leftarrow 1, \dots, n$ **do**
    simulate $\nu_t^1, \dots, \nu_t^N \overset{\text{i.i.d}}{\sim} \mathcal{N}(0, I)$
    set $U_t^i = (J_{t+1,t})^T (J_{t,t})^{-1} U_{t-1}^i + R_t^l \nu_t^i$ ▷ backsubstitution
    set $X_t^i = v_t^l + U_t^i$
    calculate $\hat{v}_t^{l+1}$ ▷ Equation (3.38)
    calculate covariances ▷ Equation (3.38)
  end for
  set $\hat{\psi}^{l+1} = \left(\hat{v}^{l+1}, \hat{R}^{l+1}, \hat{J}^{l+1}\right)$
  set $l = l + 1$
until $\hat{\psi}^l$ converged
return $\hat{\psi}_{\text{CE}} = \hat{\psi}^l$

Section 3.5.1. When matrices are only positive-semi definite, replacing inverses with generalized inverses still yields a valid model. Additionally, determining the optimal parameters (v, C, R) or (v, J, R) is numerically stable, involving only inversion of small matrices. Compare this with solving Equation (3.29), where we need to employ a numerical scheme to solve for the diagonal entries of Ω.

After having determined $\hat{\psi}_{\text{CE}}$ for model (3.30), generating N samples requires only $\mathcal{O}(Nnm^2)$ operations, whereas sampling from model (3.22) requires $\mathcal{O}(nm^3 + Nnm^2)$ operations, as we need an initial run of the Kalman filter. Unless $N < m$, this difference is negligible, and the case where $N < m$ is not really of interest, as we would expect importance sampling to require a much larger number of samples, i.e. $N \gg m$.

However, the two algorithms presented in this section also come with some drawbacks, especially if the dimension m of states is large. This affects the algorithms in multiple ways: when m is large, computation of the Cholesky decomposition in Theorem 3.12 becomes more time-intensive. Additionally, the dimension of the parameter ψ increases quadratically in m, so we expect convergence to be slower, requiring a larger sample size N to find the optimal $\hat{\psi}_{\text{CE}}$. For an empirical study in this direction, see Section 3.7.

3.5.3 Central Limit Theorems for Importance Sampling in PGSSMs

Consider a PGSSM with states $X = (X_0, \dots, X_n)$ and observations $y = (y_0, \dots, y_n)$. The target of interest is then $\mathbf{P}^X = \mathbb{P}^{X|Y=y}$ or $\mathbf{P}^S = \mathbb{P}^{S|Y=y}$, if such a signal exists. As argued in the discussion surrounding Equation (3.25) the two targets are equivalent. Using a similar approach to the on presented in Section 3.3, it seems obvious that both the CE-method and EIS fulfill a central limit theorem: we are constructing Gaussian proposals which form an exponential family, and so we should be able to apply Theorem 3.6 and Theorem 3.9 directly to this setting.

However, we have to be somewhat more careful: the assumptions of the central limit theorems have to be checked thoroughly. Additionally, upon closer inspection, we see that the proposal distributions created by EIS do not necessarily form a natural exponential family, as we will see later. Lastly, the proposal we generate are Gaussian, which allows us to simplify some of the technical assumptions made earlier.

We will formulate all results in the matrix formulation of SSMs, see (Durbin and Koopman, 2012, Section 4.13). This form considers $X \in \mathbf{R}^{(n+1)m}$, $Y \in \mathbf{R}^{(n+1)p}$ and so on, ignoring the Markov-structure introduced by the SSM. However, as we have seen in Equation (3.32), the Markov-structure is still present, if only in the precision matrix of the states X.

We begin with the CE-method. As the precision matrix is the natural parameter for the multivariate Gaussian exponential family, we see that model (3.30), parameterized by $(P^{-1}v, P)$, with P as in Equation (3.32), form a natural exponential family. Thus, we can apply Theorem 3.6 to obtain a central limit theorem when applying the CE-method for this model.

Lemma 3.12 (Markov-proposal forms exponential family)**.** *Let $\mathbf{G}_\psi$, $\psi \in \Psi$ be the family of Gaussian proposals from Equation (3.30), reparameterized by*

$$\psi = (Pv, P)\,,$$

where P is as in Equation (3.32). Then $(\mathbf{G}_\psi)_{\psi\in\Psi}$ form an exponential family.

Proof. As

$$\Psi \subseteq \left\{(\Sigma^{-1}\mu, \Sigma^{-1}) | \mu \in \mathbf{R}^{(n+1)m}, \Sigma \in \mathbf{R}^{((n+1)m)\times((n+1)m)} \text{ positive definite}\right\},$$

it suffices to show that Ψ is a subspace, i.e. closed under addition and scalar multiplication. That Ψ is closed under scalar multiplication is obvious. For $(P_1v_1, P_1), (P_2v, P_2) \in \Psi$ we have

$$(P_1v_1, P_1) + (P_2v_2, P_2) = \big((P_1 + P_2)(P_1 + P_2)^{-1}(P_1v_1 + P_2v_2, P_1 + P_2)\big)\,.$$

Furthermore, as P_1 and P_2 possess the sparsity structure given by Equation (3.32), so does $P_1 + P_2$, so $(P_1v_1, P_1) + (P_2v_2, P_2) \in \Psi$. □

Thus, the proposals $(\mathbf{G}_\psi)_{\psi\in\Psi}$ form a natural exponential family, a sub-family of the full Gaussian exponential family. Its sufficient statistic is $T(x) = \begin{pmatrix} x \\ xx^T \end{pmatrix}$. The central limit theorem for the CE-method follows:

Theorem 3.13 (CLT for the CE-method in PGSSMs)**.** *Let $\mathbf{G}_\psi$ be as in Lemma 3.12 and let $\mathbf{G} \gg \mathbf{P}^X$ be a proposal distribution. Suppose the following additional assumptions hold:*

(i) $w, w\,\mathrm{id}, w\,\mathrm{id}^2 \in L^2(\mathbf{G})$,

(ii) $\mathbf{P}^X$ *posses all fourth order moments, and*

(iii) the covariance matrix of $\mathbf{P}^X$ *is positive-definite.*

Then $\hat{\psi}_{CE}$ fulfills a CLT of the form

$$\sqrt{N}\left(\hat{\psi}_{CE} - \psi_{CE}\right) \to \mathcal{N}(0, BMB)$$

where B and M are as in Theorem 3.6.

Proof. We will check that all assumptions of Theorem 3.6 are fulfilled.

That $\psi_{\mathrm{CE}} \in \Psi$ is the unique maximizer of Equation (3.13) follows from Proposition 3.2, as the full Gaussian exponential family has non-degenerate Fisher information. That $T \in L^2(\mathbf{P})$ follows from the definition of T and the existence of forth order moments. □

The case for EIS is more involved. Let us start with the simplest case where $n = 0$, where there is only a single observation $Y = y_0 \in \mathbf{R}^m$. Indeed, all SSMs may be viewed this way, by simply ignoring the time-dependence structure and vectorizing all involved states, signals and observations. In this setting, proposal densities for $\mathbf{P}^X$ are of the form

$$\begin{aligned} p_\psi(x|z) &\propto p_\psi(z|x)p(x) \\ &\propto \det(\Omega^{-1}) \exp\left(-\frac{1}{2}(z - Bx)^T\Omega^{-1}(z - Bx)\right) \det(\Sigma^{-1}) \exp\left(-\frac{1}{2}(x-\mu)^T\Sigma^{-1}(x-\mu)\right), \end{aligned}$$

which suggests $\psi = \left(B\Omega^{-1}z, B^T\Omega^{-1}B\right)$. However, unless B is invertible, the exponential family under consideration will, in general, fail to fulfill the uniqueness properties required for consistency and the central limit theorem, e.g. Lemma 3.9 can fail to apply. Additionally, working with $\psi = \left(B\Omega^{-1}z, B^T\Omega^{-1}B\right)$ is tedious, as we have to take care of B potentially being rank-deficient. Instead, we will focus on the target $\mathbf{P}^S$ from which we can reconstruct $\mathbf{P}^X$, as long as $s = Bx$ has a $\mathbf{P}^S$ a.s. solution. As the support of $\mathbf{P}^S = \mathbb{P}^{S|Y=y}$ can only be smaller than that of $\mathbb{P}^S$, this is always the case. For simplicity, we assume that B has full row-rank, i.e. $\mathrm{image}(B) = \mathbf{R}^{(n+1)p}$

Furthermore, the proofs of Theorem 3.8 and Theorem 3.9 only involve the densities of the proposal through the log-weights, up to additive constants that do not depend on s. In our setting, we can write the log-weights as

$$\log w_\psi(s) = \log p(s|y) - \log g_\psi(s|z) = \log p(y|s) - \log g_\psi(z|s) - (\log p(y) - \log g_\psi(z)).$$

Now $g_\psi(z|s)$ is just a Gaussian natural-exponential family with parameter $\psi = (\Omega^{-1}z, \Omega^{-1})$ and sufficient statistic $T(x) = \begin{pmatrix} x \\ xx^T \end{pmatrix}$. The parameter space is

$$\Psi = \left\{(\Omega^{-1}z, \Omega^{-1})\middle| z \in \mathbf{R}^{(n+1)p}, \Omega \in \mathrm{BDiagSPD}((\mathrm{n}+1), \mathrm{p})\right\}$$

where $\mathrm{BDiagSPD}((\mathrm{n}+1), \mathrm{p})$ consists of all block-diagonal matrices Ω whose $n+1$ blocks on the diagonal are symmetric, positive-definite matrices of dimension $p \times p$.

In this setup, we can prove the central limit theorem for EIS.

Theorem 3.14 (CLT for EIS in PGSSMs)**.** *Let $(\mathbf{G}_\psi)_{\psi\in\Psi}$ be the family of proposals with densities $g_\psi(\cdot|z)$, as described above. Assume that B has full row-rank and let $\mathbf{G} \gg \mathbf{P}^S$ be a proposal with weights w. Furthermore, assume that the following conditions hold for $T_{s,i} = \begin{pmatrix} x_{s,i} \\ x_{s,i}x_{s,i} \end{pmatrix}$, $s = 0,\dots,n$, $i = 1,\dots,m$.*

(i) $wT_{s,i}T_{s',j} \in L^2(\mathbf{G})$ *for* $i,j = 1,\dots,m$ *and* $s,s' = 0,\dots,n$.

(ii) $\log p \in L^4(\mathbf{P}^S)$ *and*

(iii) $\mathrm{Cov}_{\mathbf{P}^S}(T)$ *is non-singular and* $\psi_{EIS} \in \operatorname{int}\Psi$.

Then $\hat{\psi}_{EIS}$ fulfills a CLT of the form

$$\sqrt{N}\left(\hat{\psi}_{CE} - \psi_{CE}\right) \to \mathcal{N}(0, BMB),$$

where B and M are as in Theorem 3.9.

Proof. We adapt the proof of Theorem 3.9 to account for the new setup. The assumptions are the same, except that we can drop the assumption that $T_{s,i} \in L^4(\mathbf{P}^S)$, as $\mathbf{P}^S$ possess all finite moments.

Consider the weights $\log w_\psi = \log p(s|y) - \log g_\psi(s|z)$ and recall that EIS solves the optimization problem

$$\min_{\psi\in\Psi} \mathbf{P}^S\left[\log w_\psi - \mathbf{P}^S[\log w_\psi]\right].$$

Now

$$\begin{aligned}\log w_\psi - \mathbf{P}^S[\log w_\psi] &= \log p(y|s) - \log g_\psi(z|s) - (\log p(y) - \log g_\psi(z)) \\ &= \log p(y|s) - \psi^T T(s) + \frac{(n+1)p}{2}\log 2\pi - Z(\psi) - (\log p(y) - \log g_\psi(z)),\end{aligned}$$

which motivates setting $\log \tilde{w}_\psi = \log p(y|s) - \psi^T T(s)$ and $\lambda = \mathbf{P}^S \log \tilde{w}_\psi = \frac{(n+1)p}{2}\log 2\pi - Z(\psi) - (\log p(y) - \log g_\psi(z))$. This is precisely the setup from Equation (3.19) which is all that is necessary for Theorem 3.9 to apply. □

Notice that we did not give the precise structure of B and M for both CLTs. The reason for this is that although we have imposed additional structure (Gaussian proposals), the matrices involved in the asymptotic covariance matrix are not more tractable.

Let us close this section with a short recapitulation on what we have achieved. We have seen that both the CE-method and EIS are able to exploit the Markov-structure of PGSSM, albeit in different ways.

The CE-method does not apply well to the GLSSM-approach, the reason being, that matching the covariance matrix of the target to the proposal cannot be achieved by looking at marginals only. Instead, the GLSSM-approach, which exploits the Markov-structure in the precision matrix, is more suited for the CE-method. As the Markov-approach contains proposals that directly form an exponential family, the associated CLT follows naturally.

EIS is able to use the GLSSM-approach, which has two benefits. First, the number of parameters is smaller, especially when there is a linear signal — which is often the case in applications. Second, the optimization problem solved in EIS can be broken down into multiple smaller problems, see Equation (3.27). While the proposals for EIS do not form an exponential family, we still obtain Theorem 3.14 by focusing on the signals and noting that the objective function is still, after appropriate reparametrization, a linear least squares problem of the parameters of interest, which is all that is necessary for the CLT to hold.

Similar to the CLTs in Section 3.3, we argue that Theorem 3.13 and Theorem 3.14 are widely applicable. The integrability assumptions on weights and targets are natural if we want importance sampling with Gaussian proposals to work, while the remaining assumptions are required for the optimal parameters ψ_{CE} and *peis* to exist and be unique.

However, while the CLTs provide theoretical justifications for using the two methods, the practical applicability, especially numerical stability, especially when the number of samples N is low, does not follow from them. We will come back to this point in Section 3.7.

3.6 Inference in PGSSMs

Once we have chosen a suitable PGSSM to model the observations $(y_t)_{t=0,\dots,n}$, we are interested in statistical inferences. This is a two-part procedure: first we must estimate the unknown hyperparameters θ, which we will do by maximum likelihood estimation. Then we have to obtain a description of the conditional distributions of interest, e.g. the conditional distribution of states given observations or the conditional distribution of future, yet unavailable, observations.

3.6.1 Maximum likelihood estimation

Until now, we have assumed that the SSM under consideration is completely known, i.e. we have access to the true transition and observation kernels. For the models considered in this thesis (Chapter 4), this is unrealistic, as they are not based on concrete physical processes but are rather statistical approximations of the true underlying dynamics. The transition densities of, e.g., Equation (3.4) will depend on the covariance matrix of innovations, of which we have no a priori knowledge and for negative binomially distributed observations the overdispersion parameter r will be unknown. Let us denote by $\theta \in \mathbf{R}^l$ the vector of these hyperparameters. To make this dependence explicit, we will introduce subscripts θ where appropriate, i.e. $\mathbf{P}_\theta$ is a target distribution that additionally depends on θ, p_θ its density et cetera. This section is loosely based on (Durbin and Koopman, 2012, Chapter 7 & 11) and (Chopin and Papaspiliopoulos, 2020, Chapter 14).

To determine a suitable value of θ, multiple options are available. Here, we opt for a frequentist approach, using maximum likelihood estimation to determine an optimal $\hat{\theta}$. Therefore, given observations $y \in \mathbf{R}^{(n+1)\times p}$, $\hat{\theta}$ maximizes the likelihood $p_\theta(y)$ and can be obtained as the global maximum of the following optimization problem:

$$\max_{\theta\in\Theta} p_\theta(y).$$

For numerical stability, we should maximize the log-likelihood instead, i.e. solve

$$\max_{\theta\in\Theta} \log p_\theta(y). \tag{3.40}$$

Here $\Theta \subseteq \mathbf{R}^l$ is the parameter space. To solve this optimization problem using gradient ascent algorithms, we need access to both the likelihood and its derivatives. Thus, in the following, we will assume that $\theta \mapsto \log p_\theta(y)$ is sufficiently smooth, to apply these methods, i.e. it has continuous derivatives of second order.

While the Kalman-filter (Algorithm 1) allows analytical computation of this likelihood GLSSMs, in general SSMs it is numerically intractable. The reason for this is that

$$p_\theta(y) = \int p_\theta(x, y)\mathrm{d}\mu(x)$$

is a high-dimensional integral, which is hard to evaluate numerically. Instead, we will use importance sampling to estimate the likelihood. For this, let us regard $p_\theta(x, y)$ as an unnormalized density in x. The missing integration constant is then just $p_\theta(y)$ and the normalized density is $p_\theta(x|y)$. If $\mathbf{G} \gg \mathbf{P}_\theta$ is a proposal distribution whose density g with respect to μ we can evaluate analytically, i.e. not only up to a constant, we see that for the unnormalized weights $\tilde{w}_\theta(x) = \frac{p_\theta(x,y)}{g(x)}$, that $p_\theta(y) = \mathbf{G}[\tilde{w}_\theta]$. Thus we may estimate the likelihood by

$$\widehat{p_\theta(y)} = \frac{1}{N}\sum_{i=1}^{N} \tilde{w}_\theta(X^i)$$

for $X^1, \dots, X^N \overset{\text{i.i.d}}{\sim} \mathbf{G}$ and $N \in \mathbf{N}$. To evaluate the gradient, notice that as $\nabla_\theta p_\theta(x,y) = p_\theta(x,y)\nabla_\theta \log p_\theta(x,y)$, we have, provided we can exchange integration and differentiation,

$$\begin{aligned}\nabla_\theta p_\theta(y) &= \nabla_\theta \int p_\theta(x,y)\,\mathrm{d}\mu(x) = \int p_\theta(x,y)\nabla_\theta \log p_\theta(x,y)\,\mathrm{d}\mu(x) \\ &= \mathbf{G}[\tilde{w}_\theta \nabla_\theta \log p_\theta(x,y)],\end{aligned}$$

and so we may estimate the gradient by

$$\widehat{\nabla_\theta p_\theta(y)} = \frac{1}{N}\sum_{i=1}^N \tilde{w}_\theta(X^i)\nabla_\theta \log p_\theta(X^i, y)$$

Similarly, we can estimate the log-likelihood by Plug-In

$$\widehat{\log p_\theta(y)} = \log\left(\frac{1}{N}\sum_{i=1}^N \tilde{w}_\theta(X^i)\right) \tag{3.41}$$

and its gradient, using the fact that the gradient of $\log f$ for $f : \mathbf{R}^l \to \mathbf{R}$ is $\frac{1}{f}\nabla_\theta f$, by

$$\begin{aligned}\widehat{\nabla_\theta \log p_\theta(y)} &= \left(\frac{1}{N}\sum_{i=1}^N \tilde{w}_\theta(X^i)\right)^{-1}\left(\frac{1}{N}\sum_{i=1}^N \tilde{w}_\theta(X^i)\nabla_\theta \log p_\theta(X^i,y)\right) \\ &= \sum_{i=1}^N W_\theta^i \nabla_\theta \log p_\theta(X^i, y)\end{aligned}$$

where $W_\theta^i = \frac{\tilde{w}_\theta(X^i)}{\sum_{i=1}^N \tilde{w}_\theta(X^i)}$ are the auto-normalized weights. Note that, by Jensen's inequality, these estimates are biased.

To solve the optimization problem (3.40) we will again employ CRNs. If the densities involved are twice differentiable, this device ensures that the random objective function $\theta \mapsto \sum_{i=1}^N \tilde{w}_\theta(X^i)$ is twice differentiable, and so we can indeed apply gradient ascent to find a local maximum. This is an advantage of performing global importance sampling over SMC, i.e. particle filter, methods. To avoid collapse to a single particle, SMC methods perform intermediate resampling steps, which make the objective function discontinuous. While particle smoothing methods can mitigate this problem, they are more expensive than standard SMC and, as the importance sampling estimates of the log-likelihood and its gradient are biased, the usual requirements for stochastic approximation methods are not fulfilled. For a more thorough discussion of the challenges maximum likelihood estimation with SMC methods faces, we recommend (Chopin and Papaspiliopoulos, 2020, Chapter 14).

While MLEs have a strong frequentist foundation, let us stress that, for the models that we investigate in Chapter 4, the frequentist properties of the estimates are not of interest. The reason for this is that a frequentist interpretation requires us to imagine, at least hypothetically, an infinite repetition of the data-generating process. For the data at hand, such repetition is nonsensical: the pandemic is a "one-off" event that will not be replicated under even approximately similar circumstances. Therefore, we will choose to view the estimation procedure more as a hyper-parameter tuning step, rather than true frequentist inference. While we can compute asymptotic confidence intervals for $\hat{\theta}$, see, e.g., (Durbin and Koopman, 2012, Chapter 11.6), (Chopin and Papaspiliopoulos, 2020, Chapter 14.8), these are not of practical interest for similar reasons.

As an alternative to modeling θ as fixed, but unknown, and performing maximum-likelihood estimation to obtain $\hat{\theta}$, one might also model θ as random with prior density $p(\theta)$, such that the full model becomes $p(x,y,\theta) = p(x,y|\theta)p(\theta)$. In this setup, sometimes called the Bayesian treatment of SSMs (Durbin and Koopman, 2012, Section 13.1), the main interest still lies in the posterior density $p(x,\theta|y)$, which, depending on the model at hand, can drastically increase the difficulty of the problem: even if $p(x,y|\theta)$ is an analytically tractable model such as a GLSSM, unless the prior is chosen to be conjugate, one has to resort to, e.g., MCMC-methods.

By the structure of the model, Equation (3.2), the log density and its gradient can be computed efficiently by

$$\log p_\theta(x,y) = \log p_\theta(x_0) + \sum_{t=1}^{n} \log p_\theta(x_t|x_{t-1}) + \log p_\theta(y_t|x_t, y_{t-1})$$
$$\nabla_\theta \log p_\theta(x,y) = \nabla_\theta \log p_\theta(x_0) + \sum_{t=1}^{n} \nabla_\theta \log p_\theta(x_t|x_{t-1}) + \nabla_\theta \log p_\theta(y_t|x_t, y_{t-1}),$$

respectively.

Similarly, when proposing with a GLSSM or Markov-proposal for a PGSSM, the weights have similar structure, see Equations (3.24) and (3.31), which makes calculation of $\tilde{w}$ efficient.

For the remainder of this section, let us consider the GLSSM-proposal obtained by the LA or EIS for a PGSSM with linear signal, as this is the main setting of Chapter 4. For this we obtain

$$\tilde{w}_\theta(x) = \tilde{w}_\theta(s) g(z) \frac{p_\theta(y|s)}{g(z|s)} = g(z) \prod_{t=0}^{n} \frac{p_\theta(y_t|s_t)}{g(z_t|s_t)},$$

where $s_t = B_t x_t$, $t = 0, \dots, n$, is the signal, and so the log-likelihood is given by

$$\log p_\theta(y) = \log g_\theta(z) + \log \mathbb{E}\left(w_\theta(S)|Y = y\right) \tag{3.42}$$

and can be estimated by

$$\widehat{\log p_\theta(y)} = \log g_\theta(z) + \log \left(\frac{1}{N} \sum_{i=1}^{N} \prod_{t=0}^{n} \frac{p_\theta(y_t|S_t^i)}{g(z_t|S_t^i)} \right). \tag{3.43}$$

Notice that $\log g_\theta(z)$ is the likelihood in a GLSSM, which can be computed efficiently by the standard Kalman filter (Algorithm 1). As in the GLSSM-approach we propose with an GLSSM whose state density $g(x)$ and observation matrices B_t, $t = 0, \dots, n$ are equal to those of the target, the log-likelihood $\log g_\theta(z)$ also depends on θ. The estimated gradient of the log-likelihood is

$$\widehat{\nabla_\theta \log p_\theta(y)} = \nabla_\theta \log g_\theta(z) + \sum_{i=1}^{N} W_\theta^i \sum_{t=0}^{n} \nabla_\theta \log p_\theta(y_t|S_t^i).$$

The gradient of the GLSSM log-likelihood can be obtained either numerically or analytically by employing the Kalman filter and smoother (Koopman and Shephard, 1992), however, numerical evaluation may be faster if the dimension of θ is small compared to the length of the time series, as evaluating the likelihood only requires a single application of the Kalman filter.

As the observation densities $g(z_t|s_t)$ do not depend on θ, their derivatives do not appear in the above estimate. However, when using EIS to determine an optimal proposal, the parameter $\psi = (z, \omega)$ implicitly depends on θ. Accounting for this yields the gradient

$$\widehat{\nabla_\theta \log p_\theta(y)} = \nabla_\theta \log g_\theta(z) + \sum_{i=1}^{N} W_\theta^i \left(\sum_{t=0}^{n} \nabla_\theta \log p_\theta(y_t|S_t^i) - \nabla_\theta \log g_\theta(z_t|S_t^i) \right), \tag{3.44}$$

as $\nabla_\theta \frac{1}{g_\theta(z|s)} = -\frac{1}{g_\theta(z|s)} \nabla_\theta \log g_\theta(z|s)$. The computation of this additional term is much more involved, as the parameters z, Ω are found through an iterative numerical scheme. Instead, we favor numerical differentiation of the whole procedure to evaluate the likelihood at θ, including the method of finding an optimal importance sampling scheme.

As an alternative one may try keeping proposal $\mathbf{G}$ fixed, which would avoid calculation of the involved derivatives in the previous equation. However, this makes the calculation of weights more involved, as then $p_\theta(x) \neq g(x)$. Additionally, we would expect the target $p_\theta(x|y)$ to be quite sensitive to small changes in θ, as θ will likely contain parameters related to the covariance structure of model,

leading to fast degeneration of weights. Nevertheless, a combination of analytical and numerical gradient descent steps may improve the performance of the optimization procedure, but is beyond the scope of this thesis.

As a single evaluation of the log-likelihood can become very expensive we want our procedure to be as efficient as possible. To this end, (Durbin and Koopman, 1997) provides several improvements to the basic algorithm if the model is a PGSSM with a linear signal. Their contributions consist of a bias correction for the log-likelihood, the use of antithetic and control variables to reduce Monte-Carlo error for importance sampling and a deterministic initialization procedure. Let us briefly summarize these ideas, adapted to our notation. As the computational gains for control variates in the presence of antithetic variables seem to be limited, we do not give the same level of detail here, for an in-depth analysis, we refer the reader to the source.

For bias reduction, a second-order Taylor series expansion shows that for $\tilde{w}_\cdot = \frac{1}{N}\sum_{i=1}^N \tilde{w}(X^i)$,

$$\begin{aligned}\mathbb{E}\left(\log \tilde{w}_\cdot\right) - \log \mathbf{G}\tilde{w} &= \mathbb{E}\log\left(1 + \frac{\tilde{w}_\cdot - \mathbf{G}\tilde{w}}{\mathbf{G}\tilde{w}}\right) \\ &= \frac{\tilde{w}_\cdot - \mathbf{G}\tilde{w}}{\mathbf{G}\tilde{w}} - \frac{1}{2}\left(\frac{\tilde{w}_\cdot - \mathbf{G}\tilde{w}}{\mathbf{G}\tilde{w}}\right)^2 + \mathcal{O}_p(N^{-\frac{3}{2}}),\end{aligned}$$

provided $\tilde{w} \in L^3(\mathbf{G})$. Thus, estimating the second order term by $-\frac{\hat{\sigma}^2}{2N\tilde{w}_\cdot}$, where $\hat{\sigma}^2$ is the empirical variance of the unnormalized weights, we can perform a bias reduction by estimating

$$\widehat{\log p_\theta(y)} = \log\left(\tilde{w}_\cdot\right) + \log g_\theta(z) + \frac{\hat{\sigma}^2}{2N\tilde{w}_\cdot} \tag{3.45}$$

The second improvement of (Durbin and Koopman, 1997) is the use of antithetic variables and control variates, a device to reduce Monte-Carlo variance. The main idea of an antithetic variable is to construct for each sample X^i, $i = 1, \ldots, N$, another sample $\tilde{X}^i$ that has the same distribution as X^i, but is negatively correlated with X^i. This has two effects: first of all, we increase the number of samples used for importance sampling and second, as the new samples are negatively correlated with the old samples, the Monte-Carlo variance is reduced. The computation of these samples is usually much faster than creating new samples, which requires the use of the expensive FFBS or simulation smoother algorithms.

Definition 3.6 (antithetic variable)**.** Let $X, \tilde{X} \in \mathbf{R}^k$ be two random variables with the same distribution, $\mathcal{L}(X) = \mathcal{L}(\tilde{X})$ and $f : \mathbf{R}^k \to \mathbf{R}$. Then $\tilde{X}$ is called an antithetic variable of X for f, if $\operatorname{Cov}\Big(f(\tilde{X}), f(X)\Big) < 0$. If $k = 1$ and f is the identity, we just say that $\tilde{X}$ is an antithetic variable of X.

(Durbin and Koopman, 1997) introduce two antithetic variables: balanced for location and balanced for scale, both of which are tailored to the multivariate normal distribution.

Definition 3.7 (antithetic variable balanced for location and scale, (Durbin and Koopman, 1997))**.** Let $X \sim \mathcal{N}(\mu, \Sigma)$ for $\mu \in \mathbf{R}^k$ and $\Sigma \in \mathbf{R}^{k\times k}$ positive definite. We call

$$\tilde{X} = \mu + (\mu - X) \tag{3.46}$$

the (entry-wise) antithetic balanced for location. If $L \in \mathbf{R}^{k\times k}$ is a Cholesky root of Σ and

$$X = \mu + L\varepsilon$$

with $\varepsilon \sim \mathcal{N}(0, I)$, let $c = \varepsilon^T\varepsilon \sim \chi^2_k$ and $c' = F^{-1}_{\chi^2_k}(1 - F_{\chi^2_k}(\sqrt{c}))$. We call

$$\check{X} = \mu + \sqrt{\frac{c'}{c}}\,(X - \mu) \tag{3.47}$$

the antithetic balanced for scale.

Lemma 3.13. *In the above definition, $\tilde{X}_i$ is an antithetic variable of X for the coordinate functions $f_i : \mathbf{R}^k \to \mathbf{R}$, $f_i(x) = x_i$, $i = 1, \ldots, k$. Furthermore, $\tilde{c}$ is an antithetic variable of c.*

Proof. It is easy to see that $\tilde{X}$ has the same distribution as X. Furthermore

$$\operatorname{Cov}\left(f_i(X), f_i(\tilde{X})\right) = \operatorname{Cov}\left(2\mu_i - X_i, X_i\right) = -\Sigma_{i,i} < 0.$$

For c and $\tilde{c}$, let $U = F_{\chi^2_k}(c)$, then $U \sim \operatorname{Unif}(0,1)$ and $\tilde{U} = 1 - U = F_{\chi^2_k}(\tilde{c})$. As $\tilde{U} \sim \operatorname{Unif}(0,1)$ as well, $\mathcal{L}(c) = \mathcal{L}(\tilde{c})$. In (Whitt, 1976, Lemma 2.3) it is shown that for any pair of real-valued random variables (Y, W) with CDF H and marginal CDFs F, G, it holds

$$\operatorname{Cov}(Y, W) = \int_{\mathbf{R}^2} H(y, w) - F(y)G(w)\,\mathrm{d}y\,\mathrm{d}w,$$

and, furthermore, by (Whitt, 1976, Theorem 2.1 and Lemma 2.4) that the joint CDF of $(c, \tilde{c})$ is $(y, w) \mapsto \max\{0, F(y) + G(w) - 1\}$, where F is the CDF of c and G the CDF of $\tilde{c}$. As

$$a + b - 1 = ab + a(1 - b) + b - 1 = ab - (1 - a)(1 - b) < ab$$

for all $a, b \in (0, 1)$, we have

$$\begin{aligned}\operatorname{Cov}(c, \tilde{c}) &= \int_{\mathbf{R}^2} H(y, w) - F(y)G(w)\,\mathrm{d}y\,\mathrm{d}w \\ &= \int_{\mathbf{R}^2} \max\{0, F(y) + G(w) - 1\} - F(y)G(w)\,\mathrm{d}y\,\mathrm{d}w < 0.\end{aligned}$$

□

Let us mention that, by the properties of the standard multivariate normal distribution, $c = \|u\|$ and $\frac{u}{\|u\|}$ are independent. Writing

$$X = \mu + \|u\| L \frac{u}{\|u\|} = \mu + \|u\| \frac{X - \mu}{\sqrt{c}},$$

we see that

$$\check{X} = \mu + \sqrt{\tilde{c}} \frac{X - \mu}{\sqrt{c}}$$

has the same distribution as X, as $\tilde{c} \sim \mathcal{L}(\|u\|^2)$ and is independent of $\frac{X-\mu}{\sqrt{c}}$.

Given a GLSSM-proposal and samples $X^1, \ldots, X^N$ from it, we can calculate these antithetic variables efficiently: for the location balanced antithetic we can calculate the mean using the Kalman-smoother and for the scale balanced antithetic we can calculate c and c' using the inverse CDF of the χ^2_k distribution and the standard normal samples used to sample X^i in the first place, for which fast implementations are readily available. Incidental, we obtain a third antithetic,

$$\breve{X} = \mu - \sqrt{\frac{c'}{c}}(X - \mu) \tag{3.48}$$

for free. We can then estimate the log-likelihood in Equation (3.45) by replacing each occurrence of $\tilde{w}_\theta(X^i)$ by

$$\frac{1}{4}\left(\tilde{w}_\theta(X^i) + \tilde{w}_\theta(\tilde{X}^i) + \tilde{w}_\theta(\check{X}^i) + \tilde{w}_\theta(\breve{X}^i)\right). \tag{3.49}$$

As the procedure to evaluate the likelihood by importance sampling becomes expensive as the dimension of the model increases, (Durbin and Koopman, 1997) recommend finding an initial value $\hat{\theta}_0$ by maximizing a deterministic version of Equation (3.41). For this, denote by s^* the mode of the linear signal, conditional on the pseudo-observations z. As S follows a multivariate Gaussian, s^* is

also the mean which can be computed efficiently by the Kalman or signal-smoother. Approximating the conditional expectation in Equation (3.42) by $w_\theta(s^*)$ then yields

$$\log p_\theta(y) \approx \log g_\theta(z) + \log w_\theta(s^*), \tag{3.50}$$

which can be evaluated without simulation by the LA. A better approximation can be obtained by performing a fourth-order Taylor expansion of $s \mapsto w_\theta(s)$ around the mode s^*, which yields

$$\log p_\theta(y) \approx \log g_\theta(z) + \log w_\theta(s^*) + \log\left(1 + \frac{1}{8}\sum_{t=1}^{n}\sum_{j=1}^{m} l_{t,j}^{(4)}(s^*)v_{t,j}^2\right), \tag{3.51}$$

where $l^{(4)}$ is the fourth derivative of the log-weights $s \mapsto \log w_\theta(s)$ and $v_{t,j}$ is the conditional variance $\mathrm{Var}\,(S_{t,j}|Z=z)$ in the proposal. Again, we refer the interested reader to the source for the details.

Algorithm 9 Maximum likelihood estimation in a PGSSM with linear signal using EIS.

Require: parameterized PGSSM with linear signal, initial $\theta^0 \in \Theta$, observations $y \in \mathbf{R}^{(n+1)p}$, number of samples N

function APPROX_LOGLIK(θ)
  obtain LA of the PGSSM for θ ▷ Algorithm 5
  obtain mode s^* and conditional variances $v_{t,j}$ from the LA ▷ Algorithms 1 and 2
  return approximate log-likelihood ▷ Equation (3.50) or Equation (3.51)
end function

function ESTIMATE_LOGLIK(θ)
  obtain LA of the PGSSM for θ ▷ Algorithm 5
  obtain EIS proposal $\mathbf{G}_{(z,\Omega)}$ ▷ Algorithm 6, LA as initial values
  sample N signals S^i from $S|Z=z$ in EIS ▷ Algorithm 3 or signal smoother
  obtain mode s^* in EIS proposal ▷ Algorithm 2 or signal smoother
  calculate antithetic variables $\tilde{S}^i, \check{S}^i, \breve{S}^i$ ▷ Equations (3.46) to (3.48)
  set $\tilde{w}_\theta^i = \frac{1}{4}\left(\tilde{w}_\theta(X^i) + \tilde{w}_\theta(\tilde{X}^i) + \tilde{w}_\theta(\check{X}^i) + \tilde{w}_\theta(\breve{X}^i)\right)$ Equation (3.49)
  set $\tilde{w}_\cdot = \frac{1}{N}\sum_{i=1}^N \tilde{w}_\theta^i$
  set $\hat{\sigma}^2 = \frac{1}{N-1}\sum_{i=1}^N \left(\tilde{w}_\theta^i - \tilde{w}_\cdot\right)^2$
  calculate $\widehat{\log g_\theta(z)}$ ▷ Algorithm 1
  return $\widehat{\log p_\theta(y)}$ ▷ Equation (3.45)
end function

maximize APPROX_LOGLIK with initial value θ^0 ▷ numerically
set θ^0 to optimal value
maximize ESTIMATE_LOGLIK with initial value θ^0 and CRNs ▷ numerically
set $\hat{\theta}$ to optimal value
return $\hat{\theta}$

The resulting procedure to find the MLE $\hat{\theta}$ in a PGSSM with linear signal is summarized in Section 3.6.1. Notice that we use CRNs to ensure numerical convergence. The numerical optimization can be performed using any standard solver such as the BFGS algorithm (Nocedal and Wright, 2006, Chapter 6.1). We cannot give guarantees that this procedure produces the true MLE, i.e. finds the global maximizer. However, as we have discussed earlier, we are not interested in frequentist properties of $\hat{\theta}$ but see the estimation procedure as a hyperparameter tuning step. Thus, a local maximum may well be sufficient. Nevertheless, checking different starting points and random number seeds should be used to get as close as possible to the global maximum.

Notice that our discussion implies that we cannot reuse a GLSSM proposal used for θ at another θ', as $p_{\theta'}(x) \neq g_\theta(x)$. While we can still calculate the weights using the general Equation (3.41), we presume that the old proposal is not a good choice for the new target. The reason for this is

that θ will usually contain parameters related to the covariance structure of the innovations and observations, and these parameters usually affect many, if not all states or observations. For example, it is common to model states that perform a random walk with common innovation variance σ^2 as an element of θ. As the distributions lie in a high-dimensional space, slight misspecification of the covariance structure will drastically deteriorate the performance of importance sampling.

If computations are so involved that we want to avoid running the optimal importance sampling scheme as much as possible, one could try, if the model under investigation allows for it, to split θ into (θ_x, θ_y) where θ_x only affects the state transitions and θ_y only affects the observation densities. Then a coordinate ascent scheme could be employed, where the update step for θ_y can reuse the proposal, provided that θ_y does not change too much and the observation density $p_\theta(y|x)$ is not too sensitive to changes in θ_y, which should imply that the proposal is still close enough to give good importance sampling performance. Then numerical differentiation is only required to update θ_x.

3.6.2 Posterior inference

Once we have chosen θ (by maximum likelihood estimation), and thus a concrete PGSSM with which to perform statistical inference, we are interested in, e.g., the conditional distribution of states X given observations Y, or functionals thereof. Here we will assume, for computational reasons, that the PGSSM has a linear signal, otherwise the same arguments can be applied to the states directly as well, at the expense of higher computation cost.

At our disposal we will have, after obtaining a GLSSM proposal using the EIS method, signal samples $S^i \in \mathbf{R}^{(n+1)\times p}$, $i = 1, \ldots, N$ and associated auto-normalized weights W^i. Let $\mathfrak{X} \in \mathbf{R}$ be a univariate random variable which is conditionally independent of the observations Y given the signal S, i.e. $\mathfrak{X} \perp Y|S$, whose conditional expectation and variance given Y exist, as well as a regular version of this conditional distribution. $\mathfrak{X}$ can be a marginal of X, a scalar function of X, a future or missing observation, or function thereof. We will assume that we can sample from $\mathfrak{X}|S$. This is reasonable for all scenarios we are interested in: states and signals are jointly Gaussian, so samples can be obtained using the FFBS (Algorithm 3), and the distribution of missing or future observations, conditional on states, is tractable in the models we consider. The following paragraphs are based on (Durbin and Koopman, 2012, Section 11.5), but stated in more general terms using $\mathfrak{X}$.

We are then interested in estimating several quantities: the conditional expectation $\mathbf{E}(\mathfrak{X}|Y)$, the conditional variance $\mathrm{Var}(\mathfrak{X}|Y)$ or α-quantiles of the conditional distribution $\mathfrak{X}|Y$. By the assumed conditional independence, we have

$$\mathbb{E}(\mathfrak{X}|Y) = \mathbb{E}(\mathbb{E}(\mathfrak{X}|S)|Y),$$

and, assuming that $\mathbb{E}(\mathfrak{X}|S)$ is known analytically, we may estimate the conditional expectation by

$$\sum_{i=1}^{N} W^i \mathbb{E}\left(\mathfrak{X}|S = S^i\right).$$

In the case that $\mathbb{E}(\mathfrak{X}|S)$ is not known analytically, but we can simulate from the conditional distribution $\mathfrak{X}|S$, we can obtain samples $\mathfrak{X}^i$, $i = 1, \ldots, N$ where $\mathfrak{X}^i$ is a draw from $\mathfrak{X}|S = S^i$. By the conditional independence $\mathfrak{X} \perp Y|S$, we have $p(\mathfrak{x}, s|y) = p(\mathfrak{x}|s)p(s|y)$, and $g(\mathfrak{x}, s|z) = p(\mathfrak{x}|s)g(s|z)$, so

$$\frac{p(\mathfrak{x}, s|y)}{g(\mathfrak{x}, s|z)} = \frac{p(s|y)}{g(s|z)} \propto \frac{p(y|s)}{g(z|s)}$$

and $(\mathfrak{X}^i, S^i), i = 1, \ldots, N$ are draws from a proposal whose auto-normalized weights coincide with W^i. Thus, we may estimate $\mathbb{E}(\mathfrak{X}|Y)$ by

$$\sum_{i=1}^{N} W^i \mathfrak{X}^i.$$

While this produces estimates with slightly larger variance (due to the additional simulation), we can control the simulation error by choosing the sample size large enough.

Similarly, by considering $\mathfrak{X}^2$, we can estimate the conditional variance, and by considering $\mathbf{1}_{\mathfrak{X}\leq x}$, we may estimate the conditional cumulative distribution function of $\mathfrak{X}$ given Y at x, which is just the empirical CDF of samples $\mathfrak{X}^i$ with associated weights W^i, $i = 1, \ldots, N$. Consequently, we can estimate the α-quantile of $\mathfrak{X}|Y$ by the α-quantile of this empirical CDF, where we use the standard convention for empirical quantiles of linear interpolation between samples to make quantiles unique, see also (Durbin and Koopman, 2012, Section 11.5.3).

3.7 Comparison of the Cross-Entropy method and Efficient Importance sampling

We now have three tools to produce Gaussian importance sampling proposals: the LA, the CE-method and EIS. Naturally, we want to choose the optimal tool for the problem at hand. In this section, we investigate under which circumstances which method is to be preferred over the others. To judge the performance of each method, we will discuss the following criteria:

- breakdown of methods,
- time and space complexity of the method,
- speed of stochastic convergence, as indicated by the asymptotic variance, for the CE-method and EIS, and
- performance of the optimal proposal, as measured by the efficiency factor, with a focus on degradation as the dimension of the target grows.

Let us elaborate on these criteria. With a breakdown of the methods, we mean settings in which either the numerical scheme diverges, produces parameters that lead to invalid proposals, i.e. negative variances, or where the proposals fail to produce consistent importance sampling estimates.

Time and space complexity of a single iteration of each method allow us to compare the theoretical computational resources required to apply the method in practice and can be used to inform our choice, provided there is no relevant difference in performance of the achieved importance sampling proposals. The speed of stochastic convergence is relevant for the CE-method and EIS as well: The smaller the asymptotic variance, the smaller we can choose the sample size N and thus decrease computation time. Similarly, numerical convergence directly affects computation time.

Finally, if one method has vastly better performance at the optimum, we might be willing to spend more time initially to save time later when we use the proposal to perform inference. Of special interest is the performance for long (large n) or fat (large m) time series, as the models we fit in Chapter 4 usually fall into one of these categories.

3.7.1 Breakdown of methods

It is generally difficult to determine whether the proposals produced by the three methods under consideration are valid, i.e. whether the second moment ρ is finite, see the discussion surrounding Example 3.2. Nevertheless, by focusing on Gaussian targets, one can employ Lemma 3.6. Let us thus begin with a classical example in which the LA fails to produce consistent importance sampling estimates.

Example 3.3 (Failure of LA)**.** Consider the Gaussian scale mixture $\mathbf{P} = \frac{1}{2}\left(\mathcal{N}(0,1) + \mathcal{N}(0,\varepsilon^{-2})\right)$ with mode $x^* = 0$, this is the same setup as in Example 3.2. We will perform importance sampling with a normal distribution $\mathbf{G}_\psi = \mathcal{N}(\mu, \sigma^2)$ for $\psi = (\mu, \sigma^2)$.

The LA is $\mathbf{G}_{\mathrm{LA}} = \mathcal{N}\left(0, \frac{1}{\varepsilon^2 - \varepsilon + 1}\right)$, whose variance goes to 1 as ε goes to 0, so the LA will miss close to $\frac{1}{2}$ of the total mass. For ε small enough, the variance of the LA will be smaller than $\frac{1}{2\varepsilon^2}$, whence the second moment of the weights is infinite (Lemma 3.6) and importance sampling with $\mathbf{G}_{\mathrm{LA}}$ is inconsistent.

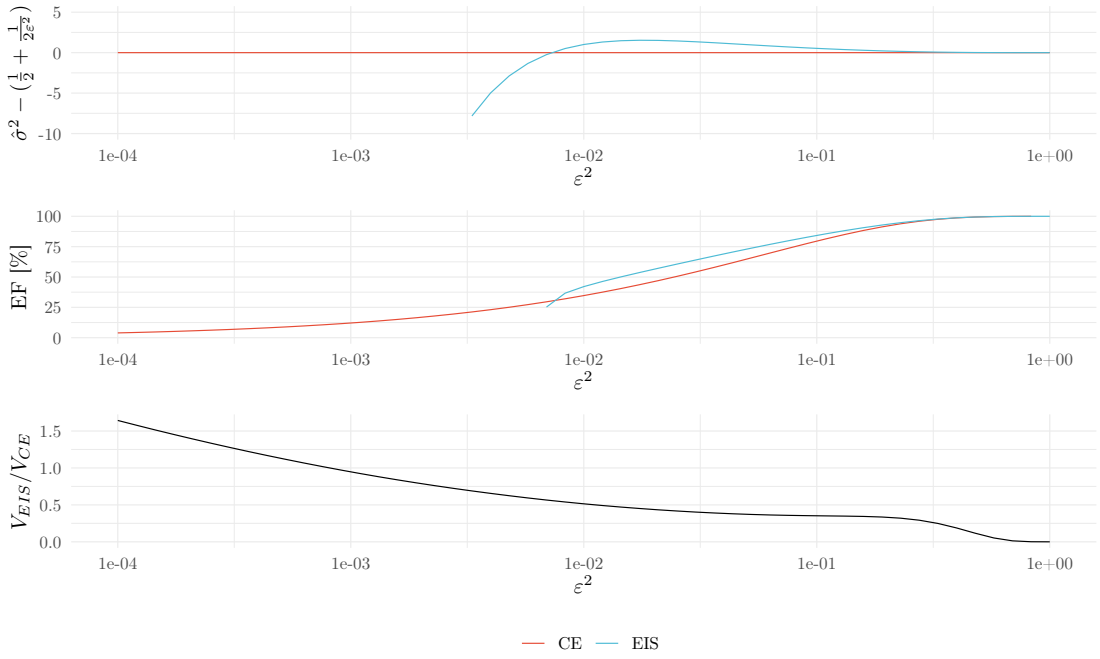

Figure 3.3: Performance of the CE-method and EIS for Example 3.3. The **top** figure shows the excess variance, with positive values corresponding to importance sampling proposals that provide consistent estimates. The **middle** figure shows the degeneration of the efficiency factor as ε^2 goes to 0. The **bottom** figure shows the asymptotic relative efficiencies of both methods, with EIS outperforming the CE-method for practically relevant values of ε^2.

The CE-method minimizes the KL-divergence between $\mathbf{P}$ and $\mathbf{G}_\psi$ and the optimal proposal is given by $\mathbf{G}_{\text{CE}} = \mathcal{N}(0, \sigma^2_{\text{CE}})$, where $\sigma^2_{\text{CE}} = \frac{1}{2}\left(1 + \varepsilon^{-2}\right)$ is the variance of $\mathbf{P}$, as the CE-method matches the first and second moments in this case. As $\sigma^2 > \frac{1}{2}\varepsilon^{-2}$, the weights have finite second moment, and importance sampling with $\mathbf{G}_{\text{CE}}$ is consistent.

As EIS does not yield analytically tractable proposals in this setting, we resort to a simulation study. Using the same setup as described in Example 3.4, we replicate $M = 100$ times $\hat{\psi}_{\text{EIS}}$ for varying levels of ε^2, averaging over the M runs. The resulting excess variances, i.e. $\widehat{\sigma^2}_{\text{EIS}} - \left(\frac{1}{2} + \frac{1}{2\varepsilon^2}\right)$ and $\sigma^2_{\text{CE}} - \left(\frac{1}{2} + \frac{1}{2\varepsilon^2}\right)$, efficiency factors and asymptotic efficiencies are displayed in Figure 3.3. We see that for small ε^2, EIS is inconsistent, while the CE-method stays consistent. However, as is to be expected, for small ε^2, the efficiency factor becomes very small for both methods, as the tails of both proposals are thinner than those of the target.

Regarding the asymptotic relative efficiencies, we see that $V_{\text{EIS}} < V_{\text{CE}}$ when ε^2 is large, and only for very small ε^2, i.e. mixtures where one component has very different tail behavior than the other, the CE-method has smaller asymptotic variance.

In the EGSSM setting EIS may produce invalid proposals, as estimates of the variance component in the weighted least squares regression are not guaranteed to be negative. Thus EIS may produce negative variances. To deal with this, the original EIS paper (Richard and Zhang, 2007, Section 3.2) recommends either inflating the prior or setting the parameters in question to arbitrary fixed values. Alternatively using a more expensive constrained linear least squares solver, such as a conjugate-gradient method (Branch, Coleman, and Y. Li, 1999) or the BVLS (bounded variable least squares) solver (Stark and Parker, 1995) may be appropriate, as is re-running the EIS procedure with a different random seed. Finally, in the EGSSM setting, we could also identify the corresponding observation as missing, similar to the argument presented in Section 3.5.1 for the CE-method.

method	single iteration (time)	single iteration (space)	simulation (time)
LA	$\mathcal{O}(np^3)$	$\mathcal{O}(np^2)$	$\mathcal{O}(n(p^3+m^3+Nm^2))$
EIS	$\mathcal{O}(n(m^2+p^3+Np^2))$	$\mathcal{O}(Np+n(p^2+m^2))$	$\mathcal{O}(n(p^3+m^3+Nm^2))$
CE-method	$\mathcal{O}(n(Nm^2+m^3))$	$\mathcal{O}(Nm+nm^2)$	$\mathcal{O}(Nnm^2)$

Table 3.2: Computational complexities of importance sampling algorithms for EGSSM with linear signals.

The CE-method presented in Section 3.5.2 (Algorithm 8) depends on the fact that the covariance matrix of the posterior $\mathrm{Cov}\,(X|Y=y)$ is symmetric positive definite (SPD), i.e. non-singular. This might be violated if, e.g., the model contains seasonal components whose associated innovations have variance 0. In this case, the Cholesky roots involved will not be unique. Still Algorithm 8 will, as $N \to \infty$ converge a globally optimal solution, though it may not be unique.

3.7.2 Computational complexity

Throughout this section, we assume that the model in question is an EGSSM with linear signal (c.f. Definition 3.5) to simplify the treatment. This assumption benefits the LA and EIS approaches, enabling the use of the efficient simulation and signal smoother. If the observation dimension p is smaller than that of states m, these algorithms are more efficient, and we will adopt them as well. An overview of computational complexities is presented in Table 3.2. It is important to acknowledge that most operations can be parallelized in one way or the other, e.g. sampling from the proposals. Therefore the time-complexities may not accurately reflect real-world-performance. Nevertheless, they provide theoretical insight into the performance of the three methods considered.

Let us begin with a discussion of the computational complexity associated with determining the optimal parameters, $\psi_{\mathrm{LA}}, \hat{\psi}_{\mathrm{EIS}}$ and $\hat{\psi}_{\mathrm{CE}}$. In this context we focus on a single iteration and consider the number of iterations as fixed.

As the LA is based on the Kalman-smoother, the time complexity of a single iteration is $\mathcal{O}(n(m^2+p^3))$. The CE-method and EIS need to generate N samples from the current proposal. For the CE-method this amounts to $\mathcal{O}(Nnm^2)$ operations (see Section 3.5.2). For EIS, using the simulation smoother (Durbin and Koopman, 2002) requires $\mathcal{O}(n(m^2+p^3+Np^2))$ operations: we need to run the Kalman filter once, while preparing the matrices required for the simulation smoother. Then, assuming Cholesky roots of the innovation covariance matrices Σ_t are already available, only matrix-vector multiplications are necessary for the simulation smoother. Obtaining the EIS model parameters is efficient, requiring only $\mathcal{O}(n(Np^2+p^3))$ operations for constructing the n $p \times p$ design matrices and estimating the optimal parameters.

Another concern is the time required to generate N samples from the fitted model. For both the LA and EIS, this procedure requires using either the simulation smoother or the FFBS algorithm. This necessitates inverting $p \times p$ matrices in the Kalman filter and $m \times m$ matrices when simulating the states. Notably, these computational steps can be performed offline, after which the simulation of a single sample requires only $\mathcal{O}(n)$ matrix-vector multiplications. The CE-method simulation is based on applying Equation (3.30), which requires $\mathcal{O}(nm^2)$ time per sample.

With respect to space complexity, the LA implementation has to run the Kalman filter which requires $\mathcal{O}(n(p^2+m^2))$ space and storage of $\mathcal{O}(np)$ parameters. EIS has the same space requirement, yet requires needs additional $\mathcal{O}(Np)$ storage for the simulated signals — it is sufficient to store just a single set of signals at once, as we can integrate the marginal EIS step into the simulation smoother. As the weights w_t in EIS depend only on the current signals $S_t^1, \ldots, S_t^N$, they can be discarded afterwards. See Section 3.5.2 for the derivation of the $\mathcal{O}(Nm+nm^2)$ space requirement of the CE-method.

The LA has the fastest and most space-efficient iteration of the three methods because it does not require the simulation of N samples. This makes it an ideal candidate as an initial guess for the other two methods. For $p \ll m$, EIS is faster than CE-method as it is based on the signals S only,

thus having access to the efficient simulation and signal smoother algorithms. The same is true for the space complexity. If, however, $p \approx m$, there is no linear signal or the observations are not conditionally independent given the states or signals, the speed of a single iteration of EIS and CE-method are comparable. While theoretically, the CE-method performs sampling faster than the other two methods, for large numbers of samples N the difference is negligible because the additional computations only have to be performed once.

3.7.3 Relative efficiencies of finite-sample and asymptotic variances

As we have seen in the previous section, the number of samples N used to estimate ψ_{CE} and ψ_{EIS} enter linearly into the computational complexities. Naturally, we want to know how big a sample size we should choose for our procedures to estimate a proposal that is close to the true optimal value and whether one of the two simulation-based procedures requires fewer samples than the other. To answer this question we turn to the two central limit theorems, Theorems 3.6 and 3.9. If N is large, the asymptotic variances (or rather: the asymptotic standard deviations) tell us how much stochastic variation we should expect around the optimal value, and can thus guide us in choosing N. We start with two examples in an univariate setting, where both the CE-method and EIS use Gaussian proposals with either fixed variance (Example 3.4) or mean (Example 3.5).

To compare both methods we will determine the asymptotic relative efficiencies, i.e. $\frac{\mathrm{Var}\left(\hat{\psi}_{\mathrm{EIS}}\right)}{\mathrm{Var}\left(\hat{\psi}_{\mathrm{CE}}\right)}$, with values smaller than 1 indicating that EIS requires (asymptotically) fewer samples for the same precision as the CE-method. Let us note that we are comparing the efficiencies of parameters ψ, not those of derived parameters such as the standard deviation or the ESS. However, should both methods have the same optimal value, the relative efficiencies are the same for all parameters derived from ψ, by the delta method. By a continuity argument, the same is approximately true if the optimal values of the CE-method and EIS are close.

To make as much the of the following examples analytically tractable, we will apply the CE-method and EIS in a univariate and single-parameter setting. This allows us to focus on the distinctive properties of the two methods, investigating under which circumstances each method performs well or poorly. In addition, we will use Gaussian proposals where mean (or variance) is fixed and the optimal variance (mean) is obtained by the CE-methods or EIS. As such, we are able to focus on specifying of either the mean or variance and determine which of the two is more crucial to specify accurately. Additionally, the univariate setting allows us, in some cases, to derive analytical expressions of the efficiencies involved.

Example 3.4 (univariate Gaussian proposal, σ^2 fixed)**.** On $\mathbf{R}$, consider the probability measure $\mathbf{P} = p\lambda$ for the Lebesgue measure λ and assume that $\mathbf{P}$ is symmetric around 0, i.e. $p(-x) = p(x)$ for λ-a.e. $x \in \mathbf{R}$ and possesses up to third order moments. Let $\mathbf{G} = \mathbf{P}$ be a proposal, so $W \equiv 1$ and let $\mathbf{G}_\psi = \mathcal{N}\left(\sigma\psi, \sigma^2\right)$ be the single parameter natural exponential family of Gaussians with fixed variance $\sigma^2 > 0$. Then

$$\log g_\psi(x) = \psi T(x) - \frac{\psi^2}{2} + \log h(x),$$

where $T(x) = \frac{x}{\sigma}$ and $h(x)$ is the density of $\mathcal{N}(0, \sigma^2)$ w.r.t. Lebesgue measure. Note that T is centered under $\mathbf{P}$. To compare the asymptotic behavior of the CE-method and EIS we compute the asymptotic variances arising from their respective central limit theorems (Theorems 3.6 and 3.9).

By symmetry, both ψ_{CE} and ψ_{EIS} are equal to 0. The Fisher information $I(\psi)$ is equal to 1 for all ψ, so

$$V_{\mathrm{CE}} = \mathrm{Cov}_{\mathbf{P}}(T) = \frac{\tau^2}{\sigma^2}, \tag{3.52}$$

where $\tau^2 = \mathbf{P}\,\mathrm{id}^2$ is the second moment of $\mathbf{P}$.

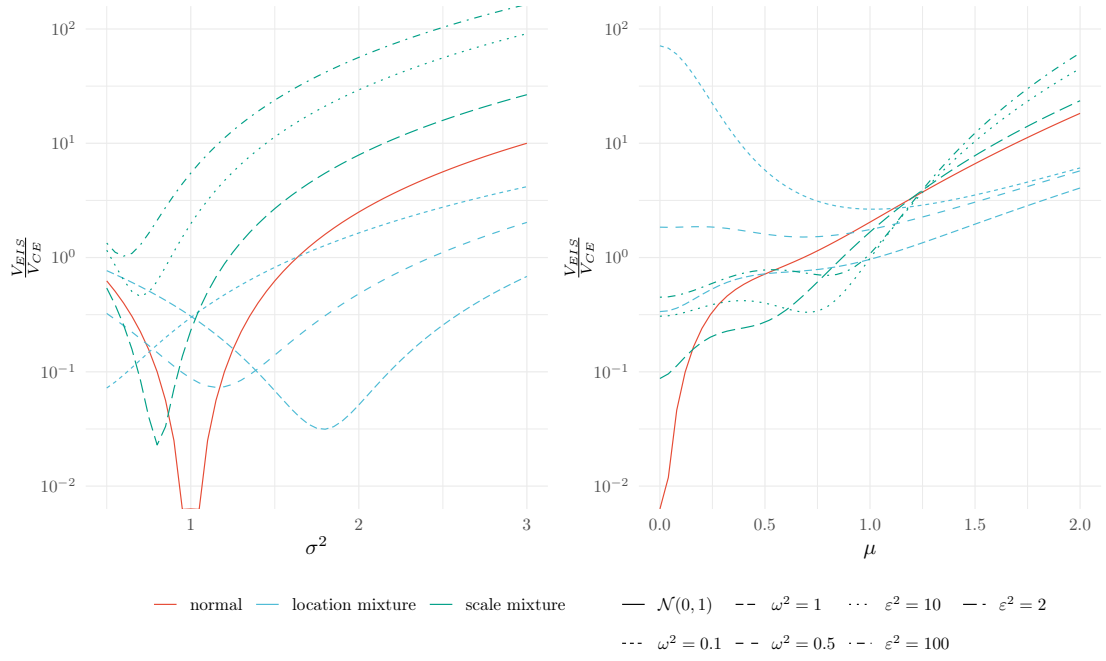

Figure 3.4: Asymptotic relative efficiency $\frac{V_{\text{EIS}}}{V_{\text{CE}}}$ for the normal distribution from Example 3.4 (left hand side) and Example 3.5 (right hand side). Here $\mathbf{P}$ is either the standard normal distribution, a Gaussian location mixture, or a Gaussian scale mixture. $\mathbf{G}_\psi$ is the normal distribution $\mathcal{N}(\mu, \sigma^2)$, where either σ^2 is fixed (left) and μ determined by the CE-method / EIS, or the other way around (right). Notice the log scale of the y-axis. As μ or σ^2 get close to their true values, EIS outperforms the CE-method in terms of asymptotic variance, see Proposition 3.5.

Additionally, $B_{\text{EIS}} = (\text{Cov}_{\mathbf{P}}(T))^{-1} = \frac{\sigma^2}{\tau^2}$ and

$$\begin{aligned} M_{\text{EIS}} &= \text{Cov}_{\mathbf{P}}\left((\log\frac{p(x)}{h(x)} - \lambda_{\text{EIS}})T\right) \\ &= \text{Cov}_{\mathbf{P}}\left((\log p - \log h - \mathbf{P}(\log p - \log h))\,T\right) \\ &= \frac{1}{\sigma^2}\int_{-\infty}^{\infty} p(x)x^2\left(\log p(x) + \frac{x^2}{2\sigma^2} - \mathbf{P}\left(\log p + \frac{\tau^2}{2\sigma^2}\right)\right)^2 \mathrm{d}x. \end{aligned}$$

Thus

$$V_{\text{EIS}} = B_{\text{EIS}} M_{\text{EIS}} B_{\text{EIS}} = \sigma^2 \frac{\gamma}{\tau^4},$$

where $\gamma = \int_{-\infty}^{\infty} p(x)x^2\left(\log p(x) + \frac{x^2}{2\sigma^2} - \mathbf{P}(\log p + \frac{\tau^2}{2\sigma^2})\right)^2 \mathrm{d}x$, and the efficiency of EIS relative to the CE-method is

$$\frac{V_{\text{EIS}}}{V_{\text{CE}}} = \frac{\sigma^4}{\tau^6}\gamma.$$

Let us now consider three exemplary choices of $\mathbf{P}$ that illustrate a target that is well-behaved (the standard normal), multimodal (a Gaussian location mixture) and has different behavior in the tails than indicated at the mode (a Gaussian scale mixture). For each target, we vary σ^2 from $\frac{1}{2}$ to 3 and obtain relative efficiencies of the CE-method and EIS either analytically or by simulation, the results are shown in the left-hand side of Figure 3.4.

We show the target densities we will consider in this example in Figure 3.5.

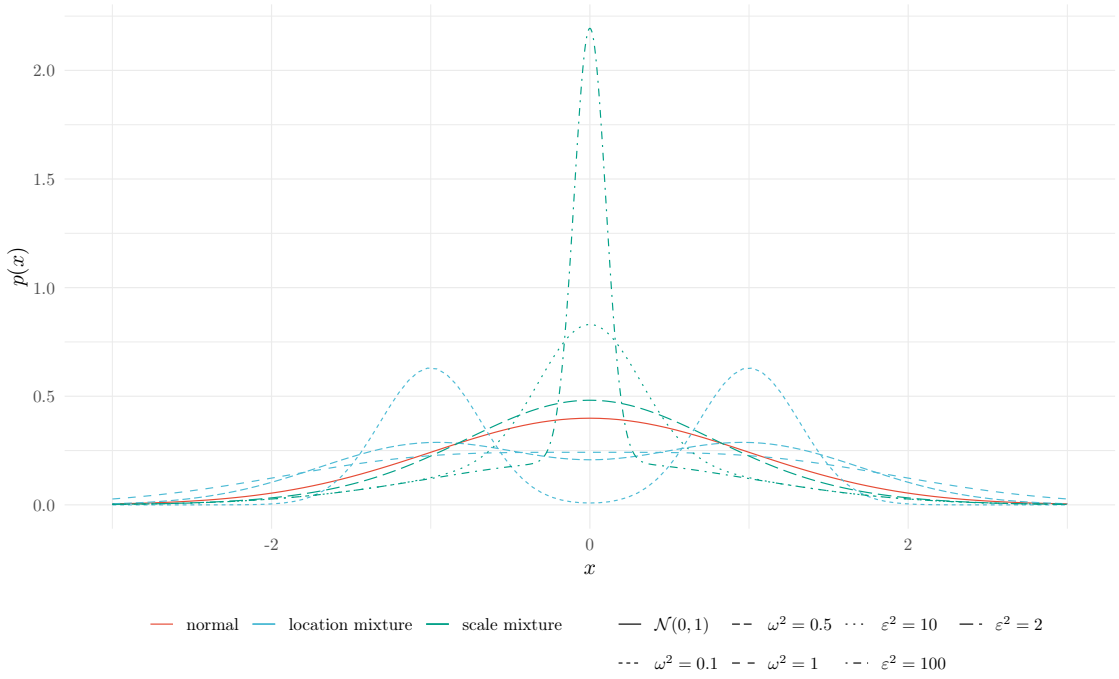

Figure 3.5: Targets used for the CE-method and EIS in Example 3.4 and Example 3.4. In addition to the standard normal distribution, we use location and scale mixtures. The location mixture is chosen for its bimodality for the smaller two values of ω^2, while the scale mixture is chosen for its different tail behavior compared to the behavior at the mode.

Normal distribution If $\mathbf{P} = \mathcal{N}(0, \tau^2)$ is a normal distribution, this reduces to

$$V_{\text{EIS}} = \frac{5}{2}\left(\frac{\tau^2}{\sigma^2} - 1\right)^2 \frac{\sigma^2}{\tau^2} = \frac{5}{2}\frac{(V_{\text{CE}} - 1)^2}{V_{\text{CE}}}$$

and so for $\tau^2 = \sigma^2$ we have $V_{\text{EIS}} = 0$, so $\hat{\psi}_{\text{EIS}}$ might converge faster than the standard $\mathcal{O}(N^{-\frac{1}{2}})$ rate. Indeed, in this case $\hat{\psi}_{\text{EIS}} = \psi_{\text{EIS}}$ a.s. for $N > 1$, see Proposition 3.5.

Gaussian location mixture Consider now the case where $\mathbf{P} = \frac{1}{2}\mathcal{N}(-1, \omega^2) + \frac{1}{2}\mathcal{N}(1, \omega^2)$ is a Gaussian location mixture. The second moment is $\tau^2 = 1 + \omega^2 = -\frac{1}{2\psi_{\text{CE}}}$. Unfortunately, there is no closed-form expression for many of the terms required for the analysis of EIS. Instead, we resort to a simulation study to determine the asymptotic variances and relative efficiencies for three different values of $\omega^2 \in \{0.1, 0.5, 1.0\}$.

To this end we draw $M = 400$ times from the distribution of $\hat{\psi}_{\text{CE}}$ and $\hat{\psi}_{\text{EIS}}$, where we use $N = 1\,000$ samples from the tractable $\mathbf{P}$ as importance samples[8]. We only iterate a single time for both procedures. From individual estimates, we estimate the asymptotic variances V_{CE} and V_{EIS} by the respective empirical variances, and determine the relative efficiency of EIS over the CE-method as $\frac{\hat{V}_{\text{EIS}}}{\hat{V}_{\text{CE}}}$. Again, we vary the fixed variance of the proposals, σ^2, from $\frac{1}{2}$ to 3. To quantify uncertainty in these asymptotic relative efficiencies, we perform the non-parametric bootstrap with 10 000 samples to estimate their standard errors $\widehat{\text{se}}_b$. $M = 400$ has been chosen to ensure that the relative bootstrap standard error $\frac{\widehat{\text{se}}_b}{\hat{V}_{\text{EIS}}/\hat{V}_{\text{CE}}}$ is less than 10% across all simulations.

Gaussian scale mixture Finally we consider $\mathbf{P} = \frac{1}{2}\left(\mathcal{N}(0,1) + \mathcal{N}(0, \varepsilon^{-2})\right)$ for $\varepsilon^2 \in \{2, 10, 100\}$, a scale mixture similar to the one seen in Example 3.3. Contrary to that example, we choose ε big,

[8] Code for all simulation studies is available in the associated GitHub repository, see Chapter A.

making the $\mathcal{N}(0,1)$ component the one with large variance, to make importance sampling with σ^2 in the range considered consistent. Here $\tau^2 = \frac{1}{2} + \frac{1}{2\varepsilon^2}$. Again, we estimate the asymptotic V_{EIS} in the same way as for the Gaussian location mixture, with $M = 100$ estimates using $N = 1000$ samples each and obtain a Monte-Carlo standard error for the asymptotic variances of 1.1×10^{-3}.

Note that for fixed σ^2 the asymptotic variance of the CE-method V_{CE} is the same in all of the examples considered, as we sample directly from the tractable $\mathbf{P}$, so V_{CE} only depends on $\mathbf{P}$ through its second moment τ^2. The asymptotic variance of EIS however depends on both τ^2 and γ, which depends on higher order moments of $\mathbf{P}$.

From the left-hand side of Figure 3.4 we can observe that in the case of $\mathbf{P} = \mathcal{N}(0,1)$ EIS has smaller asymptotic variance compared to the CE-method, as long as σ^2 is not heavily misspecified. Indeed, if $\sigma^2 = 1$ is correctly specified, by Proposition 3.5, EIS has asymptotic variance 0 and converges already for a single sample.

Consider now the case where $\mathbf{P}$ is a Gaussian location mixture. For $\omega^2 = 1$, the location mixture is unimodal with variance 2 and EIS outperforms the CE-method in terms of asymptotic variance in the range considered. For the smaller values of ω^2 considered here, the location mixture is bimodal. Close to the true variance $1 + \omega^2$, EIS still outperforms the CE-method.

For the Gaussian scale mixture, the case is less clear. Here the true variance is $\frac{1}{2} + \frac{1}{2\varepsilon^2}$. The location of the minimal relative efficiency is still close to this true variance, however, as ε^2 grows, the CE-method starts to dominate EIS. Additionally, recall from Example 3.3 that for large ε^2 EIS becomes inadmissible.

Example 3.5 (univariate Gaussian, μ fixed)**.** Consider the same setup as in Example 3.4, i.e. $\mathbf{P}$ is symmetric around 0 with second moment τ^2, but let $\mathbf{G}_\psi = \mathcal{N}(\mu, -\frac{1}{2\psi})$ be the single parameter natural exponential family of Gaussians with fixed mean μ and variance $\sigma^2 = -\frac{1}{2\psi}$.

Then

$$\log g_\psi(x) = \psi T(x) + \frac{1}{2}\log(-2\psi) - \frac{1}{2}\log 2\pi$$

for $T(x) = (x-\mu)^2$. Thus $\mathbf{P}T = \tau^2 + \mu^2$ and $\operatorname{Cov}_{\mathbf{P}} T = \nu - \tau^4 + 4\tau^2\mu^2$ where $\nu = \mathbf{P}\,\mathrm{id}^4$ and $\tau^2 = \mathbf{P}\,\mathrm{id}^2$.

By matching moments, we obtain $\psi_{\text{CE}} = -\frac{1}{2(\tau^2+\mu^2)}$ and $I(\psi_{\text{CE}}) = \frac{1}{2\psi_{\text{CE}}^2} = 2(\tau^2+\mu^2)^2$. In total

$$V_{\text{CE}} = \frac{1}{4(\tau^2+\mu^2)^4}\left(\nu - \tau^4 + 4\tau^2\mu^2\right) \tag{3.53}$$

For EIS,

$$\begin{aligned}\psi_{\text{EIS}} &= (\operatorname{Cov}_{\mathbf{P}} T)^{-1} \operatorname{Cov}_{\mathbf{P}}(T, \log p) \\ &= \left(\nu - \tau^4 + 4\tau^2\mu^2\right)^{-1} \underbrace{\int p(x)((x-\mu)^2 - \tau^2 - \mu^2)(\log p(x) - \mathbf{P}\log p(x))\,\mathrm{d}x}_{=\gamma}.\end{aligned}$$

As $B_{\text{EIS}} = \operatorname{Cov}_{\mathbf{P}} T^{-1} = \left(\nu - \tau^4 + 4\tau^2\mu^2\right)^{-1}$, we have

$$V_{\text{EIS}} = \left(\nu - \tau^4 + 4\tau^2\mu^2\right)^{-2} \mathbf{P}\left((\mathrm{id}-\mu)^4\left(\log p - \psi_{\text{EIS}}(\mathrm{id}-\mu)^2 - \mathbf{P}\log p + \psi(\tau^2+\mu^2)\right)^2\right),$$

where the last term is equal to M_{EIS}.

We now perform the same analysis as in Example 3.4, the resulting ratio of asymptotic variances is displayed in the right-hand side of Figure 3.4. In general, the variances $\sigma^2_{\text{CE}} = -\frac{1}{2\psi_{\text{CE}}}$ and $\sigma^2_{\text{EIS}} = -\frac{1}{2\psi_{\text{EIS}}}$ are different, so the ratio is no longer an asymptotic relative efficiency. However, it is still relevant as a measure of the relative speed of stochastic convergence of both methods. Additionally, we display the resulting optimal variances in Figure 3.6.

Normal distribution For the normal distribution $\mathbf{P} = \mathcal{N}(0, \tau^2)$ where $\nu = 3\tau^4$ and $\gamma = -\tau^2$, so

$$\psi_{\text{EIS}} = \frac{-\tau^2}{2\tau^2\left(\tau^2 + 2\mu^2\right)} = \frac{-1}{2(\tau^2 + 2\mu^2)}.$$

Thus the EIS proposal uses variance $\sigma^2_{\text{EIS}} = \tau^2 + 2\mu^2$, which is bigger than the variance of $\sigma^2_{\text{CE}} = \tau^2 + \mu^2$ optimal for the CE-method.

In this case the asymptotic variances are

$$V_{\text{CE}} = \frac{\tau^2(\tau^2 + 2\mu^2)}{2\left(\tau^2 + \mu^2\right)^4}$$

and

$$V_{\text{EIS}} = \frac{\mu^2\left(2\mu^6 + 45\mu^4\tau^2 + 15\tau^6\right)}{4\tau^4\left(2\mu^2 + \tau^2\right)^4},$$

which we show in the following. By standard properties of the single parameter Gaussian exponential family $I(\psi_{\text{CE}})^{-1} = \frac{\left(2\mu^2+2\tau^2\right)^2}{2}$, so $B_{\text{CE}} = \frac{2}{(2\mu^2+2\tau^2)^2}$.

Additionally,

$$\begin{aligned} M_{\text{CE}} = \text{Cov}_{\mathbf{P}}(T) &= \mathbf{P}\left(\left((\text{id} - \mu)^2 - \tau^2 - \mu^2\right)^2\right) \\ &= \mathbf{P}\left(\left(\text{id}^2 - \tau^2 + 2\mu\,\text{id}\right)^2\right) \\ &= \mathbf{P}\left(\text{id}^4 - 2\,\text{id}^2\,\tau^2 + 4\mu\,\text{id}^3 + \tau^4 + 4\mu^2\,\text{id}^2\right) \\ &= \nu + 4\mu^2\tau^2 - \tau^4, \end{aligned}$$

as $\mathbf{P}\,\text{id}^3 = 0$ and $\mathbf{P}\,\text{id}^2 = \tau^2$. In total

$$V_{\text{CE}} = B_{\text{CE}} M_{\text{CE}} B_{\text{CE}} = \frac{4\left(\nu + 4\mu^2\tau^2 - \tau^4\right)}{\left(2\mu^2 + 2\tau^2\right)^4} = \frac{\nu + 4\mu^2\tau^2 - \tau^4}{4\left(\mu^2 + \tau^2\right)^4}.$$

For EIS, we have $\log p(x) = -\frac{1}{2}\frac{x^2}{\tau^2} - \frac{1}{2\sqrt{\pi\tau^2}}$, so the log-weights are, up to an additive constant, given by

$$-\frac{1}{2}\frac{\text{id}^2}{\tau^2} - T\psi_{\text{EIS}}.$$

M_{EIS} is then given by

$$\mathbf{P}\left((\text{id} - \mu)^4\left(\log w - \mathbf{P}\log w\right)^2\right)$$

which is the expectation of a sixth order polynomial with respect to the standard normal distribution $\mathbf{P}$, so its value is analytically tractable and turns out to be[9]

$$M_{\text{EIS}} = \frac{\mu^2\left(2\mu^6 + 45\mu^4\tau^2 + 15\tau^6\right)}{\left(2\mu^2 + \tau^2\right)^2}.$$

Gaussian location and scale mixture To estimate asymptotic relative efficiencies for the Gaussian location and scale mixtures, for the same targets as in Example 3.4, we again perform a simulation study with the same parameters ($M = 400$ repetitions, 10 000 bootstrap samples estimate the standard error of estimation). Here the choice of M leads to a relative standard error of at most 11%.

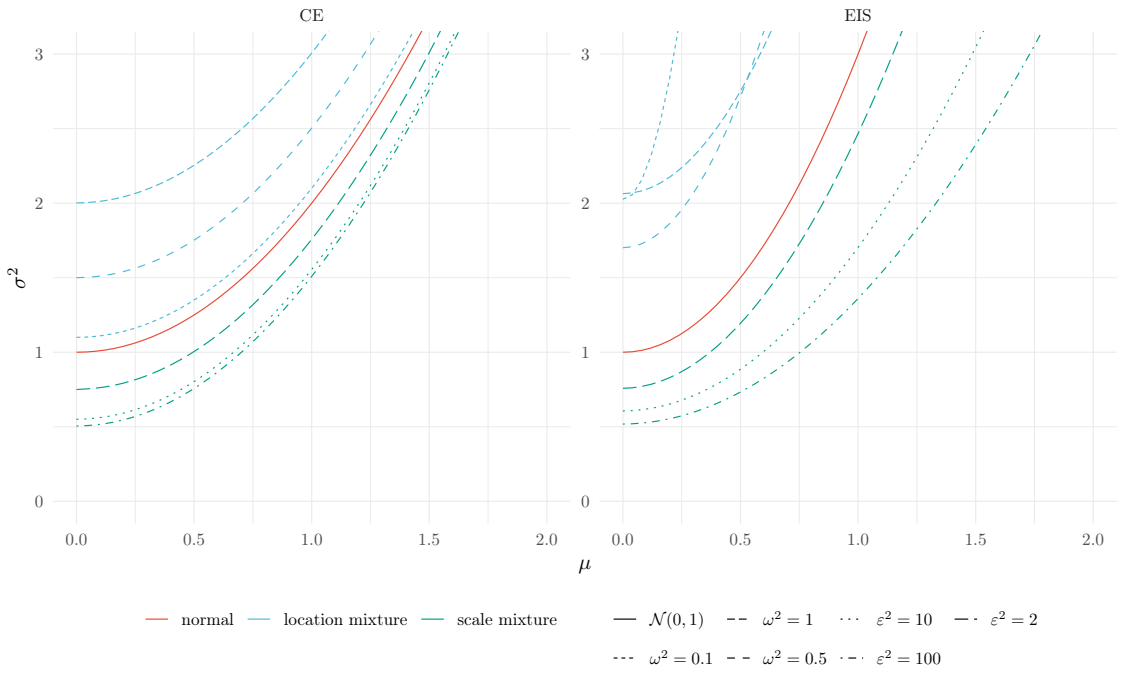

Figure 3.6: Optimal variances σ^2_{CE} / σ^2_{EIS} for the CE-method (left) and EIS (right) as a function of the misspecified mean μ. The variances produced by EIS tend to be larger than those produced by the CE-method.

On the left-hand side of Figure 3.4 we see that for μ close to the optimal value, EIS has smaller asymptotic variance than the CE-method, except for the two bimodal location measures. Again, due to the finite sample convergence of EIS, Proposition 3.5, the asymptotic variance V_{EIS} goes to 0 as $\mu \to 0$. As μ is further from the true 0 the ratio of asymptotic variances starts to grow.

In Figure 3.6 we see that, except for the extreme scale mixtures, EIS tends to produce proposals that have a larger variance than those produced by the CE-method. As we will see in the discussion of Figure 3.8, this might be advantageous for EIS as proposals with a small variance run the risk of missing a large part of the probability mass of the target.

Finally, we compare the CE-method and EIS in a situation closer to the applications in Chapter 4.

Example 3.6 (Growth factor SSM)**.** Consider the following EGSSM: The states are given by

$$X_t = \begin{pmatrix} \log I_t \\ \log \rho_{t+1} \end{pmatrix}, t = 0, \dots, n$$

with

$$X_{t+1} = \begin{pmatrix} \log I_{t+1} \\ \log \rho_{t+2} \end{pmatrix} = \begin{pmatrix} \log I_t + \log \rho_{t+1} \\ \log \rho_{t+1} + \varepsilon_{t+1} \end{pmatrix}, t = 0, \dots, n-1$$

where $\varepsilon_{t+1} \sim \mathcal{N}(0, \sigma^2)$ and $X_0 \sim \mathcal{N}(x_0, \Sigma_0)$. The observations Y_t follow a conditional Poisson distribution $Y_t \sim \text{Pois}(I_t)$. It is easy to see that this forms an EGSSM with linear signal $\log I_t$. This model is a simplified version of the exponential growth factor model presented in Section 4.1, and we defer the reader to this section for a detailed motivation of the model.

For the initial states we set $I_0 = 1\,000$ and $\rho_1 = 1$, and let $\Sigma_0 = \begin{pmatrix} 1 & 0 \\ 0 & 0.1 \end{pmatrix}$. Finally, we choose $\sigma^2 = \frac{0.05}{n}$. This ensures that the change in $\log \rho$ over the whole time period, $\log \rho_{n+2} - \log \rho_1$ has variance 0.05, which makes large and small growth factors ρ improbable.

[9] See `03_08_comparison.ipynb` in the accompanying code for calculations.

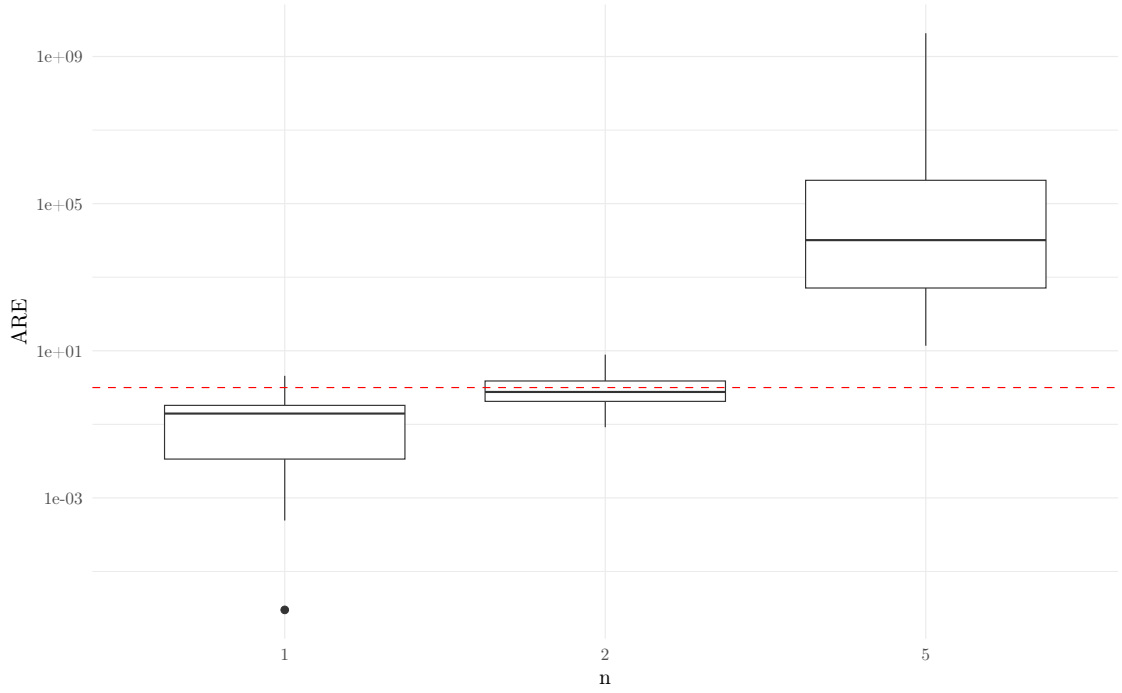

Figure 3.7: Boxplots of asymptotic relative efficiencies of EIS and the CE-method for Example 3.6. Note the log-scale of the y-axis. Values smaller than 1 indicate that the CE-method has smaller asymptotic variance, while values larger than 1 indicate that EIS has smaller asymptotic variance than the CE-method.

We then perform the following simulation protocol for varying values of n.

(i) Simulate a single observation $y = (y_0, \dots, y_n)$ from the model.

(ii) Obtain the LA to the conditional distribution $X|Y = y$.

(iii) M times, using different seeds, perform the CE-method (Algorithm 8) to obtain proposals $\mathbf{G}^1_{\text{CEM}}, \dots, \mathbf{G}^M_{\text{CEM}}$, using the LA as a starting point.

(iv) M times, using different seeds, perform EIS (Algorithm 6) to obtain proposals $\mathbf{G}^1_{\text{EIS}}, \dots, \mathbf{G}^M_{\text{EIS}}$, using the LA as a starting point.

Unfortunately, there is no straightforward way to define the relative efficiencies in this scenario. First, we are in the same scenario as in Example 3.5: EIS and the CE-method estimate different parameters. Additionally, the parameters estimated by the optimal importance sampling methods are now multivariate. To deal with this, we compare the determinants of the estimated covariance matrices of the signals $S = (\log I_0, \dots, \log I_n)$ instead.

We set the number of iterations of the CE-method and EIS to 100, which, in our experience, suffices to determine whether the numerical scheme converges or diverges. We use $M = 10$ samples to obtain the covariance matrices. For both methods we use $N = 10\,000$ samples for estimation.

The above procedure generates a single asymptotic relative efficiency for a fixed number of time points n. As the performance of importance sampling is likely influenced by the sample y, we repeat the simulation $K = 10$ times to obtain K different outcomes.

We show the resulting asymptotic relative efficiencies in Figure 3.7. For small values of n, the CE-method actually outperforms EIS in terms of asymptotic variance, but starting with $n = 5$, EIS begins to vastly outperform the CE-method.

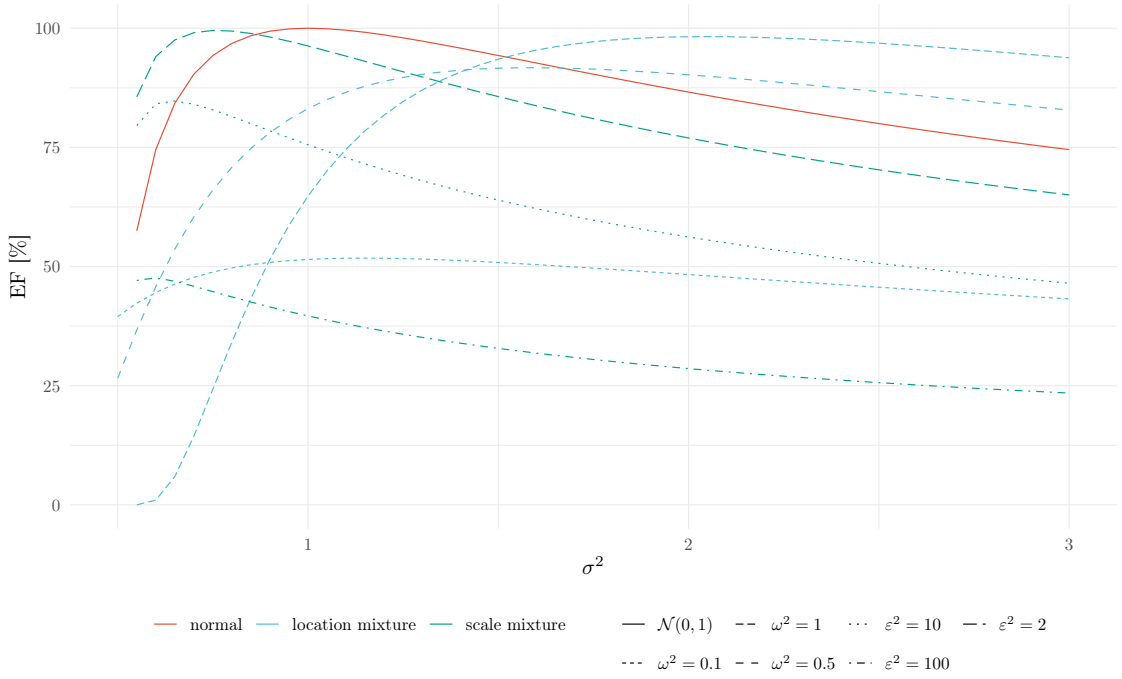

Figure 3.8: Efficiency factors of proposals for Example 3.4 in dependence of σ^2. The efficiency factor is the same for the CE-method and EIS, as the optimal μ is always 0.

3.7.4 Performance of the optimal proposal

For the performance of importance sampling the efficiency factor $\mathrm{EF} = \frac{\mathrm{ESS}}{N}$ plays an important role, see Section 3.3. Additionally, it allows a comparison of the effectiveness of importance sampling across multiple sample sizes N, indeed, as $N \to \infty$, EF converges to ρ^{-1}, where ρ is the second moment of importance sampling weights, $\int w^2 \, \mathrm{d}\mathbf{G}$.

Returning to the distributions studied in Examples 3.4 and 3.5, we now calculate the asymptotic efficiency factor

$$\mathrm{EF} = \frac{1}{\rho} \in (0, 1].$$

As the proposal is always $\mathcal{N}(\mu, \sigma^2)$ with either μ or σ^2 fixed, and $\mathbf{P}$ is a mixture of Gaussians or $\mathcal{N}(0, 1)$, ρ is analytically available, as

$$\rho = \int w^2 \mathrm{d}\mathbf{G} = \int \frac{p^2}{g^2} \mathrm{d}\mathbf{G} = \int_{-\infty}^{\infty} \frac{p^2(x)}{g(x)} \mathrm{d}x$$

can then be reduced to Gaussian integrals.

For Example 3.4, both EIS and the CE-method have, by symmetry, the same optimal $\mu = 0$. Thus the efficiency factor only depends on the fixed σ^2, see Figure 3.8, and is the same for EIS and the CE-method.

For Example 3.5 the two methods have different optimal proposals, thus also different asymptotic efficiency factors. In Figure 3.9, the first two subfigures show how the efficiency factor depends on the misspecified μ for both methods. The optimal variances are based on the results from Example 3.5, i.e. based on simulation for EIS. The right-hand subfigure shows the relative efficiency factor, i.e. the ratio of the efficiency factor for the CE-method and EIS. Here values smaller than 1 indicate that EIS has a larger efficiency factor than the CE-method.

In this figure, we can observe that, as expected, stronger misspecification in μ almost always results in a smaller efficiency factor, an exception being the scale mixture with $\varepsilon^2 = 100$ for the

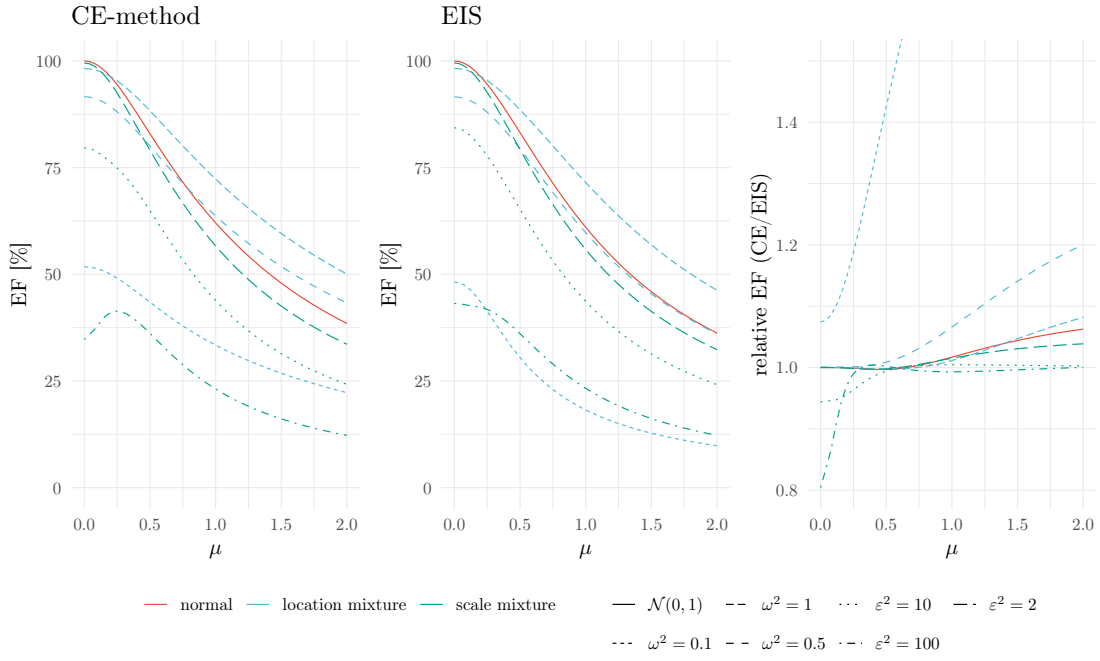

Figure 3.9: Efficiency factors of the CE-method and EIS for example Example 3.5. The **left-hand** (**middle**) figure shows the efficiency factor (in %) for the CE-method (EIS). The **right-hand** figure shows the relative efficiency factor of the CE-method vs. EIS, with values greater than 1 indicating that the efficiency factor of the CE-method is bigger than that of EIS.

CE-method. Compared to Figure 3.8, we see that already small misspecification in μ results in a large decline in EF, although we should keep in mind that this is not a fair comparison, as μ and σ^2 live on different scales. If $\mu = 0$ is correctly specified, both methods have comparable performance, except for extreme cases of the mixture models, i.e. when $\omega^2 = 0.1$ or when $\varepsilon^2 = 100$. For small misspecification of μ, this remains true, but for larger misspecification, the CE-method has a larger efficiency factor, especially for the bimodal location mixture with $\omega^2 = 0.1$, where the performance of EIS deteriorates.

Let us also return to the SSM from Example 3.6. We use a similar simulation routine to estimate efficiency factors:

(i) Simulate a single observation $y = (y_0, \ldots, y_n)$ from the model.

(ii) Obtain $\mathbf{G}_{\text{LA}}$ by the LA.

(iii) Obtain $\mathbf{G}_{\text{CEM}}$ by the CE-method, using the LA as a starting point.

(iv) Obtain $\mathbf{G}_{\text{EIS}}$ by EIS (Algorithm 6), using the LA as a starting point.

(v) Draw $N = 10\,000$ samples from each proposal and estimate the efficiency factor by Equation (3.10).

Again, we repeat this procedure 10 times for varying levels of n and use 100 iterations of for all three methods, as well as 10 000 samples to estimate the optimal proposal. The resulting efficiency factors are presented in Figure 3.10. As expected, the efficiency factor declines as n grows for all methods. For small n, both EIS and the CE-method produce better proposals — as measured by the efficiency factor — than the LA. There are some issues for the LA and EIS for $n = 1$, which we believe is due to the initialization scheme that is optimized with multiple observations in mind. From our experience, it is also the case that the optimal parameters for EIS are close to the optimal parameters produced by the LA - which may explain the bad performance of EIS in this case.

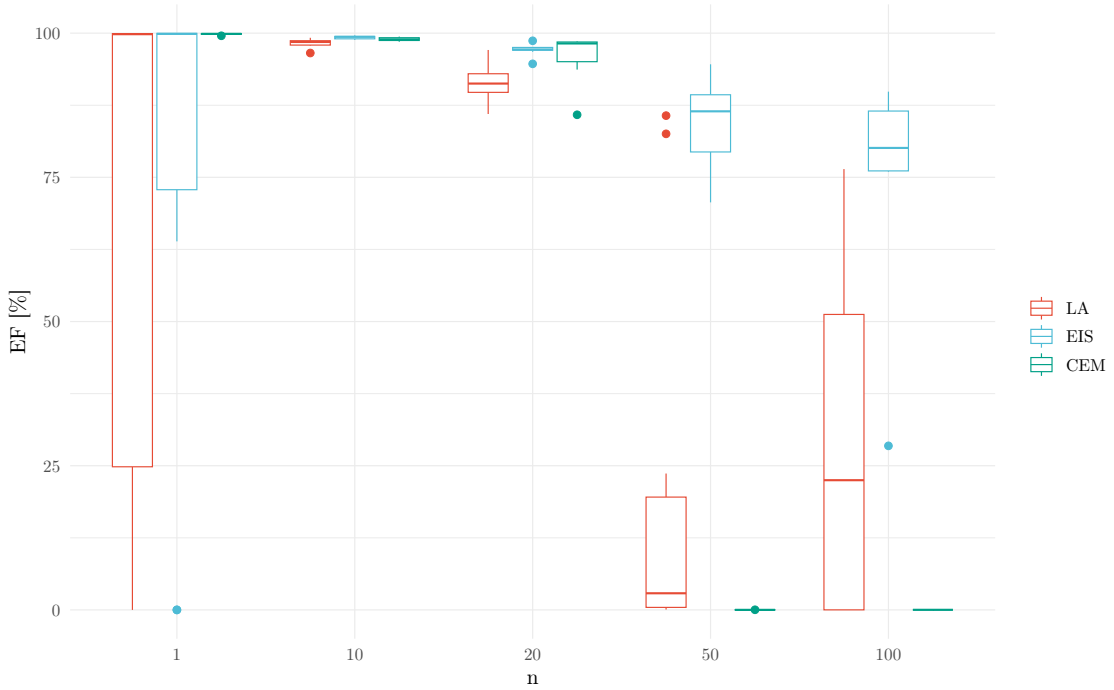

Figure 3.10: Boxplots of efficiency factors for the SSM from Example 3.6. Note that the x-axis is not to scale, presenting only the values that n takes in the simulations.

n	LA	EIS	CEM
1	0	0	0
10	0	0	0
20	0	2	2
50	0	2	5
100	2	4	9

Table 3.3: Number of invalid efficiency factors (out of $K = 10$) per size n and method. This includes cases where either the numerical scheme of the method failed to converge, or the proposal generated is numerically singular to the target.

Up to $n = 20$, the CE-method produces adequate proposals, however, with starting at $n = 50$, the performance deteriorates. Additionally, we had already seen in the previous section, that the asymptotic variance of the CE-method grows much more rapidly than that of EIS.

In addition to these observations, we report some numerical issues which result in invalid efficiency factors. The number of occurrences are displayed in Section 3.7.4. Again, the CE-method is much more unstable than the LA or EIS, with the LA having the least amount of dropout. As both methods use the LA as their initial value, we would expect such numerical issues when the LA provides bad proposals - which is the case for some proposals at $n = 100$.

3.8 Conclusion

This chapter provides a comprehensive comparison of the CE-method and EIS. Crucially, we provide the CLTs Theorems 3.6 and 3.9 (Section 3.3) and made the CE-method feasible for state space models (Section 3.5). These theoretical insights facilitate the comparisons in Section 3.7, allowing us to bridge the gap between communities that have, to the best of the authors' knowledge, developed separately from one another.

The main insight we can derive from the examples in Section 3.7 is that the main obstacle the CE-method faces in applications is likely not that its optimal proposal is far away from the target, but rather that its asymptotic variance may be too large to facilitate fast finite-sample convergence. This in turn leads to proposals that are far away from the optimal one, which in high-dimensional settings results in poor importance sampling performance. As we have seen in Section 3.7.4, the efficiency factor at the optimal proposal is — for most scenarios studied — comparable between the CE-method and EIS, as long as both methods are equipped with a sufficiently large sample size to ensure convergence. Additionally, in Figure 3.6 we saw that EIS tends to produce proposals with larger variances. Following Lemma 3.6 proposals with larger variance can be seen as preferable, as small variance may lead to inadmissible proposals.

Let us stress that the methods we used to obtain the two CLTs can be applied to other methods that find optimal proposals, such as the VM-method or the recent neural importance sampling (Müller et al., 2019), and can guide the choice of importance sampling methods in applications.

In total, we recommend using EIS over the CE-method for the following reasons:

- the asymptotic variance of EIS seems to be smaller, especially if the target is close to a Gaussian (Proposition 3.5),
- EIS is computationally more efficient, as it can be implemented in terms of the efficient simulation smoother and can exploit structure of the linear signal, if it is present and
- the least-squares regression seems numerically stable and available in many numerical libraries.

Chapter 4

Analysis of selected models

Contributions of this chapter

The main contribution of this chapter is to apply the methods derived in Chapter 3 to selected inference and prediction problems in the context of COVID-19 in Germany. Each model is an extension of model we have used during the COVID-19 pandemic to produce forecasts of cases, deaths and hospitalizations. As all content of this chapter is newly contributed, we give a short overview over the improvements that these models contribute.

Removing reporting delays and weekday effects The model developed in this section is based on the `ILM-EKF` model that Thomas Hotz and the author have submitted to the ECDCs COVID-19 ForecastHub. The original model was also based on a SSM, however fit with an extended Kalman-filter, ignoring the integer nature of the data at hand. This model also did not include delays and was based on reproduction numbers.

Regional growth factor model This model is based on the `ITWW-county_repro` model that Thomas Hotz, Tyll Krüger, Jan Pablo Burgard, Przemyslaw Biecek, Viktor Bezborodov, Marcin Bodych and the author have submitted to both the German-Polish COVID-19 ForecastHub and the ECDC's ForecastHub. This model was not based on a SSM, but rather ignored the dependencies over time. Additionally, it was based on reproduction numbers, which were fit to the incidence data using methods from small-area estimation. The main idea for this model is available in (Heyder et al., 2022).

Nowcasting hospitalizations The model designed in this section is based on the `ILM-prop` model that Thomas Hotz and the author submitted to the German NowcastHub. Again, this model was note based on a SSM. It quantified the uncertainty by past performance, which requires a substantial amount of computation - something that the model presented in this section avoids.

Having established the practical advantages of EIS over the CE-method in the previous chapter, we now demonstrate the usefulness of SSMs for epidemiological modeling. We present three applications: accounting for reporting artifacts (Section 4.1), modeling regional effects (Section 4.2), and performing fore- and nowcasting (Section 4.3). These applications illustrate how SSMs provide a flexible modeling framework that allows practitioners to tailor interpretable models to specific research questions.

The models we present in this chapter are not based on compartmental models, but rather on the epidemiological indicators presented in Section 2.2. We prefer these methods, as the compartmental models require their users to make a lot of assumptions regarding the dynamics of the epidemics, e.g. whether reinfections can or cannot occur, whether population size is fixed or not and also distributional assumptions for the transition rates between compartments. Such assumptions are difficult to verify in practice, and the influence of deviation from them is too. Basing, the infection dynamics solely on the exponential growth factor only assumes that cases grow exponentially, which is theoretically and empirically justified. Additionally, the parameters in compartmental models may be harder to interpret, compared to, e.g., the exponential growth factor; see Section 2.2.4.

Before we present our results, we give a short overview over similar work, in particular those that leverage SSMs to perform inference or short-term predictions for COVID-19.

One prominent approach involves modeling disease dynamics with growth factors. (Arroyo-Marioli et al., 2021) develop a local level model for the log-growth factor based on a classical SIR model, which allows them to derive reproduction numbers. Their model is fully Gaussian and can be fitted using the Kalman smoother. Similarly, (Ives and Bozzuto, 2021) present a similar local level model for the log-growth factor, but assume observations to follow a quasi-Poisson distribution, modeling the growth of deaths instead of the reported cases. Their model is fitted using the extended Kalman filter for US counties.

An alternative strategy derives state space models directly from epidemiological theory. (Lal, Huang, and Z. Li, 2021) and (Keller et al., 2022) derive SSMs from a time-discretized version of ODE-based compartmental models. In this framework, (Lal, Huang, and Z. Li, 2021) assume conditionally Gaussian observations, but the dependence between states and observations is non-linear, so the EnKF was used to fit the model. Taking a fully Bayesian perspective, (Keller et al., 2022) use a negative binomial distribution for cases, hospitalizations, and deaths. They adopt a fully Bayesian view putting priors on hyperparameters and derive posterior distributions of interest by Hamiltonian Monte-Carlo.

The third approach leverages asymptotic theory for computational efficiency. (O'Dea and Drake, 2022) for example implement this approach, exploiting a CLT for compartmental models, to obtain a Gaussian approximation to the states' dynamics. The model can then be fitted using the EKF.

From this overview, we see that most existing SSMs rely on compartmental models to represent epidemic dynamics. In contrast, the models we present in this section provide an alternative approach based on epidemiological indicators rather than compartmental structures. This offers practitioners simpler, more interpretable models with fewer assumptions about disease dynamics, providing greater flexibility when addressing specific research questions.

Unless noted otherwise, all computations are performed on a Macbook Air M3 (2024) with 16GB RAM and are fitted in less than one hour of computation time.

check that this is true

An exception is the larger model in Section 4.2, see there for details on runtime.

4.1 Removing reporting delays and weekday effects

Retrospective analysis of reported cases is one of the fundamental tasks in epidemiological monitoring (see Section 2.1). Such analyses require the finest temporal resolution possible to link changes in the epidemics spread to concrete dates, e.g. the enforcement of NPIs. However, as we have demonstrated in Section 2.3, the available data are contaminated by the reporting process, most notably the

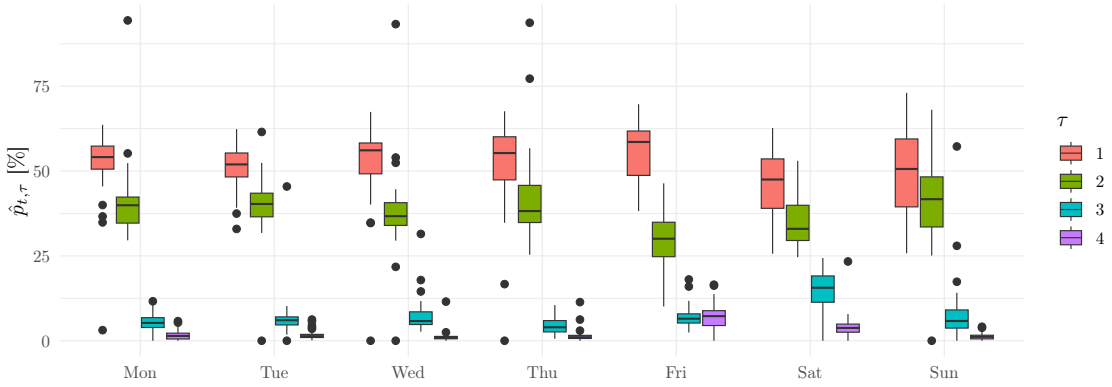

Figure 4.1: Box plots of delay probabilities $\hat{p}_{t,\tau}$ by weekday of case reporting date t. As there are systematically fewer cases reported on Sunday, there is a small weekday effect: $p_{t,1}$ for Saturdays, $p_{t,2}$ for Fridays, $p_{t,3}$ for Thursdays and $p_{t,4}$ for Wednesdays are small compared to other days.

weekday effects, reporting delays, and reporting artifacts associated with events such as public holidays.

While aggregation to the weekly level can mitigate these distortions, see Section 4.2, modeling on the daily level facilitates better retrospective analyses and as such it is the goal of this section.

Here, we use the previously described RKI case incidence data discussed in Section 2.3. As demonstrated in Figure 2.3 **A** and Figure 2.4, most delays are fewer than 4 days. Therefore, ignoring any cases reported with longer delays, we obtain for any reporting date t four observations, which we denote by

$$Y_t = (Y_{t,1}, \dots, Y_{t,4}) \in \mathbf{N}_0^4.$$

Here $Y_{t,\tau}$, $\tau = 1, \dots, 4$, is the number of newly reported cases for reporting date t with delay τ, such that $Y_{t,\cdot} = \sum_{\tau=1}^{4} Y_{t,\tau}$ is the total number of cases reported for reporting date t with delay ≤ 4. Let $\hat{p}_{t,\tau} = \frac{Y_{t,\tau}}{Y_{t,\cdot}}$ denote the empirical delay probability for day t with delay τ. We have already observed in Figure 2.3 that $Y_{t,\cdot}$ is subject to weekday effects, and analogous to hospitalizations (Figure 2.5), there is small variation across weekdays of $\hat{p}_{t,\tau}$, especially if t or $t + \tau$ falls on a weekend, as shown in Figure 4.1.

To produce accurate retrospective analyses of the daily growth factor, we will construct a SSM that accounts for these delays, weekday effects and epidemics' dynamics. This model will enable us to better understand the delay process, accommodate periods of inconsistent reporting, and generate daily growth factors useful for the interpretation of NPI efficacy.

lit rev.

The problem of accounting for reporting delays is generally termed "nowcasting" in the literature, see also Section 4.3 and the literature review therein. Here, however, we are interested in a different problem: that of reconstructing the actual course of the epidemic, i.e. removing both the reporting delay and weekday-effects.

In addition, we will demonstrate the model's utility when handling reporting artifacts not explicitly modeled, e.g. the Christmas period of 2020. SSMs handle missing data seamlessly, so removing observations in that period and fitting the model again is straightforward.

4.1.1 Model

To model the development of cases over time, we start with the exponential growth equation Equation (2.5). Let I_t be the total number of cases for reporting date t, unaffected by weekday effects and reporting delays. Ignoring variation around the mean, the exponential growth ansatz

gives

$$\log I_{t+1} \approx \log \rho_{t+1} + \log I_t$$

for the growth factor ρ_t on day t. It is then sensible to assume that the growth factor ρ_t performs a random walk on the log-scale, as we would expect large day-to-day variation of ρ_t for large values, and small variation for small values, i.e. multiplicative, rather than additive, day-to-day changes. Thus, we assume that

$$\log \rho_{t+1} = \log \rho_t + \varepsilon_{t+1,\rho}$$

for $\varepsilon_{t+1,\rho} \sim \mathcal{N}(0, \sigma_\rho^2)$. To incorporate weekday effects, consider a weekly seasonal component on the log-scale

$$\log W_{t+1} = -\sum_{s=0}^{5} \log W_{t-s} + \varepsilon_{t+1,W},$$

for $\varepsilon_{t+1,W} \sim \mathcal{N}(0, \sigma_W^2)$. Finally, to model the reporting delay probabilities $p_{t,\tau}$, $\tau = 1, 2, 3, 4$, we parameterize them by log ratios

$$q_{t,\tau} = \log \frac{p_{t,\tau}}{p_{t,4}} \qquad \tau = 1, 2, 3,$$

which also perform a random walk in time:

$$q_{t+1,\tau} = q_{t,\tau} + \varepsilon_{t+1,q,\tau},$$

with $\varepsilon_{t+1,q,\tau} \sim \mathcal{N}(0, \sigma_q^2)$ whose variance does not depend on the delay τ. To account for the weekday effect visible in Figure 4.1, we introduce three further weekday effects, for $\tau = 1, 2, 3$ let

$$\log W_{t+1}^{q,\tau} = -\sum_{s=0}^{5} \log W_{t-s}^{q,\tau} + \varepsilon_{t+1,W^{q,\tau}},$$

with $\varepsilon_{t+1,W^{q,\tau}} \sim \mathcal{N}\left(0, \sigma_{W_q}^2\right)$ and shared variance $\sigma_{W_q}^2$. We can recover the delay probabilities $p_{t,\tau}$ from the log-ratios by

$$\begin{aligned} p_{t,4} &= \frac{1}{1 + \sum_{\tau=1}^{3} \exp\left(q_{t,\tau} + \log W_t^{q,\tau}\right)}, \\ p_{t,\tau} &= \exp\left(q_{t,\tau + \log W_t^{q,\tau}}\right) p_{t,4}, \end{aligned} \tag{4.1}$$

for $\tau = 1, 2, 3$.

Finally, there are reporting artifacts and other effects that we have not yet considered in our model that contribute to the variation in the data. To account for these effects, we model daily, multiplicative, "muck" M_t, for date t, such that the total expected number of reported cases on this date is $M_t I_t$ instead of I_t. We assume that $(\log M_t)_{t=0,\ldots,n} \overset{\text{i.i.d}}{\sim} \mathcal{N}(-\frac{1}{2}\sigma_M^2, \sigma_M^2)$, independent of all other states. Thus, M_t follows a log-normal distribution with mean 1.

With these components at our disposal, we can model the observed incidences $Y_{t,\tau}$ by

$$Y_{t,\tau} | \log I_t, \log W_t, q_t, \log M_t \sim \text{Pois}\left(p_{t,\tau} \exp\left(\log I_t + \log W_t + \log M_t\right)\right), \tag{4.2}$$

conditionally independent for fixed t. Thus, W_t acts as a multiplicative factor that modulates the observed cases depending on the day of the week, and the delay probabilities distribute the total expected number of cases $M_t W_t I_t$ onto the delays. In this model, $Y_t = \sum_{\tau=1}^{4} Y_{t,\tau}$ has conditional expectation

$$\mathbb{E}\left(Y_t | \log I_t, \log W_t, q_t, \log M_t\right) = M_t W_t I_t.$$

As it is sensible to model the conditional distribution of Y_t by a Poisson distribution (see Section 2.4), we can view Equation (4.2) as a multinomial thinning of this distribution. Notice that including M_t introduces overdispersion in this Poisson distribution, similar to modeling with a negative binomial distribution.

Letting

$$X_t = \left(\log I_t, \log \rho_{t+1}, \log W_t, \ldots, \log W_{t-5}, q_{t,1}, q_{t,2}, q_{t,3}, \log W_t^{q,1}, \ldots, \log W_{t-5}^{q,3}\right)^T,$$

assuming that

$$\varepsilon_{t+1} = \begin{pmatrix} \varepsilon_{t+1,\rho} \\ \varepsilon_{t+1,W} \\ \varepsilon_{t+1,q,1} \\ \varepsilon_{t+1,q,2} \\ \varepsilon_{t+1,q,3} \end{pmatrix}$$

has independent marginals, and fixing an initial distribution of X_0 fully specifies a PGSSM for the joint distribution of (X, Y). For the initial distribution we use

$$X_0 \sim \mathcal{N}(u_0, \Sigma_0)$$

where u_0 is 0 for all elements, except to the third entry (corresponding to M_0), which we set to $-\frac{1}{2}\sigma_M^2$. For the initial covariance we use a diagonal matrix, which is based on numerical experiments (for $\log I$ and $\log \rho$) and the fact that a log-normal with parameter $\sigma^2 = 1$ (the variance of the involved normal distribution) roughly models being off by one order of magnitude[1]. We let

$$\Sigma_0 = \operatorname{diag}\left(\underbrace{5^2}_{\log I}, \underbrace{0.2^2}_{\log \rho}, \underbrace{s_M^2}_{M}, \underbrace{1}_{\log W_0}, \ldots, \underbrace{1}_{\log W_{-5}}, \underbrace{1}_{q_{0,1}}, \underbrace{1}_{q_{0,2}}, \underbrace{1}_{q_{0,3}}, \underbrace{1}_{\log W_0^{q,1}}, \ldots, \underbrace{1}_{\log W_{-5}^{q,3}}\right).$$

The model has a linear signal

$$S_t = \begin{pmatrix} \log I_t + \log W_t \\ q_{t,1} \\ q_{t,2} \\ q_{t,3} \end{pmatrix},$$

but due to the non-linear dependence of $p_{t,\tau}$ on $q_{t,\tau}$, $Y_{t,\tau}$ depends not just on $S_{t,\tau}$ but on the whole of S_t. Fortunately, this is not a problem for either the LA or EIS. For the LA (Algorithm 5), notice that the covariance matrix Ω_t is given by the inverse of the negative Hessian of $s_t \mapsto \log p(y_t|s_t)$, which is now non-diagonal. While it is not guaranteed that Ω_t is positive semi-definite during the Newton-Raphson iteration, we can still employ the Kalman filter and signal smoother to perform the iteration efficiently, see (Jungbacker and Koopman, 2007) and the discussion in Section 3.5.1. Furthermore, at the global optimum, the Hessian is negative semi-definite, so Ω_t is positive semi-definite, specifying a valid GLSSM proposal. Similarly, we may extend EIS to account for non-diagonal Ω_t. Recall from Section 3.3.3, that EIS minimizes for a given t

$$\sum_{i=1}^{N} \left(\log p(y_t|S_t^i) + \langle \Omega_t^{-1} z_t, S_t^i \rangle - \frac{1}{2} \operatorname{tr}\left(\Omega_t^{-1} S_t^i (S_t^i)^T\right) - \lambda_t\right)^2$$

over z_t, Ω_t, λ_t. Noticing that $(A, B) \mapsto \operatorname{tr}\left(A^T B\right)$ is the Frobenius inner-product, we see that this optimization problem is still a weighted linear least squares problem for $\Omega_t^{-1} z_t, \Omega_t^{-1}, \lambda_t$, when we let Ω_t^{-1} take values in the symmetric matrices in $\mathbf{R}^{p \times p}$. As the dimension of this vector space is $\frac{p(p+1)}{2}$, we may still perform the computationally efficient weighted linear least squares routine, but at an increased cost: the number of parameters increases from $2p+1$ (Ω_t diagonal) to $p + \frac{p(p+1)}{2} + 1$ (Ω_t symmetric).

The parameters of the model are $\theta = \left(\log \sigma_\rho^2, \log \sigma_W^2, \log \sigma_q^2, \log \sigma_M^2, \log \sigma_{W_q}^2\right)$, which we model on the log-scale to avoid having to take care of constraints. Given observations $Y = (Y_0, \ldots, Y_n)$ we perform maximum likelihood estimation as described in Section 3.6.1. As tuning parameters in this procedure we use 20 iterations for the LA and EIS, with relative tolerance of convergence

[1] The 1%-quantile is ≈ 0.1 and the 99%-quantile is ≈ 10.

method	$\hat{\sigma}_\rho$	$\hat{\sigma}_W$	$\hat{\sigma}_q$	$\hat{\sigma}_M$	$\hat{\sigma}_{W_q}$
manual	0.001	0.100	0.50	0.01	0.10
initial	0.015	0.024	0.12	0.14	0.81
MLE	0.015	0.024	0.12	0.14	0.81

Table 4.1: Standard deviations for the models' showcase determined either by hand, by the initial search or by maximum likelihood estimation described in Section 3.6. The difference between the initial search and the MLE is negligible and is not visible for the precision shown here.

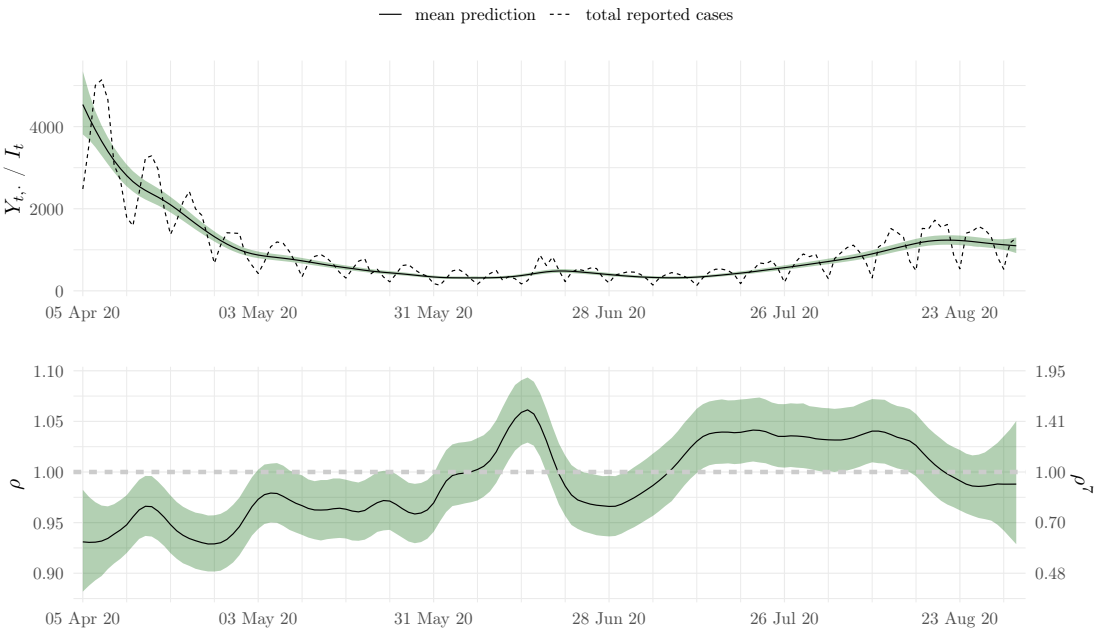

Figure 4.2: Monte-Carlo estimates of mean (black lines) and 95% prediction intervals (shaded green regions) for smoothed incidences I and daily growth factors ρ. The total reported cases with delay at most 4 days, Y_t, is shown as a dotted line. The secondary axis for the daily growth factor ρ indicates the corresponding weekly growth factors ρ^7 which are easier to interpret. The gray dashed line indicates the threshold for growth $\rho = 1$.

set to 10^{-5}. For the EIS proposals we also use 1 000 samples and all four antithetic variables, i.e. we use Equation (3.49). At the MLE we again determine the EIS proposal using the same parameters and perform inference for the conditional distribution using 10 000 samples, applying the method described in Section 3.6.2 to obtain estimates of the posterior mean, standard deviation and prediction intervals.

4.1.2 Results

Showcase We start by a showcase of the models' capability, fitting it to the reported case date in the period from April 5th to September 1st 2020, starting from the first day when 4 delays are available in the dataset to the initial period of exponential growth in the fall of 2020. We estimate the parameters $\theta = \left(\log \sigma_\rho^2, \log \sigma_W^2, \log \sigma_q^2, \log \sigma_M^2, \log \sigma_{W_q}^2\right)$ by maximum-likelihood estimation, yielding the parameters displayed in Table 4.1. There, we see that $\log \rho_t$, $\log W_t$, $q_{t,1}, q_{t,2}$ and $q_{t,3}$ vary slowly over time, compared to the faster varying $W^{q,1}, W^{q,2}, W^{q,3}$.

We show importance sampling estimates of the mean and 95% prediction intervals of the conditional distribution of I and ρ (Figure 4.2) as well as W, M and p (Figure 4.3), based on the procedure

described in Section 3.6.2. For I we additionally show the total number of reported cases with delay at most 4 days, $Y_{t,\cdot} = Y_{t,1} + \cdots + Y_{t,4}$, as a sanity check. Indeed, I is a smoothed version of Y, which removes weekday-effects and small discrepancies in reporting, as these effects are captured by the W and M terms.

For the daily growth factor ρ we additionally display the corresponding weekly growth factors ρ^7 on the secondary axis. We see that uncertainty for ρ is roughly constant over time, except close to the beginning and end of the time period considered here. We see that until June 2020 ρ is below 1, followed by a short skip above 1 during the local outbreak highlighted in Figure 2.2 and a return to $\rho < 1$ until beginning of July 2020. We will deal with this sudden increase and the following decrease more extensively in the following section. From the middle of July 2020 to the middle of August 2020, ρ is consistently above 1, with a slight dip at the end of August, before rising above 1 again. That cases are, or will be, rising exponentially is easier to infer from ρ compared to I, as ρ, or ρ^7 for that matter, directly quantifies the increase in cases. Thus, this sustained period of exponential growth could have been a warning sign to policymakers of the buildup of infections in the population, which only became noticeable in the cases starting in October 2020.

For the muck term M, we see that is centered around 1 and allows capturing variation of the reported cases that is not captured by other terms in the model. As M follows a log Normal distribution, its variance is $\left(\exp\left(\sigma_M^2\right) - 1\right) \exp\left(2(-\frac{1}{2}\sigma_M^2) + \sigma_M^2\right) = \exp\left(\sigma_M^2 - 1\right)$, so M has standard deviation ≈ 0.12 for the MLE from Table 4.1, consistent with Figure 4.3. As such, we expect the reported cases to vary around $\pm 24\%$ on any given day, due to residual effects not captured by the weekday effect. We also investigated qq-plots of the mean predictions of M, which indicate that there might be some outliers, e.g. those around the local outbreak in June 2020, present. To improve the fit, we could replace the distribution of M by, e.g., a t-distribution with a low degree of freedom, allowing for heavier tails. The LA for such a model can still be found efficiently, see (Durbin and Koopman, 2012, Section 11.7.2), so the methods of this section are still applicable. However, we deem such a modification to be outside the scope of this thesis.

The weekday effect W exhibits the expected seasonal pattern: on Sundays, which are marked by the minor breaks in the figures' grid, W is below 1, while it is high for Tuesdays, Wednesdays and Thursdays. Over the period considered, this pattern is quite stable, with only slight changes over time: W is slightly larger for Mondays and Fridays at the end of the period compared to the beginning. By construction, we have $\overline{\log W_t} = \frac{1}{7}\sum_{\tau=-3}^{3} \log W_{t-\tau} \approx 0$ for all t, so Jensen's inequality suggests $\frac{1}{7}\sum_{\tau=-3}^{3} W_{t-\tau} \gtrapprox 1$. However, the practical difference is small:

$$\frac{1}{7}\sum_{\tau=-3}^{3} \mathbb{E}(W_{t-\tau}|Y) \approx 1.05,$$

for $t = 3, \ldots, n-3$, with small standard deviation. Consequently, we could correct I_t for the bias introduced by W by an increase of 5% (or, more precisely, consider $I_t \bar{W}_t$).

Finally, for the delay probabilities, we compute both the signals probabilities, given by Equation (4.1), and a smoothed version, obtained by setting $\log W_t^{q,\tau}$ to 0 in Equation (4.1). From Figure 4.3, we see that starting in the middle of April, reporting became faster, with a larger share of cases being reported with a delay of only a single day. While this seems to reverse at the end of the considered period, this is likely due to the reporting artifacts at the end of August, indicated by the large spike in $p_{t,2}$.

reporting artifacts in Christmas season 2020 Now that we have seen an application of the model, we use it to demonstrate how easily we can incorporate missing or faulty observations. Recall from Figure 2.2 the problem of reporting artifacts during the 2020 Christmas season. In Figure 4.4 we show undesirable effects of directly applying our model to the data in this period. In this figure, the red lines correspond to inferences made using all available observations, while turquoise lines correspond to inferences made where we remove all observations from December 19th 2020 until January 17th 2021, marked by the gray background in the figure.

We can fit both models using the same methods, as we only have to replace the observation matrices B_t for missing dates t by zero matrices and the conditional distribution of $Y_{t,\tau}|S_t$ by δ_0, while

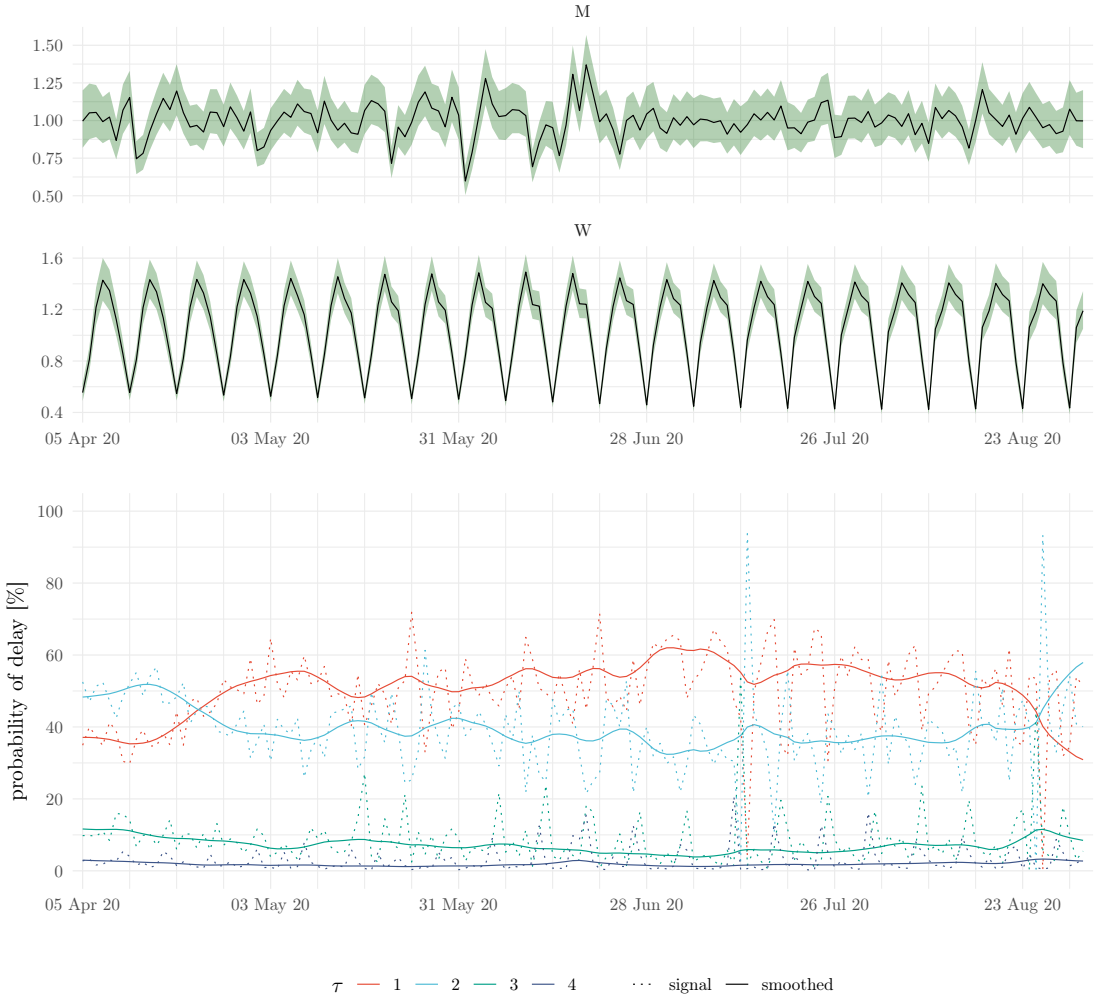

Figure 4.3: Importance sampling estimates of mean (black lines) and 95% prediction intervals (green ribbons) for weekday effect, "muck" and delay probabilities in the showcase model, based on the method described in Section 3.6.2. We omit the small prediction intervals for delay probabilities for better readability. Note that all variables are not included directly in the model, but may be written as a function of states, either taking the exponential or converting from log-ratios to probabilities. The minor breaks in the x-axis grid indicate Sundays.

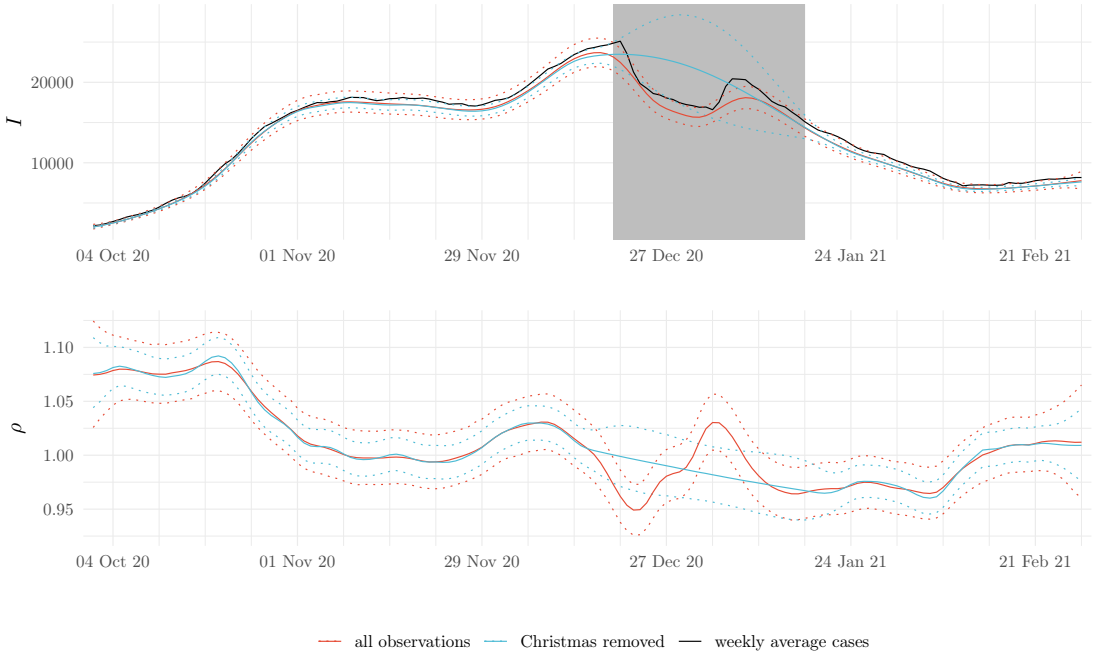

Figure 4.4: Importance sampling estimates of 95% prediction intervals and means of the conditional distribution of I and ρ given reported cases for the reporting delay model applied to the period of October 1st 2020 until February 28th 2021. For I we additionally show weekly average reported cases as in Figure 2.2.

replacing $Y_{t,\tau}$ by 0 for $\tau = 1, \ldots, 4$. In the approximating LAs and EIS proposals we set z_t and Ω_t to the zero vector and matrix, respectively.

For the model using all available data, we see that the reporting artifacts affect both the incidences I and growth factors ρ, with a sharp decrease in ρ during the holidays, followed by a sharp increase in the new year. For the model that has the flawed observations removed, we see that both I and ρ behave more smoothly, as the estimated standard deviations, displayed in Table 4.2, are also smaller. The price we pay for this smoother transition is larger uncertainty where observations are now missing, i.e. the 95% prediction intervals are larger in this period than those for the model with all data available. However, when data are available, the prediction intervals for the second model are smaller, as its estimated standard deviations are smaller. The means, however, tend to agree rather well.

In Figure 4.5 we additionally show the expected smoothed delay probabilities based on Equation (4.1) where we set the weekday effects to 0. There, we see that starting on December 24th, the reporting pattern exhibits strong irregular behavior (recall that the reported cases for December 24th correspond to December 23rd to December 20th for delays $\tau = 1, \ldots, 4$) for the model using all observations. Additionally, in January, we a large spike in $p_{t,1}$, which could correspond to a backlog of cases being reported all at once. Again, the model that has the Christmas period removed, proceeds much smoother.

4.1.3 Discussion

As we can see from the exemplary results, the model allows to accurately model the evolution of reported cases over time, while taking care of unwelcome reporting artifacts such as the weekday effect, delays and changes in reporting pattern due to holidays. The estimated growth factors allow inferring about the speed at which the cases proliferate, and can thus be a valuable tool for decision makers. With our model, we can identify the almost constant exponential growth in the summer of

method	$\hat{\sigma}_\rho$	$\hat{\sigma}_W$	$\hat{\sigma}_q$	$\hat{\sigma}_M$	$\hat{\sigma}_{W_q}$
all observations					
manual	0.0150	0.024	0.12	0.140	0.81
initial	0.0126	0.032	0.37	0.110	0.91
MLE	0.0126	0.032	0.38	0.110	0.91
Christmas removed					
manual	0.0150	0.024	0.12	0.140	0.81
initial	0.0087	0.028	0.16	0.048	0.38
MLE	0.0087	0.028	0.16	0.048	0.38

Table 4.2: Estimated parameters for the model during the Christmas period, for all observations or with observations during the Christmas period (19th December 2020 until January 17th 2021) removed. The manual parameter is based on the estimate of the models' showcase, i.e. the MLE result from Table 4.1.

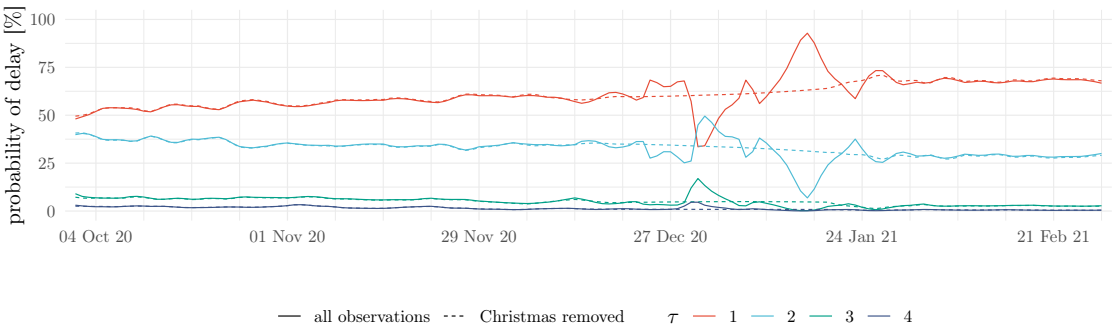

Figure 4.5: Importance sampling estimates of conditional expectation $\mathbb{E}(p_{t,\tau}|Y)$ for the two sets of Christmas observations: the full lines correspond to all reported incidences and the dashed lines to observations between December 19th 2020 and January 17th 2021 removed. When using all observations, we clearly see the effect of the Christmas holidays, with a drop in next day reporting during the holidays, and an increase in next day reporting in the middle of January.

2020 (Figure 4.2), which is difficult to see by only looking at the number of reported cases, due to the reporting artifacts and low number of cases.

As our model explicitly models reporting delays, we can infer about them as well. From Figures 4.3 and 4.5 we can see that during the first year of the epidemic, reporting became faster: while only about 40% of cases were reported with delay of one day in April 2020, that fraction rose to more than 60% at the end of 2020, excluding the noisy Christmas period. By including reporting delays, our model is also capable of performing now- and forecasts of future reported cases. For forecasts, we evaluate the performance of seven day predictions from this model in the following section.

The SSM nature of our model has the additional advantage of being capable of naturally handling missing observations, either actual missing observations or synthetically missing observations, such as in the Christmas period. By removing available observations from the model, we are able to create a what-if scenario, letting the model automatically fill-in the faulty observations. Let us hasten to add that this should not be confused with redistributing the number of cases observed in the Christmas period to better fit the model, as we have not included any restrictions on the total number of cases being equal to the observed number of cases in this period. Technically, this is possible, by adding $\log I_{t-1}, \dots, \log I_{t-D+1}$, where D is the number of days removed, to the states and adding a single observation of $\sum_{s=0}^{D-1} I_{t^*-s}$ at time t^*, the first day after the Christmas period is over. Removing the observations from December 19th 2020 to January 17th 2021 removes a total of 551 031 cases. In the Christmas model, the predictive distribution of cases for this time period has mean 618 000 (standard deviation 59, 000) with a 95% prediction interval of (511 000, 743 000) (all numbers rounded to the next thousand due to Monte Carlo error). Thus, our reconstruction of the total number of cases is compatible with the total number of cases removed, albeit slightly overestimating the total number of cases.

While we believe that our model already captures many of the relevant effects for modeling the daily evolution of cases, there are several worthwhile extensions conceivable. We here give an incomplete list of potential improvements:

- We have only used the reporting date in our model, but the data include also information (for some cases) on the symptom onset date. Including this would also allow to better remove the weekday effect, as infection dates, presumably, are less affected by weekdays than reported cases.
- In the same vein, including data on deaths would allow for estimates of the reporting dark figure, and its change over time, as long as immunization through infection and vaccination is low, i.e. at the beginning of the epidemic.

Most of these improvements require the use of additional data sources, which is straightforward to do with state space models: we just have to extend the states and dynamics accordingly.

4.2 Regional growth factor model

Modeling the epidemics spread on a regional level allows us to differentiate between localized and global outbreaks, such as the one in June 2020, highlighted in Figure 2.2. Additionally, regional level prediction and growth factors are of interest on their own, because NPIs are enforced on the regional level. Moreover, having access to the spread on the regional level enables, e.g., regression of the growth rate against regional covariates, which in turn sheds light on which factors drive the epidemic.

Instead of modeling the number of cases per day and with delay as we did in Section 4.1, we will now model the total number of cases reported within one week for every county in Germany. Here we assume that a sufficient time period has passed, i.e. several days, see Figure 2.3, such that the total number of cases is known sufficiently well. This weekly approach has several advantages: First, aggregating over the weekly data gets rid of the weekday effect, at the expense of a lower time resolution. Second, if we are interested in a retrospective analysis, it is sensible to assume all cases have been reported already, so we can avoid modeling the reporting delays.

However, modeling cases on the regional level comes with its own challenges, as we have to take care of accounting for the spatial spread, as well as an exchange between regions, cf. Section 2.4.

4.2.1 Model

Similar to the last section, we start by modeling the evolution of cases in time. We now have incidences $I_{t,r}$ reported for reporting date t and region r, where there are a total of R regions. For Germany we use the $R = 400$ counties as of the Gebietsreform 2021, which united the free city Eisenach with the county of Wartburgkreis (Freistaat Thüringen, n.d.). This has several implications for the raw data published by the RKI:

- For data published before 30. June 2021, cases were reported separately for Eisenach and the Wartburgkreis. In pre-processing the data on the county level, we merge these two regions into a single one.
- The RKI reports cases for Berlin's districts separately. Again, we aggregate all of them into a single number of cases for Berlin.

Again, we model the evolution of cases by

$$\log I_{t+1,r} \approx \log I_{t,r} + \log \rho_{t+1,r} \tag{4.3}$$

where $\rho_{t+1,r}$ is the weekly growth factor in region r. Now we deviate from the previous model and model

$$\log \rho_{t,r} = \overline{\log \rho_t} + u_{t,r},$$

where $\overline{\log \rho_t}$ is the average growth rate and $u_{t,r}$ is the difference between the growth rate in region r and the country wide average. We will model $u_{t,r}, r = 1, \dots, R$ to be jointly Gaussian, but correlated, which will enable us to model regional dependencies. To motivate our choice for the covariance structure, let us consider how cases are transferred between regions first.

As we are modeling cases on a regional level, we have to account for an exchange of cases as well. To illustrate our approach, suppose that we have for region r S^r many secondary cases generated where the primary case belongs to region r, but the secondary case may belong to another region r'. Here "belonging to" signifies that the case is reported in that region, which means that the infectee has registered their center of living to be in this region. Denote by $p_{r,r'}$ the fraction of such cases and set $p_{r,r} = 1 - \sum_{r' \neq r} p_{r,r'}$.

Under these assumptions, the newly reported cases in region r are

$$\tilde{S}^r = \sum_{r'=1}^{R} p_{r',r} S^{r'} = (P^T S)_r$$

for $P = (p_{r,r'})_{r,r'=1,\dots,R} \in \mathbf{R}^{R \times R}$. As $P\mathbf{1} = \mathbf{1}$, P is a stochastic matrix. Assuming now that $S^r, r = 1, \dots, R$ are random and i.i.d. with variance σ_S^2, we have

$$\operatorname{Cov}\left(\tilde{S}\right) = \operatorname{Cov}\left(P^T S, P^T S\right) = \sigma_S^2 P^T P.$$

However, modeling the correlation of newly reported cases turns out to be difficult: the cases will surely be modeled by a Poisson or Negative Binomial distribution, so we would have to decide on a copula to introduce this dependency structure. While this is feasible in principle, we opt for an easier way. Instead of modeling correlated incidences $I_{t+1,r}$, we model correlated growth rates $\log \rho_{t+1,r}$, by taking $\operatorname{Cov}(u_t)$ to be $\sigma_S^2 P^T P$. By Equation (4.3), conditional on $I_{t,r}$, this also captures regional correlation, without having to specify an involved joint distribution for the incidences. Note however, that this is just a convenient modeling choice whose aim is to replicate the covariance structure of the — somewhat artificial — case of having i.i.d. number of secondary cases across all regions.

As elaborated in Section 2.4, we want the regional effects $u_{t,r}$ to be both flexible, but also, in some sense, stable over time. Thus, it makes sense to model u_t as a stationary process in time. The

simplest, non-trivial, stationary process is a vector-autoregressive process

$$u_{t+1} = \alpha u_t + \varepsilon_{t+1,u}$$

where $\alpha \in (-1, 1)$ and $\varepsilon_{t+1,u} \sim \mathcal{N}(0, \Gamma)$, where Γ is a positive definite matrix. By the above discussion, we set $\Gamma = (1-\alpha^2)\sigma_S^2 P^T P$ so that the stationary distribution of $u_t, t = 0, \dots, n$ is $\mathcal{N}(0, \sigma_S^2 P^T P)$.

To setup our SSM, let $X_t = \left(\overline{\log \rho_{t+1}}, u_{t,1}, \dots, u_{t,R}\right)^T \in \mathbf{R}^{R+1}$. For the observations, we let $Y_t = (I_{t,1}, \dots, I_{t,R})^T$, the number of cases observed in regions $1, \dots, R$ in the t-th week.

We then model the number of cases at time $t+1$ in region r, $I_{t+1,r}$ to follow a negative binomial distribution, conditional on the states X_t to be

$$I_{t+1,r} | I_t, \overline{\log \rho_t}, u_{t,r} \sim \text{NegBinom}\left(\overline{\rho}_t \exp(u_{t,r}) P^T I_t, r\right),$$

conditionally independent. While the previous observations I_t are now conditioned on as well, recall from our discussion in the beginning of Chapter 3, that this is not problematic.

To fully specify the model, we have to provide the transfer probabilities $p_{r,r'}$. For these, we use official data by Germany's federal employment agency on commuters. We use two datasets: the number of employees subject to social security contributions per county (Bundesagentur für Arbeit, Statistik, 2021) and the number of commuters per county (Bundesagentur für Arbeit, Statistik, 2024). We use the number of commuters per county from December 2022, which are no longer directly available on the homepage of the federal employment agency, but can be obtained through the Pendleratlas interface. In any case, these data are additionally available in the accompanying zenodo repository of this thesis

link to it

. Notice that both datasets are dated after the Gebietsreform in June 2021. Counties are uniquely identified by the Allgemeiner Gemeinde Schlüssel (AGS), a five-digit code, which are also available in the RKI dataset.

In this dataset a commuter is someone whose center of living (as registered with the German authorities) is a different county than the county of their workplace. For two regions r, r' we let n_r be the total number of employees subject to social security contributions per county and $c_{r,r'}$ be the number of commuters from county r to county r', with $c_{r,r} = n_r - \sum_{r' \neq r} c_{r,r'}$. From these data, we calculate $q_{r,r'} = \frac{c_{r,r'}}{n_r}$, the fraction of socially insured employees that have their center of life in region r, but are registered to work in region r'.

As this is only a crude approximation to the actual exchange between regions, we let

$$p_{r,r'} \propto \bar{q} + (1-\bar{q}) \frac{q_{r,r'}}{\sum_{r'' \neq r} q_{r,r''} + C q_{r,r}} \qquad r' \neq r$$

where we interpret $\bar{q}$ as a constant socket of exchange between regions and $C \geq 1$ as an additional proportion of stay at home inhabitants that are not captured by $q_{r,r}$, e.g. elderly or children. The proportionality is owed to $\sum_{r'=1}^{R} p_{r,r'} = 1$. Let us highlight some instances of P.

If $\bar{q} = 0$ and $C = 1$, then $p_{r,r'} = q_{r,r'}$, which would distribute secondary cases according to the commuting given by the official data from Germany's federal employment agency.

If $\bar{q} = 1$ or $\bar{q} \to 1$ with fixed C, $P = \frac{1}{R} J \in \mathbf{R}^{R \times R}$, where J is the matrix with all entries equal to 1. We can interpret this as choosing the region a secondary case is reported in as uniformly as random across all regions, regardless of the original region of the primary case.

If $\bar{q} \in [0, 1)$ and $C \to \infty$, then $P \to I \in \mathbf{R}^{R \times R}$, where I is to identity matrix. In this setting all regions evolve independently of one another. Thus, the model is flexible enough to account for these practically relevant scenarios, and interpolate between them.

Our final model is parameterized by

$$\theta = \left(\log \sigma_S^2, \operatorname{logit} \alpha, \log(C-1), \operatorname{logit} \bar{q}, \log \sigma^2_{\overline{\log \rho}}, \log r\right),$$

where we reparameterized to an unconstrained $\theta \in \mathbf{R}^6$. The model has a linear signal

$$S_t = (\log \rho_t + u_{t,r})_{r=1,\dots,R},$$

which makes inference fast, as the approximating GLSSM in the LA and EIS method only requires $\mathcal{O}(n\,R)$ many parameters. Again, we use MLE to estimate θ, using the methods from Section 3.6.

describe setup/parameters

We aggregate the reported cases from the RKI on a weekly level. We orient ourselves at the ECDC's ForecastHub, whose guidelines read

> Forecast horizons should use the Epidemiological Week (EW) format, defined by the US CDC. Each week starts on Sunday and ends on Saturday. [2]

Thus, the observations $I_{t,r}$ $t = 0, \dots, n$ and $r = 1, \dots, R$ consist of the number of reported cases in region r that were reported from the t-th Sunday up until the t-the Saturday in the period of interest and for identification purposes we identify t with the t-th Saturday in the period under consideration.

4.2.2 Results

We will demonstrate the usefulness of our new model by applying it to two scenarios. First, recalling the local outbreak highlighted in Figure 2.2, occurring in the middle of June 2022 (T. Günther et al., 2020), we show that using our model gives reasonable estimates of growth rates when incidences are low and local outbreaks can occur, which can then be used to give sensible forecasts, outperforming baseline models on the country as well as the regional level. We will use this as a **showcase** of the models capabilities, and comment on the estimated parameters, especially P, which accounts for cross-regional infections. Second, we show that our model is able to give reasonable **one-week ahead forecasts** of COVID-19 cases by comparing its predictive performance to that of real-time forecasts created in the ECDC's ForecastHub from April 2021 to January 2022.

showcase Similar to the last section, we start out with a motivational example on the capabilities of our model. For this, we use the local outbreak highlighted in Figure 2.2, which occurred in the middle of June 2020 (T. Günther et al., 2020). We consider the time period from 25 April 2020[3] up until 20 June 2020 as observations, consider the observation on 27 June 2020 to be missing, and fit the SSM to this data. Figure 4.6 shows the number of reported cases used to fit this model, aggregated to the whole of Germany. The local outbreak accounts for a total of 1 413 cases in the county of Gütersloh between 17 June 2020 and 23 June 2020 (see (T. Günther et al., 2020, Figure 1)), noticeable in this figure by the large jump between 13 June 2020 (2324 cases) and 20 June 2020 (3872 cases).

We fit the model using maximum likelihood estimation and present the estimated parameters in Table 4.3. The estimated auto-regressive parameter α is negative, which has can be interpreted as follows: when a region's log-growth factor is above the country-wide average at time t, it tends to decrease below the average in the following week. Similarly, regions with below-average growth factors tend to increase back toward the mean. This negative autocorrelation is sensible for the low-incidence setting we consider here, where large outbreaks are typically localized and temporary, rather than sustained.

The standard deviation of the average growth rate, $\sigma_{\overline{\log \rho}}$, is small compared to that of the spatial effect, σ_S. This is visible from Figure 4.7 as well, where we show the predicted median growth factors (not on the log scale) for the model with a blue dashed line ($\overline{\log \rho_t}$) and boxplots for the

[2] https://github.com/european-modelling-hubs/covid19-forecast-hub-europe/wiki/targets-and-horizons
[3] Recall that this weekly observation includes cases reported from 19 April 2020 to 25 April 2020.

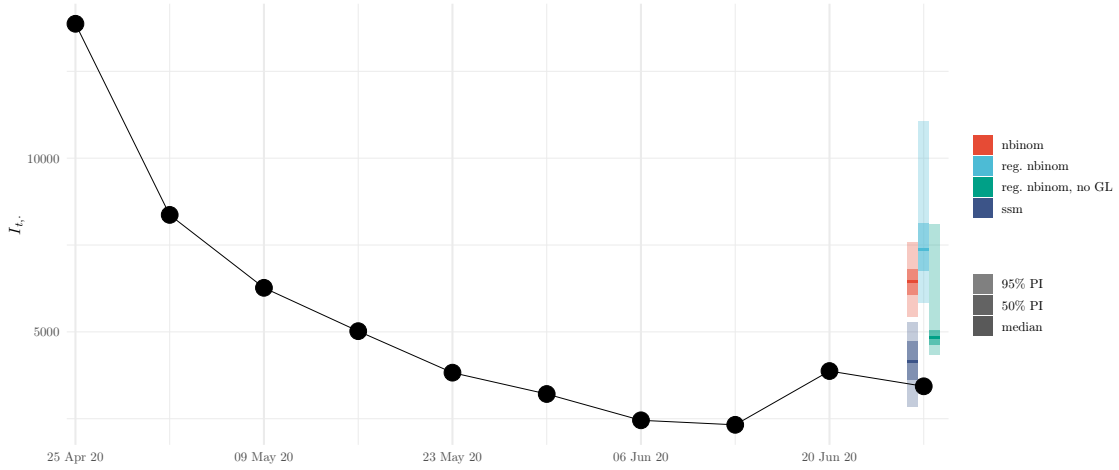

Figure 4.6: Incidences $I_{t,\cdot} = \sum_{r=1}^{R} I_{t,r}$ in Germany in the period under consideration in the regional showcase model. We additionally show predictions (median, 50% and 95% prediction intervals) as shaded regions for three different approaches: the SSM presented in this section and three negative binomial baselines (see text for details). The SSM approach is the only approach with the actual incidences ending up within the 95% prediction interval, the three baselines completely miss this target. Note that all four prediction intervals are located at 27 June 2020, but are shifted horizontally for better visibility.

parameter	estimate
α	-0.218
$\sigma_{\overline{\log \rho}}$	0.177
σ_S	0.866
$\bar{q}$	0.049
C	2.406
r	19.518

Table 4.3: Estimated parameters for the regional showcase model.

median growth rates for each county (summarized by blue boxplots). Here we can see that the variation over time at the county level is much larger than that at the country level, which is also evident when examining $\log \rho_{t,r}$ directly (figures not shown).

The estimated proportion of stay at home inhabitants, $C \approx 2.4$, is remarkably close to the Germany-wide ratio of total inhabitants to employees subject to social security contributions, which is 2.5—despite the model having no direct access to total population data. The estimated overdispersion parameter r indicates significant overdispersion in the data: as explained in Example 3.1, the variance of a NegBinom distribution with mean μ and overdispersion parameter r is $1 + \frac{\mu}{r}$ times larger than that of a Poisson distribution with the same mean.

This overdispersion becomes practically significant when $\mu \geq r$, as this corresponds to at least doubling the variance compared to a Poisson model. For the date of 20 June 2020, this threshold was exceeded by 32 out of 400 counties, indicating that overdispersion was relevant for the larger counties during this period.

Having fitted the model, we can use it to obtain forecasts for the next observation, that on 27 June 2020, using the techniques detailed in Section 3.6.2. We show predictions (median, 50% and 95% prediction intervals) in Figure 4.6, indicated by the blue regions. As the predictions on the country level consist of those on the regional level, we additionally use the data on total inhabitants in a county, capping the number of predicted cases by the total inhabitants, that is we predict in region

r with samples

$$\min\left\{\log \rho^i_{T,r} I_{T-1,r}, \text{pop}_r\right\},$$

where $i = 1, \ldots, N$, T is the index for which we want to perform predictions and pop_r is the total number of inhabitants in each region.

To assess the performance, we compare it to three simple baseline models.

- The `nbinom` model uses a NegBinom distribution with mean $\mu = 6451.1$ set to the country wide growth factor from 13 June 2020 to 20 June 2020 ($\rho = 1.67$) times the total number of cases reported for Germany for 20 June 2020 ($I_{t,\cdot} = 3872$). The overdispersion parameter is estimated by fitting the model to past observations with maximum likelihood estimation, resulting in $r = 143.1$. The median and prediction intervals presented in the figure are given by the respective quantiles of this distribution.
- The `reg.nbinom` model uses the same strategy, but applied to observations on the county level, estimating an individual r for each county. To take care of unrealisticly high growth factors, we cap all growth factors at 3. Should the empirical growth factor be infinite or indeterminante due to the number of old cases being 0, we set it to 1. The median and prediction intervals presented in the figure are obtained by simulating 10 000 samples from each county, independently, then taking empirical prediction intervals on the number of cases aggregated to the country level. We also apply the same capping strategy by the total number of inhabitants as for the `ssm` model.
- The `reg.nbinom no GL` model is the same as the `reg.nbinom` model, but with cases for the county of Gütersloh set to 0.

It is clear from Figure 4.6 that the `ssm` approach outperforms the baseline models: it is the only model where the prediction interval contains, or is even close to the true observation. There are multiple reasons for this behavior. First, the simple `nbinom` overpredicts the number of total cases because the number of reported cases from the local outbreak in Gütersloh county dominate the country-wide development of cases. While the regional level `reg.nbinom` model is able to account for this, the empirical growth factor for Gütersloh is $\hat{\rho}_{T,\text{Gütersloh}} = 11.7$ with 856 cases reported for 20 June 2020, which results in $\approx 10\,000$ cases predicted for that county alone. Recalling that we have capped the growth factor at 3, the `reg.nbinom` model would only predict $\approx 2\,600$ cases, which is still noticeable in the predictions. The best of the three baseline models — in terms of predictive performance for this single observation — is the `reg.nbinom no GL` model, where we have removed Gütersloh from the prediction completely. However, it still overpredicts by a relevant margin which we attribute to the fact that the same effect — albeit less pronounced may be at work in other counties: due to small numbers of reported cases there are many large outliers in the empirical growth factors, see Figure 4.7.

Another advantage of the `ssm` model are the regional and country level growth factors we obtain. In Figure 4.7 we show median estimates of these growth factors, together with their empirical counterparts, i.e. the growth factors used in the `nbinom` and `reg.nbinom` baseline models (without the cap at $\rho = 3$ introduced there). In this figure, we observe that the country level estimates of the growth factor are smaller for the SSM approach, compared to the empirical one. The reason for this is that $\overline{\log \rho_t}$ is not the logarithm of a country wide growth factor, but the mean (on the log-scale) of all regional growth factors, so by Jensen's inequality it has to be smaller than the country level growth factor. Its estimate is close to the median growth factor on the county level, indicated by the bar in the blue boxplots. For the county level growth factors in this figure, we additionally observe less variation of growth factors across counties due to the regularization our model imposes.

Finally, we can interpret the entries in P, which informs both the redistribution of cases between regions, and the covariance of regional effects u_t. As P is a 400×400 matrix, we focus only on a small section of it: the counties in the federal state of Saxony. Saxony is interesting because it contains two large cities ("Leipzig, Stadt" and "Dresden, Stadt") with commuters commuting from the surrounding area to these cities. In the fitted model, this results in a larger row-sum for the indices associated with these cities, see the right-hand side of Figure 4.8.

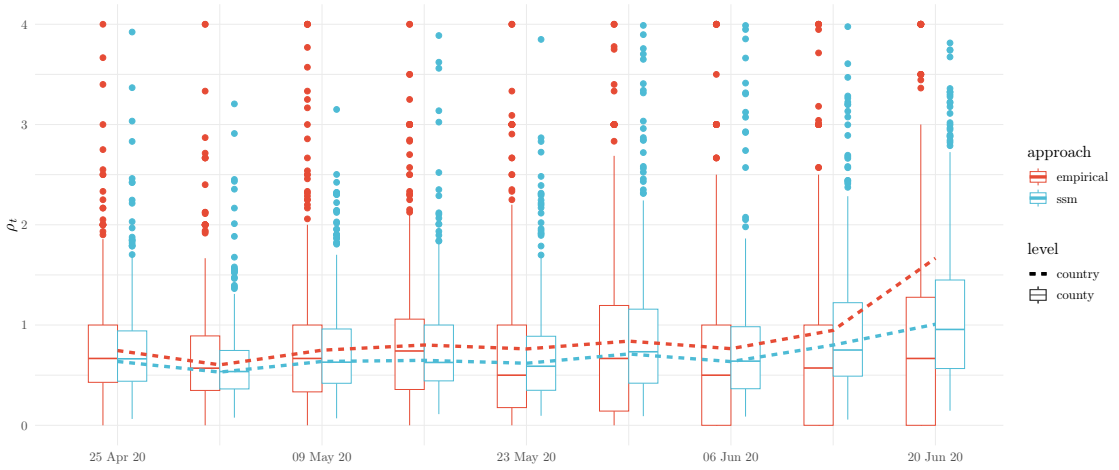

Figure 4.7: Growth factors for the showcase model estimated by the SSM approach (blue boxplots and lines) and the empirical approach (red boxplots and lines). For the 400 counties in Germany, we summarize the estimated growth factors with boxplots. The top of the y-axis is cutoff at $\rho = 4$ omitting the many outliers produced by both approaches, which is due to the overall small number of reported cases. The estimates of the SSM approach tend to be more concentrated than those based on the empirical approach, as the SSM approach regularizes the (log-)growth rates both in time an space. While the country level estimates (shown by dashed lines) mostly agree, they diverge at the end of the observational period, as the local outbreak (T. Günther et al., 2020) has less of an impact in the SSM approach.

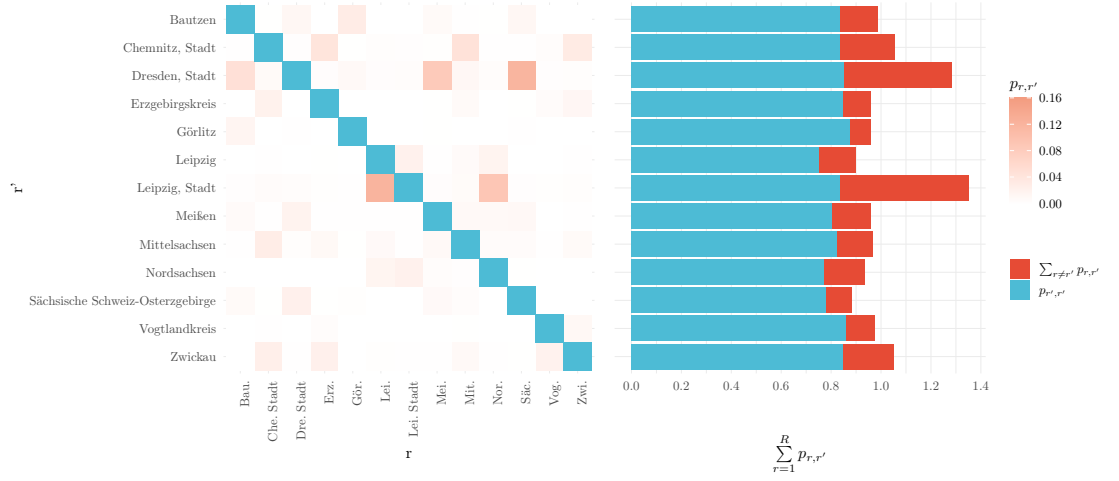

Figure 4.8: We show part of the estimated P for the showcase example for Saxonian counties. On the left-hand side we present $p_{r,r'}$ for r, r' in Saxony. As the diagonal elements are much larger than the off-diagonal ones, we only apply the color gradient to the off-diagonal elements. The right-hand shows the proportion of in-county infections $p_{r',r'}$ (blue bars) and out-of-county infections $\sum_{r \neq r'} p_{r,r'}$ (red bars). For the two big cities, "Leipzig, Stadt" and "Dresden, Stadt", we see a larger influx of cases, compared to the more rural regions, e.g. "Görlitz".

one-week ahead forecasts In the last section we have seen that our regional SSM provides accurate forecasts in a low incidence setting. We now want to investigate if that holds true in higher incidence settings. To that end, we will compare the predictions made by our model to that of some models that participated in the German and Polish COVID-19 ForecastHub (Bracher et al., 2021a; Bracher et al., 2022) and European COVID-19 ForecastHub (Sherratt et al., 2023), collaborative forecasting challenges for COVID-19 cases, deaths and hospitalizations. From 10 October 2020, the German and Polish COVID-19 ForecastHub (German and Polish FCH) gathered weekly real-time forecasts for cases and deaths in Germany and Poland on the national and sub-national level. The participating teams were required to submit their forecast in a standardized format, providing selected quantiles from their predictive distributions. To evaluate the predictive performance of our model, we compare it to three models submitted to the Hub:

- The `baseline` model takes the number of reported cases for this week as next weeks median, and adds uncertainty based on the past behavior of the epidemic.
- The `ensemble` model produces forecasts by averaging all submission to the German and Polish COVID-19 ForecastHub, i.e. for each predictive quantile of one-week ahead cases, its predictive quantile is the average of all submissions for the same day, target and quantile, see (Sherratt et al., 2023) for details.
- The `itww` model makes predictions based on a county-level reproduction number model, with forecasts based on repeated simulations from the renewal equation Equation (2.2). See (Heyder et al., 2022) for details.

We chose to focus on models submitted to the German and Polish FCH instead of the European FCH for two reasons. First, the European FCH uses the JHU COVID-19 data (Dong, H. Du, and Gardner, 2020a) as truth, rather than the RKI data. The German and Polish FCH uses a dataset curated by the ECDC instead, which is closer to the RKI as it is based on the TESSy reports from the RKI. Second, as the German and Polish FCH was explicitly gathering forecasts for Germany (and Poland), we expect the models submitted to it to create more accurate forecasts than the ones submitted to the European FCH.

For the `ensemble` model we use a combination of the `KITCOVIDhub-median-baseline` model, submitted to the German and Polish FCH and the `EuroCOVIDhub-ensemble` model, submitted to the European FCH: Starting with 10 April 2021, the `KITCOVIDhub-median-baseline` only aggregates subnational forecasts, not national ones. Instead the `EuroCOVIDhub-ensemble` is used in the German and Polish FCH from that date on, and so we do the same. The switch is indicated in Figure 4.9 by a vertical line.

To obtain the predictions for the `ssm` model, we aim at replicating the setup of the ForecastHubs as closely as possible. While the Hubs were active, forecasts could be submitted each Monday to predict the number of newly reported cases between the last Saturday and the next. For each forecast — e.g. the first made for 17 October 2020 — we use as observations the number of weekly reported cases that were available the Monday before — e.g. on 12 October 2020 — as reported by the RKI on that day. Of those, we use the last 9 weeks of weekly reported cases as observations and mark the last observation, that for the date to be forecasted, as missing.

To fit the model, we use an abbreviated fitting and prediction procedure: we use only the initial guess of the parameter, $\hat{\theta}_0$ (Section 3.6.1) which is obtained by at most 10 iterations of a gradient descent procedure. Using this parameter, we obtain the LA (Algorithm 5) of the posterior distribution and produce forecasts of the last, missing observation by using 1000 samples from the LA, using the approach detailed in Section 3.6.2. The whole procedure can run in approximately 10 minutes for a single forecast on a consumer grade Macbook Air M3 with 16GB of RAM.

To evaluate the quality of the forecasts, we use a the true value the RKI used throughout this thesis, i.e. the dataset published on 5 May 2023, see Section 2.3.1.

We show median, 50% and 95% prediction intervals of all four models in Figure 4.9. For the `baseline` model, we see that carrying forward the last observation results in over- or underpredctions in times of decline or growth. The `ensemble` model provides prediction intervals of medium size, and has

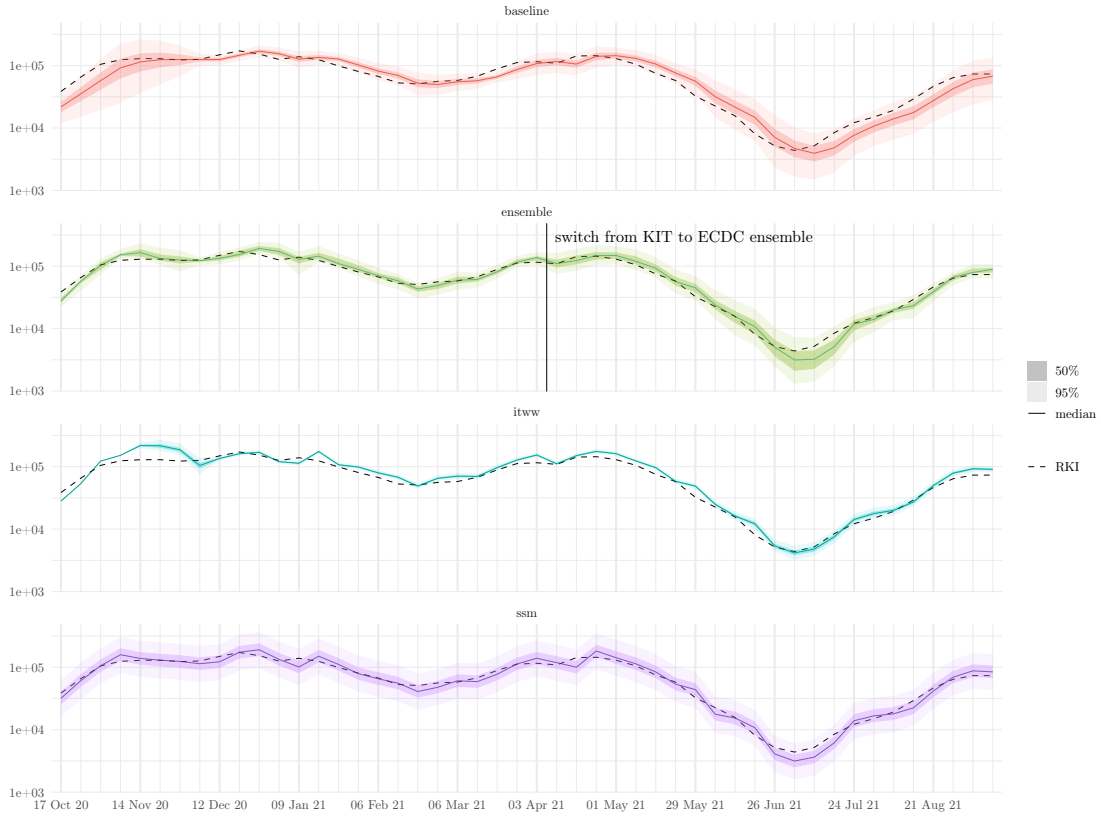

Figure 4.9: Comparison of the 67 one-week ahead forecasts (showing median, 50% and 95% prediction intervals) produced by four different model: three from the ForecastHubs (`baseline`, `ensemble`, `itww`) and our novel `ssm` approach. Note the log-scale of the y-axis. The minor and major x-axis gridlines correspond to the forecasting dates. For the `ssm` approach, each forecast is obtained by a single run of the model, with the observations to be forecasts missing. The true reported cases after one week are indicated by a dashed line. Notice the log-scale of the y-axis. While the prediction intervals provided by the `baseline` and `itww` models occasionally miss the true reported cases, the `ensemble` and `ssm` approach provides more adequate coverage, see also Table 4.4 for a quantitative comparison of the four approaches.

metric	baseline	ensemble	itww	ssm
MAE	14,654.00	9,750.84	16,531.37	10,149.94
WIS	8,707.22	5,595.53	12,708.90	6,795.43
WIS components				
sharpness	3,023.82	2,459.09	890.01	5,074.88
underprediction	3,239.05	776.09	1,293.94	832.67
overprediction	1,753.83	1,934.32	9,789.56	448.63
rescaled MAE	690.52	426.03	735.40	439.25
coverage				
coverage 50% PI [%]	37.50	43.75	18.75	75.00
coverage 95% PI [%]	91.67	91.67	41.67	100.00
relative to baseline				
MAE	1.00	0.67	1.13	0.69
WIS	1.00	0.64	1.46	0.78

Table 4.4: Quantitative comparison of the four approaches to one-week ahead forecasts. All metrics are averaged across the 67 one-week ahead forecasts made by each model. To be consistent with the weighted interval score (WIS) we use the median as the point forecast for the mean absolute error (MAE). For the WIS we show additional the decomposition into four components and the relative performance, when compared to the `baseline`, of the `ensemble`, `itww` and `ssm`.

close to nominal coverage (see Table 4.4). The `itww` model has very narrow prediction intervals, which often miss the true reported cases completely, resulting in overall bad performance. Our novel `ssm` approach has much wider prediction intervals, but also provides quite precise point predictions.

To make the comparison more rigorous, we evaluate the predictions made by the four models by several forecasting performance metrics, as shown in Table 4.4. We use three different metrics:

- the mean absolute error, where we take the median of the predictive distribution as a point forecast and average the absolute error between this point forecast and the RKI truth over all 67 observations,
- the weighted interval score(Bracher et al., 2021b), a proper scoring rule which approximates the continuous ranked probability score. It takes into account the whole predictive distribution, i.e. the centered prediction intervals provided in the forecasts. Lower values of WIS are better, and WIS can be decomposed into components measuring over- and underprediction as well as sharpness (length of predictive intervals). Finally, we also report
- the empirical coverage of 50% and 95% prediction intervals.

Additionally, we report the decomposition of the WIS into its four components and the MAE and WIS relative to the baseline model, to quickly identify which of the three other models outperforms the baseline model.

For the MAE, we see that the `ensemble` model obtains the best performance, followed closely by the `ssm` model, then the `baseline` model and finally, worse than the `baseline`, the `itww` model. While the MAE is dominated by the errors in periods of high incidence, we follow the argument of (Bracher et al., 2021b, Section 5), which encourages the use of the MAE over relative performance measures, such as the mean absolute percentage error (MAPE), as using the MAE as a performance metric incentivizes models to report predictive medians. Additionally, the MAE is one of the components in the decomposition of the WIS, making the two metrics compatible with one another.

For the WIS, we observe a similar ranking as for the MAE, with a slight difference: the `ensemble` model performs better relative to the baseline for WIS and the `ssm` model performs slightly worse. However, such comparisons should be treated carefully, as none of the measures reported here come with uncertainties attached and are based on only 67 forecasts.

As for the decomposition of the WIS into its four components, we see that for all models, except

the `itww` model, substantial contributions come from the sharpness component, which penalizes large prediction intervals. For the `ssm` model, it is by far the largest component of the WIS, while for the `baseline` model underprediction (due to the long increase at the end of the forecasting period) and for the `ensemble` model overprediction are on a comparable level. The `itww` model has a high WIS largely due to overprediction and, to lesser extent, underprediction.

For the empirical coverage of the prediction intervals, we observe similiar results: the best calibration of the 50% and 95% prediction intervals is achieved by the `ensemble` model, while the `baseline` model prodcues too narrow 50% prediction intervals. The `itww` model produces too narrow forecasts, and the `ssm` model too wide ones.

From this comparison we can speculate that the `ssm` model would benefit from slight rescaling of the prediction intervals, while the `itww` model could benefit from larger prediction intervals.

As expected, the `ensemble` model outperforms all models — this is consistent with the results from almost all such forecasting hubs, e.g. (Bracher et al., 2021a; Bracher and Wolffram, 2021; Bracher et al., 2022; Ray et al., 2020; Sherratt et al., 2022; Wolffram et al., 2023). However, the `ssm` model is a close second, except for its somewhat large uncertainty intervals. In this analysis it should be mentioned that the model is in no way calibrated to perform accurate forecasts, i.e. we did not perform model selection (e.g. by Akaike's Information Criterion) or include predictive performance in the parameter fitting procedure.

4.2.3 Discussion

consider Armbruster2024Networkbased, Armillotta2023Inference

4.3 Nowcasting hospitalizations

Judging the severity of the COVID-19 epidemic has been an ongoing challenge since its inception. As immunization against COVID-19 rose, strict enforcement of social distancing rules eased and testing regimes became less strict, case incidences became a less reliable and harder to interpret indicator of epidemic severity. Instead, more direct indicators of morbidity, such as the number of deaths and ICU admissions and occupancy have come to the fore. But these indicators are late due to the substantial delays between infection and occurrence. An alternative indicator that captures the morbidity caused by COVID-19, but is earlier than the others, is the number of hospitalizations of positive COVID-19 cases.

While hospitalizations occur earlier, they still come with substantial delay between the infection and subsequent admission to hospital. Additional difficulties arise due to delays in reporting, i.e. the time it takes until the hospital reports the new case to the national health authorities. The problem of accounting for delays in reporting for occurred, but not yet reported events has been termed **nowcasting**, i.e. forecasting of the indicator at time "now". Predicting the number of hospitalizations is thus a mixture of both forecasting — which reported COVID-19 cases will end up in the hospital — and nowcasting — which cases have yet to be reported — and we will use the term nowcasting in this section to mean this predictive mixture. We focus on the situation in Germany where data on hospitalizations has been available since April 2021 provided by the German federal health care authority, the Robert Koch-Institut (RKI), via Github (Robert Koch-Institut, 2021). Recall from Section 2.3.2 that the hospitalization incidence is reported on a daily basis and consists of weekly rolling sums of hospitalizations. For each day, it counts the hospitalizations with associated reporting dates of COVID-19 infections occurring in the week prior of that day.

In the period from November 2021 to March 2024, the German COVID-19 NowcastHub (Wolffram et al., 2023) has gathered daily submissions of nowcasts of the German hospitalization incidence from eight different research groups, using a variety of nowcasting approaches. The submissions are aggregated into different ensemble models which provides more accurate nowcasts than any individual model. Together with his supervisor Thomas Hotz, the author of this thesis has contributed the "ILM-prop" model, which is based on a regression on the number of reported cases available at the time of nowcast, as well as uncertainty quantification based on past model performance.

In this section, we will extend the ILM-prop model by designing a SSM that captures the main ideas present in that model, but provides prediction intervals based on the SSM, rather than past model performance as the ILM-prop model does (see below for details on the model setup). This allows the model to adapt to changing circumstances faster and comes with the usual benefits of interpretability of SSMs. Before we discuss our approach in more detail, let us provide some context for nowcasting in general.

The origin of nowcasting lie in accounting for incurred, but not reported claims in the actuarial sciences (Kaminsky, 1987), delays in reporting for AIDS (Lawless, 1994; Zeger, See, and Diggle, 1989) and other infectious diseases (Farrington et al., 1996). Popular statistical approaches include methods from survival analysis (Lawless, 1994) and generalized linear regression (Zeger, See, and Diggle, 1989). In the survival analysis setting one commonly models the reverse time discrete hazard parametrically and assumes multinomial sampling of the final number of cases, potentially accounting for overdispersion. Such models have been applied in frequentist (Midthune et al., 2005) and Bayesian (An Der Heiden and Hamouda, 2020; Höhle and An Der Heiden, 2014) settings. The generalized linear regression approach has origins in the chain ladder model from actuarial sciences (Renshaw and Verrall, 1998) and models the observed counts in the reporting triangle by a Poisson or negative binomial distribution. For both approaches, available covariates can be incorporated in a straightforward way. In the setting of real-time nowcasting, it is often beneficial to incorporate epidemic dynamics into the model, this can be achieved by splines (Höhle and An Der Heiden, 2014; van de Kassteele et al., 2019) or by a latent process of infections (McGough et al., 2020).

Nowcasting methods have wide application in accounting for reporting delays (Midthune et al., 2005), early outbreak detection (Bastos et al., 2019; Salmon et al., 2015), and, in the recent COVID-19 epidemic, improving real-time monitoring of epidemic outbreaks (Akhmetzhanov, 2021; An Der Heiden and Hamouda, 2020; F. Günther et al., 2021; Schneble et al., 2021). Evaluating a forecasting model in a real-time public health setting is advantageous as it avoid hindsight bias (Desai et al., 2019), however nowcasting approach may have difficulties with bias and properly calibrated uncertainty if used in a real-time setting. This includes rapidly changing dynamics (F. Günther et al., 2021; van de Kassteele et al., 2019), both of the delay distribution and the underlying epidemic, retrospective changes in data (Midthune et al., 2005) and long delays with few observed cases (Noufaily et al., 2015).

To avoid the aforementioned hindsight bias one can make their predictions publicly available in real-time (Bracher et al., 2021a; Ray et al., 2020). For the hospitalizations in Germany, we have participated in the German COVID-19 NowcastHub (*Nowcasts Der COVID-19 Hospitalisierungsinzidenz* 2022) since November 2021 where nowcasts are available in a public Github repository (*Hospitalization Nowcast Hub* 2022) with the "ILM-prop" model. The ideas, especially the model and the "double-weekday effect", discussed this section are based on this model. However, the "ILM-prop" model is based on simple point estimates for the proportion of hospitalizations per reported case, neglecting regularization over time. In this thesis we extend this model to the SSM setting of this thesis and investigate if the increased model complexity results in improved performance. In particular, we want to reduce computation time, as the previous model quantified uncertainty by past model performance, which requires running the model many times. If prediction uncertainty is based on predicting future observations in a SSM, we can reduce computation time drastically. However, this is only worthwhile, if the predictive performance is comparable to the computationally more intensive model.

To predict the number of hospitalizations we consider the reporting process of both reported COVID-19 cases and reported hospitalizations. Recall that the reporting date of a COVID-19 case is shared for both the case and its hospitalization, i.e. the case and hospitalization are linked through this date.

As hospitalizations are only available as 7-day rolling sums, we use 7-day rolling sums for daily reported incidences as well. To avoid dealing with the double weekday effect of both reporting date of the case and reporting date of the hospitalization (see Figure 2.5) we divide the future hospitalizations we wish to predict into chunks of one week, which gets rid of the weekday effect for the hospitalizations, see the next section for details. Our prediction of each of these weekly chunks

then consists of the fraction of hospitalizations of reported cases in the past.

We use the publicly available data from the RKI discussed in Section 2.3 on daily reported COVID-19 cases (Robert Koch-Institut, 2024c) and weekly reported hospitalizations (Robert Koch-Institut, 2024a). Both datasets are available on a daily basis.

Recall from Section 2.3 that COVID-19 cases are described by their date of reporting, and are subject to reporting delay and hospitalizations are reported by the *reporting date of the associated case*, and are subject to delay as well. As the date of symptom onset is not known for a substantial amount of incident cases, and is not reported for hospitalized cases, we focus our analysis on the date of reporting.

4.3.1 Model

In line with the structure of the data, we let $H^a_{t,t+\tau}$ be the number of weekly hospitalizations in age group a with case reporting date $t-1,\dots,t-7$ that are known on the day $t+\tau$, aggregated over all states. We suppress the dependence on age group in the following for ease of notation, keeping in mind that we only model a single age group within each model, ending up with seven models (including one for the "all ages" aggregate age group).

As we focus on same-day nowcasting, our goal is to predict on day t $H_{t,t+D}$ the number of hospitalizations reported D days into the future, for simplicity assume that the maximal delay considered, D, is a multiple of 7. We decompose this target into a weekly telescoping sum

$$H_{t,t+D} = H_{t,t} + \sum_{k=1}^{D/7} (H_{t,t+7k} - H_{t,t+7(k-1)}),$$

where $H_{t,t}$ is already known on day t and $H_{t,t+7k} - H_{t,t+7(k-1)}$ is the increment in the hospitalization incidence from the $(k-1)$-st week to the k-th week. Recalling that any case attached to the hospitalization incidence on this date has case reporting date t we now crucially assume that the hospitalization reporting process consists of two independent events: hospitalization and its delayed reporting. More formally, let I^7_t be the seven-day case incidence (again, modeled separately for every age group) on day t, defined in the same fashion as the hospitalization incidence. Thus,

$$I^7_t = \sum_{\tau=1}^{7} I_{t-\tau,t}$$

where for $\tau = 1,\dots,7$ $I^7_{t-\tau,t}$ is the number of cases with reporting date $t-\tau$ known on date t. Note that, similar to the hospitalization incidence, I^7_t does not contain cases with reporting date t, but rather cases with reporting dates $t-1,\dots,t-7$. While cases are also affected by reporting delays, these delays are on the order of days, rather than weeks, cf. Figure 2.3, and averaging over the past week means that I^7_t is subject to only minor, negligible, reporting delays. We thus model

$$H_{t,t+7k} - H_{t,t+7(k-1)} | I^7_t, p_{t,k} \sim \text{Poisson}\left(\lambda_{t,k}\right) \qquad \lambda_{t,k} = I^7_t p_{t,k}, \tag{4.4}$$

conditionally independent for all t and k. Here $p_{t,k}$ is the proportion of reported cases I^7_t that will become hospitalized after k weeks. For simplicity of notation, let $H_{t,t-7} = 0$, so that $H_{t,t} - H_{t,t-7} = H_{t,t}$ has conditional rate $\lambda_{t,0} = I^7_t p_{t,0}$.

Figure 4.10 displays the empirical delay probabilities $\hat{p}_{t,k} = \frac{H_{t,t+7k} - H_{t,t+7(k-1)}}{I^7_t}$ for the period of the NowcastHub for $k = 0, 1, 2, 3$.

Ignoring noisy day-to-day variation, we see that within an age group, the delay probabilities evolve roughly in parallel (on the log-scale). This encourages us split the delayed hospitalization probabilities $p_{t,k}$ for all t and k into two parts

$$p_{t,k} = p_t q_{t,k}$$

where p_t is the time-varying proportion of hospitalization and $q_{t,0},\dots,q_{t,\frac{D}{7}}$ comprise the delay distribution. To make this identifiable we impose that $\sum_{k=0}^{\frac{D}{7}} q_{t,k} = 1$. Figure 4.10 implies that the

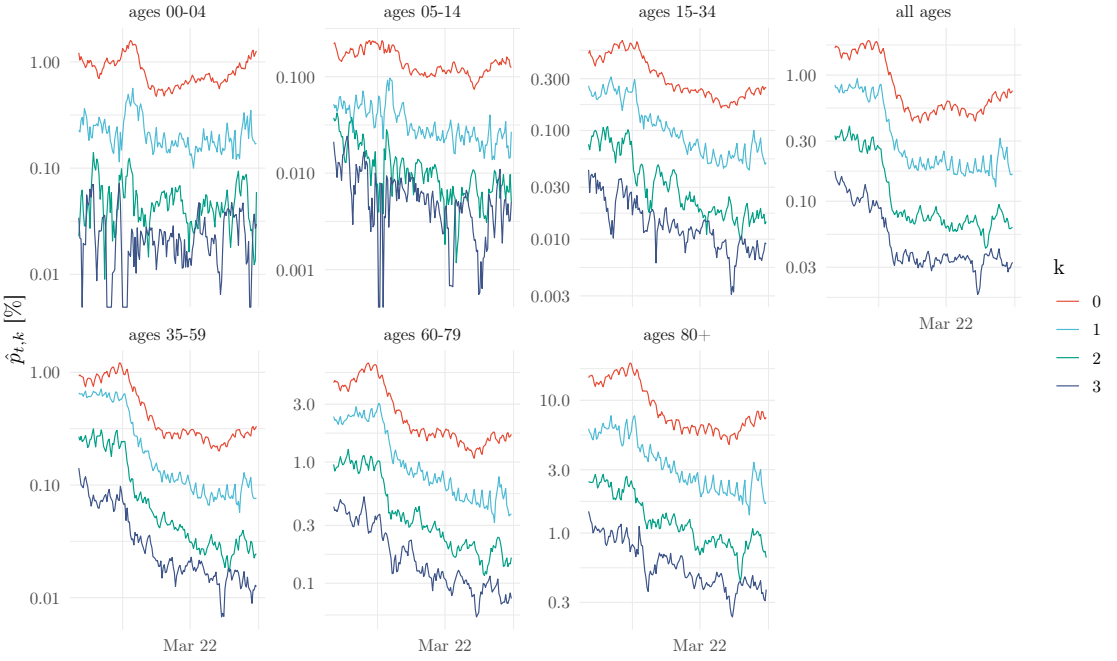

Figure 4.10: Empirical hospitalization probabilities $\hat{p}_{t,k}$ by date t and delay k for the NowcastHub period. The probabilities are given in percent. Note the different scales of the logged y-axes across different age groups. Zeroes are indicated by data points at the bottom of the y-axis, e.g. for age group 00-04.

delay probabilities evolve rather smoothly, so we let the log-probabilities $\log p_t$ perform a second order random walk, i.e. we model

$$\begin{aligned} \log p_{t+1} &= \log p_t + v_t \\ v_{t+1} &= v_t + \varepsilon_{t+1,v}. \end{aligned}$$

For the delay distribution, we first reparameterize to consecutive conditional probabilities

$$q^c_{t,k} = \frac{q_{t,k}}{1 - \sum_{l=1}^{k-1} q_{t,l}},$$

i.e. $q^c_{t,k}$ is the probability of a delay of exactly k weeks, conditional on having at least k weeks of delay. This reparameterization is a diffeomorphism from the open simplex $\left\{ p \in \mathbf{R}^{D/7+1}_{>0} \middle| \|p\|_1 = 1 \right\}$ to $(0,1)^{D/7} \times \{1\}$ which has the advantage that $q_{t,k}$ only depends on $q^c_{t,l}$ for $l \leq k$ (rather than all of them, as was the case for the model in Section 4.1). We then model the logits of these reparameterized delay probabilities to perform independent random walks

$$\operatorname{logit} q^c_{t+1,k} = \operatorname{logit} q^c_{t,k} + \varepsilon_{t+1,q,k}$$

for $\varepsilon_{t+1,q,k} \sim \mathcal{N}(0, \sigma_q^2)$.

From Figure 4.10 we additionally observe a weekday effect, at least for small k. Thus, we additionally add two multiplicative weekday effects for q^c_0 and q^c_1, i.e. we modify (4.4) to be

$$\lambda_{t,k} = I_t p_t q_{t,k} W_{t,k} \qquad \text{for } k = 0, 1, \tag{4.5}$$

where $W_{t,0}$ and $W_{t,1}$ are two independent, multiplicative weekday effects as for the model in Section 4.1. The choice of having two weekday effects here is based on balancing the dimension of the model, and thus the computational resources required to run inferences and predictions,

with its explainability and is based on numerical experiments. A more rigorous analysis, e.g. using information criteria, could be run as well, but is outside the scope of this thesis.

We assume that the innovations

$$\begin{aligned}\varepsilon_{t+1} &= \left(\varepsilon_{t+1,v}, \varepsilon_{t+1,q,0}, \ldots, \varepsilon_{t+1,q,D/k-1}, \varepsilon_{t+1,W,0}, \varepsilon_{t+1,W,1}\right) \\ \operatorname{Cov}\left(\varepsilon_{t+1}\right) &= \Sigma_{t+1} = \operatorname{diag}\left(\sigma_p^2, \sigma_q^2, \ldots, \sigma_q^2, \sigma_W^2, \sigma_W^2\right)\end{aligned}$$

are centered, independent across all t and Gaussian.

These considerations lead to a PGSSM with linear signal: Let the states and signals be given by

$$\begin{aligned}X_t &= \left(\log p_t, \operatorname{logit} q_{t,0}, \ldots, \operatorname{logit} q_{t,D/7}, \log W_{t,0}, \ldots, \log W_{t-5,0}, \log W_{t,1}, \ldots, \log W_{t-5,1}\right)^T \\ S_t &= \begin{pmatrix} e_1 & \mathbf{0}_p & e_2 & \ldots & e_p & e_2 & \mathbf{0}_{p\times 5} & e_3 & \mathbf{0}_{p\times 5}\end{pmatrix} X_t \\ &= \left(\log p_t, \operatorname{logit} q_{t,0} + \log W_{t,0}, \operatorname{logit} q_{t,1} + \log W_{t,1}, \operatorname{logit} q_{t,2}, \ldots, \operatorname{logit} q_{t,\frac{D}{7}-1}\right)^T\end{aligned}$$

and let the observations be

$$Y_t = \left(H_{t,t}, H_{t,t+7} - H_{t,t}, \ldots, H_{t,t+D} - H_{t,t+D-7}\right)^T$$

with conditional distribution given by Equation (4.4) where $\lambda_{t,k}$ is given by Equation (4.5).

For the initial distribution of use $X_0 \sim \mathcal{N}(\mathbb{E}X_0, \Sigma_0)$ where

$$\mathbb{E}X_0 = \begin{pmatrix} \log p_0 \\ 0 \\ \ldots \\ 0 \end{pmatrix}$$

and $\Sigma_0 = \sigma_0^2 I$ is a multiple of the identity matrix. We chose these initial conditions as they only introduce two further unknown parameters, making them amenable to maximum likelihood estimation. Of course specifying the same (large) variance σ_0^2 for all states may simultaneously over- and under-estimate the initial variance in some components. As an alternative, one could implement the diffuse initialization of the Kalman filter, see (Ansley and Kohn, 1985; Koopman, 1997).

The model is parameterized by

$$\theta = \left(\log \sigma_p^2, \log \sigma_q^2, \log \sigma_W^2, \log \sigma_0^2, \log p_0\right)$$

which we estimate by MLE.

To fit the model for all age groups, we use at most 100 iterations for all occurences of the LA, with a convergence threshold set to 10^{-5} relative difference in z and Ω. We use the same method for EIS, where we additionally use $1,000$ samples to determine the optimal proposal, starting with the proposal given by th LA.

For MLE, we use $1,000$ samples to determine the maximum likelihood estimate of the parameters, initializing at the initial guess given by Section 3.6.1. To obtain prediction intervals of the states, signals and missing observations we use $10,000$ samples. To estimate the ESS we use $10,000$ samples. Note that all sample sizes are given before constructing the three antithetic variables.

4.3.2 Results

To demonstrate the capabilities of our model, we fit it the analysis period of the NowcastHub, i.e. to the period from 22nd November 2021 to 29th April 2022 (Wolffram et al., 2023). We do this for each of the seven age groups, including all age-groups together, the 00+ age group. For each of these age groups, we fit the model as described in last subsection.

In the original NowcastHub the truth against which nowcasts were to be evaluated was set to the data available 100 days after the last date of the study period, 8th August 2022, under the

Age group	EF [%]	weeks of delay
A00-04	15	5
A05-14	7	5
A15-34	4	7
A35-59	48	7
A60-79	93	8
A80+	98	8
A00+	97	8

Table 4.5: Efficiency factors (in %) and weeks of delay for the seven models (one per age group) presented in this section. For younger age groups, there are few long delays, which causes numerical instabilities due to the consecutive conditional probability parametrization chosen in this section. For each of the age groups, we chose the longest delays that still allowed for a reasonable fit, with a maximum delay of 8 weeks. While the efficiency factor for A15-34 is quite low, we use a large enough number of samples for the prediction of states and signals, so the ESS is still sufficiently large.

assumptions that there would be no late reporting after such a long period. However, it turns out that the hospitalization incidence is still subject to relevant data revisions long after the date of reporting of the COVID-19 case has passed see (Wolffram et al., 2023, Section 3.7). Thus, we choose to focus on a delay of 42 days (6 weeks), similar to the time horizon of 40 days proposed as an alternative target in the same section in that work.

For the younger age groups, long delays are rare (see also Figure 4.10), which leads to numerical instabilities in the consecutive logit parametrization. If such numerical instabilities occur, we manually choose the maximum delay (in weeks) that still produces a reasonable model fit, which we define here as an EF above 2.5%. We show the resulting weeks of delay and EF in Table 4.5. The resulting posterior distributions of interest are displayed in Figure 4.11.

We see that, generally, hospitalization probabilities p_t grow larger as the age group under consideration becomes older; note the logarithmic y-axis. The exception here is the youngest age group A00-04. While infants are vulnerable to COVID-19 (Havers et al., 2024), this may also be explained by circumstantial testing in hospitals: children in age group A05-14 were largely subjected to mandatory testing at school, so we would expect the darkfigure of unreported cases in age group A00-04 to be large compared to the older age groups. Let us stress that interpretations of our results are contingent on taking the considerations from Section 2.3 into account. Nevertheless, we see p_t drop in all age groups, except A00-A04, over the period considered. This is consistent with the rise of the Omicron variant of SARS-CoV-2 (Robert Koch-Institut, 2024e) which is associated with milder progression of disease.

We also observe a pronounced weekday effect $W_{t,0}$ across all age groups, with a smaller proportion of I_t^7 reported as hospitalized already on day t if t is a Sunday, as indicated by the vertical grid lines in Figure 4.11. To compensate, $W_{t,1}$ is large when $W_{t,0}$ is small. Again, A00-04 exhibits a more pronounced weekday effect, but the general pattern is consistent across all age groups. On the right-hand side of Figure 4.11 we see the delay probabilities $q_{t,k}$ for $k = 0, \dots, 3$, as well as the average delay (in weeks)

$$\bar{\tau}_t = \sum_{k=0}^{\frac{D}{7}} k q_{t,k},$$

for all age groups. We can observe that starting in the middle of December 2021 the delays got (on average) shorter, only to rise again in the middle of January.

Real-time nowcasting of hospitalization incidences To evaluate the predictive capabilities of our model, we use it to perform retrospective nowcasting of hospitalizations, emulating the setting of the German NowcastHub. We focus on same-day nowcasting, i.e. only nowcasting for

Figure 4.11: For each of the seven age groups (indicated by color and linetype), we show means of the smoothing distribution for the first four delay probabilities $q_{t,k}$, $k = 0, \ldots, 3$, the smoothed probabilities of hospitalization p_t and the two weekday effects $W_{t,0}, W_{t,1}$. Recall that we fit a separate model for each age group. For the smoothed delay probabilities, we additionally show 95% prediction intervals. Note the log-scale of the y-axis for the smoothed delay probabilities.

the current day, with a maximum delay of 6 weeks, performing all predictions for every age group separately. Let us call this model `SSM` in the remainder of this section.

For every day, s say, in the period of 22nd November 2021 to 29th April 2022 we fit the model to the data of the past 100 days that were available on day s. Thus, the observations of the model consist of y_t for $s - 100 < t \leq s$, but as

$$y_t = (H_{t,t}, H_{t,t+7} - H_{t,t}, \ldots, H_{t,t+D} - H_{t,t+D-7}),$$

the k-th component of y_t is missing whenever $t + 7(k-1) > s$. Taking the last day, s, as an example $H_{s,s}$ is made available to the model, but $H_{s,s+7k}$ for $k > 0$ is not, and so $y_s = (H_{s,s}, \mathbf{NA}, \ldots, \mathbf{NA})$ where $\mathbf{NA}$ indicates missing observations. Similarly, the last observation for which the second component is available is $y_{s-7} = (H_{s-7,s-7}, H_{s-7,s} - H_{s-7,s-7}, \mathbf{NA}, \ldots, \mathbf{NA})$ and so on.

Similar to the other models in this thesis, we can include these missing observations in a straightforward manner, by setting the corresponding rows of B_t to 0, setting the same entries of s_t to $-\infty$, such that $\lambda_{t,k} = 0$, and replacing missing observations by 0. For the approximating GLSSMs, we fix the rows and columns of Ω_t and entries of z_t that correspond to missing signals s_t to 0. To make fitting the 158 resulting models computationally feasible, we omit the MLE step and fit the model using only the initial value from Section 3.6.1.

To nowcast the total number of hospitalizations, we use the method described in Section 3.6.2, i.e. using MC-integration to estimate quantiles of $H_{s,D}$. Accordingly, we draw N samples from the smoothing distribution $S_s^i | Z = z$ with weights W^i and, conditional on these samples, $\tilde{Y}_s^i | S_s^i \sim \text{Poisson}\left(\exp S_s^i\right)$, independent of everything else, where we fix the first component be the known $y_{s,1} = H_{s,s}$. In total, we obtain N draws $H_{s,D}^i = H_{s,s} + \sum_{k=1}^{D/7} \tilde{Y}_{s,k}^i$ with associated weights W^i from which we can estimate the desired quantiles. We use the same quantiles as in the NowcastHub, i.e. the $2.5\%, 10\%, 25\%, 50\%, 75\%, 90\%, 97.5\%$ quantiles.

To assess the predictive performance of our model, we compare its predictions to the `ILM-prop42` and the revised ensemble model, `MeanEnsemble` tailored to a maximum delay of 40 days from (Wolffram et al., 2023, Section 3.7).

The main idea of the `ILM-prop42` model is similar to the rationale for the `SSM` model: The fraction of hospitalized cases should vary slowly over time, so that one can estimate these fractions from available data. However, the `ILM-prop42` model is not based on an underlying SSM, but rather estimates the fraction of hospitalized cases by

$$\widehat{p_{t,k}} = \frac{H_{t-7k,7k} - H_{t-7k,7\cdot(k-1)}}{I_{t-7k}} = p_{t-7k,k}$$

for $k = 1, \ldots, K$ and predicts using

$$\widehat{H_{t,D}} = H_{t,t} + (\widehat{p_{t,1}} + \cdots + \widehat{p_{t,K}})\, I_t.$$

Thus, $\widehat{p_{t,k}}$ depends on data that are associated with infections k weeks ago, which makes the model slow to react to fast changes. Prediction intervals are constructed by fitting a log-normal distribution to past predictions of the model, and so the uncertainty is based on past model performance.

The `MeanEnsemble` model is constructed from all submissions to the NowcastHub. Its point predictions and prediction intervals are based on averaging across all models that submitted a valid nowcast on that day — see (Wolffram et al., 2023) for details.

We present the resulting 95% prediction intervals for all three models in Figure 4.12. Here we can see that all three models provide reasonable forecasts with mostly adequate prediction intervals. Two period of time stand out: The period from January 2022 to February 2022 and late April 2022. In the first period, the ILM-prop42 model overpredicts the 7-day hospitalizations by a large margin, with comparatively small uncertainty intervals. As the uncertainty intervals are based on past performance, the model catches up eventually in the middle of February (after 6 weeks). This could be due to the Omicron variant that became the dominant variant in January / February 2022. It is more infectious than the previously dominant Delta variant, but causes less severe outcomes.

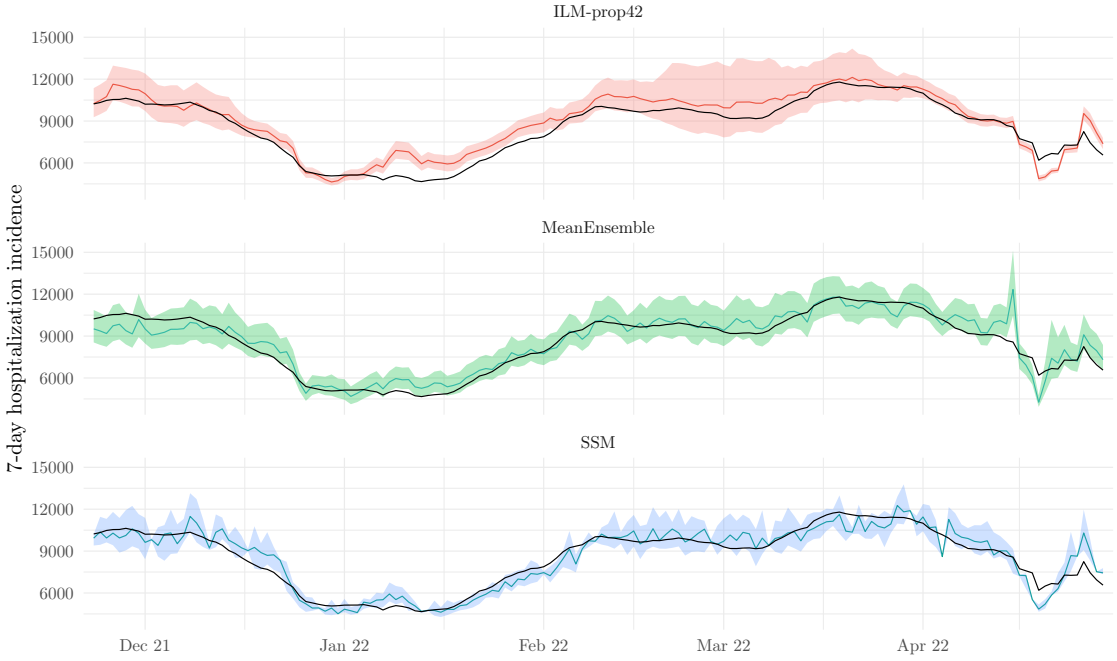

Figure 4.12: 95% prediction intervals for the three nowcasting models. The true hospitalization count, as reported after 6 weeks, is marked in all subfigures by a solid black line.

This is problematic for the `ILM-prop42` model, as it takes 6 weeks to catch up to this new baseline. For late April, we see that around the Easter weekend (April 15th - April 18th) all models have difficulties nowcasting the final number of cases. On these public holidays reporting of cases (and thus hospitalizations) was performed late, which causes problems for all three models.

For each model, we additionally quantify the nowcasting performance by the mean absolute error, the empirical coverage of the 50% and 95% prediction intervals and the weighted interval score (WIS) (Bracher et al., 2021b), a score that approximates the continuous ranked probability score. Lower values of WIS are better, and WIS can be decomposed into components measuring over- and underprediction as well as sharpness (length of predictive intervals). These performance metrics are displayed in Section 4.3.2.

In this table we see that the `MeanEnsemble` model outperforms all other models in most aspects,

	ILM-prop42	MeanEnsemble	SSM
Mean Absolute Error	589.3	**502.9**	526.4
Coverage 95% PI [%]	69.0	**86.7**	67.7
Coverage 50% PI [%]	42.4	**46.2**	29.1
WIS	377.6	**282.7**	352.1
WIS components			
Sharpness	101.4	110.2	**75.3**
Underprediction	**33.9**	40.5	100.5
Overprediction	162.5	**61.6**	97.0

Table 4.6: Average nowcasting performance metrics of the three models for hospitalization. The weighted interval score (WIS) is additionally decomposed into sharpness and under/over-prediction (see (Bracher et al., 2021b) and (Wolffram et al., 2023, Section 2.5) for details). For each metric, the best value has been highlighted by boldface.

with an exception for the sharpness — the `SSM` model has smaller prediction intervals — and the underprediction component — the `ILM-prop42` overpredicts, especially between January 2022 to March 2022. However, the interesting comparison is between the `ILM-prop42` and `SSM` model, as we expect the ensemble model to outperform any single model.

Comparing these two models, we see that the `SSM` performs better than the `ILM-prop42` model in most metrics. The mean absolute error over the period considered is smaller and closer to the ensemble. The WIS is smaller as well, but, taking the ensemble as a baseline, the difference is not as striking as for the mean absolute error. However, the coverage metrics of the `SSM` are worse than those of `ILM-prop42` and `SSM` produces smaller prediction intervals overall, making it overconfident. In total, the `SSM` model tends to produce better point forecasts, but `ILM-prop42` is better calibrated — which is sensible, as its prediction intervals are informed by past performance of the model. This explains why the WIS for `SSM` is only slightly smaller than that of `ILM-prop42`.

4.3.3 Discussion

Before we start a discussion on the performance, advantages and disadvantages of our model, let begin with a discussion of the indicator we are aiming to nowcast. Let us stress that its value on a given date does not represent the current occupancy of hospitals in Germany with COVID-19 patients but is rather an approximation to the morbidity caused by COVID-19 on that date. The reason for this discrepancy is that hospitalizations are attributed to the reporting date of the associated case, not that of hospitalization. While the reporting date of the hospitalization can be recovered from the publicly available data, the date of hospitalization cannot. Additionally, no information on the duration of stay is available, making it impossible to create an indicator for the occupancy of hospitals based solely on data provided by the RKI. Nevertheless, the indicator was used to decide on which countermeasures to implement, so it still seems worthwhile to nowcast it, or similar indicators in the future.

The SSM introduced in this section offers several distinct advantages for retrospective analysis of hospitalization incidence. First, the model is highly interpretable, as each component corresponds directly to epidemiologically meaningful quantities such as the probability of hospitalization, the delay distribution, and the weekday effects. Second, the flexible structure of the SSM allows for straightforward incorporation — or leaving out, as shown for the real-time nowcasting — of weekday effects, which is essential for accurately capturing reporting patterns observed in the data. Third, the computational efficiency of the model is notable: fitting and generating predictions typically requires only a few minutes for a single day of nowcasts, making it practical for large-scale retrospective studies. A minor drawback is that some manual tuning of initial states and hyperparameters is required to ensure robust model performance, but this is manageable given the overall transparency and speed

Compared to the `ILM-prop42` model, the `SSM` reacts more quickly to sudden changes in the underlying dynamics, as seen during the Omicron wave in early 2022. The computational cost of the SSM remains negligible, even with increased model complexity. However, the need for parameter fitting introduces the possibility of instability or suboptimal choices, which requires careful attention. A potential avenue for further improvement would be to combine the point forecasts from the SSM with the prediction interval strategy employed in the ILM-prop, to combine the strengths of both models.

Compared to other approaches in the COVID-19 NowcastHub, that tended to exclusively focus on modeling the delay distribution with parametric and non-parametric models, our `SSM` model, similar to the `ILM-prop42` model, sidesteps this complex delay structure by decomposing delayed hospitalizations into weekly chunks and incorporating case data. As cases and hospitalizations are explicitly linked by the case reporting date we forecast the number of hospitalizations in each chunk based on the current incidences and past fractions of hospitalizations in a comparable weekly chunk.

The comparison of the three models in the previous section is not completely free of bias. After all, the `SSM` model was created and fit retrospectively, while both the `ILM-prop42` and `MeanEnsemble` models were created in a live setting under preregistration, which makes the nowcasts more honest.

Chapter 5

Discussion

Let us look back on the insights gained in this thesis and put the theoretical and applied results into a broader picture. To this end, let us give answers to the questions raised in Chapter 1 and see how far we have come. First, let us reiterate the ambitious goal of this thesis detailed in the introduction: provide mathematically sound statistical tools that allow practitioners to design and fit models suited for the epidemiological data arising in an ongoing epidemic. To this end we have contributed results to three areas, from more applied to more abstract:

- the results of concrete models applied to COVID-19 in Germany in Chapter 4,
- the general modeling strategy of PGSSMs for epidemiological models in the same chapters, as well as Section 2.4, and
- the rigorous mathematical study of the computational methods used to fit these models, especially the comparison of EIS and the CE-method in Chapter 3.

reformulate locality of epidemics more generally, effects particular to question at hand

In Chapter 2 we highlighted the need for explainable statistical models in infectious disease epidemiology. Throughout this thesis we use COVID-19 as a driving example, which is owed to the fact that this thesis is a product of this particular epidemic. However, the core questions surrounding past, current and future development of cases and derived indicators is of essence for all epidemics outbreaks, including seasonal influenza and other respiratory diseases

cite hubs, fraser influenze models

. As a solution to this challenging task, we presented SSMs, in particular PGSSMs, as a flexible framework for modeling the high-dimensional time-series data we are faced with. The wide range of applications in Chapter 4 demonstrates the flexibility of SSMs as a modeling tool.

We have seen that the widely available data surrounding the epidemic, in particular daily reports on infections and hospitalizations, can be leveraged to fit PGSSMs and the fitted models allow for straight-forward interpretation. While the fitting procedures for these models can be quite involved, the models themselves, especially the temporal dynamics, are not, an as such our analyses can be disseminated to statisticians and practitioners alike. However, the interpretability of all models presented in this thesis is hampered by the quality of data available. Indeed, large constituents of our models are purely for dealing with weekday effects, and reporting delays.

The final contribution of this thesis is a mathematically rigorous analysis of the performance of the importance sampling methods used in the applications (Chapter 4). To the authors' knowledge, Theorems 3.6 and 3.9 gives the first joint analysis of the CE-method and EIS, and sheds insight on the poor performance of the CE-method in practice: we can expect its asymptotic covariance to be larger than that of EIS, as its meat matrix M is fixed, whereas that of EIS can be expected to be small when the optimal proposal is close to the target.

Appendix A

Reproducibility and code

All code used in to create figures and tables in this thesis is written in Python and R

cite

and available as open source software. Python is used for simulations, while R is used to create figures and tables of these results.

The code is split into two software packages:

- Importance Sampling for State Space Models (`isssm`)[1] is a Python package developed by the author. It implements frequentist inference for SSMs using the general methods described in this thesis, in particular the CE-method and EIS for PGSSMs.
- The SSMs for Epidemiology `ssm4epi` package contains Python and R code particular to this thesis, i.e. the code needed to reproduce all results and figures in this thesis.

The `ssm4epi` package is available as Jupyter Notebooks organized by chapters of this thesis. To reproduce the results of this thesis, follow the instructions in the associated documentation

ref to doc

. Simulations use a fixed seed that is set at the beginning of each notebook to ensure reproducibility.

The data produced by these Jupyter notebooks are available on zenodo

put them there

, and can be reproduced by running the notebooks. Figures and tables in this thesis that depend on simulation results can be reproduced similarly, using Jupyter notebooks with an R kernel. Dependent R packages can be found in the `setup.R` file in this thesis' GitHub repository.

[1] https://stefanheyder.github.io/isssm

Bibliography

Abbott, S. et al. (June 1, 2020). "Estimating the Time-Varying Reproduction Number of SARS-CoV-2 Using National and Subnational Case Counts." In: *Wellcome Open Res* 5, p. 112. ISSN: 2398-502X. DOI: 10.12688/wellcomeopenres.16006.1.

Adamik, B. et al. (May 5, 2020). *Mitigation and Herd Immunity Strategy for COVID-19 Is Likely to Fail*. DOI: 10.1101/2020.03.25.20043109. Pre-published.

Agapiou, S. et al. (Jan. 14, 2017). *Importance Sampling: Intrinsic Dimension and Computational Cost*. DOI: 10.48550/arXiv.1511.06196. arXiv: 1511.06196 [stat]. Pre-published.

Akhmetzhanov, A. R. (2021). "Estimation of Delay-Adjusted All-Cause Excess Mortality in the USA: March-December 2020." In: *Epidemiology and Infection*. DOI: 10.1017/s0950268821001527. PMID: 34210370.

An Der Heiden, M. et al. (Apr. 22, 2020). "Schätzung Der Aktuellen Entwicklung Der SARS-CoV-2-Epidemie in Deutschland – Nowcasting." In: *Epidemiologisches Bulletin*. DOI: 10.25646/6692.4.

Ansley, C. F. et al. (1985). "Estimation, Filtering, and Smoothing in State Space Models with Incompletely Specified Initial Conditions." In: *The Annals of Statistics*, pp. 1286–1316. JSTOR: 2241356. URL: https://www.jstor.org/stable/2241356 (visited on 10/15/2024).

Arroyo-Marioli, F. et al. (Jan. 13, 2021). "Tracking R of COVID-19: A New Real-Time Estimation Using the Kalman Filter." In: *PLOS ONE* 16.1. DOI: 10.1371/journal.pone.0244474. PMID: 33439880.

Assimakis, N. et al. (2012). "Information Filter and Kalman Filter Comparison: Selection of the Faster Filter." In: *Information Engineering*. Vol. 2. 1, pp. 1–5. URL: http://madam.users.uth.gr/papers/3%20IJIE_2012.pdf (visited on 06/24/2024).

Bastos, L. S. et al. (2019). "A Modelling Approach for Correcting Reporting Delays in Disease Surveillance Data." In: *Statistics in Medicine*. DOI: 10.1002/sim.8303.

Bazaraa, M. S. et al. (2006). *Nonlinear Programming: Theory and Algorithms*. 3. ed. Hoboken, NJ: Wiley-Interscience. 853 pp. ISBN: 978-0-471-48600-8.

Bengtsson, T. et al. (2008). "Curse-of-Dimensionality Revisited: Collapse of the Particle Filter in Very Large Scale Systems." In: *Probability and statistics: Essays in honor of David A. Freedman* 2, pp. 316–334. DOI: 10.1214/193940307000000518.

Billingsley, P. (1995). *Probability and Measure*. 3rd ed. Wiley Series in Probability and Mathematical Statistics. New York: Wiley. 593 pp. ISBN: 978-0-471-00710-4.

Biswas, M. et al. (Dec. 9, 2020). "Association of Sex, Age, and Comorbidities with Mortality in COVID-19 Patients: A Systematic Review and Meta-Analysis." In: *Intervirology* 64.1, pp. 36–47. ISSN: 0300-5526. DOI: 10.1159/000512592.

Borchering, R. K. et al. (Sept. 1, 2023). "Public Health Impact of the U.S. Scenario Modeling Hub." In: *Epidemics* 44, p. 100705. ISSN: 1755-4365. DOI: 10.1016/j.epidem.2023.100705.

Bracher, J. et al. (Aug. 27, 2021a). "A Pre-Registered Short-Term Forecasting Study of COVID-19 in Germany and Poland during the Second Wave." In: *Nat Commun* 12.1 (1), p. 5173. ISSN: 2041-1723. DOI: 10.1038/s41467-021-25207-0.

Bracher, J. et al. (Nov. 23, 2021). *Comparison and Combination of COVID-19 Hospitalization Nowcasts in Germany*. URL: https://osf.io/mru75/.

Bracher, J. et al. (Feb. 12, 2021b). "Evaluating Epidemic Forecasts in an Interval Format." In: *PLoS Comput Biol* 17.2. Ed. by V. E. Pitzer, e1008618. ISSN: 1553-7358. DOI: 10.1371/journal.pcbi.1008618.

Bracher, J. et al. (Oct. 31, 2022). "National and Subnational Short-Term Forecasting of COVID-19 in Germany and Poland during Early 2021." In: *Commun Med* 2.1 (1), pp. 1–17. ISSN: 2730-664X. DOI: 10.1038/s43856-022-00191-8.

Branch, M. A. et al. (Jan. 1999). "A Subspace, Interior, and Conjugate Gradient Method for Large-Scale Bound-Constrained Minimization Problems." In: *SIAM J. Sci. Comput.* 21.1, pp. 1–23. ISSN: 1064-8275, 1095-7197. DOI: 10.1137/S1064827595289108.

Brauner, J. M. et al. (Feb. 19, 2021). "Inferring the Effectiveness of Government Interventions against COVID-19." In: *Science* 371.6531, eabd9338. ISSN: 0036-8075, 1095-9203. DOI: 10.1126/science.abd9338.

Britton, T. et al. (2019). *Stochastic Epidemic Models with Inference*. Ed. by T. Britton et al. Springer.

Brooks, S. et al., eds. (2011). *Handbook for Markov Chain Monte Carlo*. Boca Raton: Taylor & Francis. 592 pp. ISBN: 978-1-4200-7941-8.

Brown, L. D. (1986). *Fundamentals of Statistical Exponential Families: With Applications in Statistical Decision Theory*. Lecture Notes-Monograph Series v. 9. Hayward, Calif: Institute of Mathematical Statistics. 283 pp. ISBN: 978-0-940600-10-2.

Bundesagentur für Arbeit, Statistik (2021). *Sozialversicherungspflichtig beschäftigte nach ausgewählten merkmalen (quartalszahlen)*. Amtliche Statistik. Nürnberg, Deutschland: Bundesagentur für Arbeit. URL: https://statistik.arbeitsagentur.de/Statistikdaten/Detail/202109/iiia6/beschaeftigung-sozbe-svb-kreise-merkmale/svb-kreise-merkmale-d-0-202109-xlsx.xlsx?__blob=publicationFile&v=1.

– (2024). *Pendleratlas*. Pendleratlas - Statistik der Bundesagentur für Arbeit. URL: https://statistik.arbeitsagentur.de/DE/Navigation/Statistiken/Interaktive-Statistiken/Pendleratlas/Pendleratlas-Nav.html.

Burgard, J. P. et al. (Aug. 31, 2021). "Regional Estimates of Reproduction Numbers with Application to COVID-19." arXiv: 2108.13842 [stat]. URL: http://arxiv.org/abs/2108.13842 (visited on 09/30/2021).

Byambasuren, O. et al. (Dec. 31, 2020). "Estimating the Extent of Asymptomatic COVID-19 and Its Potential for Community Transmission: Systematic Review and Meta-Analysis." In: *Journal of the Association of Medical Microbiology and Infectious Disease Canada* 5.4, pp. 223–234. DOI: 10.3138/jammi-2020-0030.

Chan, J. C. C. et al. (Sept. 1, 2012). "Improved Cross-Entropy Method for Estimation." In: *Stat Comput* 22.5, pp. 1031–1040. ISSN: 1573-1375. DOI: 10.1007/s11222-011-9275-7.

Chan, J. C. C. et al. (May 1, 2012). *Marginal Likelihood Estimation with the Cross-Entropy Method*. DOI: 10.2139/ssrn.2055042. Pre-published.

Chatterjee, S. et al. (Apr. 1, 2018). "The Sample Size Required in Importance Sampling." In: *Ann. Appl. Probab.* 28.2. ISSN: 1050-5164. DOI: 10.1214/17-AAP1326.

Chopin, N. et al. (Feb. 1, 2017). "Leave Pima Indians Alone: Binary Regression as a Benchmark for Bayesian Computation." In: *Statist. Sci.* 32.1. ISSN: 0883-4237. DOI: 10.1214/16-STS581.

Chopin, N. et al. (2020). *An Introduction to Sequential Monte Carlo*. Springer Series in Statistics. Cham, Switzerland: Springer. 378 pp. ISBN: 978-3-030-47844-5.

Cori, A. (2021). *EpiEstim: Estimate Time Varying Reproduction Numbers from Epidemic Curves*. manual. URL: https://CRAN.R-project.org/package=EpiEstim.

Cover, T. M. et al. (2006). *Elements of Information Theory*. 2nd ed. Hoboken, N.J: Wiley-Interscience. 748 pp. ISBN: 978-0-471-24195-9.

Danielsson, J. et al. (1993). "Accelerated Gaussian Importance Sampler with Application to Dynamic Latent Variable Models." In: *Journal of Applied Econometrics* 8.S1, S153–S173. ISSN: 1099-1255. DOI: 10.1002/jae.3950080510.

Desai, A. N. et al. (Aug. 2019). "Real-Time Epidemic Forecasting: Challenges and Opportunities." In: *Health Security* 17.4, pp. 268–275. ISSN: 2326-5094. DOI: 10.1089/hs.2019.0022.

Diekmann, O. et al. (2013). *Mathematical Tools for Understanding Infectious Diseases Dynamics*. Princeton Series in Theoretical and Computational Biology. Princeton: Princeton University Press. 502 pp. ISBN: 978-0-691-15539-5.

Dong, E. et al. (2020a). *COVID-19 Data Repository by the Center for Systems Science and Engineering (CSSE) at Johns Hopkins University*. Johns Hopkins University. URL: https://github.com/CSSEGISandData/COVID-19.

Dong, E. et al. (May 1, 2020b). "An Interactive Web-Based Dashboard to Track COVID-19 in Real Time." In: *The Lancet Infectious Diseases* 20.5, pp. 533–534. ISSN: 1473-3099, 1474-4457. DOI: 10.1016/S1473-3099(20)30120-1. PMID: 32087114.

Du, Z. et al. (July 1, 2022). "Reproduction Numbers of Severe Acute Respiratory Syndrome Coronavirus 2 (SARS-CoV-2) Variants: A Systematic Review and Meta-analysis." In: *Clinical Infectious Diseases* 75.1, e293–e295. ISSN: 1058-4838. DOI: 10.1093/cid/ciac137.

Durbin, J. et al. (2012). *Time Series Analysis by State Space Methods*. 2nd ed. Oxford Statistical Science Series 38. Oxford: Oxford University Press. 346 pp. ISBN: 978-0-19-964117-8.

Durbin, J. et al. (Sept. 1, 1997). "Monte Carlo Maximum Likelihood Estimation for Non-Gaussian State Space Models." In: *Biometrika* 84.3, pp. 669–684. ISSN: 0006-3444. DOI: 10.1093/biomet/84.3.669.

– (2002). "A Simple and Efficient Simulation Smoother for State Space Time Series Analysis." In: *Biometrika* 89.3, pp. 603–616. DOI: 10.1093/biomet/89.3.603.

Ehre, M. et al. (Mar. 31, 2023). "Certified Dimension Reduction for Bayesian Updating with the Cross-Entropy Method." In: *SIAM/ASA J. Uncertainty Quantification* 11.1, pp. 358–388. DOI: 10.1137/22M1484031.

Engbert, R. et al. (Dec. 8, 2020). "Sequential Data Assimilation of the Stochastic SEIR Epidemic Model for Regional COVID-19 Dynamics." In: *Bull Math Biol* 83.1, p. 1. ISSN: 1522-9602. DOI: 10.1007/s11538-020-00834-8.

Engel, M. et al. (Jan. 15, 2023). "Bayesian Updating and Marginal Likelihood Estimation by Cross Entropy Based Importance Sampling." In: *Journal of Computational Physics* 473, p. 111746. ISSN: 0021-9991. DOI: 10.1016/j.jcp.2022.111746.

Evensen, G. (1994). "Sequential Data Assimilation with a Nonlinear Quasi-Geostrophic Model Using Monte Carlo Methods to Forecast Error Statistics." In: *Journal of Geophysical Research: Oceans* 99.C5, pp. 10143–10162. ISSN: 2156-2202. DOI: 10.1029/94JC00572.

Farrington, C. P. et al. (1996). "A Statistical Algorithm for the Early Detection of Outbreaks of Infectious Disease." In: *Journal of The Royal Statistical Society Series A-statistics in Society*. DOI: 10.2307/2983331.

Flaxman, S. et al. (Aug. 2020). "Estimating the Effects of Non-Pharmaceutical Interventions on COVID-19 in Europe." In: *Nature* 584.7820, pp. 257–261. ISSN: 1476-4687. DOI: 10.1038/s41586-020-2405-7. PMID: 32512579.

Fraser, C. (Aug. 22, 2007). "Estimating Individual and Household Reproduction Numbers in an Emerging Epidemic." In: *PLoS ONE* 2.8. Ed. by A. Galvani, e758. ISSN: 1932-6203. DOI: 10.1371/journal.pone.0000758.

Fraser, D. et al. (Aug. 1969). "The Optimum Linear Smoother as a Combination of Two Optimum Linear Filters." In: *IEEE Trans. Automat. Contr.* 14.4, pp. 387–390. ISSN: 0018-9286. DOI: 10.1109/TAC.1969.1099196.

Freistaat Thüringen (n.d.). *Thüringer Gesetz- und Verordnungsblatt Nr. 12/2019*. Gesetz- und Verordnungsblatt. Erfurt. URL: https://parldok.thueringer-landtag.de/ParlDok/dokument/72572/gesetz_und_verordnungsblatt_nr_12_2019.pdf.

Frühwirth-Schnatter, S. (1994). "Data Augmentation and Dynamic Linear Models." In: *Journal of Time Series Analysis* 15.2, pp. 183–202. ISSN: 1467-9892. DOI: 10.1111/j.1467-9892.1994.tb00184.x.

"Discrete Spatial Variation" (2010). In: *Handbook of Spatial Statistics*. Ed. by A. E. Gelfand et al. CRC Press. ISBN: 978-0-429-13650-4.

Günther, F. et al. (2021). "Nowcasting the COVID-19 Pandemic in Bavaria." In: *Biometrical Journal* 63.3, pp. 490–502. ISSN: 1521-4036. DOI: 10.1002/bimj.202000112.

Günther, T. et al. (Dec. 7, 2020). "SARS-CoV-2 Outbreak Investigation in a German Meat Processing Plant." In: *EMBO Molecular Medicine* 12.12, e13296. ISSN: 1757-4676. DOI: 10.15252/emmm.202013296.

Gupta, S. et al. (Nov. 2020). *Mandated and Voluntary Social Distancing During The COVID-19 Epidemic: A Review*. DOI: 10.3386/w28139. National Bureau of Economic Research: 28139. Pre-published.

Haberman, S. J. (1989). "Concavity and Estimation." In: *The Annals of Statistics* 17.4, pp. 1631–1661. ISSN: 0090-5364. DOI: 10.1214/aos/1176347385. JSTOR: 2241655.

Hart, W. S. et al. (May 1, 2022). "Generation Time of the Alpha and Delta SARS-CoV-2 Variants: An Epidemiological Analysis." In: *The Lancet Infectious Diseases* 22.5, pp. 603–610. ISSN: 1473-3099, 1474-4457. DOI: 10.1016/S1473-3099(22)00001-9. PMID: 35176230.

Havers, F. P. et al. (Sept. 26, 2024). "COVID-19–Associated Hospitalizations and Maternal Vaccination Among Infants Aged <6 Months — COVID-NET, 12 States, October 2022–April 2024." In: *MMWR Morb. Mortal. Wkly. Rep.* 73.38, pp. 830–836. ISSN: 0149-2195, 1545-861X. DOI: 10.15585/mmwr.mm7338a1.

Heyder, S. et al. (2022). "Regional Estimates of Reproduction Numbers with Application to COVID-19." In: *Progress in Industrial Mathematics at ECMI 2021*. Ed. by M. Ehrhardt et al. Mathematics in Industry. Cham: Springer International Publishing, pp. 163–171. ISBN: 978-3-031-11818-0. DOI: 10.1007/978-3-031-11818-0_22.

Heyder, S. et al. (Oct. 4, 2023). "Measures of COVID-19 Spread." In: *Covid-19 pandisziplinär und international: Gesundheitswissenschaftliche, gesellschaftspolitische und philosophische Hintergründe*. Ed. by A. Kraemer et al. Medizin, Kultur, Gesellschaft. Wiesbaden: Springer Fachmedien, pp. 51–66. ISBN: 978-3-658-40525-0. DOI: 10.1007/978-3-658-40525-0_3.

Höhle, M. et al. (2014). "Bayesian Nowcasting during the STEC O104:H4 Outbreak in Germany, 2011." In: *Biometrics* 70.4, pp. 993–1002. ISSN: 1541-0420. DOI: 10.1111/biom.12194.

Homem-de-Mello, T. (July 20, 2007). "A Study on the Cross-Entropy Method for Rare-Event Probability Estimation." In: *INFORMS Journal on Computing*. DOI: 10.1287/ijoc.1060.0176.

Hospitalization Nowcast Hub (Oct. 31, 2022). KITmetricslab. URL: https://github.com/KITmetricslab/hospitalization-nowcast-hub (visited on 11/09/2022).

Hotz, T. et al. (Apr. 18, 2020). "Monitoring the Spread of COVID-19 by Estimating Reproduction Numbers over Time." arXiv: 2004.08557 [q-bio, stat]. URL: http://arxiv.org/abs/2004.08557 (visited on 07/20/2020).

Hughes, T. D. et al. (Mar. 18, 2023). "The Effect of SARS-CoV-2 Variant on Respiratory Features and Mortality." In: *Sci Rep* 13.1, p. 4503. ISSN: 2045-2322. DOI: 10.1038/s41598-023-31761-y.

Ives, A. R. et al. (Jan. 5, 2021). "Estimating and Explaining the Spread of COVID-19 at the County Level in the USA." In: *Communications Biology* 4.1 (1), pp. 1–9. ISSN: 2399-3642. DOI: 10.1038/s42003-020-01609-6.

Jazwinski, A. H. (1970). *Stochastic Processes and Filtering Theory*. New York: Academic Press. 376 pp.

Johnson, N. L. et al. (1994). *Continuous Univariate Distributions*. 2nd ed. Wiley Series in Probability and Mathematical Statistics. New York: Wiley. 2 pp. ISBN: 978-0-471-58495-7 978-0-471-58494-0.

Julier, S. J. et al. (July 28, 1997). "New Extension of the Kalman Filter to Nonlinear Systems." In: Signal Processing, Sensor Fusion, and Target Recognition VI. Vol. 3068. International Society for Optics and Photonics, pp. 182–194. DOI: 10.1117/12.280797.

Jungbacker, B. et al. (Dec. 1, 2007). "Monte Carlo Estimation for Nonlinear Non-Gaussian State Space Models." In: *Biometrika* 94.4, pp. 827–839. ISSN: 0006-3444. DOI: 10.1093/biomet/asm074.

Kaminsky, K. S. (Apr. 1, 1987). "Prediction of IBNR Claim Counts by Modelling the Distribution of Report Lags." In: *Insurance Mathematics & Economics* 6.2, pp. 151–159. DOI: 10.1016/0167-6687(87)90024-2.

Kappen, H. J. et al. (Mar. 1, 2016). "Adaptive Importance Sampling for Control and Inference." In: *J Stat Phys* 162.5, pp. 1244–1266. ISSN: 1572-9613. DOI: 10.1007/s10955-016-1446-7.

Katzfuss, M. et al. (Oct. 1, 2016). "Understanding the Ensemble Kalman Filter." In: *The American Statistician* 70.4, pp. 350–357. ISSN: 0003-1305, 1537-2731. DOI: 10.1080/00031305.2016.1141709.

Keller, J. P. et al. (2022). "Tracking the Transmission Dynamics of COVID-19 with a Time-Varying Coefficient State-Space Model." In: *Statistics in Medicine* 41.15, pp. 2745–2767. ISSN: 1097-0258. DOI: 10.1002/sim.9382.

Kermack, W. O. et al. (Aug. 1927). "A Contribution to the Mathematical Theory of Epidemics." In: *Proc. R. Soc. Lond. A* 115.772, pp. 700–721. ISSN: 0950-1207, 2053-9150. DOI: 10.1098/rspa.1927.0118.

Khailaie, S. et al. (Jan. 28, 2021). "Development of the Reproduction Number from Coronavirus SARS-CoV-2 Case Data in Germany and Implications for Political Measures." In: *BMC Medicine* 19.1, p. 32. ISSN: 1741-7015. DOI: 10.1186/s12916-020-01884-4.

Khazaei, Y. et al. (Nov. 2, 2023). "Using a Bayesian Hierarchical Approach to Study the Association between Non-Pharmaceutical Interventions and the Spread of Covid-19 in Germany." In: *Sci Rep* 13.1, p. 18900. ISSN: 2045-2322. DOI: 10.1038/s41598-023-45950-2.

Kong, A. (1992). "A Note on Importance Sampling Using Standardized Weights." In: *University of Chicago, Dept. of Statistics, Tech. Rep* 348, p. 14.

Kong, A. et al. (Mar. 1994). "Sequential Imputations and Bayesian Missing Data Problems." In: *Journal of the American Statistical Association* 89.425, pp. 278–288. ISSN: 0162-1459. DOI: 10.1080/01621459.1994.10476469.

Koopman, S. J. (Dec. 1997). "Exact Initial Kalman Filtering and Smoothing for Nonstationary Time Series Models." In: *Journal of the American Statistical Association* 92.440, pp. 1630–1638. ISSN: 0162-1459, 1537-274X. DOI: 10.1080/01621459.1997.10473685.

Koopman, S. J. et al. (1992). "Exact Score for Time Series Models in State Space Form." In: *Biometrika* 79.4, pp. 823–826. ISSN: 0006-3444. DOI: 10.2307/2337237. JSTOR: 2337237.

Koopman, S. J. et al. (Jan. 2, 2015). "Numerically Accelerated Importance Sampling for Nonlinear Non-Gaussian State-Space Models." In: *Journal of Business & Economic Statistics* 33.1, pp. 114–127. ISSN: 0735-0015, 1537-2707. DOI: 10.1080/07350015.2014.925807.

Koopman, S. J. et al. (2019). "Modified Efficient Importance Sampling for Partially Non-Gaussian State Space Models." In: *Statistica Neerlandica* 73.1, pp. 44–62. ISSN: 1467-9574. DOI: 10.1111/stan.12128.

Lal, R. et al. (Aug. 19, 2021). "An Application of the Ensemble Kalman Filter in Epidemiological Modelling." In: *PLOS ONE* 16.8, e0256227. ISSN: 1932-6203. DOI: 10.1371/journal.pone.0256227.

Laplace, P. S. (Aug. 1986). "Memoir on the Probability of the Causes of Events." In: *Statistical Science* 1.3, pp. 364–378. ISSN: 0883-4237, 2168-8745. DOI: 10.1214/ss/1177013621.

Lauer, S. A. et al. (2020). "The Incubation Period of Coronavirus Disease 2019 (COVID-19) from Publicly Reported Confirmed Cases: Estimation and Application." In: *Annals of internal medicine* 172.9, pp. 577–582. DOI: 10.7326/M20-0504.

Lauritzen, S. L. (1996). *Graphical Models*. Oxford Statistical Science Series 17. Oxford : New York: Clarendon Press ; Oxford University Press. 298 pp. ISBN: 978-0-19-852219-5.

Lawless, J. F. (1994). "Adjustments for Reporting Delays and the Prediction of Occurred but Not Reported Events." In: *Canadian Journal of Statistics* 22.1, pp. 15–31. ISSN: 1708-945X. DOI: 10.2307/3315826.n1.

Liang, K.-Y. et al. (May 1995). "Inference Based on Estimating Functions in the Presence of Nuisance Parameters." In: *Statistical Science* 10.2, pp. 158–173. ISSN: 0883-4237, 2168-8745. DOI: 10.1214/ss/1177010028.

Liesenfeld, R. et al. (Sept. 1, 2003). "Univariate and Multivariate Stochastic Volatility Models: Estimation and Diagnostics." In: *Journal of Empirical Finance* 10.4, pp. 505–531. ISSN: 0927-5398. DOI: 10.1016/S0927-5398(02)00072-5.

Lloyd-Smith, J. O. et al. (Nov. 2005). "Superspreading and the Effect of Individual Variation on Disease Emergence." In: *Nature* 438.7066, pp. 355–359. ISSN: 1476-4687. DOI: 10.1038/nature04153.

McGough, S. F. et al. (2020). "Nowcasting by Bayesian Smoothing: A Flexible, Generalizable Model for Real-Time Epidemic Tracking." In: *PLOS Computational Biology*. DOI: 10.1371/journal.pcbi.1007735. PMID: 32251464.

MichaelKreil et al. (June 16, 2022). *RKI-Corona-Daten-Archiv*. ard-data. URL: https://github.com/ard-data/2020-rki-archive (visited on 08/18/2024).

Midthune, D. N. et al. (Mar. 1, 2005). "Modeling Reporting Delays and Reporting Corrections in Cancer Registry Data." In: *Journal of the American Statistical Association* 100.469, pp. 61–70. ISSN: 0162-1459. DOI: 10.1198/016214504000001899.

Morf, M. et al. (Aug. 1975). "Square-Root Algorithms for Least-Squares Estimation." In: *IEEE Transactions on Automatic Control* 20.4, pp. 487–497. ISSN: 1558-2523. DOI: 10.1109/TAC.1975.1100994.

Mossong, J. et al. (Mar. 25, 2008). "Social Contacts and Mixing Patterns Relevant to the Spread of Infectious Diseases." In: *PLOS Medicine* 5.3, e74. ISSN: 1549-1676. DOI: 10.1371/journal.pmed.0050074.

Müller, T. et al. (Oct. 10, 2019). "Neural Importance Sampling." In: *ACM Trans. Graph.* 38.5, 145:1–145:19. ISSN: 0730-0301. DOI: 10.1145/3341156.

Neiswanger, W. et al. (July 23, 2014). "Asymptotically Exact, Embarrassingly Parallel MCMC." In: *Proceedings of the Thirtieth Conference on Uncertainty in Artificial Intelligence*. UAI'14. Arlington, Virginia, USA: AUAI Press, pp. 623–632. ISBN: 978-0-9749039-1-0.

Nocedal, J. et al. (2006). *Numerical Optimization*. Second edition. Springer Series in Operation Research and Financial Engineering. New York, NY: Springer. 664 pp. ISBN: 978-0-387-30303-1 978-1-4939-3711-0.

Noufaily, A. et al. (2015). "Modelling Reporting Delays for Outbreak Detection in Infectious Disease Data." In: *Journal of The Royal Statistical Society Series A-statistics in Society*. DOI: 10.1111/rssa.12055.

Nowcasts Der COVID-19 Hospitalisierungsinzidenz (2022). URL: https://covid19nowcasthub.de/ (visited on 11/09/2022).

O'Dea, E. B. et al. (Feb. 16, 2022). "A Semi-Parametric, State-Space Compartmental Model with Time-Dependent Parameters for Forecasting COVID-19 Cases, Hospitalizations and Deaths." In: *Journal of The Royal Society Interface* 19.187, p. 20210702. DOI: 10.1098/rsif.2021.0702.

Rao, C. R. (2002). *Linear Statistical Inference and Its Applications*. 2. ed., Paperback ed. Wiley Series in Probability and Statistics. New York: Wiley. 625 pp. ISBN: 978-0-471-21875-3.

Ray, E. L. et al. (Aug. 22, 2020). "Ensemble Forecasts of Coronavirus Disease 2019 (COVID-19) in the U.S." In: *medRxiv*, p. 2020.08.19.20177493. DOI: 10.1101/2020.08.19.20177493.

Renshaw, A. E. et al. (1998). "A Stochastic Model Underlying the Chain-Ladder Technique." In: *British Actuarial Journal* 4.4, pp. 903–923. DOI: 10.1017/S1357321700000222.

Richard, J.-F. et al. (Dec. 1, 2007). "Efficient High-Dimensional Importance Sampling." In: *Journal of Econometrics* 141.2, pp. 1385–1411. ISSN: 0304-4076. DOI: 10.1016/j.jeconom.2007.02.007.

Ripley, B. D. (2009). *Stochastic Simulation*. Vol. 316. John Wiley & Sons.

Robert Koch-Institut (Oct. 1, 2021). *COVID-19-Hospitalisierungen in Deutschland*. Version 2021-10-01. Zenodo. DOI: 10.5281/ZENODO.5519056.

– (Feb. 7, 2022). *SARS-CoV-2 Infektionen in Deutschland*. Version 2022-02-07. Zenodo. DOI: 10.5281/ZENODO.4681153.

– (Aug. 19, 2024a). *COVID-19-Hospitalisierungen in Deutschland*. Version 2024-08-19. Zenodo. DOI: 10.5281/ZENODO.5519056.

– (Aug. 2024b). *COVID-19-Hospitalisierungen in Deutschland*. DOI: 10.5281/zenodo.13340547.

– (Aug. 18, 2024c). *SARS-CoV-2 Infektionen in Deutschland*. Version 2024-08-18. Zenodo. DOI: 10.5281/ZENODO.4681153.

– (Aug. 2024d). *SARS-CoV-2 Infektionen in Deutschland*. DOI: 10.5281/zenodo.13337137.

– (Oct. 23, 2024e). *SARS-CoV-2 Sequenzdaten aus Deutschland*. Version 2024-10-22. Zenodo. DOI: 10.5281/ZENODO.5139363.

Rubinstein, R. Y. (Sept. 1, 1999). "The Cross-Entropy Method for Combinatorial and Continuous Optimization." In: *Methodology and Computing in Applied Probability* 1.2, pp. 127–190. ISSN: 1573-7713. DOI: 10.1023/A:1010091220143.

Rubinstein, R. Y. et al. (2004). *The Cross-Entropy Method: A Unified Approach to Combinatorial Optimization, Monte-Carlo Simulation and Machine Learning*. New York, NY: Springer New York. ISBN: 978-1-4757-4321-0.

Rubinstein, R. Y. et al. (Nov. 6, 2009). "How to Deal with the Curse of Dimensionality of Likelihood Ratios in Monte Carlo Simulation." In: *Stochastic Models* 25.4, pp. 547–568. ISSN: 1532-6349. DOI: 10.1080/15326340903291248.

Salmon, M. et al. (2015). "Bayesian Outbreak Detection in the Presence of Reporting Delays." In: *Biometrical Journal*. DOI: 10.1002/bimj.201400159. PMID: 26250543.

Salzberger, B. et al. (Apr. 1, 2021). "Epidemiology of SARS-CoV-2." In: *Infection* 49.2, pp. 233–239. ISSN: 1439-0973. DOI: 10.1007/s15010-020-01531-3.

Schäfer, F. et al. (Jan. 2021). "Sparse Cholesky Factorization by Kullback–Leibler Minimization." In: *SIAM J. Sci. Comput.* 43.3, A2019–A2046. ISSN: 1064-8275. DOI: 10.1137/20M1336254.

Schneble, M. et al. (Mar. 2021). "Nowcasting Fatal COVID-19 Infections on a Regional Level in Germany." In: *Biometrical Journal* 63.3, pp. 471–489. ISSN: 0323-3847, 1521-4036. DOI: 10.1002/bimj.202000143.

Schneider, W. (1986). *Der Kalmanfilter Als Instrument Zur Diagnose Und Schätzung Variabler Parameter in Ökonometrischen Modellen*. Arbeiten Zur Angewandten Statistik Bd. 27. Heidelberg: Physica-Verlag. 490 pp. ISBN: 978-3-7908-0359-4.

Shephard, N. (1994). "Partial Non-Gaussian State Space." In: *Biometrika* 81.1, pp. 115–131. DOI: 10.1093/biomet/81.1.115.

Shephard, N. et al. (Sept. 1, 1997). "Likelihood Analysis of Non-Gaussian Measurement Time Series." In: *Biometrika* 84.3, pp. 653–667. ISSN: 0006-3444. DOI: 10.1093/biomet/84.3.653.

Sherratt, K. et al. (June 16, 2022). *Predictive Performance of Multi-Model Ensemble Forecasts of COVID-19 across European Nations*. DOI: 10.1101/2022.06.16.22276024. Pre-published.

Sherratt, K. et al. (Apr. 21, 2023). "Predictive Performance of Multi-Model Ensemble Forecasts of COVID-19 across European Nations." In: *eLife* 12. Ed. by A. Wesolowski et al., e81916. ISSN: 2050-084X. DOI: 10.7554/eLife.81916.

Song, J. et al. (May 1, 2021). "Maximum Likelihood-Based Extended Kalman Filter for COVID-19 Prediction." In: *Chaos, Solitons & Fractals* 146, p. 110922. ISSN: 0960-0779. DOI: 10.1016/j.chaos.2021.110922.

Stark, P. B. et al. (1995). "Bounded-Variable Least-Squares: An Algorithm and Applications." In: *Computational Statistics* 10, pp. 129–129. URL: https://digitalassets.lib.berkeley.edu/sdtr/ucb/text/394.pdf (visited on 06/05/2024).

Tierney, L. et al. (Mar. 1986). "Accurate Approximations for Posterior Moments and Marginal Densities." In: *Journal of the American Statistical Association* 81.393, pp. 82–86. ISSN: 0162-1459, 1537-274X. DOI: 10.1080/01621459.1986.10478240.

Tierney, L. et al. (Sept. 1989). "Fully Exponential Laplace Approximations to Expectations and Variances of Nonpositive Functions." In: *Journal of the American Statistical Association* 84.407, pp. 710–716. ISSN: 0162-1459, 1537-274X. DOI: 10.1080/01621459.1989.10478824.

Tomori, D. V. et al. (Mar. 26, 2021). "Individual Social Contact Data Reflected SARS-CoV-2 Transmission Dynamics during the First Wave in Germany Better than Population Mobility Data – an Analysis Based on the COVIMOD Study." In: p. 2021.03.24.21254194. DOI: 10.1101/2021.03.24.21254194.

Van de Kassteele, J. et al. (2019). "Nowcasting the Number of New Symptomatic Cases during Infectious Disease Outbreaks Using Constrained P-Spline Smoothing." In: *Epidemiology*. DOI: 10.1097/ede.0000000000001050. PMID: 31205290.

Van der Vaart, A. W. (2000). *Asymptotic Statistics*. Cambridge: Cambridge University Press.

Wallinga, J. et al. (Feb. 22, 2007). "How Generation Intervals Shape the Relationship between Growth Rates and Reproductive Numbers." In: *Proc. R. Soc. B.* 274.1609, pp. 599–604. ISSN: 0962-8452, 1471-2954. DOI: 10.1098/rspb.2006.3754.

Wallinga, J. et al. (Sept. 15, 2004). "Different Epidemic Curves for Severe Acute Respiratory Syndrome Reveal Similar Impacts of Control Measures." In: *American Journal of Epidemiology* 160.6, pp. 509–516. ISSN: 0002-9262. DOI: 10.1093/aje/kwh255.

White, H. (1982). "Maximum Likelihood Estimation of Misspecified Models." In: *Econometrica* 50.1, pp. 1–25. ISSN: 0012-9682. DOI: 10.2307/1912526. JSTOR: 1912526.

Whitt, W. (Nov. 1976). "Bivariate Distributions with Given Marginals." In: *The Annals of Statistics* 4.6, pp. 1280–1289. ISSN: 0090-5364, 2168-8966. DOI: 10.1214/aos/1176343660.

Willrich, N. et al. (Nov. 25, 2021). "Update: Erfassung der SARS-CoV-2-PCR-Testzahlen in Deutschland und die Entwicklung der Testzahlen in ärztlichen Praxen." In: DOI: 10.25646/9306.

Wolffram, D. et al. (Aug. 11, 2023). "Collaborative Nowcasting of COVID-19 Hospitalization Incidences in Germany." In: *PLOS Computational Biology* 19.8, e1011394. ISSN: 1553-7358. DOI: 10.1371/journal.pcbi.1011394.

Wu, N. et al. (May 1, 2023). "Long-Term Effectiveness of COVID-19 Vaccines against Infections, Hospitalisations, and Mortality in Adults: Findings from a Rapid Living Systematic Evidence Synthesis and Meta-Analysis up to December, 2022." In: *The Lancet Respiratory Medicine* 11.5, pp. 439–452. ISSN: 2213-2600, 2213-2619. DOI: 10.1016/S2213-2600(23)00015-2. PMID: 36780914.

Zeger, S. L. et al. (1989). "Statistical Methods for Monitoring the AIDS Epidemic." In: *Statistics in Medicine* 8.1, pp. 3–21. DOI: 10.1002/sim.4780080104.

Zhang, W. et al. (Jan. 2014). "Applications of the Cross-Entropy Method to Importance Sampling and Optimal Control of Diffusions." In: *SIAM J. Sci. Comput.* 36.6, A2654–A2672. ISSN: 1064-8275. DOI: 10.1137/14096493X.

Zhu, X. et al. (Oct. 1, 2021). "Extended Kalman Filter Based on Stochastic Epidemiological Model for COVID-19 Modelling." In: *Computers in Biology and Medicine* 137, p. 104810. ISSN: 0010-4825. DOI: 10.1016/j.compbiomed.2021.104810.

Symbols

R_c	case reproduction number
R_t	time-varying reproduction number
$X_{:t}$	$(X_0, \ldots, X_t)$ for $t \in \mathbf{N}_0$
$X_{s:t}$	$(X_s, \ldots, X_t)$ for $s, t \in \mathbf{N}_0$, $s < t$
$\mathbf{R}_{>0}$	positive real numbers
Θ	set of all parameters
Pois	Poisson distribution
ρ	growth factor
θ	a parameter
d	doubling time
p	generic density
r	exponential growth rate
$test$	doubling
w	generation time distribution
$\mathbf{N}_0$	Natural numbers, including 0
$\mathbf{N}$	Natural numbers, excluding 0
$\mathbf{R}^{p \times m}$	matrices with p rows and m columns of real entries
$\mathbb{E}$	expected value

Abbreviations

BLUP best linear unbiased predictor. 54

CDF cumulative distribution function. 83

CE-method Cross-Entropy method. ix, 2, 22, 25, 40, 45–49, 51, 53–56, 58–60, 62–65, 68–71, 73–75, 83–96, 99, 129, 131

CLT central limit theorem. 51, 52, 57, 59, 74–76, 95, 96, 99

COD curse of dimensionality. 49

COVID-19 Coronavirus disease 2019. 1, 2, 5–7, 9–11, 14–16, 18, 31, 98, 99, 111, 115, 123, 129

CRN common random number. 48, 71, 77, 81

ECDC European Centre for Disease Prevention and Control. 115

EF efficiency factor. 41–43, 123

EGSSM Exponential Family Partially Gaussian state space model. 34, 35, 61–63, 70, 72, 84, 85, 91

EIS Efficient Importance Sampling. ix, 2, 22, 25, 32, 40, 45, 54–56, 59, 60, 62–65, 71, 73–75, 78, 81–96, 99, 102, 103, 106, 111, 122, 129, 131

EKF Extended Kalman filter. 29, 31, 99

EnKF Ensemble Kalman filter. 29, 31, 99

ESS effective sample size. 40–42, 45, 60, 86, 122, 123

European FCH European COVID-19 ForecastHub. 115

FFBS Forwards Filter, Backwards Sampling. 31, 79, 82

German and Polish FCH German and Polish COVID-19 ForecastHub. 115

GLSSM Gaussian linear state space model. ix, 22, 25, 26, 28–32, 60–63, 65, 70, 71, 75–78, 80–82, 102, 111, 125

ICU intensive care unit. 10

IS Importance Sampling. 36

JHU CSSE Johns Hopkins University Center for Systems Science and Engineering. 10

KL-divergence Kullback Leibler divergence. 2, 25, 38–40, 45, 46, 54, 68

LA Laplace approximation. ix, 22, 35, 45, 60, 62, 63, 70, 78, 81, 83, 85, 92, 94, 95, 102, 104, 106, 111, 115, 122

MAE mean absolute error. 117

MC-integration Monte-Carlo integration. 19, 35, 62

MCMC Markov chain Monte Carlo. 25, 35, 36, 49, 60, 77

MLE maximum likelihood estimator. 25, 29, 77, 81, 103, 107, 111, 122, 125

MSE mean-squared error. 38, 41

NPI non-pharmaceutical intervention. 5, 6, 8, 14, 17, 18, 99, 100, 108

PGSSM Partially Gaussian state space model. 25, 32, 34, 36, 37, 62, 63, 73–76, 78, 79, 81, 82, 102, 122, 129, 131

PSD positive semi-definite. 29

RKI Robert Koch-Institut. 1, 6, 10–12, 14, 15, 100, 109–111, 115, 117, 118, 120, 127

SARS-CoV-2 Severe acute respiratory syndrome coronavirus 2. 5, 123

SMC sequential Monte Carlo. 25, 35, 36, 77

SPD symmetric positive definite. 31, 41, 85

SSM state space model. 2, 23–26, 32, 35, 44, 45, 59, 60, 63, 65, 73, 74, 76, 77, 91, 94, 95, 98–100, 108, 110–115, 119, 125, 127, 129, 131

UKF unscented Kalman filter. 29, 30

VM-method Variance-Minimization method. 60, 96

WIS weighted interval score. 117, 118

Declaration

Put your declaration here.

Ilmenau, 2025-10-05 20:45:33+02:00